Cytosolic RECONnaissance:
Host Strategies for Sensing and Controlling Bacteria

Adelle P. McFarland

A dissertation
submitted in partial fulfillment of the
requirements for the degree of

Doctor of Philosophy

University of Washington
2018

Reading Committee:
Joshua J. Woodward, Chair
Daniel B. Stetson
Kevin Hybiske

Program Authorized to Offer Degree
Molecular and Cellular Biology

University of Washington

Abstract

Cytosolic RECONnaissance:
Host Strategies for Sensing and Controlling Bacteria

Adelle P. McFarland

Chair of the Supervisory Committee:
Joshua J. Woodward
Department of Microbiology

Cyclic dinucleotides (CDNs) of bacterial and host origin mediate cytosolic immune responses through the stimulator of interferon genes (STING) signaling pathway, though evidence suggests alternative receptors exist. We identified the oxidoreductase RECON as a high-affinity host receptor specific for bacterial CDNs. RECON's enzyme activity was inhibited by bacterial CDNs, which bound in the substrate and cosubstrate sites. During bacterial infection of macrophages, RECON antagonized STING activation by acting as a molecular sink for CDNs. In hepatocytes, RECON negatively regulated NF-κB activation via its enzymatic activity. Loss of RECON resulted in increased NF-κB activation and reduced bacterial survival. Therefore, CDN inhibition of RECON promotes a proinflammatory, antibacterial state.

We investigated the molecular pathways by which RECON controls inflammation and found that several branches of the arachidonic acid inflammatory cascade were involved. At the top of the cascade, free arachidonic acid levels were significantly elevated in the absence of RECON, which correlated with the formation of large lipid droplets. Genetic deletion of the cytosolic phospholipase A2, which liberates arachidonic acid from phospholipids, in RECON-deficient cells restored the inflammatory response to WT levels. The reactive lipid aldehyde 4-hydroxynonenal (4-HNE), which is a byproduct of arachidonic acid peroxidation, was elevated in RECON-deficient cells following TLR stimulation. 4-HNE was determined to be a bonafide RECON substrate

that specifically enhanced *Nos2* expression. Interestingly, a separate branch of the arachidonic acid cascade was found to govern *Il6* expression distinct from the pathway described for *Nos2*. Dysregulated COX-mediated prostaglandin synthesis was discovered in RECON-deficient cells by comprehensive eicosanoid profiling. Accordingly, inhibition of COX-2 activity reduced *Il6* but not *Nos2* expression. Finally, although RECON controlled *Nos2* via augmented NF-κB activation, we found that the MEK-ERK pathway was critical for *Il6* expression. Overall, RECON's targeting of inflammatory arachidonic acid oxidation metabolites provides a molecular explanation for how this enzyme operates as a regulator of multiple gene induction programs.

In addition to its role as a regulator of innate immune gene activation, we also characterized the effects of RECON on the infection cycle of the intracellular bacterium *Listeria monocytogenes*, which secretes cyclic diadenosine monophosphate (c-di-AMP) into the cytosol of infected host cells. Remarkably, *L. monocytogenes* exhibited significantly enhanced cell-to-cell spread in RECON-deficient hepatocytes. *L. monocytogenes* actin tail lengths were significantly longer and there was a larger number of faster moving bacteria in the absence of RECON. Complementation experiments demonstrated that the effect of RECON on *L. monocytogenes* spread and actin tail lengths was linked to its enzymatic activity. Augmented NF-κB activation in the absence of RECON was responsible for the enhanced *L. monocytogenes* cell-to-cell spread. Finally, we found that increased NF-κB-dependent iNOS expression and nitric oxide production was sufficient to drive *L. monocytogenes* spread. This work revealed a novel host-pathogen interaction, whereby *L. monocytogenes* secretion of c-di-AMP inhibits RECON, drives augmented NF-κB activation and nitric oxide production, and enhances intercellular spread.

To gain insights into how RECON functions *in vivo*, we generated mice deficient in RECON. Following systemic challenge *L. monocytogenes*, RECON-deficient mice exhibited increased survival and reduced bacterial loads. Apart from its role in infection, we found that RECON deficiency promoted aberrant low-level inflammation in the small intestines. The absence of RECON was associated with alterations in the microbiota, with aberrant expansion of segmented filamentous bacteria. These findings demonstrate that RECON functions in intestinal homeostasis and that the inflammatory programs under its control are protective during systemic bacterial infection. Collectively, the work presented in this dissertation establishes RECON as an innate immune sensor and modulator of cell-intrinsic metabolites that promote antibacterial immunity.

Acknowledgements

A great number of people contributed to this work. First and foremost, I would like to recognize and thank my graduate advisor, Josh Woodward, for his unwavering support and ideas. The many directions I was able to explore would not have happened without his curiosity, generosity, encouragement, and fortitude. We made the best team, which I know will continue for the rest of our careers. I would also like to thank Ram Savan, who has been a mentor to me since the first day I started a career in research. My success has largely been aided by his insights, recommendations, and support.

I am very grateful for the time, ideas and positivity of my committee. Brad Cookson, Ferric Fang, Kevin Hybiske, and Dan Stetson provided outstanding encouragement and enthusiasm from the outset of my graduate training, which gave me a great deal of confidence.

Our work on RECON benefited from the resources and ideas of many people. Dan Stetson and Michael Gale, Jr. provided key mouse lines. Dan Portnoy generously supplied many *Listeria monocytogenes* strains. Kamakshi Sureka, Tu Anh Huynh, Shivam Zaver and Michelle Reniere contemplated many data, and I am grateful for their feedback. I would also like to thank our co-authors, who are named at the beginning of each published chapter. Our work was elevated by their expertise, thoughtfulness and time.

Carrying out my Ph.D. work in the Department of Microbiology afforded me the opportunity to interact with dedicated and fun graduate students and faculty. It was an enriching environment that broadened my interests and knowledge. Additionally, the graduate students, post-docs and faculty in the Department of Immunology were also a source of encouragement for me. In particular, I am grateful to the members of the Ram Lab for their friendship and for supplying endless laughter.

This is for my family.
To my mother and father, Morgan and Gregory,
who modeled a love of knowledge and the value of being kind.
To my sisters, Lila, Shelley and Kristina,
who I miss every minute that we are not together.
To my nieces and nephew,
who brought a new purpose to my life.

Table of Contents

List of Figures

List of Tables

Chapter 1

Introduction: Microbial Sensing in the Cytosol

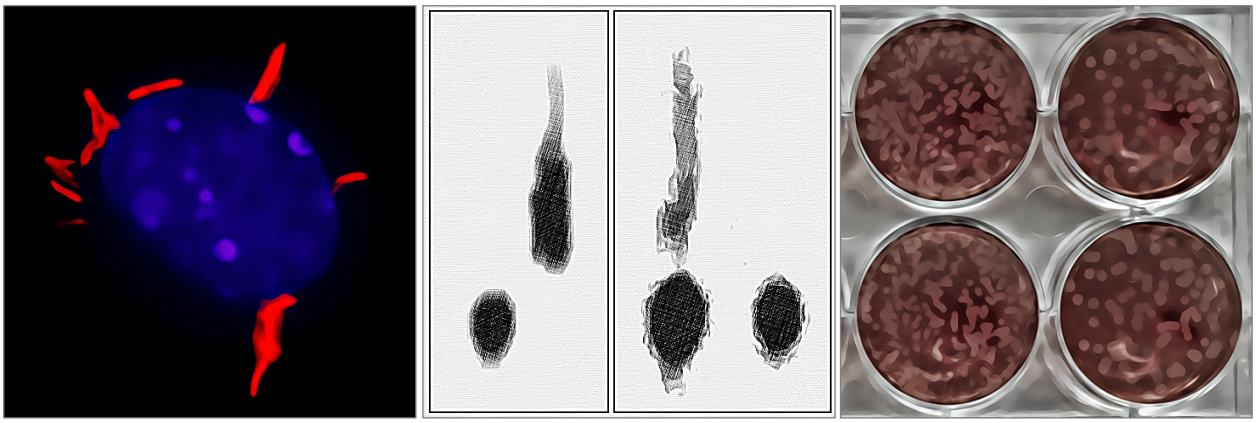

1.1 Cytosolic surveillance of cyclic dinucleotides

Host cells have evolved a sophisticated arsenal of germ-line encoded pattern recognition receptors (PRRs) that detect a vast array of microorganisms in distinct tissues and cellular compartments. Cytoplasmic sensors monitor for microbes that gain access to the host cell cytosol following breach of the plasma membrane or intracellular invasion. This sensing is achieved through detection of invariant molecular patterns associated with microorganisms or cell stress responses that indicate the presence of a pathogen. Engagement of a PRR by a microbial product triggers a signal transduction pathway that ultimately shapes cellular function to regain sterility. Many of the cellular changes are mediated through activation of transcription factors, such as nuclear factor κB (NF-κB), mitogen-activated protein kinases (MAPKs) and/or interferon regulatory factors (IRFs) (*1*). Classically, PRR engagement results in recruitment and activation of kinase activity that serves as the driving force of these signaling cascades. For example, retinoic acid-inducible gene I (RIG-I)-like receptors (RLRs), which recognize viral and bacterial RNA species in the cytoplasm, activate the IKK kinase complex and TANK-binding kinase 1 (TBK1), leading to NF-κB and IRF3 activation, respectively (*2*).

A newly discovered arm of cytosolic sensing involves the PRR STING (stimulator of interferon genes), which mediates nucleic acid sensing by binding cyclic dinucleotides (CDNs) resulting in activation of the TBK1-IRF3 signaling axis (*3-6*). CDNs have recently emerged as central players in the innate immune response to bacterial and viral

infections. Mammals synthesize 2′3′-cGAMP downstream of cytosolic DNA detection of bacterial and viral origin (*7-10*). Bacteria produce c-di-GMP, c-di-AMP and 3′3′-cGAMP as second messengers that regulate a variety of cellular processes (*11, 12*). C-di-GMP regulates motility and biofilm formation while 3′3′-cGAMP regulates metal-reducing activity and host colonization in *Geobacter* and *Vibrio cholera*, respectively (*12-14*). C-di-AMP, the only essential CDN, regulates bacterial growth, cell wall homeostasis and central metabolism (*15-17*). C-di-AMP is implicated in STING-dependent type I interferon (IFN) induction during infection with the intracellular pathogens *Listeria monocytogenes*, *Chlamydia* spp., *Mycobacterium tuberculosis*, and Group B *Streptococcus* (*3, 4, 18-23*). Given the widespread conservation and central physiological function of these metabolites, CDNs likely play a role in a diverse array of bacterial-host interactions.

1.2 Bacterial cyclic di-AMP is an ideal PAMP

To maximize detection of a diverse set of organisms using a limited number of germ-line encoded receptors, the innate immune system targets conserved and essential components of microbial cells. The diadenylate cyclase responsible for c-di-AMP production is broadly conserved among most major phyla of bacteria (*22*) (Figure 1.1). Due to its small molecule chemical nature and essentiality among the many bacterial pathogens and commensals in the Firmicutes and Bacteroidetes phyla, c-di-AMP is difficult for organisms to evolve away from or to chemically alter to mask immune detection. Based on these characteristics, c-di-AMP is an ideal signature of bacterial presence. Furthermore, c-di-AMP is considered to be a special class of PAMP, known as PAMP-PV or vita-PAMP, because it is produced by viable bacteria (Figure 1.2) (*24, 25*). Therefore, its presence signals to the host that a live bacterium is present, and when found within the cytosol, a sterile space, is a strong indication that a live pathogen is present (Figure 1.2).

To date, STING-dependent detection of c-di-AMP during infection by a variety of organisms, including *L. monocytogenes*, *C. trachomatis*, *M. tuberculosis*, *S. aureus*, and *Streptococcus agalactiae* has been reported (*18, 19, 23, 26, 27*). *S. agalactiae* and *M. tuberculosis* have been reported to utilize specific phosphodiesterases to degrade extracellular c-di-AMP to evade immune sensing (*23, 27*), a tell-tale sign that immune detection of c-di-AMP is indeed detrimental to microbial survival. Together with the

widespread conservation of c-di-AMP and its essential nature in many organisms, these findings support c-di-AMP immune detection as a broadly conserved and highly significant area of study.

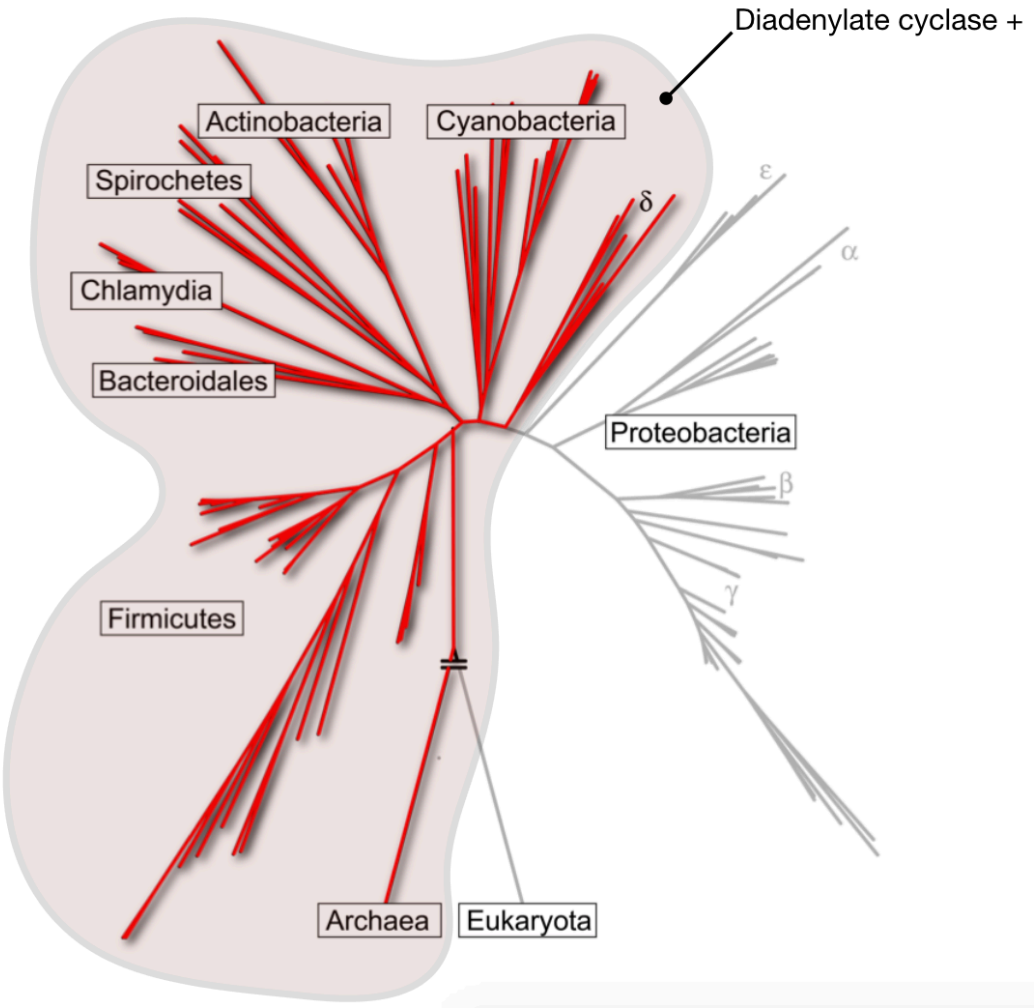

Figure 1.1. Widespread distribution of the diadenylate cyclase across bacterial phyla. All bacterial phyla, excluding most Proteobacteria, encode a diadenylate cyclase. Eukaryotes do not encode a diadenylate cyclase and therefore, do not produce c-di-AMP.

1.3 Enzymes as sensors and regulators of immunity

The integration of sensor function with control of enzyme activity is a newly emerging paradigm in innate sensing. Upon binding to cytosolic DNA, cyclic GMP-AMP synthase (cGAS) is activated and synthesizes 2′3′-cGAMP which engages STING and triggers a

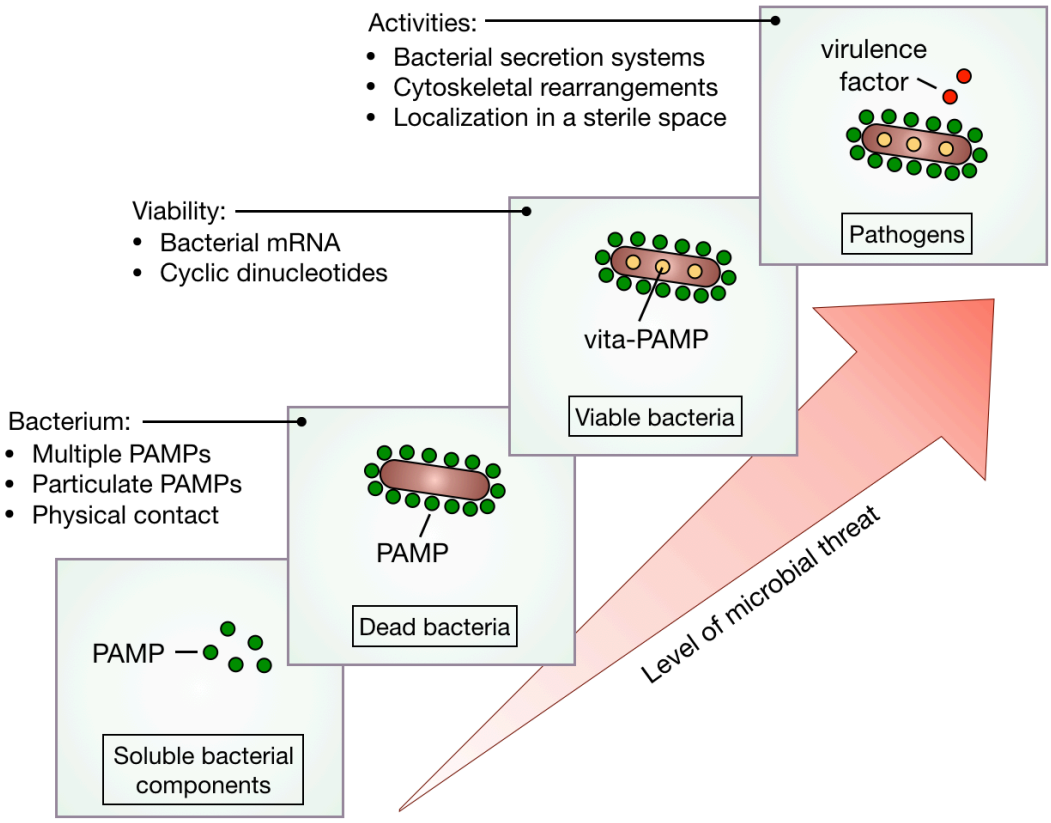

Figure 1.2. Context and type of PAMP determine immune responses. Soluble versus particulate PAMPs can signify to a host cell whether a physical bacterium is present. Vita-PAMPs, like bacterial mRNA and cyclic dinucleotides, signify life and therefore a potentially viable threat. At the highest tier, the activities of a pathogen and localization within the cytosol prompt a robust immune response. This schematic was adapted from Blander and Sander, *Nat Rev Immunol* (2012) (*24*).

type I IFN response (*8-10*). From what is currently known, the enzymatic function of cGAS is solely to produce the second messenger 2′3′-cGAMP. However, metabolic enzymes can also serve as innate sensors. For instance, binding of N-acetylglucosamine, a sugar subunit found in bacterial peptidoglycan, to hexokinase blocks glycolysis, triggers its release from the mitochondrial outer membrane, and induces activation of the NLRP3 inflammasome (*28*).

Examples of crosstalk between intrinsic cellular metabolism and immune sensing are numerous. Over the past 15 years, cholesterol and intracellular sterols have been studied for their ability to modulate immune responses (reviewed in (*29*)). During LPS stimulation, sensing of oxysterols by the liver X receptor (LXR) suppresses NF-κB activation (*30*). However, oxysterols have LXR-independent roles and can function as

pro-inflammatory mediators. For example, the oxysterol 25-hydroxychosterol (25HC), which is a cholesterol oxidation product synthesized by cholesterol-25-hydroxylase (Ch25h), can amplify inflammation in virally-infected macrophages by promoting AP-1 DNA binding (*31*). On the other hand, restraint of cholesterol levels by Ch25h during macrophage LPS stimulation is critical to prevent mitochondrial damage, which can trigger AIM2 inflammation activation and IL-1β production (*32*). Therefore, depending on the context, Ch25h and oxysterols can assume either proinflammatory or anti-inflammatory roles. Indeed, many enzymes involved in cellular metabolism behave in this two-faced fashion, conditionally dictated by the inflammatory stimuli, cell type, and substrate repertoire.

1.4 Introduction to RECON

In the following chapters of this dissertation, we report on the identification and characterization of the bacterial cyclic dinucleotide sensor RECON. RECON is an enzyme belonging to the aldo-keto reductase superfamily, first cloned in 1999 from mouse stomach (*33*). Only having ever been studied as a recombinant protein in enzyme assays, the role of this enzyme in cellular physiology and immunity was completely unknown. In Chapter 2, our initial discovery of RECON as a c-di-AMP-binding protein and controller of NF-κB-mediated inflammatory gene expression is described. The work presented in Chapter 3 provides evidence that RECON's enzymatic activity regulates arachidonic acid-derived metabolites that feed into TLR-induced inflammatory cascades. The excess production of nitric oxide via increased iNOS expression is a key feature of RECON-controlled inflammation that we have extensively studied. Chapter 4 reveals a surprising relationship between c-di-AMP, RECON and nitric oxide production and the intercellular spread of *Listeria monocytogenes*. Finally, the generation of RECON-deficient mice and initial phenotype characterizations related to bacterial pathogenesis and intestinal homeostasis are the subjects of Chapter 5. Collectively, this dissertation establishes RECON as an innate immune sensor and modulator of cell-intrinsic metabolites that promote antibacterial immunity.

Chapter 2

Initial Discovery and Characterization of RECON

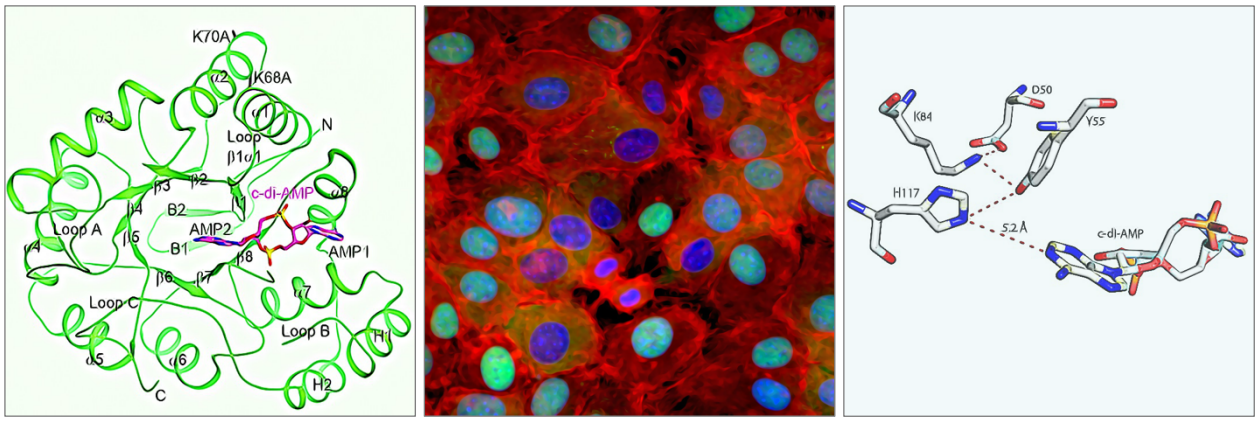

The following work has been published as: McFarland, A.P., Shukun, L., Ahmed-Qadri, F., Zuck, M., Thayer, E.F., Goo, Y.A., Hybiske, K., Tong, L., Woodward, J.J. "Sensing of Bacterial Cyclic Dinucleotides by the Oxidoreductase RECON Promotes NF-κB Activation and Shapes a Proinflammatory Antibacterial State." *Immunity* 46.3 (2017): 433-445.

2.1 Summary

Cyclic dinucleotides (CDNs) of bacterial and host origin mediate cytosolic immune responses through the STING signaling pathway, though evidence suggests alternative receptors exist. We performed pulldowns using CDN-conjugated beads and identified the oxidoreductase RECON as a high-affinity host receptor specific for bacterial CDNs. RECON enzyme activity was inhibited by bacterial CDNs, and the co-crystal structure revealed that CDN binding blocked the substrate and cosubstrate sites. During bacterial infection of macrophages, RECON antagonized STING activation by acting as a molecular sink for CDNs. In hepatocytes, which are deficient in STING, RECON negatively regulated NF-κB activation via its enzymatic activity. Loss of RECON activity resulted in increased NF-κB activation and reduced bacterial survival, therefore CDN inhibition of RECON promoted a proinflammatory, antibacterial state. These findings identify RECON as a cytosolic pattern recognition receptor specific for bacterial CDNs that shapes STING and NF-κB inflammatory gene expression.

2..2 Background

The extensive characterization of pattern recognition receptors (PRRs) that detect microbial ssRNA, dsRNA or dsDNA has revealed the existence of multiple PRRs that detect similar nucleic acid species. For example, several cytosolic PRRs, including DDX41, DHX9, DHX36, IFI16, DAI, AIM2 and cGAS, have been implicated in dsDNA detection, although for some of these receptors, such as IFI16, their ability to bind dsDNA does not necessarily translate into *in vivo* importance during infection (*7, 34, 35*). Cyclic dinucleotides (CDNs) have recently emerged as central players in the innate immune response to bacterial and viral infections and are detected by the ER-localized sensor STING (stimulator of interferon genes). STING mediates nucleic acid sensing by binding CDNs resulting in activation of the TBK1-IRF3 signaling axis (*3-6*).

Although PRR activation by CDNs is a relatively recent discovery, our understanding of CDN detection by host cells lags significantly behind other nucleic acid species. STING and DDX41 are the only two known PRRs that bind CDNs and downstream responses are aimed at the induction of type I IFN. Interestingly, STING-deficient mice do not exhibit altered bacterial burden or survival during infection with CDN-producing bacteria, such as *L. monocytogenes* or *M. tuberculosis* (*4, 36*), suggesting that activation of STING does not significantly influence the innate response to infection with these pathogens. However, mice infected with *L. monocytogenes* or *M. tuberculosis* producing altered levels of c-di-AMP exhibit profound differences in bacterial loads and survival in an IFN-independent manner, with increased c-di-AMP production correlating with increased host resistance and vice versa (*19, 37, 38*). The discordant phenotypes between STING-deficient mice and c-di-AMP production suggests the existence of additional host receptors that engage bacterial CDNs.

In the work presented in this chapter, we aimed to identify host proteins that interact with bacterial CDNs. We found that the oxidoreductase, aldo-keto reductase family 1, member C13 (AKR1C13), which we refer to as RECON (REductase COntrolling NF-κB) specifically bound to the bacterial nucleotides c-di-AMP and 3′3′-cGAMP, but not mammalian 2′3′-cGAMP. RECON bound c-di-AMP with high affinity, altering STING activation during *L. monocytogenes* infection by acting as an intracellular sink for this CDN. In addition, c-di-AMP bound to RECON in the substrate and cosubstrate binding sites, thereby inhibiting its enzyme activity. We found that loss of RECON enzyme

activity increased NF-κB activity that resulted in augmented inflammatory gene activation and reduced bacterial survival. Taken together, our data reveal a role for RECON in the shaping of an antibacterial state distinct from the antiviral type I IFN response mediated by the CDN sensing axis comprised of STING and DDX41.

2.3 Bacterial cyclic dinucleotides bind and inhibit the oxidoreductase RECON

2.3.1 C-di-AMP sepharose pulldowns identify RECON

To identify host proteins that interact with bacterial CDNs, we performed pulldowns from lysates of mouse spleen, liver and lung with c-di-AMP sepharose (Figures 2.1A and 2.1B). The oxidoreductase, aldo-keto reductase family 1, member C13 (AKR1C13; protein

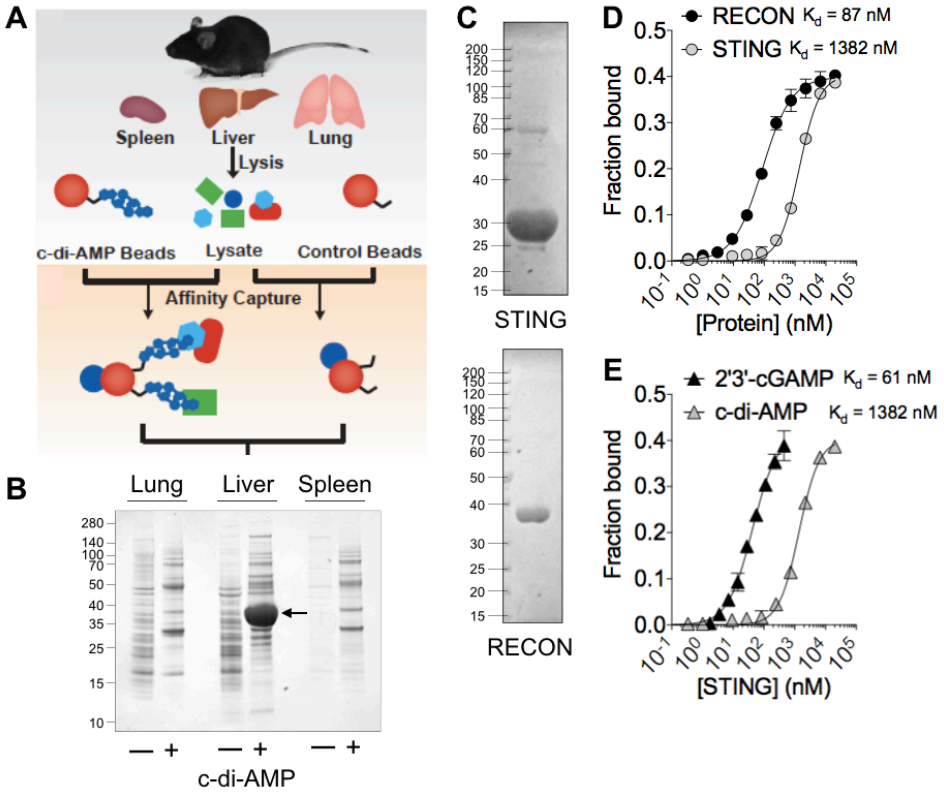

Figure 2.1. C-di-AMP binds the oxidoreductase RECON. (A) Schematic diagram of chemical proteomics used to identify c-di-AMP interacting proteins (image modified from Sureka et al., 2014). (B) SDS-page analysis of pulldowns from mouse organ lysates with c-di-AMP (+) or control (-) sepharose. (C) SDS-page gels of purified, recombinant STING and RECON. (D) Binding titration of ^{32}P-c-di-AMP with RECON or STING. Kd values are indicated. (E) Binding titration of ^{32}P-2′3′-cGAMP or ^{32}P-c-di-AMP with STING. Data are representative of at least two independent experiments with similar results. In all panels, error bars represent ± SEM of technical replicates.

herein referred to as RECON) was identified by mass spectrometry as the highly abundant protein in c-di-AMP liver pull-downs. Biochemical characterization using purified recombinant protein confirmed that RECON bound to c-di-AMP (Figures 2.1C and 2.1D). The affinity of this interaction was significantly higher than that observed between c-di-AMP and STING, with RECON binding to c-di-AMP 16 times more tightly. The binding of c-di-AMP by RECON was comparable to the affinity of STING for 2′3′-cGAMP (Figure 2.1E), consistent with STING specificity for the endogenously produced 2′3′-cGAMP nucleotide and RECON specificity for exogenously produced bacterial c-di-AMP.

2.3.2. Bacterial CDNs but not host-derived 2′3′-cGAMP bind RECON

Only the addition of cold c-di-AMP, but not a variety of other cold nucleotides, could interfere with ^{32}P-c-di-AMP binding to RECON (Figure 2.2A). By competing all of the known CDNs against ^{32}P-c-di-AMP, we found that RECON also bound 3′3′-cGAMP, but not c-di-GMP or host-derived 2′3′-cGAMP, whereas all cold CDNs competed off ^{32}P-c-di-AMP from STING (Figure 2.2B). Therefore, RECON specifically binds to bacterial CDNs and not the host-derived 2′3′-cGAMP. RECON exhibits both dehydrogenase and reductase activity and can turn over a broad spectrum of substrates (*33, 39*). We found that in the presence of c-di-AMP, RECON's enzyme activity was completely inhibited (Figures 2.2C and 2.2D). Consistent with our nucleotide binding studies, bacterial-derived 3′3′-cGAMP, but not host-derived 2′3′-cGAMP, also inhibited RECON activity (Figure 2.2E). Both c-di-AMP and 3′3′-cGAMP inhibited RECON activity by 50% at concentrations near 300 nM, even in the presence of 200 μM NADPH.

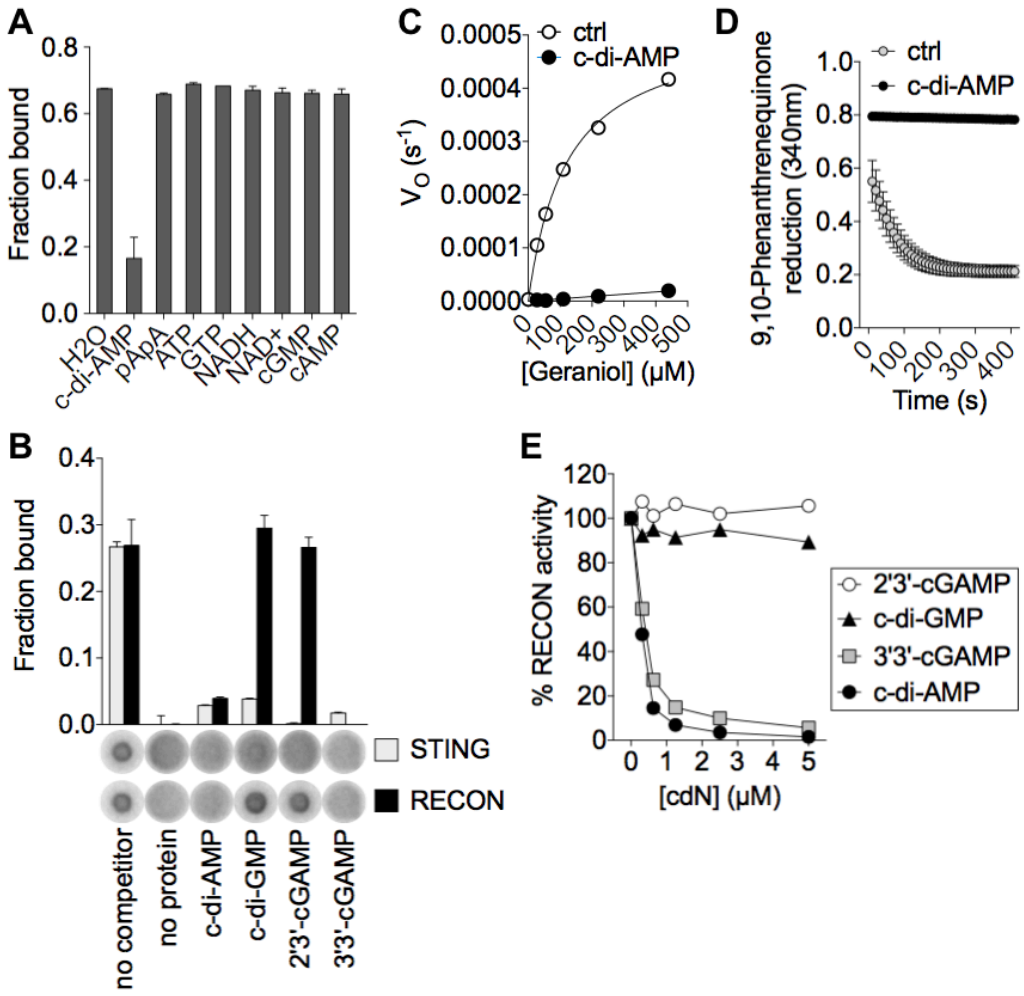

Figure 2.2. Bacterial cyclic dinucleotides inhibit RECON. (A) Binding of RECON with ^{32}P-c-di-AMP in the presence of competing unlabeled nucleotides (200 μM). (B) Binding of RECON or STING with ^{32}P-c-di-AMP in the presence of competing unlabeled cyclic dinucleotides, each at 400 μM concentration. (C) Michaelis–Menten kinetics of RECON with the substrate geraniol and cosubstrate NAD+ in the presence or absence of 1 μM c-di-AMP. (D) Oxidation of NADPH in the presence or absence of c-di-AMP as measured by 340 nm absorbance during RECON enzymatic activity with the substrate 9,10-Phenanthrenequinone. (E) RECON enzyme activity in the presence of increasing concentrations of the indicated CDNs. Substrate was 9,10-PQ and cosubstrate was NADPH. Data are plotted as percent of activity without CDN added. Data are representative of at least two independent experiments with similar results. In all panels, error bars represent ± SEM of technical replicates.

2.4 Crystal structure and the binding mode of c-di-AMP in RECON

We determined the crystal structure of the c-di-AMP-RECON complex at 1.5 Å resolution. The atomic model had good agreement with the crystallographic data and the

expected bond lengths, bond angles and other geometric parameters (Table 2.1). RECON adopts the TIM barrel fold with eight parallel β-strands (β1- β8) surrounded by 8 crossover α -helixes (α1-α8) (Figure 2.3A) common to aldo-keto reductase superfamily members (*40*). RECON also has a two-stranded anti-parallel β-sheet (B1 and B2) that caps the N-terminal end of the central barrel, and two additional helixes H1 (inserted between β7 and α8) and H2 (after α8) located on the side of the structure (Figure 2.3A). The active site of the enzyme is located at the top of the structure, near the C-terminal end of the central barrel, and several large loops (loops A, B and C, and loop β1α1) form the NAD+ and substrate binding sites (Figure 2.3B). Although the structure of the c-di-AMP complex exhibits a very small rms distance of 0.3 Å among equivalent Cα atoms in the NAD+ complex (PDB entry 3LN3) (Figure 2.3B), important differences between the two structures exist in the active site.

Clear electron density was observed for c-di-AMP based on the crystallographic analysis at 1.5 Å resolution (Figure 2.3C). The compound is an extended conformation where the two adenine bases adopt anti confirmations in nearly the same plane as the phosphodiester ring. The c-di-AMP binding site is in a deep crevice at the top of the central barrel (Figures 2.3A and 2.3D). One AMP molecule (AMP1) of c-di-AMP has essentially the same position as the AMP portion of the NAD+ cosubstrate, while the other AMP (AMP2) has small overlap with the nicotinamide ring (Figure 2.3E) and is positioned mostly in the substrate-binding site (Figure 2.3B) (*41*).

The N6 and N7 atoms of the AMP1 adenine base are recognized by hydrogen-bonding to the side chain of Asn280 (helix α8), and N6 also interacts with the side chain of Glu279 (α8) (Figure 2.3F). The adenine base is flanked by the side chain of Glu276 (α8) on one face and those of Leu219 (loop B) and Ala253 (α7) on the other. The phosphate group of AMP1 hydrogen-bonds with the main-chain amides of Leu219 and Thr221 (loop B). The adenine base of AMP2 is π-stacked with the side chain of Tyr24 (β1α1 loop) on one face and is flanked by the side chains of Tyr216 (β7) and Leu306 (loop C) on the other (Figure 2.3F). This base is pointed toward the catalytic tetrad of the enzyme, composed of Asp50, Tyr55, Lys84, and His117. The 2′ hydroxyl of the ribose is hydrogen-bonded to the main-chain amide of Gly217 (loop B). Several water molecules are in and near the c-di-AMP binding site, including one which mediates hydrogen-bonding interactions between the N1 atom of AMP2 and the catalytic Tyr55 and His117 residues (Figure 2.3F).

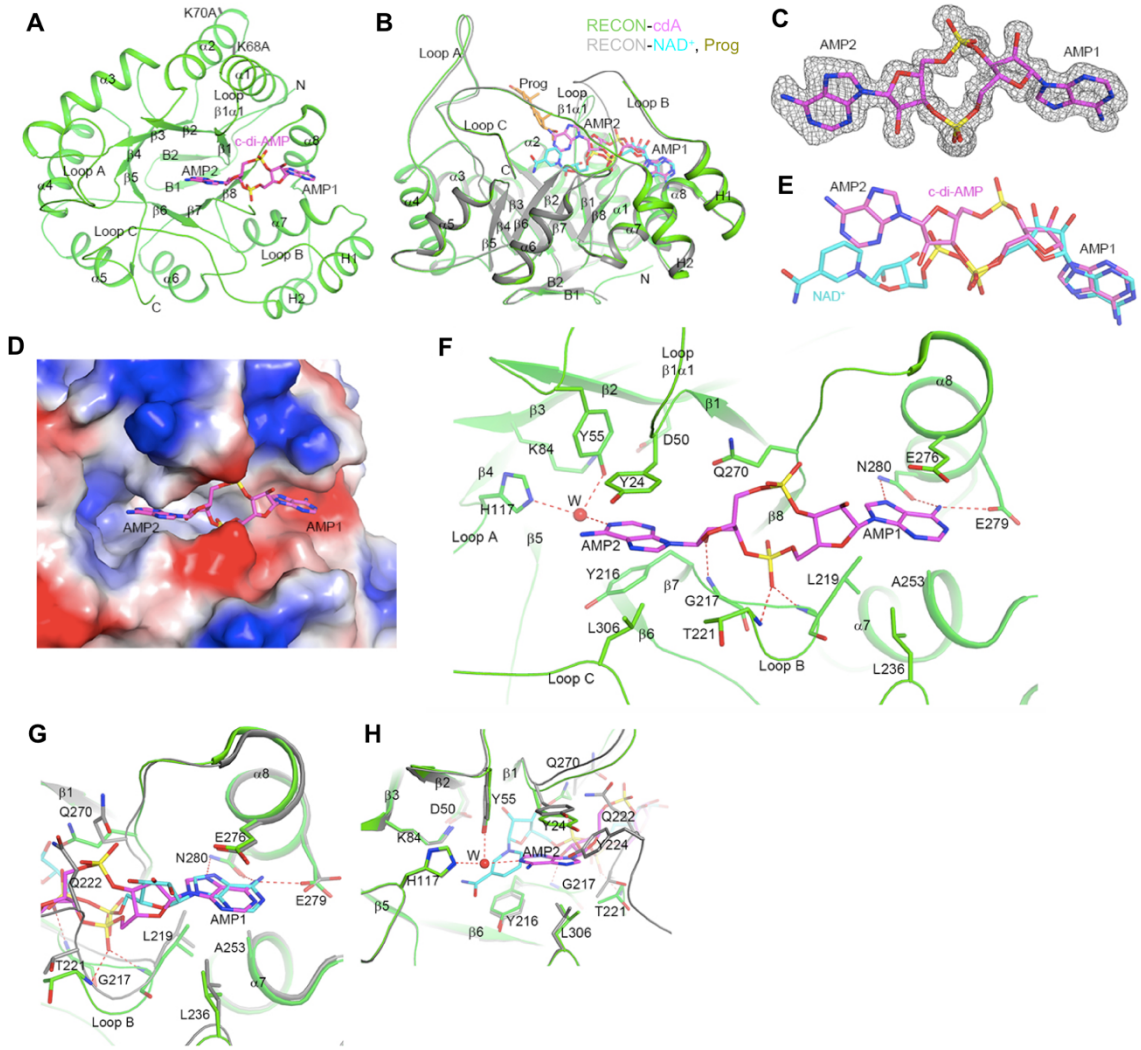

Figure 2.3. C-di-AMP blocks the NAD+ and substrate binding sites of RECON. (A) Schematic drawing of structure of RECON (green) in complex with c-di-AMP (magenta, stick models). The view is down the central barrel of the structure. The two Lys to Ala mutation sites are labeled. (B) Overlay of structure of RECON (green) in complex with c-di-AMP (magenta, stick models) and that of RECON (gray) in complex with NAD+ (cyan, stick models) (PDB entry 3LN3). The view is related to that of panel A by a 90° rotation around the horizontal axis. The bound position of the progesterone substrate (Prog) to AKR1C1 is also shown (orange, stick models) (Couture et al., 2003). (C) Side views of (A) with two residue-mutations indicated. Omit Fo–Fc electron density for c-di-AMP at 1.5 Å resolution, contoured at 2.5σ. (D) Molecular surface of RECON near c-di-AMP, colored by electrostatic potential. (E) Comparison of the binding modes of c-di-AMP (magenta) and NAD+ (cyan) to RECON. All structure figures were produced with PyMOL (www.pymol.org). (F) Detailed interactions between c-di-AMP and RECON. Hydrogen-bonding interactions are indicated with dashed lines (red). Residues involved in interactions with c-di-AMP are labeled. A water molecule is shown as a red sphere and labeled W. (G) Overlay of the binding sites of NAD+ (cyan) and c-di-AMP (magenta) near the first nucleotide (AMP1) of c-di-AMP. (H) Overlay of the binding sites of NAD+ (cyan) and c-di-AMP (magenta) near the second nucleotide (AMP2) of c-di-AMP.

Compared to the structure of the NAD+ complex, most residues in the AMP1 binding site assume the same conformation (Figure 2.3G). In contrast, substantial conformational differences are observed for residues in the AMP2 binding site (Figure 2.3H). Tyr24 and the β1α1 loop move closer by ~1 Å to the adenine base, enabling π stacking between the two aromatic moieties. Residues 222-231 of loop B are disordered in the c-di-AMP complex due to clashes of Gln222 and Tyr224 with AMP2. The side chain of Gln270 assumes a different rotamer in the c-di-AMP complex to avoid steric clash with the phosphate group of AMP2 (Figure 2.3G). Even though c-di-AMP uses the NAD+ binding site and assumes a conformation of similar length as NAD+, only one nucleotide has close overlap with NAD+. The other nucleotide deviates significantly from the NAD+ envelope, exploring a different region of the target protein. This should confer selectivity to the compound, so that it will not inhibit all NAD+/NADP+ binding proteins.

Table 2.1. Summary of Crystallographic Information. *Related to Figure 2.3.*

Structure	c-di-AMP complex
Space group	$P2_12_12_1$
Cell dimensions	
a (Å)	48.6
b (Å)	75.4
c (Å)	88.4
a (°)	90
b (°)	90
g (°)	90
Wavelength (Å)	1.74
Resolution[1] (Å)	25-1.50 (1.55-1.50)
No. of observations	295,963
R_{merge} (%)	7.8 (24.2)
I/σI	11.2 (3.0)
Redundancy	5.7 (3.0)
No. of reflections	52,009
Completeness (%)	98.9 (92.7)
R_{work} (%)	0.168 (0.178)
R_{free}[2] (%)	0.186 (0.195)
R.m.s deviations	
Bond lengths (Å)	0.006
Bond angles (°)	0.98
Ramachandran plot	
Favored (%)	99.4
Allowed	0.6
Outliers	0

1. The numbers in parentheses are for the highest resolution shell.
2. 5% of the reflections were selected for free R calculation.

2.5 Loss of RECON augments inflammatory gene expression

2.5.1 *Ifnb1* inversely correlates with *Akr1c13* expression in iBMDMs

To interrogate the effects of RECON on host innate immune responses during infection, we characterized the transcriptional response to *L. monocytogenes*, an organism that secretes c-di-AMP and triggers STING-dependent type I IFN expression during infection of macrophages (Figure 2.4A) (*3, 4, 20*). We measured the expression of IFN-β (gene *Ifnb1*) 4 hours post-infection (hpi) in immortalized bone marrow-derived macrophages (iBMDMs) that overexpressed *Akr1c13* (MSCV-*Akr1c13*), had reduced levels of *Akr1c13* expression via RNAi using a short hairpin RNA (sh-*Akr1c13*), or were transduced with control scrambled short hairpin RNA (sh-Control) and observed an inverse correlation with *Akr1c13* expression, whereby high amounts of *Ifnb1* transcripts correlated with low amounts of *Akr1c13* transcripts and vice versa (Figures 2.4B and 2.4C). Given that RECON binds c-di-AMP with higher affinity than STING, these observations suggest that RECON antagonizes STING activation by decreasing the bioavailability of c-di-AMP during infection.

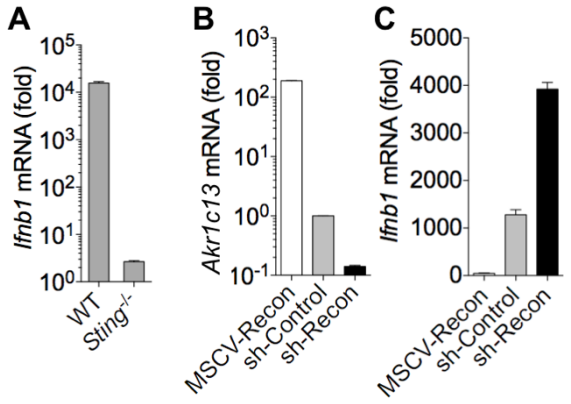

Figure 2.4. Loss of RECON during *L. monocytogenes* infection augments *Ifnb1* expression. (A) *Ifnb1* expression in WT or *Sting*-deficient primary BMDMs 4 hpi. (B) Expression of *Akr1c13* mRNA in iBMDM cell lines with altered *Akr1c13* expression. (C) Expression of *Ifnb1* mRNA in iBMDM cell lines with altered *Akr1c13* expression infected with *L. monocytogenes* for 4 h. Data are representative of three or more independent experiments with similar results. qRT-PCR data were performed in technical duplicates or triplicates and were normalized to uninfected sh-Control iBMDM cells. In all panels, error bars represent ± SEM.

2.5.2 Inflammatory genes inversely correlate with RECON levels

We ran a focused TaqMan mouse immune panel on sh-Control, sh-*Akr1c13* and MSCV-*Akr1c13* iBMDMs infected with *L. monocytogenes* for 4 hours. *Ccl5*, *Cxcl10*, *Cxcl11*, *Il1b* and *Nos2* were all induced during *L. monocytogenes* infection, and, similar to *Ifnb1*, there was a strong inverse correlation between their expression and *Akr1c13* levels (Figure 2.5A). Thus, loss of RECON is associated with increased inflammatory gene expression. *Clc5* (RANTES), *Cxcl10* (IP-10) and *Cxcl11* (I-TAC) are potent chemoattractants for activated T cells, IL-1β is a proinflammatory cytokine that activates innate and adaptive cellular responses, while *Nos2* encodes for inducible nitric oxide synthase (iNOS) (*42*, *43*). *Akr1c13* expression itself was not significantly altered during infection, therefore transcriptional regulation of *Akr1c13* does not appear to be involved in the response to *L. monocytogenes* in iBMDMs (Figure 2.5B).

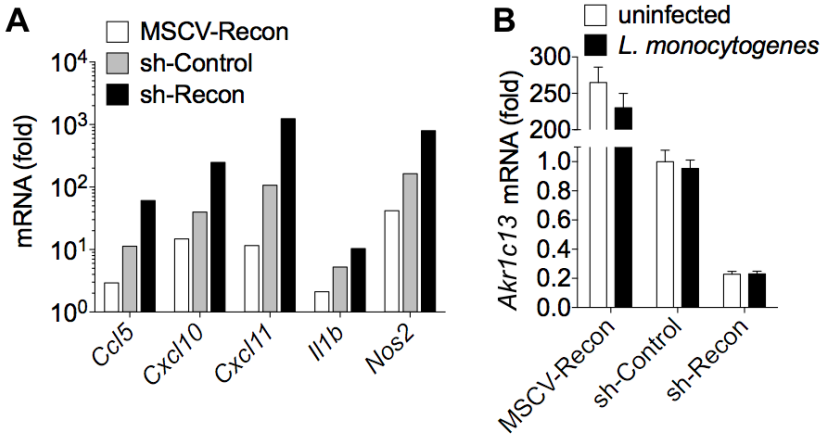

Figure 2.5. Loss of RECON during *L. monocytogenes* infection augments inflammatory gene expression. (A) TaqMan array expression of *Ccl5*, *Cxcl10*, *Cxcl11*, *Il1b* and *Nos2* mRNA in iBMDM cell lines with altered *Akr1c13* expression infected with *L. monocytogenes* for 4 h. (B) Expression of *Akr1c13* mRNA in uninfected or *Lm*-infected (4 hpi) iBMDM cell lines with altered *Akr1c13* expression. Data were performed in technical triplicates and were normalized to uninfected sh-Control iBMDM cells. Error bars represent ± SEM.

2.5.3 RECON affects inflammatory gene expression through STING- and IFN-independent pathways

The RECON-dependent expression of *Nos2* was of interest, considering the important role of nitric oxide in host defense against pathogenic bacteria (*44*). The effect of RECON

on *Nos2* transcription resulted in differences in nitric oxide production, as measured by Griess assay (Figures 2.6A and 2.6B). Since feedback from IFN-β is known to enhance induction of Toll-like receptor (TLR)-stimulated genes, including iNOS (*42*), we also examined inflammatory gene expression during *L. monocytogenes* infection in the presence of an IFNAR1 blocking antibody (Figures 2.6C) and following treatment with the TLR2 ligand Pam3CSK4or NOD1 ligand Tri-DAP (Figures 2.6D and 2.6E). In all cases, we observed that loss of RECON augmented *Nos2* expression, even when *Ifnb1* expression was similar across the cell lines. Therefore, RECON affects expression of *Nos2* and other inflammatory genes through a STING- and IFN-independent pathway.

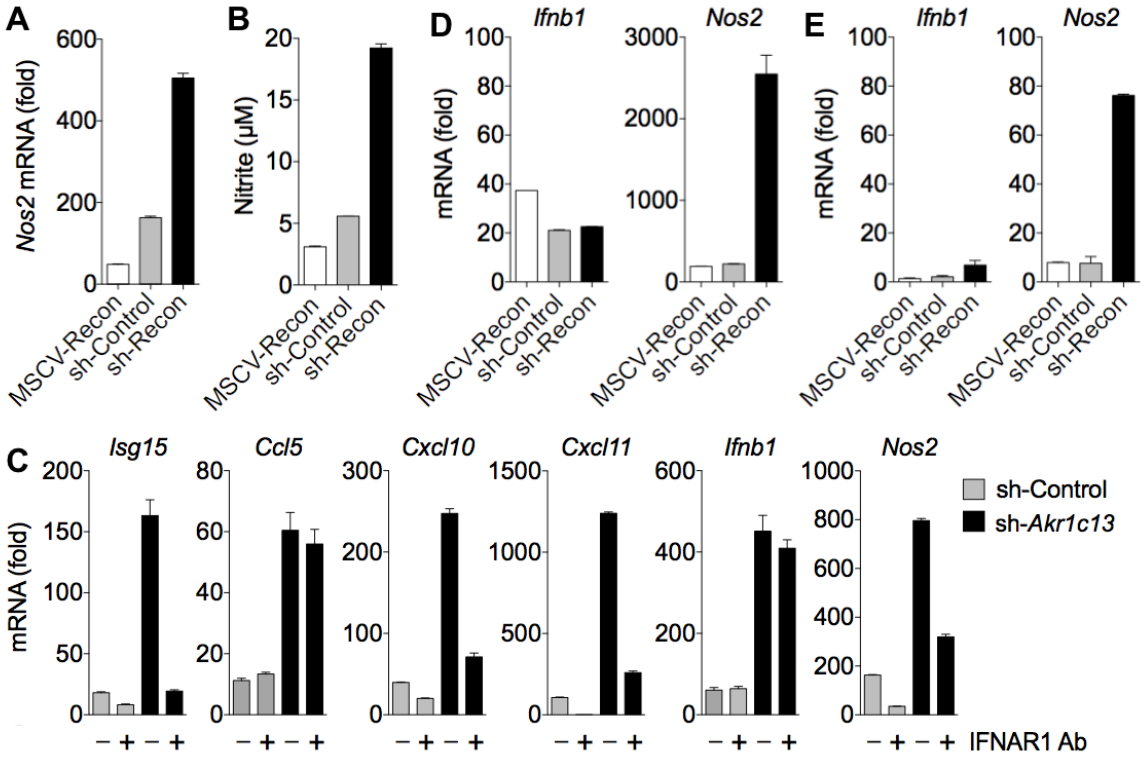

Figure 2.6. RECON affects inflammatory gene expression through STING- and IFN-independent pathways. (A) Expression of *Nos2* mRNA at 4 hpi with *L. monocytogenes* (*Lm*). (B) Nitrite levels in iBMDM supernatants 20 hpi with *Lm*. (C) Expression of inflammatory genes in sh-Control (grey bars) or sh-*Akr1c13* (black bars) iBMDM cell lines infected with *Lm* for 4 h in the presence (+) or absence (-) of an IFNAR1 blocking antibody (Ab). (D, E) Expression of *Ifnb1* and *Nos2* in iBMDMs treated with Pam3CSK4 (D) or Tri-DAP (E) for 4 h. Data are representative of two or more independent experiments with similar results. qRT-PCR data were performed in technical duplicates or triplicates and were normalized to uninfected/unstimulated sh-Control iBMDM cells. In all panels, error bars represent ± SEM.

2.6 Bacterial CDN responses are controlled by RECON and elicit STING-independent host responses

2.6.1 RECON acts as a sink for c-di-AMP and dampens the STING response

Engagement of TLRs by pathogen-associated molecular patterns (PAMPs) leads to MyD88-dependent gene expression. We studied the contribution of this pathway as well as STING activation in primary BMDMs. Infection of WT, *Sting*-deficient, or *Myd88/Tlr3*-deficient primary BMDMs resulted in expression of *Ccl5*, *Cxcl10*, *Cxcl11* and *Ifnb1* that was almost entirely STING-dependent (Figure 2.7A). We assessed the effect of RECON on the direct ability of CDNs to activate the STING-dependent genes in macrophages.

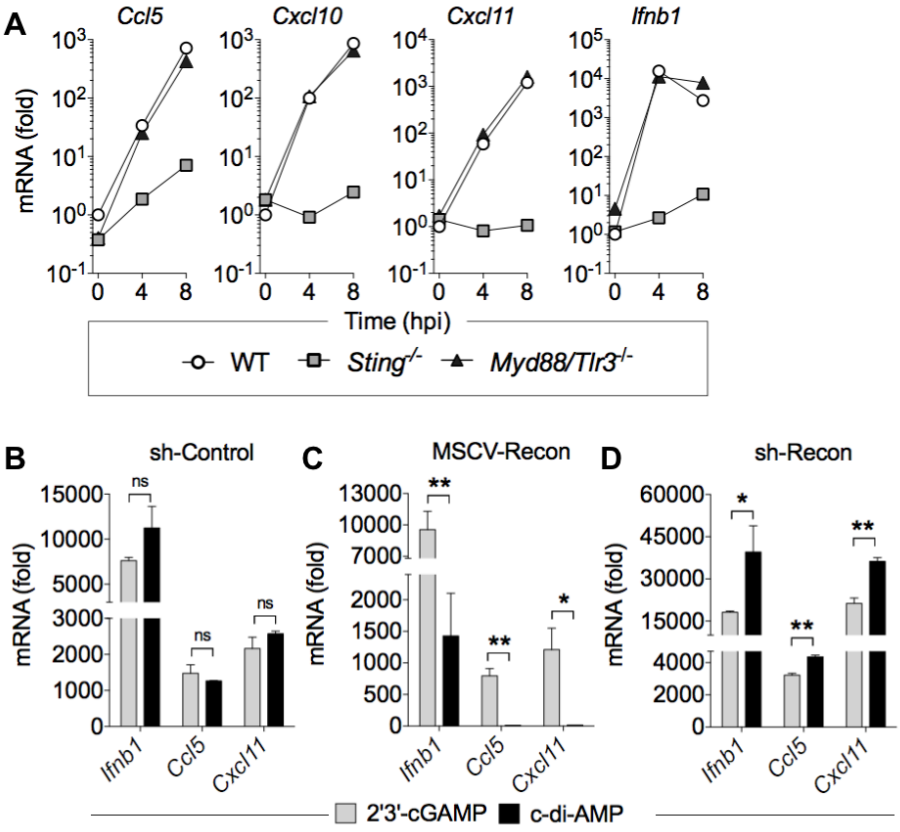

Figure 2.7. Bacterial cyclic dinucleotide responses are controlled by RECON and elicit STING-independent host responses. (A) Expression of *Ccl5*, *Cxcl10*, *Cxcl11*, and *Ifnb1* mRNA in WT, *Sting*-deficient, or *Myd88/Tlr3*-deficient primary BMDMs infected with *L. monocytogenes* for 4 h and 8 h. (B-D) Expression of *Ifnb1*, *Ccl5*, and *Cxcl11* in sh-Control (B), MSCV-*Akr1c13* (C) or sh-*Akr1c13* (D) iBMDMs treated with c-di-AMP or 2′3′-cGAMP for 4 h. Data are representative of two or more independent experiments with similar results. (B-D) Data are the means of five biological replicates pooled. qRT-PCR data were performed in technical duplicates or triplicates and were normalized to uninfected WT BMDMs. In all panels, error bars represent ± SEM.

Our biochemical data demonstrated that RECON only binds to bacterial CDNs, c-di-AMP and 3′3′-cGAMP, and not the host-derived 2′3′-cGAMP (Figure 2.2B). We did not observe a significant difference between the effects of c-di-AMP and 2′3′-cGAMP in sh-Control iBMDMs (Figure 2.7B). However, MSCV-*Akr1c13* iBMDMs treated with c-di-AMP had a significantly impaired ability to induce *Ifnb1*, *Ccl5* and *Cxcl11* compared with 2′3′-cGAMP (Figure 2.7C). The opposite trend was observed in the sh-*Akr1c13* iBMDMs, where c-di-AMP elicited increased gene expression over 2′3′-cGAMP (Figure 2.7D). These data strengthen a model in which RECON acts as a sink for c-di-AMP and dampens the STING response.

2.6.2 C-di-AMP increases nitric oxide production in the presence and absence of STING

In primary BMDMs infected with *L. monocytogenes*, *Nos2* expression kinetics significantly differed from *Ifnb1* and the chemokines. Early *Nos2* induction was MyD88-dependent and STING-independent, whereas late expression was partially restored in the MyD88-deficient cells but was stunted in STING-deficient cells (Figure 2.8A). These data are consistent with the idea that IFN feedback promotes *Nos2* expression during *L. monocytogenes* infection. To study the effect of CDNs on iNOS directly, and in the absence of IFN feedback, we co-stimulated primary BMDMs with Pam3CSK4 or Tri-DAP and c-di-AMP. Although c-di-AMP induced an IFN response during co-stimulation with both Pam_3CSK_4 and Tri-DAP, we only observed increased nitric oxide production during co-stimulation with Tri-DAP (Figure 2.8B). There was no measurable nitrite production in cells treated only with CDNs without TLR or NOD ligand.

We studied this effect further using *Sting*-deficient primary BMDMs. Neither 2′3′-cGAMP nor c-di-AMP induced an IFN response in STING-deficient cells, as expected; however, in the absence of STING, c-di-AMP but not 2′3′-cGAMP increased nitric oxide production during co-stimulation with Tri-DAP (Figure 2.8C and 2.8D). The ability of c-di-AMP but not 2′3′-cGAMP to increase nitric oxide in the absence of STING establishes that c-di-AMP can affect antimicrobial responses through other pathways. The synergy of c-di-AMP with NOD1 but not TLR2 stimulation correlates with the *in vivo* importance of these pathways to host bacterial clearance, whereby NOD1-deficient mice are highly susceptible to *L. monocytogenes* infection while TLR2-deficient mice show equivalent resistance to WT mice (*45*, *46*).

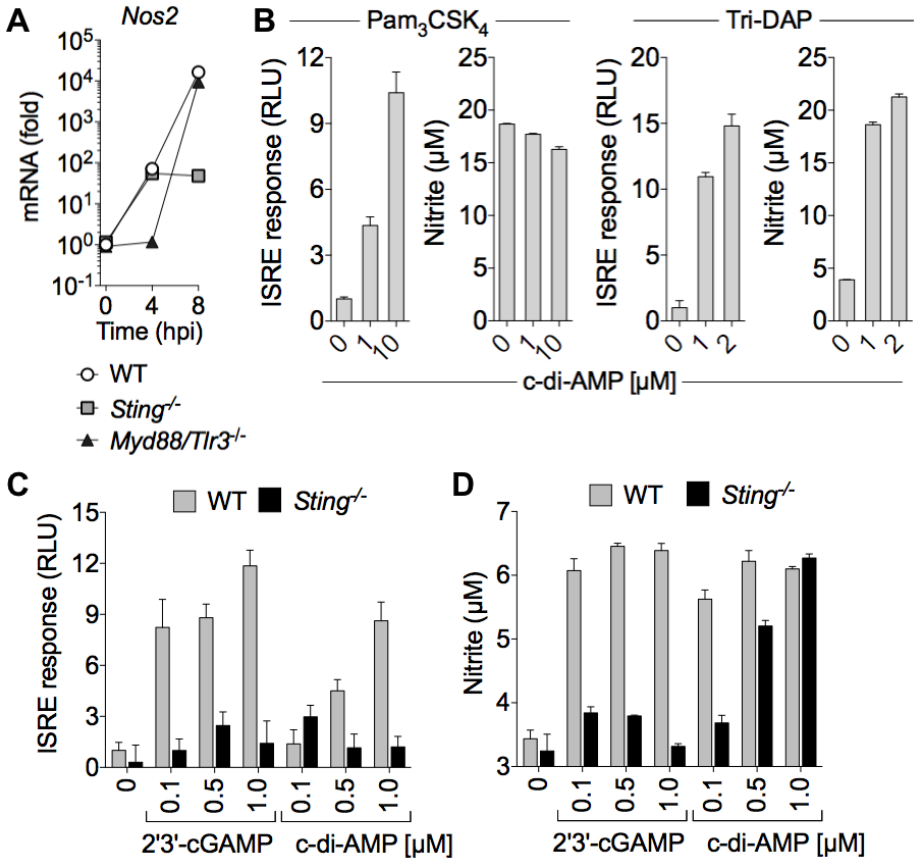

Figure 2.8. C-di-AMP increases nitric oxide production in the presence and absence of STING. (A) Expression of *Nos2* mRNA in WT, *Sting*-deficient, or *Myd88*/*Tlr3*-deficient primary BMDMs infected with *L. monocytogenes* for 4 h and 8 h. (B) Primary BMDMs were co-stimulated with c-di-AMP and Pam3CSK4 or Tri-DAP for 20 h. Supernatants were used to determine the ISRE response and nitrite levels. (C, D) WT or *Sting*-deficient primary BMDMs were co-stimulated with the indicated CDNs and Tri-DAP for 20 h. Supernatants were used to determine the ISRE response (C) and nitrite levels (D). ISRE luciferase data is plotted as the fold change in relative luciferase units (RLU) with TLR or NOD stimulation in the absence of CDNs set at 1 (N=6). Data are representative of two or more independent experiments with similar results. qRT-PCR data were performed in technical triplicates and were normalized to uninfected WT BMDMs. In all panels, error bars represent ± SEM.

2.7 RECON is a negative regulator of NF-κB activation

2.7.1 Generation of RECON-deficient TIB73 hepatocytes

Our investigations in macrophages revealed that RECON augmented *Nos2* expression in a STING- and IFN-independent manner. Induction of *Nos2* is dependent on NF-κB activation, so we further explored the potential link between RECON and NF-κB. We

used the embryonically-derived murine hepatocyte cell line, TIB73, because RECON is highly expressed in hepatocytes, and mice with obstructed NF-κB activation specifically in hepatocytes are unable to clear *L. monocytogenes*, even in the presence of NF-κB-competent immune cells (*47*). Additionally, a recent study has shown that primary human and murine hepatocytes do not express STING (*48*), therefore the use of this cell type would allow us to study NF-κB activation without complications from IFN feedback.

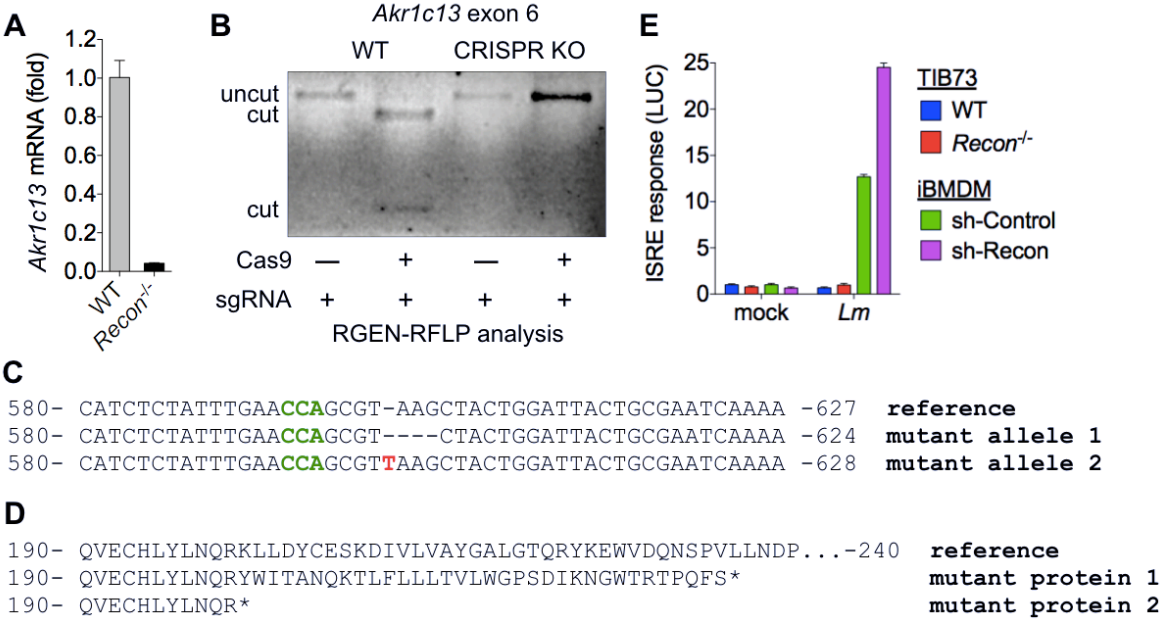

Figure 2.9. Generation of a TIB73 CRISPR/Cas9 *Akr1c13*-deficient clonal cell line. (A) Steady-state expression of *Akr1c13* mRNA in WT and *Akr1c13*-deficient TIB73 cell lines. (B) RGEN-RFLP analysis of exon 6 PCR fragments from WT or *Akr1c13*-deficient TIB73 cells. Data are representative of three independent experiments with similar results. (C) Sequence results from TOPO-cloning of WT (reference) and *Akr1c13* mutant alleles. N = 20 clones sequenced. Green nucleotides indicate the location of the PAM site. (D) Protein sequences as translated from sequences in (C). (E) ISRE response of supernatants from TIB73 or iBMDMs infected with *L. monocytogenes* for 18 h. Luciferase data is plotted as the fold change in relative luciferase units (RLU) compared to untreated (mock) TIB73 WT supernatants (N = 6). Error bars represent ± SD of biological replicates. Data are representative of two independent experiments with similar results.

Using CRISPR/Cas9-based site-directed mutagenesis, we introduced mutations in the *Akr1c13* gene in TIB73 hepatocytes. Although there is no commercially available RECON-specific antibody, the resulting clonal RECON-deficient cell line had significantly reduced levels of *Akr1c13* mRNA (<5% of WT), likely due to nonsense-

mediated decay, and contained two mutated compound heterozygous alleles (one with a 3 base pair insertion, one with a single base pair deletion), both of which encoded premature stop codons (Figures 2.9A-D). We also confirmed the absence of STING signaling in this cell line, as we were unable to detect *Ifnb1* or *Isg15* expression in either WT or *Akr1c13*-deficient TIB73 hepatocytes infected with *L. monocytogenes*. Likewise, supernatants from infected cells elicited no ISRE response compared with supernatants from iBMDMs (Figure 2.9E).

2.7.2 Loss of RECON augments NF-κB activity

Infection of TIB73 hepatocytes with *L. monocytogenes* induced expression of *Il6*, *Nos2*, *Ccl5* and *Cxcl11*, and, similar to the results in macrophages, loss of RECON augmented their expression (Figures 2.10A-C). Similarly, the expression of these genes in *Akr1c13*-deficient hepatocytes was elevated in response to TLR2, TLR4 and NOD1 stimulation. Multiple NF-κB inhibitors (Celastrol, BAY 11-7082 and MG-132) blocked *Nos2* expression during *L. monocytogenes* infection in both WT and *Akr1c13*-deficient cells without affecting bacterial replication (Figures 2.10D-G). Consistent with the gene expression data, the activity of an NF-κB luciferase reporter was increased in the absence of RECON following stimulation with bacterial TLR ligands or *L. monocytogenes* infection (Figure 2.10H). Interestingly, the absence of RECON did not affect *Il6* gene expression or luciferase activation following stimulation with the NF-κB activator TNF-α (Figures 2.10I and 2.10J). Together, these data demonstrate that loss of RECON augments NF-κB activity and that this effect might only occur alongside detection of other bacterial MAMPs.

2.7.3 RECON-deficient TIB73 cells exhibit increased phosphorylation of IKKα and NF-κB p65 following TLR stimulation

We examined the influence of RECON on components of the NF-κB signaling pathway. We observed an increased ratio of nuclear to cytoplasmic p65 NF-κB in *Akr1c13*-deficient hepatocytes compared to WT cells at 1 hpi as assessed by microscopy, and this translocation was blocked by the addition of an NF-κB inhibitor (Figures 2.11A-C).

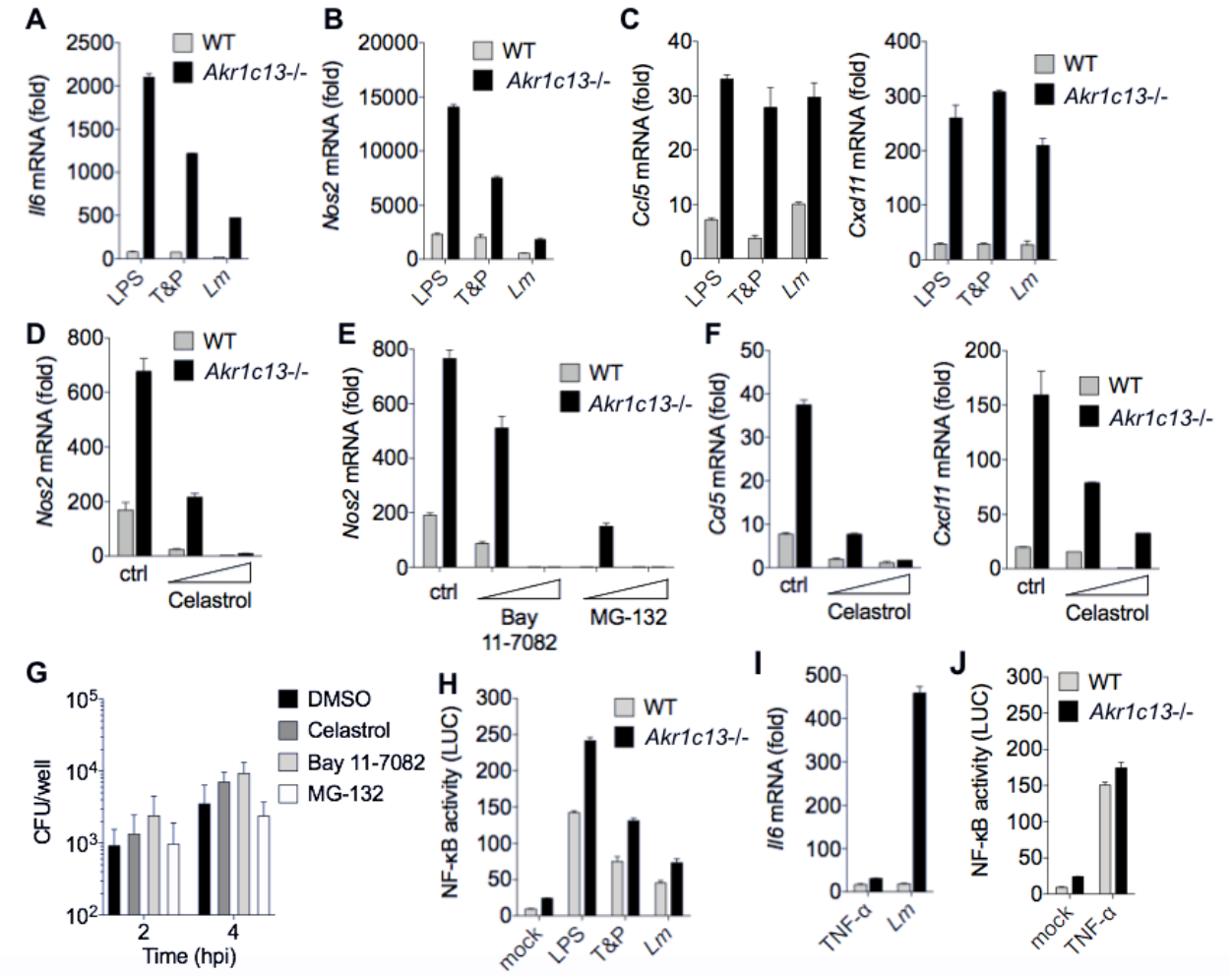

Figure 2.10. RECON is a negative regulator of NF-κB activation. (A-C) Expression of *Il6* (A), *Nos2* (B), or *Ccl5* and *Cxcl11* (C) at 2 h post-treatment with the indicated ligands or *L. monocytogenes* infection of WT or *Akr1c13*-deficient TIB73 hepatocytes. T&P = Tri-DAP + Pam_3CSK_4 co-stimulation. (D, E) Expression of *Nos2* in TIB73 cells pre-treated for 1 h with DMSO (ctrl), with the NF-κB inhibitor celastrol (0.1 and 1 μM) (E), or with the NF-κB inhibitors BAY 11-7082 (1 and 10 μM) or MG-132 (2 and 20 μM) (E). (F) Expression of *Ccl5* or *Cxcl11* in TIB73 cells pre-treated for 1 h with DMSO (ctrl) or the NF-κB inhibitor celastrol (0.1 and 1 μM). (G) WT TIB73 cells infected with *L. monocytogenes* in the presence of the indicated inhibitors or DMSO. CFU were enumerated at 2 and 4 hpi (N=4). Data are pooled from two independent experiments. Error bars represent ± SD of biological replicates. (H) NF-κB luciferase activity measured from WT or *Akr1c13*-deficient TIB73 hepatocytes treated with the indicated ligands for 6 h. The data are presented as luciferase units divided by the eGFP transfection control fluorescence (LUC) (N=6). (I) Expression of *Il6* in WT or *Akr1c13*-deficient TIB73 hepatocytes treated with TNF-α for 2 h. (J) NF-κB luciferase activity measured from WT or *Akr1c13*-deficient TIB73 hepatocytes treated with TNF-α for 6 h (N=6). Error bars represent ± SD of biological replicates. Data are representative of two or more independent experiments with similar results. qRT-PCR data were performed in technical duplicates or triplicates and were normalized to untreated (mock) WT TIB73 cells. Unless otherwise notes, error bars represent ± SEM of technical replicates.

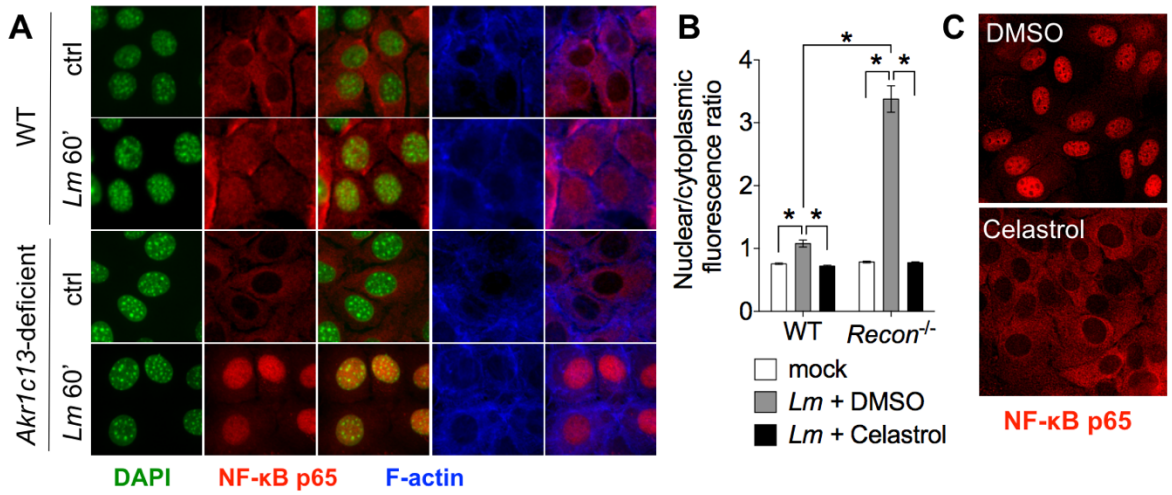

Figure 2.11. RECON is a negative regulator of NF-κB p65 nuclear translocation. (A) Microscopy analysis of WT (top) or *Akr1c13*-deficient (bottom) TIB73 hepatocytes infected with *L. monocytogenes* for 1 h. DAPI (green), NF-κB p65 (red), and F-actin (blue). (B) Quantification of the nuclear/cytoplasmic ratio of NF-κB p65 fluorescence of data presented in (A). N=100-120 cells for each treatment. Error bars represent ± SD of biological replicates (*P < 0.0001, unpaired Student's t test). (C) Microscopy analysis of TIB73 cells pre-treated with celastrol for 1 h and then infected with *L. monocytogenes* for 1 h. Images are of *Akr1c13*-deficient TIB73 cells. Data are representative of three independent experiments with similar results.

We observed increased phosphorylation of p65 by Western blot in *Akr1c13*-deficient cells co-stimulated with Tri-DAP + Pam3CSK4 (Figure 2.12), which was consistent with the increased nuclear localization we observed by microscopy (Figure 2.11). Additionally, the peak of p65 phosphorylation occurred earlier in the absence of RECON (20 versus 40 min). Blots for the inhibitory protein IκBα revealed that after transient degradation (between 20-40 min), its abundance increased over basal levels in WT cells (60-120 min), while they did not rise above the basal state in *Akr1c13*-deficient cells, indicating that the loss of RECON promoted sustained activation of the pathway. We also observed increased phosphorylation of IKKα occurring at 20-40 min in the *Akr1c13*-deficient cells. Thus, the augmentation of NF-κB signaling in the absence of RECON appears to occur at two points – at the level of phospho-IKKα, which would result in increased initiation of the signaling cascade, and phospho-p65, which would result in increased p65 nuclear translocation and DNA binding activity.

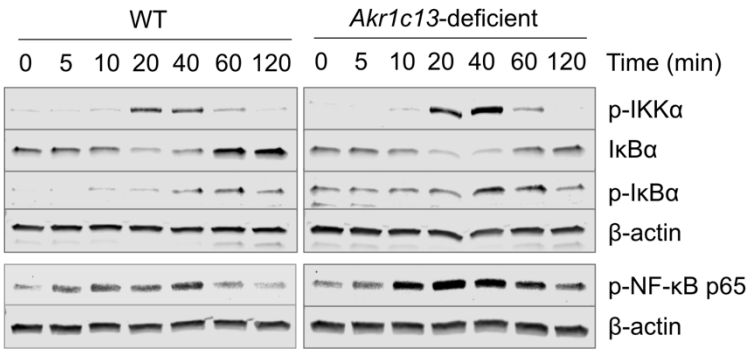

Figure 2.12. RECON-deficient cells exhibit enhanced phosphorylation of the NF-κB pathway. Western blot of proteins in the NF-κB pathway; WT or *Akr1c13*-deficient TIB73 hepatocytes were co-stimulated with Tri-DAP + Pam3CSK4 for the indicated times (5-120 min). β-actin is shown as a loading control. Data are representative of two independent experiments with similar results.

2.8 Loss of RECON's enzymatic activity promotes inflammation

2.8.1 Generation of catalytically dead RECON

To segregate the role of RECON's enzyme activity from its effects as a nucleotide sink, we mutated the invariant H117 residue that functions as a general acid/base in a proton relay network during oxidative/reductive catalysis by AKRs (*49*). The H117 residue is

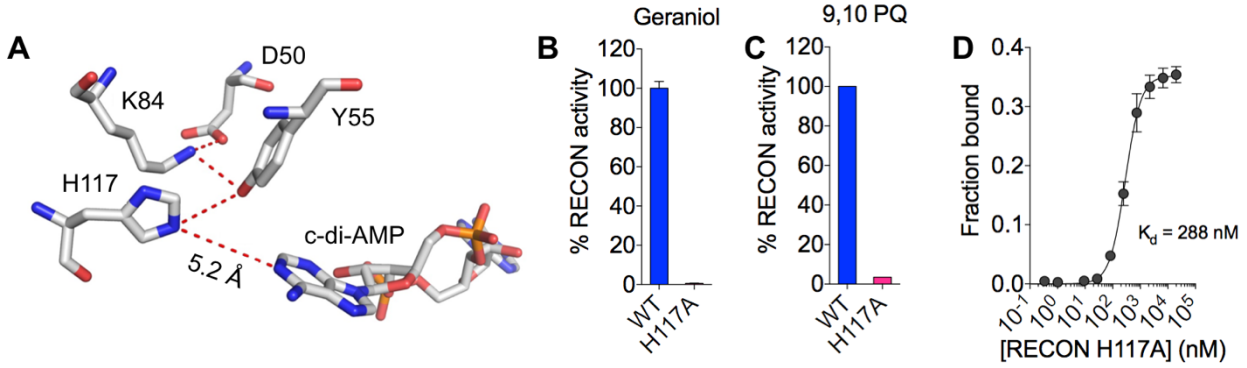

Figure 2.13. Generation of catalytically dead RECON with H117A mutation. (A) The conserved residues of the catalytic tetrad of RECON are shown with the measured proximity between H117 and bound c-di-AMP. (B, C) Percent enzyme activity of WT or the H117A mutant RECON. Substrates used were geraniol with the cosubstrate NAD+ (B) or 9,10-Phenanthrenequinone (PQ) with the cosubstrate NADPH (C). (D) Binding titration of c-di-AMP with the H117A mutant RECON using ^{32}P-c-di-AMP. Kd value is indicated. Data are from one of two independent experiments with similar results. Error bars represent ± SEM.

more than 5 Å away from c-di-AMP, and thus it is unlikely that it would play an important role in c-di-AMP binding (Figure 2.13A). Accordingly, mutation of H117 to alanine (H117A mutant) abolished RECON's enzymatic activity while maintaining high affinity c-di-AMP binding (Figures 2.13B-D).

2.8.2 Loss of RECON catalytic activity drives augmented NF-κB activity

We stably expressed H117A or WT RECON in *Akr1c13*-deficient hepatocytes and determined that their *in vivo* c-di-AMP binding capacity was equivalent using a whole cell lysate DRaCALA assay (Figure 2.14A and 2.14B). Complementation of the *Akr1c13*-deficient cells with WT RECON reversed the augmentation of NF-κB-driven luciferase

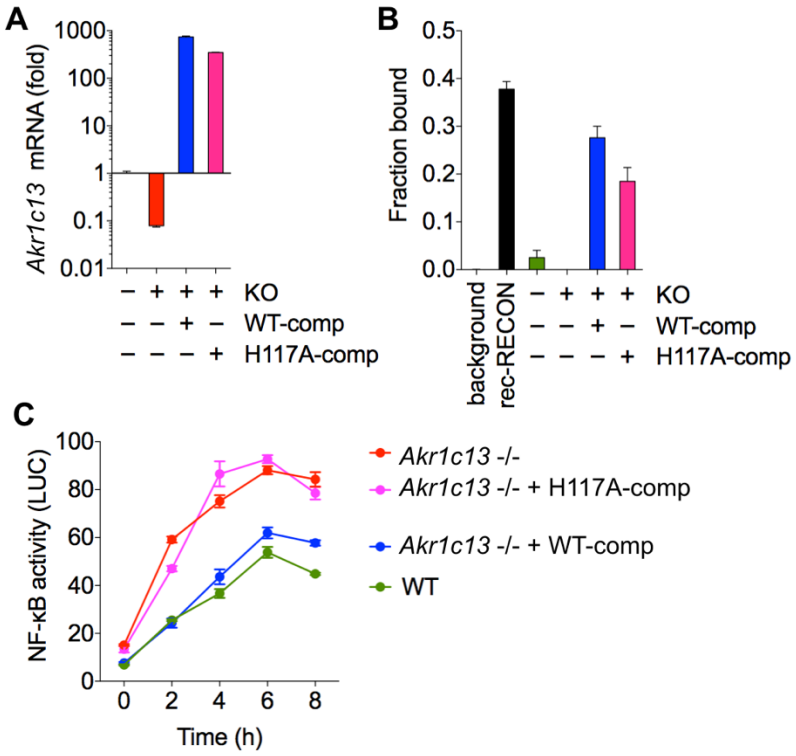

Figure 2.14. Loss of RECON enzymatic activity promotes NF-κB activation. (A) Steady-state expression of *Akr1c13* mRNA in WT, *Akr1c13*-deficient, or *Akr1c13*-deficient complemented with WT (WT-comp) or H117A (H117A-comp) RECON. (B) Binding of ^{32}P-c-di-AMP to whole cell lysates from the indicated TIB73 cell lines or to recombinant (rec) RECON as a control. (C) NF-κB luciferase activity measured from WT or *Akr1c13*-deficient TIB73 hepatocytes co-stimulated with Tri-DAP + Pam3CSK4 for the indicated times. The data are presented as luciferase units divided by the eGFP transfection control fluorescence (LUC) (N=6). Error bars represent ± SD of biological replicates. Data are from one of two (A-B) or three (C) independent experiments with similar results. Unless otherwise noted, error bars represent ± SEM.

activity following co-stimulation with Tri-DAP and Pam3CSK4 while complementation with the H117A mutant did not (Figure 2.14C). From these results, we can conclude that it is the loss of RECON enzyme activity that is driving increased NF-κB activation. These data support our hypothesis that the accumulation of a RECON substrate or substrates may be responsible for augmenting the activation of the NF-κB pathway.

2.9 RECON alters bacterial virulence in phagocytic and non-phagocytic cells

2.9.1 RECON restricts *L. monocytogenes* growth in IFN-γ-activated macrophages

We tested whether modulation of RECON levels would influence bacterial virulence. We did not observe any difference in *L. monocytogenes* bacterial growth in naïve iBMDMs expressing different levels of RECON (Figure 2.15A). This was not entirely unexpected considering that neither loss of STING nor MyD88 affects *L. monocytogenes* virulence in macrophages (Figure 2.15B), even though MyD88-deficient mice are highly susceptible to *L. monocytogenes* infection (*45*). However, we observed a significant increase in *L. monocytogenes* intracellular replication in MSCV-*Akr1c13* iBMDMs activated with IFN-γ

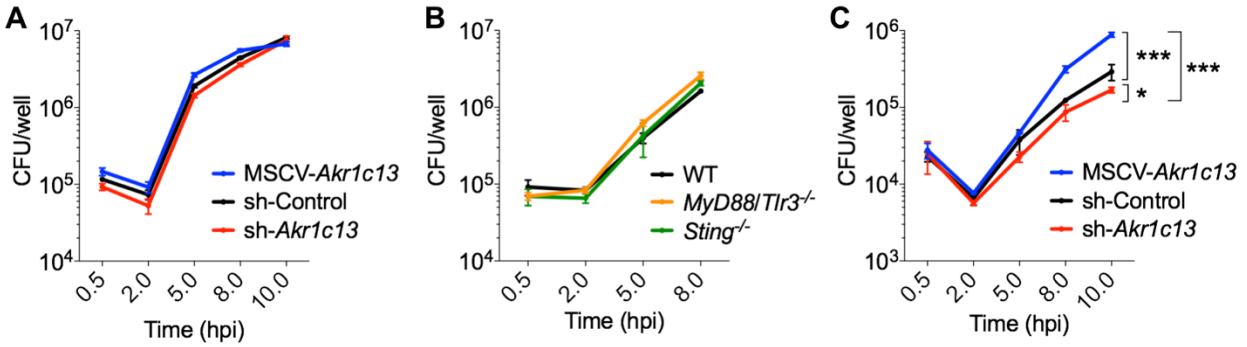

Figure 2.15. RECON-mediated inflammation alters *L. monocytogenes* growth in macrophages. (A) iBMDM cell lines (not activated with IFN-γ) with altered RECON expression were infected with *L. monocytogenes* and CFU were enumerated at the indicated times (N=3). (B) Primary WT, *Sting*-deficient, *Myd88*/*Tlr3*-deficient BMDMs were infected with *L. monocytogenes* and CFU were enumerated at the indicated times (n = 4). (C) iBMDM cell lines with altered *Akr1c13* expression were pre-treated with IFN-γ for 20 h and then infected with *Lm*. CFU were enumerated at the indicated times (0.5 h to 10 h) (N=4). Data are representative of two or more independent experiments with similar results. *$P < 0.05$, ***$P < 0.0005$, unpaired Student's *t* test of 10 hpi.

(Figure 2.15C). These data suggest that suppression of RECON drives a cell-intrinsic antibacterial state in activated iBMDMs. It has previously been reported that IFN-γ-mediated inhibition of *L. monocytogenes* growth in BMDMs is dependent on NOD1 (*46*), and earlier results showed a NOD1-specific synergy of c-di-AMP on nitric oxide production (Figure 2.8B).

2.9.2 RECON restricts *Chlamydia* spp. growth in TIB73 hepatocytes

We performed similar experiments as shown in Figure 2.15 in WT or *Akr1c13*-deficient TIB73 hepatocytes but did not observe any difference in *L. monocytogenes* intracellular growth (Figure 2.16A). In the host, *L. monocytogenes* can multiply to high numbers in the liver; therefore, we reasoned that perhaps *L. monocytogenes* has evolved mechanisms to counteract the effects of RECON suppression in this non-immune cell type. For example, *L. monocytogenes* is resistant to the antimicrobial effects of nitric oxide (*50*, *51*), which is elevated downstream of RECON inhibition. To determine if hepatocyte cell-intrinsic, antibacterial responses are influenced by RECON, we infected TIB73 hepatocytes with

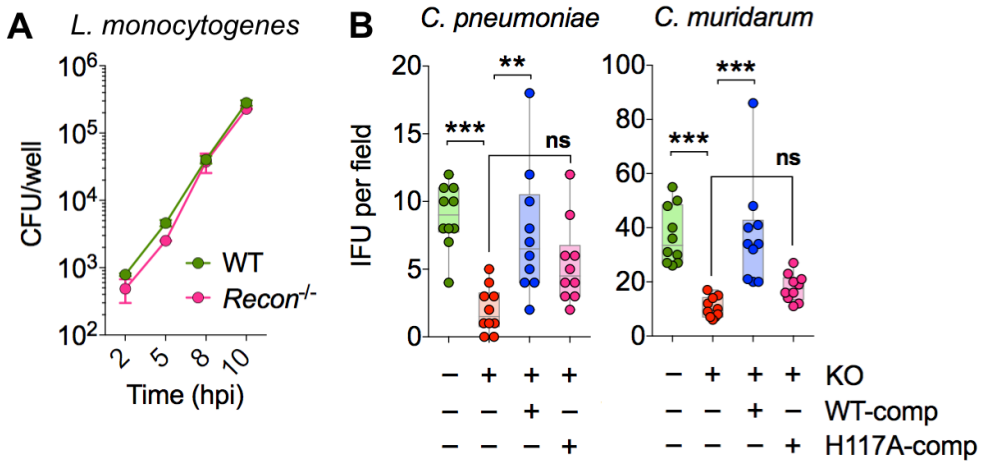

Figure 2.16. RECON-mediated inflammation alters *Chlamydia* spp. growth in TIB73 hepatocytes. (A) WT or *Akr1c13*-deficient TIB73 cells lines were infected with *L. monocytogenes* and CFU were enumerated at the indicated times (N=3). Error bars represent ± SD of biological replicates. (B) WT, *Akr1c13*-deficient (KO), or *Akr1c13*-deficient complemented with WT (WT-comp) or H117A (H117A-comp) RECON TIB73 hepatocytes were infected with *C. pneumoniae* or *C. muridarum* and inclusion forming units (IFU) were quantified after 24 h (10-20 fields were analyzed across two biological replicates per experiment). All points are shown with min to max indicated. Data are representative of two or more independent experiments with similar results. *P < 0.05, ** P < 0.001, ***P <0.0001, ordinary one-way ANOVA.

Chlamydia spp., another genus of c-di-AMP-producing, intracellular pathogens (*17, 22*). Both *C. pneumoniae* and *C. muridarum* can infect hepatocytes but do not naturally invade these cells. Infection of *Akr1c13*-deficient hepatocytes significantly reduced the growth and infectivity of both *Chlamydia* spp. (Figures 2.16B). This effect was complemented by re-introduction of WT but not H117A RECON in the *Akr1c13*-deficient cells. These data demonstrate that RECON's enzyme activity influences intracellular bacterial growth and highlights the importance of this CDN sensor in cell-intrinsic host responses.

2.10 Human AKR1C1 may bind c-di-AMP

2.10.1 Quantitative mass spectrometry proteomics identifies human AKR1C1 as a potential c-di-AMP binding protein

Analogous to what has been reported in other PRR families, mice encode an expanded number of AKR family members, specifically those in the AKR1C subfamily to which RECON belongs. Within this subfamily, mice encode eight AKRs, while humans encode four (http://www.med.upenn.edu/akr). There has been significant interest in the members of the AKR1C subfamily because they are implicated in the progression of several human cancers, including prostate and breast cancer (*52*). To determine whether any human AKR proteins bind c-di-AMP, we performed pulldowns using c-di-AMP

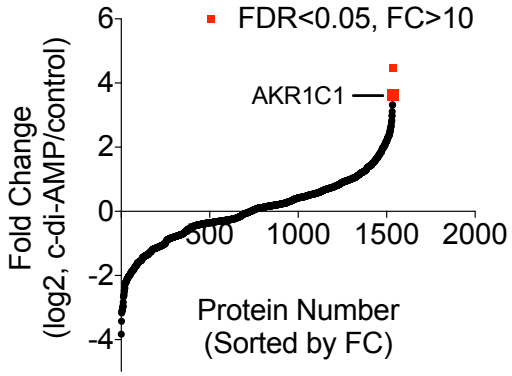

Figure 2.17. Pulldowns from HepG2 hepatocytes indicate AKR1C1 may be a human c-di-AMP binding protein. Quantitative shotgun proteomics of c-di-AMP-binding proteins. Data are sorted based upon fold change (FC) in spectral count ratio (c-di-AMP sepharose/control sepharose). Data points in red represent proteins with FC > 10 and a false discovery rate (FDR) < 0.05.

sepharose and lysates from the human hepatoma cell line HepG2. The AKR family member AKR1C1 was reproducibly and statistically significantly enriched in c-di-AMP pulldowns over the control (Figure 2.17).

2.10.2 The reference sequence AKR1C1 protein likely does not interact with c-di-AMP

AKR1C1, also known as 20-alpha-hydroxysteroid dehydrogenase, is in the same subfamily as RECON and catalyzes the reaction of progesterone to the inactive form 20-alpha-hydroxyprogesterone. It has previously been shown to be important during pregnancy and in the development of some human cancers (*53*). It has ~70% identify with RECON and, similar to RECON, it is highly expressed in the liver, stomach and small intestine. However, we were not able to confirm the pulldown results with recombinant AKR1C1 and further examination of the protein revealed that it did not exhibit any enzyme activity (Figure 2.18A-C). Previous work with other human AKRs showed recombinant proteins expressed in *E. coli* had up to 20-fold lower activity compared to native enzymes purified from human livers (*54*). Furthermore, some AKR family members require post-translational modifications for their cellular activities (*55*), so it possible that AKR1C1 expressed in *E. coli* lacked the necessary modifications for c-di-AMP binding.

We also stably overexpressed *AKR1C1* in iBMDMs and observed a slight increase in c-di-AMP binding over sh-Control iBMDMs, however we observed no effect of *AKR1C1* overexpression on *Ifnb1* expression in response to c-di-AMP (Figure 2.18D-F). It is possible that the level of AKR1C1 overexpression achieved in the iBMDMs was not enough to affect c-di-AMP intracellular pools or the use of the reference *AKR1C1* sequence (NCBI NM_001353.5) may not resolve the potential role for isoforms or different *AKR1C1* alleles that may be important for c-di-AMP binding. *AKR1C1* is a complex locus with six transcript isoforms, evidence of exon skipping, over 300 single nucleotide polymorphisms, and varying 5′ and 3′ UTR lengths (GTExPortal). Further work will be necessary to determine if AKR1C1 does interact with bacterial CDNs and whether their interaction shapes the immune response in an orthologous way to RECON. Additionally, given that many AKR members are inducibly expressed and are found in cell types other

than hepatocytes, it remains to be seen whether more mouse and human AKR family members are capable of interacting with bacterial CDNs.

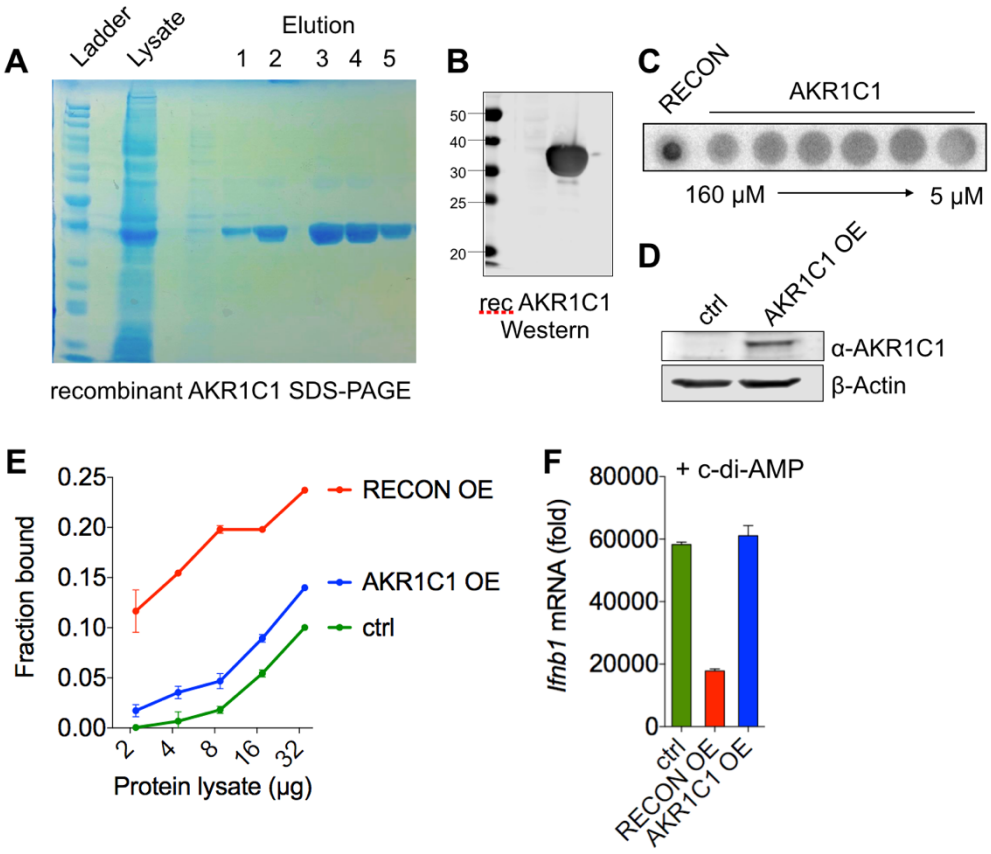

Figure 2.18. *In vitro* experiments do not reveal an interaction between the AKR1C1 reference sequence protein and c-di-AMP. (A) SDS-PAGE stained with coomassie showing purification of recombinant human AKR1C1 from *E. coli* lysates. (B) Western blot on purified, recombinant human AKR1C1 protein. (C) ^{32}P-c-di-AMP radioligand binding assay with AKR1C1 and RECON (as a control). (D) Western blot of iBMDMs overexpressing (OE) AKR1C1. Actin is shown as a loading control. (E) Binding of ^{32}P-c-di-AMP to whole cell lysates from iBMDMs overexpressing RECON or AKR1C1. (F) Expression of *Ifnb1* mRNA in the indicted iBMDMs treated with c-di-AMP (20 μM) for 4 h. qRT-PCR data were performed in technical triplicates and are normalized to untreated iBMDM sh-Control cells. All data are representative of two or more independent experiments with similar results. Error bars represent ± SEM of technical replicates.

2.11 Model: RECON orchestrates cytosolic immune surveillance by targeting bacterial cyclic dinucleotides

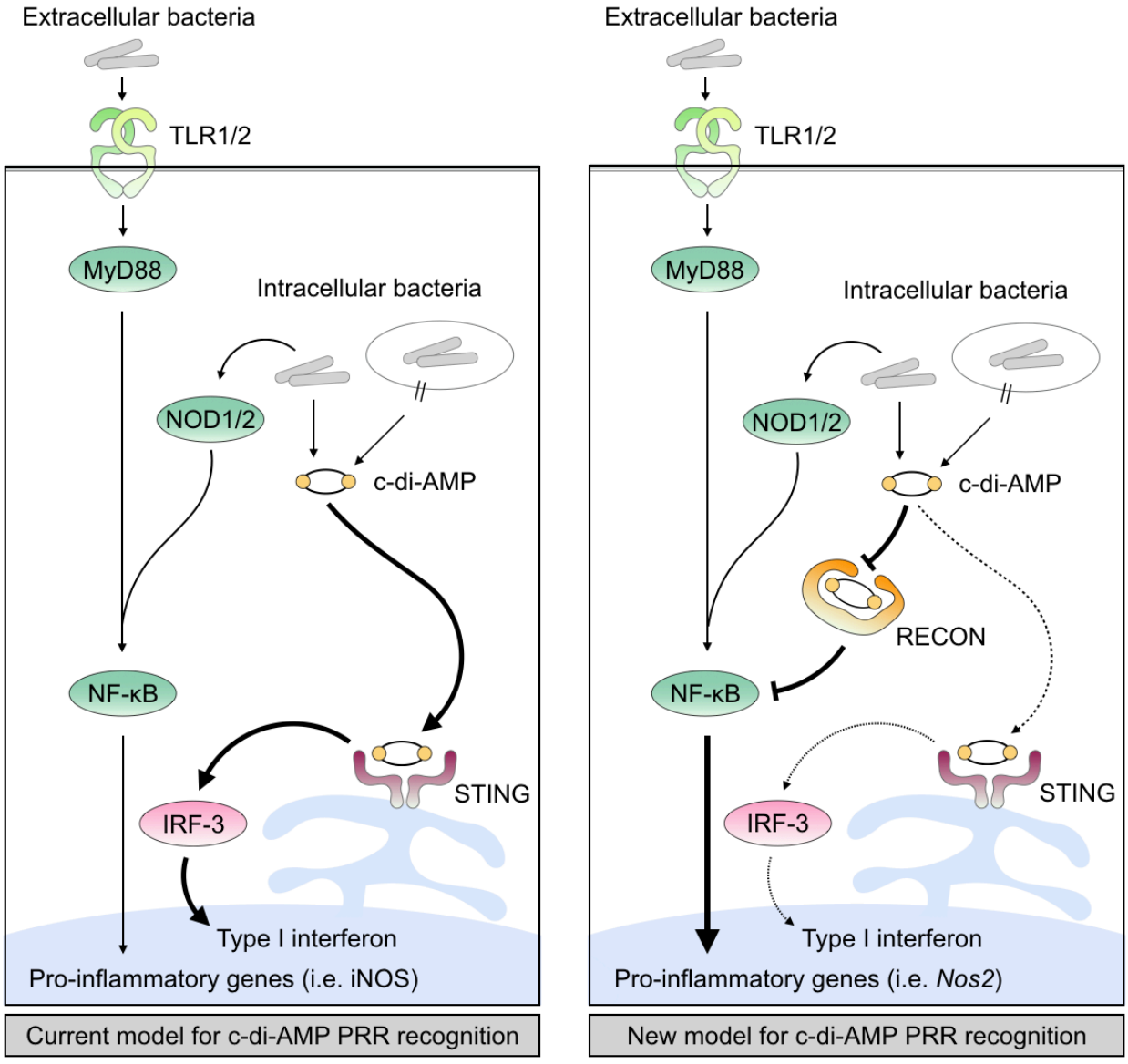

Figure 2.19. RECON orchestrates cytosolic immune surveillance by targeting bacterial cyclic dinucleotides. Our new understanding of the role of RECON in host responses suggests RECON sequesters c-di-AMP away from STING and boosts NF-κB activation by relieving an unknown inhibitory mechanism.

2.12 Discussion

Microbial nucleic acid recognition by host cell cytosolic PRRs is an important facet of innate immune responses. In the work presented in this chapter, we characterized an

oxidoreductase PRR that specifically detects canonical bacterial CDNs. Complementation studies presented here support a model whereby CDN binding modulates RECON enzymatic activity to shape downstream inflammation. These observations suggest the presence of an inflammatory mediator that is actively metabolized by RECON. The identity of the substrate or mechanism by which this mediator acts to modulate NF-κB is the subject of investigation detailed in Chapter 3. AKR family proteins have been shown to metabolize nearly all biological lipophilic metabolites, including sterols, isoprenoids, retinoids, and eicosanoids, while many AKRs, RECON included, show promiscuous activity toward a variety of substrates. Thus, the integration of sensor function with enzyme activity may provide plasticity in the host response that is dependent upon the RECON substrates available within the cell or tissue type during infection. Studies to reveal the identity and individual effects of RECON substrates on specific cellular processes will likely expand the repertoire of immunomodulatory effects of this unique enzymatic PRR.

STING has higher affinity for the non-canonical mammalian-derived 2′3′-cGAMP than for bacterial CDNs (*56*). Interestingly, some human *STING* alleles have lost the ability to bind bacterial CDNs (*8, 57*), suggesting that this pathway may not be geared towards recognizing bacterial pathogens but rather towards DNA sensing of viruses. It is clear that STING-dependent induction of type I IFN elicits a robust antiviral response. However, the role of type I IFN in bacterial infection is variable and in some cases detrimental to host clearance of c-di-AMP-producing pathogens such as *L. monocytogenes, M. tuberculosis,* and *C. muridarum*, (reviewed in (*58*)). We found that the binding of c-di-AMP by RECON dampens type I IFN induction during bacterial infection. Therefore, the inability of mammalian-derived 2′3′-cGAMP to bind RECON may maintain the cellular response geared towards type I IFN production during viral infection.

One immediate and important implication of this work is the interpretation of data relating to immune activation by c-di-AMP or bacteria that produce c-di-AMP in mouse models. Recent studies on *M. tuberculosis* have found that STING activation during infection of mouse BMDMs occurs mainly via 2′3′-cGAMP derived from cGAS, with minimal activation contributed by c-di-AMP (*19, 59*). This finding has raised questions as to whether c-di-AMP produced by *M. tuberculosis* has any role to play in infection. Given that these studies were performed in BMDMs, which express RECON, and that RECON binds c-di-AMP significantly tighter than STING, it is feasible that c-di-AMP is mediating

responses independent of STING during infection with this pathogen, as we have found occurs for *L. monocytogenes*. Future work to assess the effects of RECON targeting c-di-AMP during infection with *M. tuberculosis*, as well as the relative contribution of c-di-AMP or cGAS-derived 2′3′-cGAMP in activating STING in the absence of RECON will help to shed some light on this active area of investigation.

Another important consideration relates to the translational capacity of *Listeria* and CDN immunomodulatory studies performed in mice. The intracellular niche and immunostimulatory activity of *L. monocytogenes* have prompted the development of live, attenuated *L. monocytogenes* vaccine vectors that retain the ability to enter the cytoplasm (*60*). Similarly, the use of CDNs as adjuvants or in immunotherapeutic formulations has shown significant promise in the therapeutic protection against infectious and malignant disease (*61*). Vaccine and immunotherapeutic formulations that contain c-di-AMP and/or 3′3′-cGAMP may elicit RECON-mediated responses that may shape the outcome and interpretation of these pre-clinical studies.

In this chapter, we explored the effect of the oxidoreductase RECON during bacterial infection of macrophages and hepatocytes. RECON protein was abundantly isolated from mouse liver using c-di-AMP sepharose and the liver (specifically hepatocytes) is a principal site for *L. monocytogenes* replication following systemic dissemination (*62*). Previous work characterizing tissue-specific expression of RECON has shown that it is most highly expressed in the gastrointestinal tract and is almost exclusively restricted to this site and the liver (*63*). Data from FANTOM5, a comprehensive RNA expression analysis database, indicates that GP2+ M cells and enterocytes have the highest steady-state expression of *Akr1c13* (EntrezGene: 27384). Stellate cells, hepatocytes and bone marrow-derived macrophages were also among the top seven highest *Akr1c13*-expressing cells. Given the high expression of *Akr1c13* in the gastrointestinal tract, there are several possible effects it may have in these organs. Both *L. monocytogenes* and *Vibrio cholerae* produce RECON-targeted CDNs, while Firmicutes and Bacteroidetes, the two major bacterial phyla in the gastrointestinal tract (>95% in humans), all produce c-di-AMP (*64*, *65*). Considering this, RECON-mediated surveillance of bacterial CDNs may have widespread implications for the host immune response to bacteria, both pathogens and commensals alike.

2.13 Materials and Methods

Synthesis of c-di-AMP sepharose

C-di-AMP was enzymatically synthesized as previously described (*16, 66*). Approximately 100 mg of purified c-di-AMP nucleotide was dissolved in PBS to 200 μM. The pH of the solution was adjusted to 7.5 with NaOH and was added directly to washed epoxy-activated sepharose (2 mL) and incubated at 56°C for 2 days. The sepharose was washed and the absorbance spectrum of 50% slurry was measured to ensure nucleotide coupling. HPLC analysis of the remaining uncoupled nucleotide ensured no degradation of c-di-AMP occurred during the 2-day incubation. Remaining epoxy groups were blocked with ethanolamine following the instructions provided by GE. In parallel with this blocking step, fresh epoxy-activated sepharose was also treated with ethanolamine to generate control resin.

C-di-AMP pulldowns

Soluble lysates from mouse lung, liver and spleen or from the human hepatoma cell line HepG2 (~$1x10^9$ cells) were prepared in 30 mL of buffer (0.1 M Tris-HCl [pH 7.5], 150 mM NaCl, 0.1% v/v Tween-20, 1 mM PMSF). Lysates were incubated with rotation for 3 h at 4°C with 100 mL ethanoamine or c-di-AMP-conjugated beads as previously described (*16*). Beads were washed three times with 5 mL PBS. Samples from mouse organ homogenates were mixed with 100 μL of SDS-PAGE sample loading buffer, incubated at 56°C for 10 min, and the soluble fraction removed and analyzed by SDS-PAGE. The large band observed in the c-di-AMP pulldown from liver (Figure 2.1B) was excised and an in-gel digestion with trypsin was performed using standard protocols (http://msf.ucsf.edu/protocols.html) (*67, 68*). Mass spec sequencing was conducted by the QB3/chemistry mass spec facility at UC Berkeley. For samples from HepG2 cells, bound proteins were digested on bead with 100 ng of sequencing grade trypsin for 6 hours at 37˚C. The released peptides were processed and analyzed as previously described (*16*).

Recombinant protein expression

pSpeedET plasmid encoding *Akr1c13* (MmCD00326044; DNASU Plasmid Repository) was used for protein expression and purification in *E. coli*. The expression construct for the C-terminus of murine *Sting* was kindly provided by Russell Vance (*3*). *AKR1C1*

coding sequence was amplified from the pJP1520-AKR1C1 plasmid (DNASU repository HsCD00075735) using the following primers: FWD 5′ gaggagCATATGGATTCGAAATATCAGTGTGTG 3′ and REV 5′ gaggagCTCGA GATATTCATCAGAAAATGGATAATTAGGGG 3′. The *AKR1C1* PCR product was subcloned into a pET-20b expression vector digested with NdeI and XhoI. The plasmids for *Akr1c13*, *Sting*, and *AKR1C1* expression were transformed into Rosetta (DE3)pLysS chemically competent cells. Overnight cultures of the resulting transformed bacteria were used to inoculate 1 L of LB broth at a 1:100 dilution. Cultures were grown to OD600 0.5 and IPTG (0.5 mM) was added to induce protein expression. Cells were lysed in PBS containing PMSF (1 mM) and soluble protein was purified using Ni-NTA agarose (QIAGEN) chromatography. The resulting proteins were >95% pure as determined by SDS-PAGE with Coomassie staining.

Mutagenesis of RECON

The H117A RECON mutant was made using the QuikChange kit (Stratagene) with the following primers: Fwd 5′-GCTGGATTATGTTGATCTTTACATTATGGCATACCCAG TGCCAATGAAGTC-3′ and Rev 5′-GACTTCATTGGCACTGGGTATGCCATAATGTAA AGA TCAACATAATCCAGC-3′. It was expressed and purified using the same protocol as the WT RECON protein.

Protein crystallization

Protein solution (20 mg/mL) with 2 mM c-di-AMP was used to set up crystallization with the sitting-drop method at 20°C. Crystals were grown by mixing 1 μl protein solution with 1 μl well solution (0.2 M NaCl, 0.1 M Bis-Tris (pH 5.5), 25% (w/v) polyethylene glycol 3,350). Crystals appeared after 2 days and were transferred to the cryoprotectant containing well solution supplemented with 20% (v/v) glycerol before being flash-frozen in liquid nitrogen. The crystals belong to space group P212121 and there is one complex in the asymmetric unit.

Protein expression and purification for crystal structures

The full-length mouse *Akr1c13* gene was cloned into a pSpeedET vector with a 6-His tag and a TEV protease cleavage site at the N terminus. Crystals of wild-type RECON diffracted X-rays poorly, and several collections of lysine residues were mutated to Ala, by site-directed mutagenesis method (Agilent), to improve diffraction quality (*69*). Two

Lys residues (68 and 70) were mutated to Ala in order to produce high quality crystals. These two residues are located far from the c-di-AMP binding site, and the mutations did not perturb the structure or the interactions with c-di-AMP. The mutant was over-expressed in Escherichia coli BL21 Star (DE3) strain (Novagen). The cells were induced with 0.4 mM isopropyl β-D-1-thiogalactopyranoside for 18 h at 20°C. The harvested cells were resuspended in lysis buffer containing 50 mM phosphate (pH 7.6), 500 mM NaCl, 20 mM imidazole and lysed by sonication. Cell lysates were centrifuged for 30 min at 4°C, and the supernatant was incubated with nickel beads (Qiagen). After 2 h, beads were transferred to a gravity flow column (Bio-Rad) and washed extensively with lysis buffer. Protein was eluted with a buffer containing 50 mM phosphate (pH 7.6), 500 mM NaCl, and 500 mM imidazole. Protein eluate was further purified by gel filtration using Sephacryl S-300 column (GE Healthcare) equilibrated in a buffer containing 5 mM HEPES (pH 7.6) and 150 mM NaCl. The protein sample were concentrated to 50 mg/mL and stored at -80°C.

Data collection, structure determination and refinement

A data set at 1.5 Å resolution was collected at the X29 beamline of the National Synchrotron Light Source (NSLS). The diffraction images were processed with the HKL package (*70*). The structure was solved by the molecular replacement method using the AKR1C3 structure (PDB entry 3LN3) as the model. The structure was refined with PHENIX (*71*) and manual adjustment to the model was carried out with Coot (*72*). The crystallographic information is summarized in Table S1.

Nucleotide binding (DRaCALA) and enzyme assays

Differential radial capillary action of ligand assays (DRaCALA) were performed with recombinant proteins in binding buffer (40 mM Tris,100 mM NaCl, 20 mM MgCl2 [pH 7.5]) and analyzed as described previously (*73*). DRaCALA was performed on 50 μg of TIB73 whole cell lysates (or the indicated concentrations of iBMDM lysates) that were sonicated (40% amp, 1 sec on/off intervals for 5 sec) in binding buffer. For competition assays, 200 μM of unlabeled nucleotides (see Figure 2.2A) or cyclic dinucleotides (c-di-AMP, c-di-GMP, 2′3′-cGAMP, or 3′3′-cGAMP [purchased from BioLog]) were added prior to the addition of ^{32}P-c-di-AMP. To measure RECON enzyme activity, geraniol (10 μM) (Sigma) or 9,10-Phenanthrenequinone (25 μM) (Sigma) were supplied as substrates

with NAD+ (500 μM) or NADPH (200 μM) as cosubstrates, respectively. Substrates and cosubstrates were mixed in 1X PBS to a final reaction volume of 200 μl and initiated by addition of RECON (5 μM). CDNs were also added where indicated (see Figure 2.2E). Absorbance (340 nm) was measured on a SpectraMax M3 microplate reader, and data was collected with SoftMax Pro software. The slopes of the first 100 s of the reaction were used to calculate enzyme activity.

Cyclic dinucleotide or MAMP stimulations of macrophages

2′3′-cGAMP or c-di-AMP (BioLog) were added externally (10 μM and 20 μM, respectively) to iBMDMs or transfected into primary BMDMs with Lipofectamine 2000 (Thermo Fisher). Where indicated, cells were treated with 500 ng/mL Pam3CSK4 (InvivoGen), 1 μg/mL Tri-DAP (InvivoGen), 100 ng/mL LPS (Sigma), 100 ng/mL TNF-α (generously provided by Jessica Hamerman) or a combination of ligands (100 ng/mL Pam_3CSK_4 + 1 μg/mL Tri-DAP). For TLR/NOD1 co-stimulation experiments with CDNs, the CDNs were added to primary BMDMs 15 minutes prior to the addition of Pam3CSK4 or Tri-DAP.

Cell culture

TIB73 and ISRE-L929 cells were grown at 37°C in 5% CO2 in phenol red-free DMEM medium (GIBCO) with 10% heat-inactivated FBS (HyClone) and supplemented with 2 mM sodium pyruvate and 1 mM L-Glutamine (Thermo Fisher). J2 immortalized BMDMs (iBMDMs) and primary BMDMs were grown in the same media as above except with additional supplementation of 55 μM 2-mercaptoethanol and M-CSF harvested from L929 conditioned medium (final volume 10%). Primary BMDMs were generated as previously described (*74*). Bone marrow from WT, *Sting*-deficient or *MyD88*/*Tlr3*-deficient mice was generously provided by Daniel Stetson and Michael Gale, Jr. at the University of Washington. All protocols were reviewed and approved by the Institutional Animal Care and Use Committee at the University of Washington.

Infection assays

For infections, wild-type 10403S *L. monocytogenes* was grown in Brain Heart Infusion (BHI) media at 30°C overnight without shaking to stationary phase (OD600, 1.1-1.3). 1 mL of the culture was washed 3x and resuspended in 1 mL of 1X PBS. iBMDMs were infected as previously described (*75*) with an MOI of 0.1 (as determined by CFU

enumeration at 0.5 hpi). For some experiments iBMDMs were activated for 20 h prior to infection with 100 ng/mL of recombinant IFN-γ (PeproTech). Following initial infection (0.5 h for iBMDMs), gentamicin (50 μg/mL) was added to kill extracellular bacteria. For hepatocyte infections, $1x10^6$ TIB73 cells were seeded per well in 6-well plates the day before infection. The morning of infection, TIB73 cells were washed and placed in pre-warmed media containing 0.1% FBS. TIB73 cells were infected for 1 h with 20 μL of washed bacteria per well, resulting in a final MOI of 0.001 (as determined by CFU enumeration at 1 hpi). After 1 h, TIB73 cells were washed twice with 1X PBS and placed in pre-warmed complete media containing 10% FBS and 50 μg/mL gentamicin.

For *Chlamydia* infections, *C. pneumoniae* TW73 (University of Washington), and *C. muridarum* (University of Washington) were infected onto TIB73 hepatocytes and centrifuged at 900 x g for 1 h, then incubated at 37°C for an additional hour. Cells were rinsed twice with HBSS and fresh DMEM and incubated O/N. After 24 h, cells were rinsed, trypsinized and resuspended in DMEM, then sonicated at 20 amps for 3 x 10 second intervals. Sonicated cell/chlamydial suspensions were plated onto HeLa or Hep2 cell monolayers. Cells were infected using the same infection procedure written above, then fixed with 3.7% formaldehyde at 24 hpi to count infectious progeny. An inclusion forming units (IFU) assay was performed by staining chlamydial inclusions with an antibody to chlamydial LPS (University of Washington) and imaged by fluorescence microscopy at 20x magnification. 5-10 random fields per well were imaged to quantify the number of chlamydial inclusions per field (IFU/field).

Generation of cell lines with modified RECON expression

The open reading frame for *Akr1c13* was amplified from pSpeedET plasmid encoding *Akr1c13* (MmCD00326044; DNASU Plasmid Repository) with the following primers: Fwd 5′-gaggagctcgagATGAGCTCCAAACAGCAC-3′ and Rev 5′-gaggagGCGGCCGCTTAA TTAAGTCGCGTTAATATTCCTCC-3′. The resulting PCR product was digested with XhoI and NotI and sub-cloned into the MSCV plasmid similarly digested. MSCV-*Akr1c13* plasmid was co-transfected with VSV-G plasmid into GP2 cells using Lipofectamine 2000 (Thermo Fisher). For studies of human AKR1C1, retrovirus was produced with VSV-G and GP2 cells using pJP1520-AKR1C1 (DNASU repository HsCD00075735). Virus-containing supernatants were transferred to iBMDMs and TIB73 cells, and transduced cells were selected with 10 μg/mL puromycin for 3 days. Lentivirus-transduced

scrambled control and *Akr1c13* RNAi iBMDMs were generated using the pLKO.1 vector system, with *Akr1c13*-targeting shRNAs in the pLKO.1 vector obtained from the RNAi consortium with the following mature shRNA sequences: shRNA #1 ATTCTCTTTGA AACTCTGGGC, shRNA #4 GCCATTCAAAGCAAGATTAAA. VSV-G pseudotyped lentivirus was produced using HEK293T cells transfected using Lipofectamine 2000 (Thermo Fisher) with the appropriate pLKO.1 vector, pMD2.G, and pSPAX2. Stably transduced iBMDMs were selected with 10 μg/mL puromycin for 3 days.

Cas9 guide sequences specifically targeting *Akr1c13* were determined using http://crispr.mit.edu/. Annealed *Akr1c13*-targeting guide sequence oligos (Fwd 5′-AGTAATCCAGTAGCTTACGC-3′, Rev 5′-GCGTAAGCTACTGGATTACT-3′) were cloned into pX330-U6-Chimeric_BB-CBh-hSpCas9 (a gift from Feng Zhang (Addgene plasmid # 42230)) containing Cas9 and the sgRNA scaffold as previously described (*76*). The pX330-*Akr1c13* plasmids were transfected into TIB73 using TransIT-LT1 transfection reagent (Mirus Bio) and were clonally selected. Clones were assayed for *Akr1c13* mutation using RGEN-RFLP (RNA-guided engineered nuclease restriction fragment length polymorphism) analysis. *In vitro* transcribed sgRNA was generated using the MEGAshortscript T7 kit with the pX330-*Akr1c13*-sgRNA-Cas9 plasmid and primer 5′-TTAATACGACTCAÍCTATAGGAGTAATCCAGTAGCTTACGCG-3′ and purified with the MEGAclear kit as previously described (*77*). RGEN-RFLP genotyping was performed according to the New England BioLabs protocol with recombinant Cas9 (NEB M0386) and *Akr1c13* PCR product as the substrate DNA (Fwd 5′-TTGCAGCTGGCGTCTTTACC-3′, Rev 5′-CAGACAGCACTTGACTGACAATGC-3′). The specific disruption in *Akr1c13* was determined by TOPO PCR cloning (Thermo Fisher) and sequencing, using the same PCR product used for RGEN-RFLP analysis.

Measurement of IFN response

Supernatants from *Lm*-infected (20 hpi) or stimulated (20 h) macrophages or TIB73 hepatocytes were applied in various dilutions to the interferon responsive ISRE-L929 cells (5×10^4 cells/well, 96-well plate). Cells were incubated for 6 hours, media aspirated, and 40 μL of TNT lysis buffer (20 mM Tris, 100 mM NaCL, 1% Triton X-100) was added to each well. Finally, 40 μL of luciferase substrate solution (20 mM Tricine, 2.67 mM MgS047H20, 0.1 mM EDTA, 33.3 mM DTT, 530 μM ATP, 270 μM acetyl CoA lithium salt,

470 μM luciferin, 5 mM NaOH, 265 μM magnesium carbonate hydroxide) was added to each well and luminescence was measured using a Synergy HT (BioTek).

Microscopy and ImageJ analysis

TIB73 cells plated on coverslips (Corning BioCoat) were infected with *L. monocytogenes* for 1 h, fixed in 3.5% formaldehyde for 15 min and blocked with 10% normal goat serum for 30 min. Cells were stained with anti-NF-κB p65 antibody (Cell Signaling #8242) for 3 h, followed by anti-rabbit Alexa Fluor 488 and Alex Fluor 568 Phalloidin (Thermo Fisher A11034 and A12380). Coverslips were mounted with ProLong Gold Antifade Mountant with DAPI (Thermo Fisher). Imaging of slides was done using a Nikon Eclipse E600 microscope with a QImaging Retigia EX CCD Camera. Quantitative analyses of fluorescence were performed with ImageJ software.

NF-κB activation assays and Western blots

For NF-κB luciferase assays, TIB73 hepatocytes ($1.5x10^4$/100 μL/well) were seeded in 96-well plates and the following day co-transfected with 15 ng of pNiFty-Luc plasmid (InvivoGen) and 45 ng of eGFP plasmid using 0.5 μL TransIT-LT1 transfection reagent (Mirus Bio). Cells were stimulated 20 h post-transfection. Luciferase activity was measured as detailed above for the IFN bioassay. For NF-κB Western blots, cells were lysed in Pierce IP lysis buffer (Thermo Fisher) in the presence of protease and phosphatase inhibitors (Thermo Fisher). Protein concentrations were determined by BCA assay (Thermo Fisher), 60 μg of protein was boiled in Laemmli buffer (Bio-Rad) with 2-mercaptoethanol and Westerns were run using nitrocellulose membranes. Membranes were blocked and probed in 5% non-fat dry milk in 1X TBS with NF-κB antibodies or β-actin (Cell Signaling NF-κB pathway kit #9936). For verification of human AKR1C1 overexpression in iBMDMs, the membranes were probed with anti-AKR1C1 antibody (R&D Systems MAB6529).

qRT-PCR assays and inhibitors

RNA was extracted with the RNAqueous Total RNA Isolation Kit, DNase treated using the TURBO DNA-free Kit (Thermo Fisher) and reverse-transcribed with the iScript cDNA synthesis kit (Bio-Rad). A TaqMan Mouse Immune Panel (Thermo Fisher 4367786) was used for data presented in Figure 3C and TaqMan RT-qPCR assays were used for quantification of mouse *Akr1c13*, *Ccl5*, *Cxcl10*, *Cxcl11*, *Ifnb1*, *Il1b*, *Il6*, *Isg15,* and *Nos2*. *Hprt*

served as an endogenous control. All RT-qPCR data are plotted as the mean ± SEM of technical duplicates or triplicates. Purified anti-mouse IFNAR-1 antibody (BioLegend) (1 μg/ml) was added to cells 1 hpi with *L. monocytogenes*. NF-κB inhibitors Celastrol, BAY 11-7082, MG-132 (InvivoGen) were added to cells for 1 h prior to infection, maintained in the presence of the inhibitors during infection and then again after bacteria were washed off out to 4 hpi. All inhibitors were reconstituted in DMSO, which by itself was used as a control treatment.

Statistical analyses

Data were analyzed using Prism 6 software. Unpaired Student's t-tests were used to determine significance of data unless otherwise noted.

Accession numbers

The Research Collaboratory for Structural Bioinformatics Protein Data Bank accession number for the new structure reported in this paper is 5UXF.

Chapter 3

RECON Regulates Arachidonic Acid Metabolites

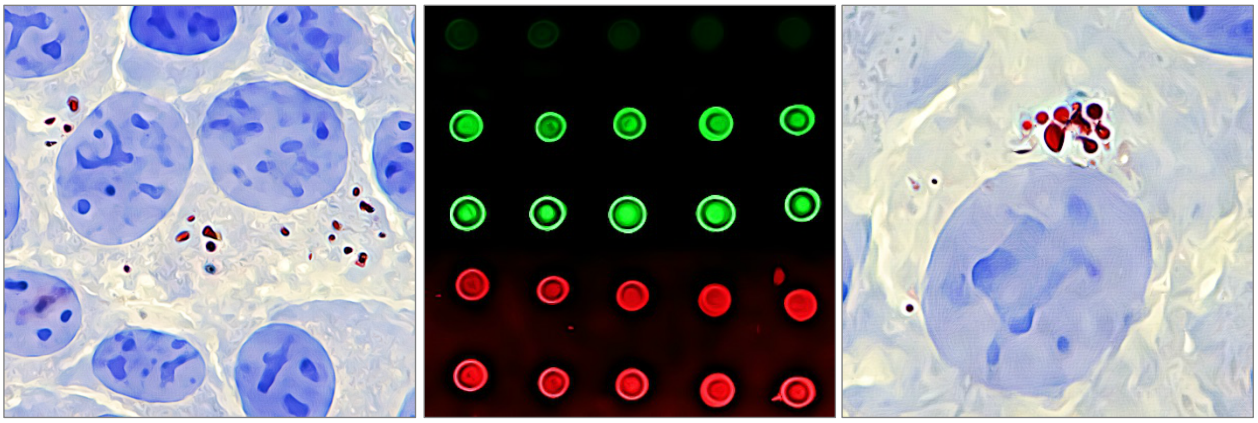

The following work has been submitted for publication as: McFarland, A.P., Glover, R., Woodward, J.J. "The aldo-keto reductase and cytosolic immune sensor RECON modulates inflammatory arachidonic acid metabolites."

3.1 Summary

The aldo-keto reductase RECON is a high affinity cytosolic sensor of bacterial-derived cyclic dinucleotides. Cyclic dinucleotide binding inhibits RECON's enzymatic activity and promotes antibacterial inflammatory gene expression. In this chapter, we sought to detail how the loss of RECON alters the cell-intrinsic inflammatory response. We found that RECON activity regulates several branches of the arachidonic acid inflammatory cascade. At the top of the cascade, free arachidonic acid levels were significantly elevated in the absence of RECON, which correlated with larger lipid droplet formation. Genetic deletion of the cytosolic phospholipase A2 (cPLA2), which liberates arachidonic acid from phospholipids, in RECON-deficient cells restored the inflammatory response to WT levels. The reactive lipid aldehyde 4-hydroxynonenal (4-HNE), which is a byproduct of arachidonic acid peroxidation that can promote inflammatory signaling, was elevated in RECON-deficient cells following TLR stimulation. 4-HNE was determined to be a bonafide RECON substrate that specifically enhanced *Nos2* expression. Interestingly, a separate branch of the arachidonic acid cascade was found to govern *Il6* expression distinct from the pathway described for *Nos2*. Dysregulated COX-mediated

prostaglandin synthesis was discovered in RECON-deficient cells by comprehensive eicosanoid profiling. Accordingly, inhibition of COX-2 activity reduced *Il6* but not *Nos2* expression. Finally, although RECON controlled *Nos2* via augmented NF-κB activation, we found that the MEK-ERK pathway was critical for *Il6* expression. Overall, these results illuminate the enzymatic functions of RECON during TLR stimulation. Its targeting of inflammatory metabolites produced by arachidonic acid oxidation provides a molecular explanation for how this enzyme operates as a regulator of multiple gene induction programs.

3.2 Background

How the magnitude of an inflammatory response to a particular microbial threat is assessed and coordinated by the host cell is an emergent theme in the field of innate immunity. At the most basic level, pattern recognition of pathogen-associated molecular patterns (PAMPs) by the host cell reveals information about the potential threat. Whether the PAMP is soluble or cell-associated, can only be produced by a living bacterium (vita-PAMP), or detected in the cytosol, can all inform about the location, viability or pathogenic potential of a microbe (*24, 25*). Likewise, the simultaneous activation of multiple pattern recognition receptors (PRRs) by several PAMPs can lead to synergistic production of inflammatory gene products. Exactly how this synergistic action is intrinsically coordinated is an active area of investigation.

We recently described the cytosolic pattern recognition receptor (PRR) named RECON (REductase COntrolling NF-κB) that detects the bacterial-derived vita-PAMP c-di-AMP (see Chapter 2 and (*78*)). RECON is a unique type of PRR; it is an NADPH-dependent aldo-keto reductase (AKR) that is inhibited upon binding its bacterial ligand. Loss of RECON's enzyme activity boosts inflammation during Toll-like receptor (TLR) or nucleotide-binding and oligomerization domain (NOD) activation, but not in conjunction with TNF-α stimulation. This suggests that RECON functions as a danger sensor and that the physiological disturbance resulting from its loss specifically synergizes with microbial-induced inflammatory cascades.

Our previous work revealed that loss of RECON augments TLR-induced NF-κB activation with increased phosphorylation of IKKα, IκBα, and p65 (see Chapter 2 and (*78*)). However, the connection between RECON's enzymatic function and TLR signaling

is unclear. There are over 60 AKRs in rodents and humans. Broadly speaking, AKRs catalyze the reduction of carbonyls to their corresponding alcohols (*33, 39, 79*). Examples of carbonyl-containing molecules that are known to be modified by AKRs include steroid hormones, prostaglandins, retinoids, isoprenoids, and lipid aldehydes (*80*). In addition to endogenously produced substrates, AKRs also modify xenobiotics and therefore have been extensively studied in the context of drug metabolism (*81*). Although much attention has been paid to the role of AKRs in the progression of human cancers owing to their turnover of steroid hormones and prostaglandins (*82, 83*), there is nearly a complete absence of their study in innate immunity despite the obvious importance of their substrates in this context.

Our current understanding of RECON's enzymatic properties is limited mainly to *in vitro* work assessing its ability to turnover panels of known AKR substrates. In these assays, RECON did not reduce steroid hormones, such as testosterone and progesterone, but was active against reactive xenobiotic carbonyls (*33, 39, 84-86*). However, RECON's *in vivo* substrate repertoire is completely unknown. Its involvement as an anti-inflammatory enzyme during TLR stimulation suggests that RECON is likely detoxifying reactive host-derived factors. Many reactive carbonyls are produced downstream of TLR stimulation from the ubiquitous inflammatory precursor arachidonic acid, which is liberated from membrane phospholipids by activated cytosolic phospholipase A2 (cPLA2) (*87-91*).

In the work presented in this chapter, we sought to understand the cellular functions of RECON following immune activation and examined whether RECON was involved in arachidonic acid metabolism. Following TLR stimulation, cells deficient in RECON exhibited significantly increased free arachidonic acid levels, suggesting there may be increased flux through this cascade. CRISPR/Cas9-mediated mutagenesis of *Pla2g4a*, which encodes the cytosolic phospholipase A2, abrogated the enhanced inflammation in RECON-deficient cells demonstrating that arachidonic acid metabolism was required for the response. Further probing of this cascade revealed that RECON alters metabolites in both non-enzymatic and enzymatic branches of arachidonic acid metabolism. Reactive lipid species produced from reactive oxygen species (ROS)-mediated arachidonic acid peroxidation were elevated in RECON-deficient cells and were sufficient to drive *Nos2* expression. In contrast, *Il6* expression was partially dependent on COX-2 activity and found to be downstream of MEK-ERK. The control of

MAPK activation by RECON was not previously known, as RECON was initially described as a regulator of NF-κB (see Chapter 2 and (*78*)). Collectively, the results presented here provide evidence that RECON functions within the arachidonic acid cascade to regulate inflammation.

3.3 RECON-deficiency alters arachidonic acid mobilization and lipid droplets

3.3.1 The absence of RECON promotes arachidonic acid mobilization

RECON functions as a negative regulator of inflammation during TLR stimulation or infection with *L. monocytogenes*. Previous characterization of RECON-deficient cells revealed augmented inflammatory gene expression, with enhanced NF-κB activation that was due to the absence of RECON's enzymatic activity (see Chapter 2 and (*78*)). RECON is an aldo-keto reductase family member, which provides some information regarding its enzymatic function, such as the potential ability to oxidize non-steroidal alcohols as well as reduce reactive carbonyls (*33, 39, 84-86*). However, the *in vivo* substrates of RECON are currently uncharacterized. When RECON (AKR1C13) was first cloned, it was identified as a possible prostaglandin F synthase (PGFS)-like enzyme due to its cross reactivity with PGFS antisera (*33*). PGFS is a synthase that functions within the arachidonic acid cascade during inflammatory responses (*92*). Following TLR stimulation, activation of the cytosolic phospholipase A2 (cPLA2) leads to the liberation of arachidonic acid, an omega-6 polyunsaturated fatty acid (PUFA), from the phospholipid bilayer (*88-91*). Arachidonic acid metabolites are ubiquitous mediators of inflammatory processes. We therefore hypothesized that in the absence of RECON, dysregulation of inflammatory arachidonic acid metabolites may promote inflammatory gene expression.

To explore this hypothesis, we employed hepatocytes, as these cells express high levels of RECON and play an important role in innate immunity via biosynthesis of secreted immunity proteins such as transferrin, lipocalin-2, serum amyloid A, and LPS-binding protein (*93*). Additionally, hepatocytes do not express STING, which is regulated by RECON via TLR-independent processes (see Chapter 2 and (*78*)), and therefore allowed us to study how loss of RECON specifically promotes TLR-dependent inflammation. To determine whether RECON influenced arachidonic acid mobilization,

we measured the levels of free arachidonic acid in supernatants from TIB73 embryonic murine hepatocytes at 5 and 20 min following stimulation with TLR2 and NOD1 ligands. Remarkably, the absence of RECON resulted in a 3-fold increase in the level of free arachidonic acid at 20 min (Figure 3.1). In comparison, there was no change in the levels of the anti-inflammatory omega-3 PUFA eicosapentaenoic acid (EPA) (*94*).

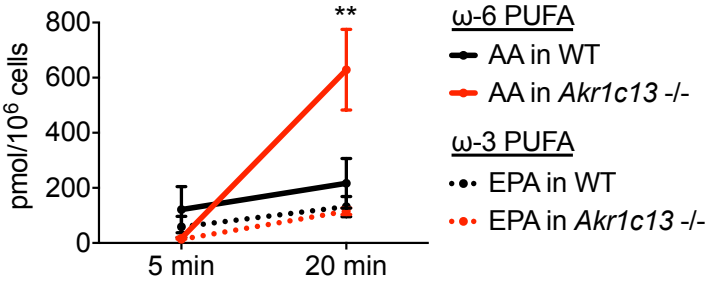

Figure 3.1. RECON-deficient hepatocytes have elevated free pools of arachidonic acid following stimulation. Levels of free polyunsaturated acids (PUFAs) arachidonic acid (AA) and eicosapentaenoic acid (EPA) determined by mass spectrometry in cell-free supernatants from *Akr1c13*-deficient or WT TIB73 cells stimulated with the TLR2 ligand Pam3CSK4 and NOD1 agonist Tri-DAP. Error bars represent ± SD (N=3). Statistical significance was determined by 2way ANOVA with post-hoc Tukey test (**p=0.0038).

3.3.2 RECON deficiency results in the formation of large lipid droplets

In light of the increased free pool of arachidonic acid in the absence of RECON, we examined whether RECON-deficiency affected the formation of lipid droplets. Lipid droplets are hubs for arachidonic acid processing because they are rich in esterified arachidonic acid and, following stimulation, are compartmentalized with cPLA2 leading to enhanced arachidonic acid mobilization (*95, 96*). Oil red O staining of TLR-stimulated hepatocytes revealed significantly larger lipid droplets were formed in the absence of RECON (Figure 3.2A-C). Although the biogenesis and hydrolysis of lipid droplets is not well understood, particularly in hepatocytes, their enlarged size supports the idea that arachidonic acid mobilization may be altered in RECON-deficient cells, which is consistent with the increase in free arachidonic acid (Figure 3.1). Together these results demonstrate that the absence of RECON increases arachidonic acid mobilization, thereby increasing the supply of this precursor for potential inflammatory cascades.

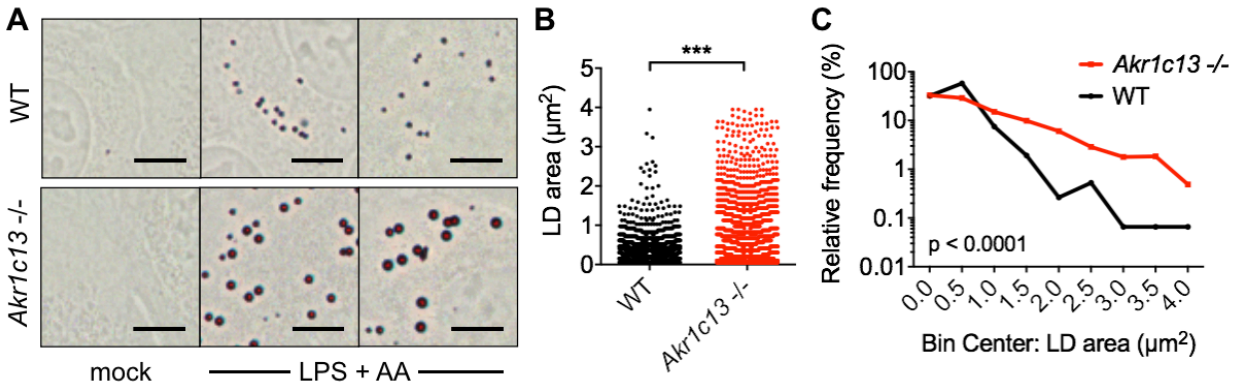

Figure 3.2. RECON deficiency results in the formation of large lipid droplets. (A) Oil Red O staining in WT or *Akr1c13*-deficient TIB73 hepatocytes stimulated with LPS and arachidonic acid (AA) for 4 h. Scale=10 μm. (B) Quantification of lipid droplet areas as shown in (A). All data points are shown (N=1500-1800). Statistical significance was determined by Mann-Whitney U test (***p<0.0001). (C) Relative frequency (percent) of the lipid droplets binned according to their area. These data are representative of three independent experiments with similar results.

3.4 cPLA2 drives inflammatory cascades in the absence of RECON

3.4.1 Chemical inhibition of PLA2 reverses augmented inflammation in RECON-deficient hepatocytes

Arachidonic acid is released from phospholipids following hydrolysis by cPLA2. To test whether the increased arachidonic acid levels may be involved in driving inflammation in the absence of RECON, we targeted cPLA2 activity. Hepatocytes were treated with the PLA2 inhibitor aristolochic acid and infected with *L. monocytogenes*. We observed a significant dose-dependent inhibition of *Il6* and *Nos2* expression (Figure 3.3A and 3.3B).

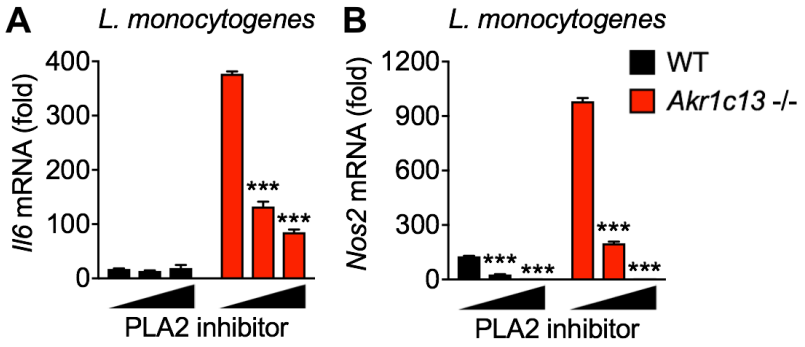

Figure 3.3. Inhibition of PLA2 blocks RECON-dependent *Nos2* and *Il6* expression. Expression of *Il6* (A) and *Nos2* (B) in WT (black bars) or *Akr1c13*-deficient (red bars) TIB73 hepatocytes infected with *L. monocytogenes* for 4 h in the presence of DMSO or the PLA2

inhibitor aristocholic acid (25 and 100 μM). *Hprt* was used as an endogenous control and the data are normalized to uninfected WT TIB73 cells. Error bars represent ± SEM of technical triplicate. Statistical significance was determined by One-way ANOVA with post-hoc Tukey test (***p<0.0001). The significances indicated in the figure represent the comparison with mock treatment with respect to either WT or RECON-deficient backgrounds. Data are representative of three independent experiments with similar results.

3.4.2 Generation of *Pla2g4a*-deficient TIB73 hepatocytes

There are several isoforms of PLA2 enzymes that may be targeted by the inhibitor aristolochic acid. The group IVA calcium-dependent cPLA2 encoded by *Pla2g4a* is known to be a central actor in the release of arachidonic acid during TLR stimulation and infection (*97-99*). We targeted the *Pla2g4a* gene using CRISPR/Cas9-mediated mutagenesis and obtained cPLA2-deficient hepatocytes as well as RECON/cPLA2-deficient cells (Figure 3.4).

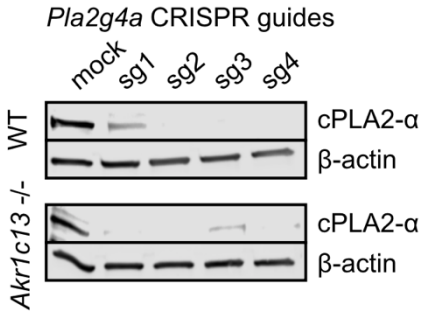

Figure 3.4. Generation of cPLA2-deficient TIB73 cell lines. Western blot analysis of cPLA2-*α* in TIB73 cells (both WT and *Akr1c13*-deficient backgrounds) mutagenized with CRISPR/Cas9 sgRNAs targeting the *Pla2g4a* gene. β-actin was used as a loading control.

3.4.3 Genetic deletion of cPLA2 in RECON-deficient cells restores *Nos2* and *Il6* gene expression to WT levels

Consistent with the PLA2 inhibitor data, mutation of cPLA2 blocked the augmented *Il6* and *Nos2* expression in RECON-deficient hepatocytes during *L. monocytogenes* infection (Figure 3.5A and 3.5B). Similarly, RECON/cPLA2-deficient cells also exhibited significantly reduced inflammation following LPS stimulation (Figure 3.5C and 3.5D).

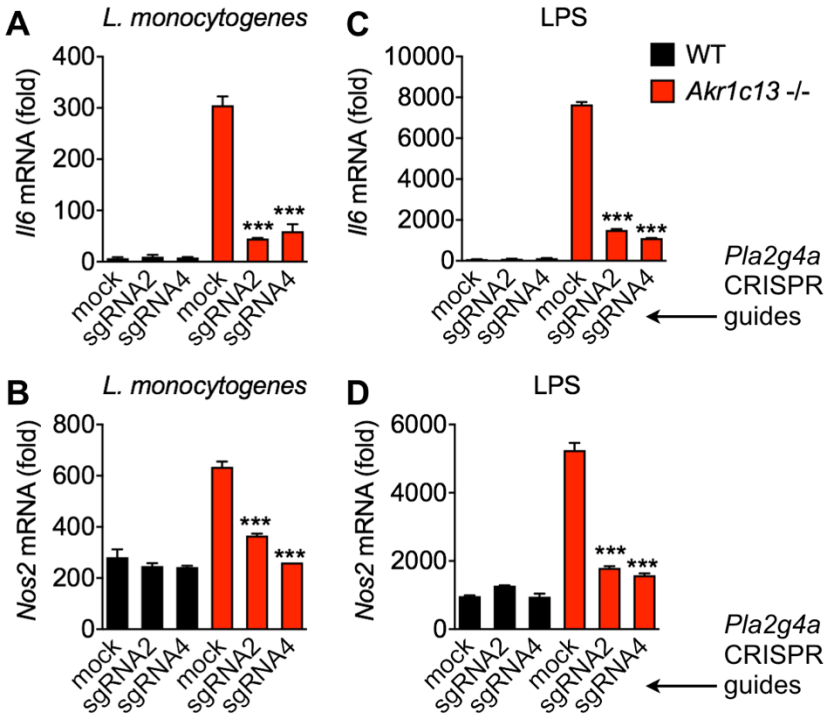

Figure 3.5. cPLA2 drives augmented *Nos2* and *Il6* expression in RECON-deficient cells. Expression of *Il6* (A, C) and *Nos2* (B, D) in the indicated TIB73 lines 2 h post-infection with *L. monocytogenes* or treatment with LPS. For all qRT-PCR data, *Hprt* was used as an endogenous control and the data are normalized to uninfected WT TIB73 cells. Error bars represent ± SEM of technical duplicate or triplicate. Statistical significance in all graphs was determined by One-way ANOVA with post-hoc Tukey test (***$p<0.0001$). The significances indicated in the figure represent the comparison with (mock) RECON-deficient cells. Data are representative of three independent experiments with similar results.

3.4.4 Genetic deletion of cPLA2 in RECON-deficient cells blocks augmented NF-κB activation

Our previous work revealed that RECON functions as a negative regulator of NF-κB activation (see Chapter 2 and (*78*)). We investigated whether the dramatic curtailing of *Il6* and *Nos2* expression in RECON/cPLA2-deficient hepatocytes was observed at the level of NF-κB activation. WT, cPLA2-deficient, RECON-deficient, or RECON/cPLA2-deficient cells were transfected with an NF-κB luciferase reporter and infected with *L. monocytogenes* or stimulated with LPS. Consistent with the gene expression analyses, the loss of cPLA2 in RECON-deficient cells diminished the augmented NF-κB activation (Figure 3.6A and 3.6B). Together, these results demonstrate that the inflammatory

program(s) controlled by RECON downstream of TLR activation involve the action of cPLA2 and arachidonic acid cascades.

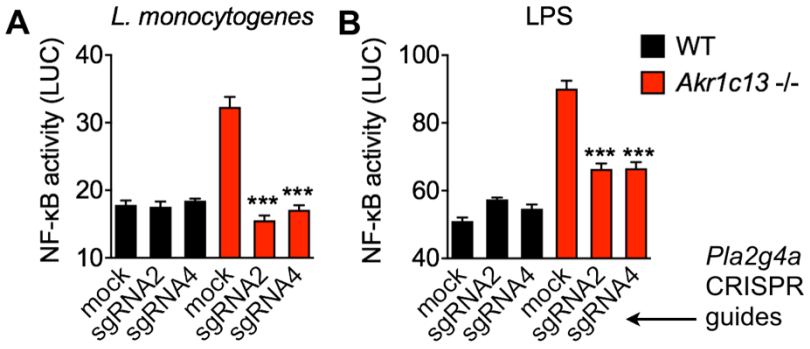

Figure 3.6. cPLA2 drives augmented NF-κB activation in RECON-deficient hepatocytes. NF-κB luciferase activity measured at 4 h from the indicated TIB73 lines infected with *L. monocytogenes* (A) or treated with LPS (B). The data are presented as luciferase units divided by the eGFP transfection control fluorescence (LUC) and normalized to unstimulated WT cells (N=6). Error bars represent ± SD. Statistical significance in all graphs was determined by One-way ANOVA with post-hoc Tukey test (***$p<0.0001$). The significances indicated in the figure represent the comparison with (mock) RECON-deficient cells. Data are representative of two independent experiments with similar results.

3.5 The lipid aldehyde 4-HNE is detoxified by RECON and specifically promotes *Nos2* expression during TLR stimulation

3.5.1 *Nos2* but not *Il6* is controlled by a cPLA2-ROS-NF-κB pathway

Free arachidonic acid can be non-enzymatically or enzymatically oxidized (*100, 101*). Non-enzymatic peroxidation of arachidonic acid by ROS produces lipid aldehydes and isoprostanes as the major end products (*101-103*). These reactive lipid species (RLS) are electrophilic and can covalently modify proteins, including signaling proteins, and these modifications can sensitize signaling pathways to activation even when ligand levels are low (*101*). Importantly, AKRs are known to function in the cellular detoxification of RLS (*103, 104*). To test whether RLS may be involved in the enhanced inflammation in the absence of RECON, we inhibited the activity of the NADPH oxidases (NOX) with diphenyleneiodonium (DPI) during *L. monocytogenes* infection. The inhibition of ROS production caused a specific block in *Nos2* expression, whereas *Il6* expression was significantly increased in RECON-deficient cells (Figure 3.7A). These surprising results

suggested that augmentation of *Nos2* and *Il6* in the absence of RECON may operate via distinct pathways, with RLS specifically enhancing *Nos2* expression.

We previously found that *Nos2* expression during stimulation of WT and RECON-deficient hepatocytes was dependent on NF-κB (see Chapter 2 and (*78*)). Given the opposite trends of *Il6* and *Nos2* with DPI, we tested whether *Il6* expression was NF-κB-dependent. Unexpectedly, the addition of the NF-κB inhibitor celastrol specifically blocked *Nos2* expression during *L. monocytogenes* infection, while the augmented *Il6* expression that occurred in RECON-deficient cells was NF-κB-independent (Figure 3.7B). These data support a model in which RECON regulation of *Nos2* but not *Il6* expression is driven via a cPLA2-RLS-NF-κB pathway.

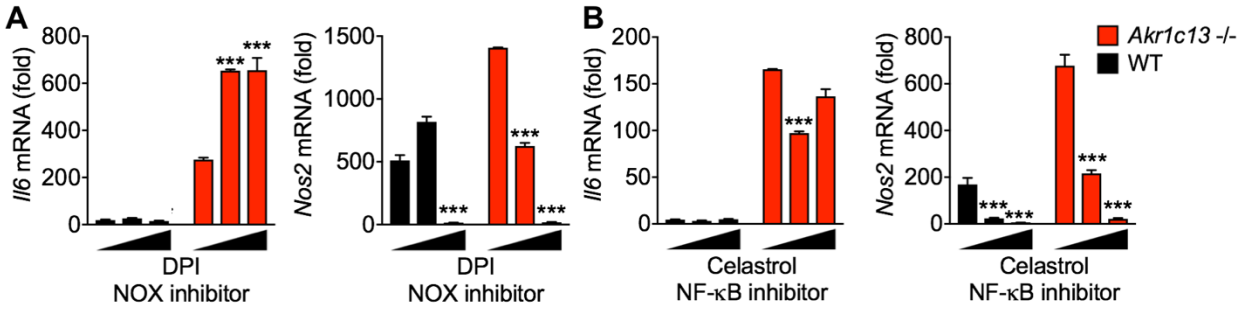

Figure 3.7. *Nos2* expression but not *Il6* is controlled by ROS and NF-κB in RECON-deficient hepatocytes. Expression of *Il6* and *Nos2* in WT (black bars) or *Akr1c13*-deficient (red bars). TIB73 hepatocytes infected with *L. monocytogenes* for 4 h in the presence of (A) diphenyleneiodonium (DPI) (NAPDH oxidase NOX inhibitor; 10 and 100 μM) or (B) celastrol (NF-κB inhibitor; 0.1 and 1 μM). DMSO treatment was used for the mock control, and the statistical significances indicated in the figure represent the comparison with DMSO mock in WT (for black bars) and RECON-deficient (for red bars) cells. Statistical significance was determined by One-way ANOVA with post-hoc Tukey test (***$p<0.0001$). *Hprt* was used as an endogenous control and the data are normalized to uninfected mock-treated WT TIB73 cells. Error bars represent ± SEM of technical duplicate or triplicate. Data are representative of at least two independent experiments with similar results.

3.5.2 The RLS 4-hydroxynoneal accumulates in the absence of RECON

The reaction of oxygen with arachidonic acid produces lipid aldehydes, including malondialdehyde (MDA) and 4-hydroxynonenal (4-HNE). 4-HNE is an abundant and well-characterized product of arachidonic acid oxidation (*103, 105, 106*). At low levels, 4-HNE has been shown to act as a signaling molecule, whereas at high levels this reactive molecule is genotoxic and cytotoxic and causes cell death (*103*). 4-HNE is detoxified in

the cytosol via several enzymes, including NADPH-dependent aldo-keto reductases (*103*, *104*). We therefore sought to determine whether 4-HNE accumulation during stimulation was altered in RECON-deficient cells. In non-pathological states, 4-HNE is estimated to exist in the low micromolar range in cell extracts (*107*). 4-HNE levels in biological samples are estimated by approximation via antibody-based detection of 4-HNE protein adducts. We utilized a flow cytometry assay to detect 4-HNE protein adducts in fixed cells. Treatment of WT hepatocytes with exogenous 4-HNE resulted in a detectable increase in the mean fluorescence intensity of 4-HNE adducts (Figure 3.8A). Comparison of WT and RECON-deficient hepatocytes following TLR2 stimulation revealed a significantly higher incidence of 4-HNE adducts in the absence of RECON (Figure 3.8B).

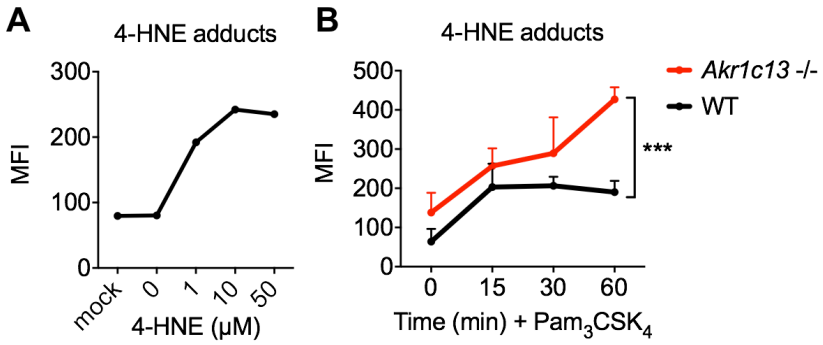

Figure 3.8. Increased levels of 4-hydroxynonenal adducts in RECON-deficient cells. (A) Mean fluorescent intensity (MFI) of 4-HNE adducts detected in 4-HNE-treated WT TIB73 cells by flow cytometry. (B) MFI of 4-HNE adducts in WT or RECON-deficient hepatocytes following stimulation with the TLR2 ligand Pam3CSK4. Error bars represent ± SD (N=3). Statistical significance was determined by 2way ANOVA (***p<0.0001). Data are representative of two independent experiments with similar results.

3.5.3 RECON directly detoxifies 4-HNE

To determine whether the difference in 4-HNE levels in hepatocytes could be the result of direct enzymatic turnover by RECON, we tested whether recombinant RECON was capable of reducing 4-HNE *in vitro* using an NADPH oxidation assay. We found RECON could detoxify 4-HNE and the reaction of RECON with 4-HNE obeyed Michaelis–Menten kinetics, with a catalytic efficiency (k_{cat}/K_M value of 1.0 x 10^5 M^{-1} min^{-1}) on par with other AKR turnover of 4-HNE reported previously (Figure 3.9A and 3.9B) (*108-110*). Together, these data demonstrate that 4-HNE is bonafide substrate of RECON and that RECON controls 4-HNE accumulation following TLR stimulation.

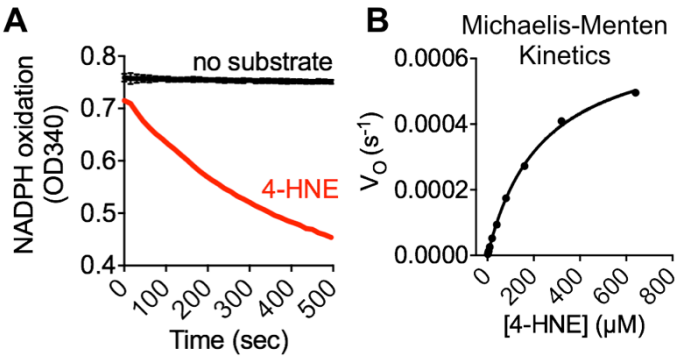

Figure 3.9. 4-HNE is a bonafide RECON substrate. (A) NADPH oxidation in the presence of RECON plus the lipid aldehyde 4-HNE. (B) Michaelis-Menten kinetics of RECON with 4-HNE and cosubstrate NADPH (k_{cat}/K_M value of 1.0 x 10^5 M^{-1} min^{-1}).

3.5.4 4-HNE promotes *Nos2* but not *Il6* expression during TLR stimulation

Given its purported roles in inflammatory gene activation (*103, 111*), we hypothesized that 4-HNE was the RLS responsible for the augmented *Nos2* expression in the absence of RECON. To test this, we added increasing amounts of 4-HNE in combination with TLR2 ligands to WT cells. Remarkably, the addition of nanomolar concentrations of 4-HNE resulted in a robust and dose-dependent augmentation of *Nos2* expression, while

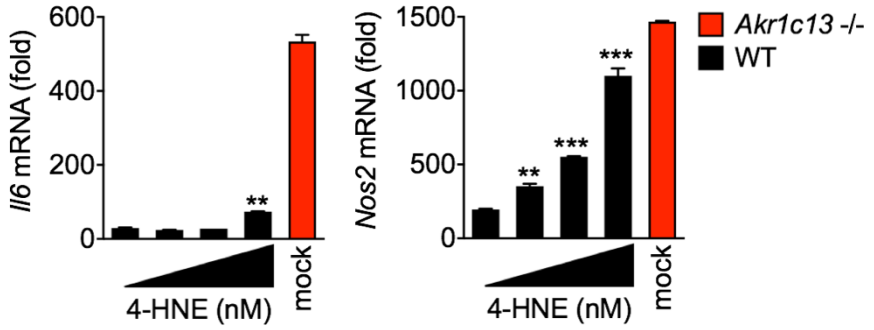

Figure 3.10. 4-HNE synergizes with TLR ligands to promote *Nos2* expression. Expression of *Il6* and *Nos2* in WT (black bars) TIB73 hepatocytes stimulated for 4 h with Pam3CSK4 or mock-treated along with increasing concentrations of 4-HNE (0.1, 1.0, 10 nM). Red bar is the gene expression in *Akr1c13*-deficient cells provided for comparison with 4-HNE-treated WT cells. Statistical significance was determined by One-way ANOVA with post-hoc Dunnett test (**p<0.001; ***p<0.0001). The significances indicated in the figure represent the comparison with Pam_3CSK_4-stimulated WT cells plus DMSO mock. *Hprt* was used as an endogenous control and the data are normalized to unstimulated mock-treated WT TIB73 cells. Error bars represent ± SEM of technical duplicate. Data are representative of three independent experiments with similar results.

Il6 expression was only marginally affected (Figure 3.10). This is consistent with our earlier findings that arachidonic acid peroxidation via ROS, which is the pathway by which 4-HNE is produced, is responsible for augmented *Nos2* expression but not *Il6* (Figure 3.7A). Taken together, the exquisite sensitivity of the hepatocytes to small changes in 4-HNE levels and specificity of the response leading to *Nos2* expression suggests that in absence of its detoxifying enzyme, RECON, accumulation of 4-HNE enhances NF-κB and *Nos2* activation downstream of TLR activation.

3.6 RECON regulates COX metabolites that promote *Il6* expression

3.6.1 Comprehensive eicosanoid profiling of RECON-deficient hepatocytes

The unexpected finding that *Il6* expression in RECON-deficient cells is cPLA2-dependent but RLS-NF-κB-independent led us to hypothesize that alterations in enzymatic arachidonic acid processing may be involved in promoting *Il6* expression. Enzymatic oxidation of arachidonic acid by cyclooxygenases (COX), lipoxygenases (LOX), and cytochrome P450 (CYP450) oxygenases produces a variety of inflammatory eicosanoids, such as prostaglandins and leukotrienes (*100, 112*). To determine which branch of arachidonic acid metabolism may be dysregulated in the absence of RECON, we performed comprehensive eicosanoid profiling on TLR-stimulated WT and RECON-deficient hepatocytes. 150 eicosanoid species were quantitatively measured by mass spectrometry, and 57 of these were detected in cell supernatants 5 minutes post-stimulation.

The most significant changes in eicosanoids observed between WT and RECON-deficient hepatocytes occurred in the COX pathway (Figure 3.11). The levels of prostaglandin (PG)A_2, PGD_2, PGE_2 and $PGF_{2\alpha}$ were all significantly altered in the absence of RECON at 5 min post-stimulation, and these trends continued through 20 min post-stimulation (Figure 3.12A). COX-1/2 action on arachidonic acid leads to the production of PGH_2, which is a precursor substrate for synthases that produce PGD_2, PGE_2, and $PGF_{2\alpha}$(*100*) (Figure 3.12B). PGE_2 can be non-enzymatically oxidized to produce PGA_2 and can also be converted into $PGF_{2\alpha}$ (*100, 112*). The roles of these PGs in inflammation is complex, as they can serve to both promote and resolve inflammation. Since the loss of

RECON associates with increased inflammation, we propose that the alteration in PG metabolism in RECON-deficient cells is a pro-inflammatory permutation.

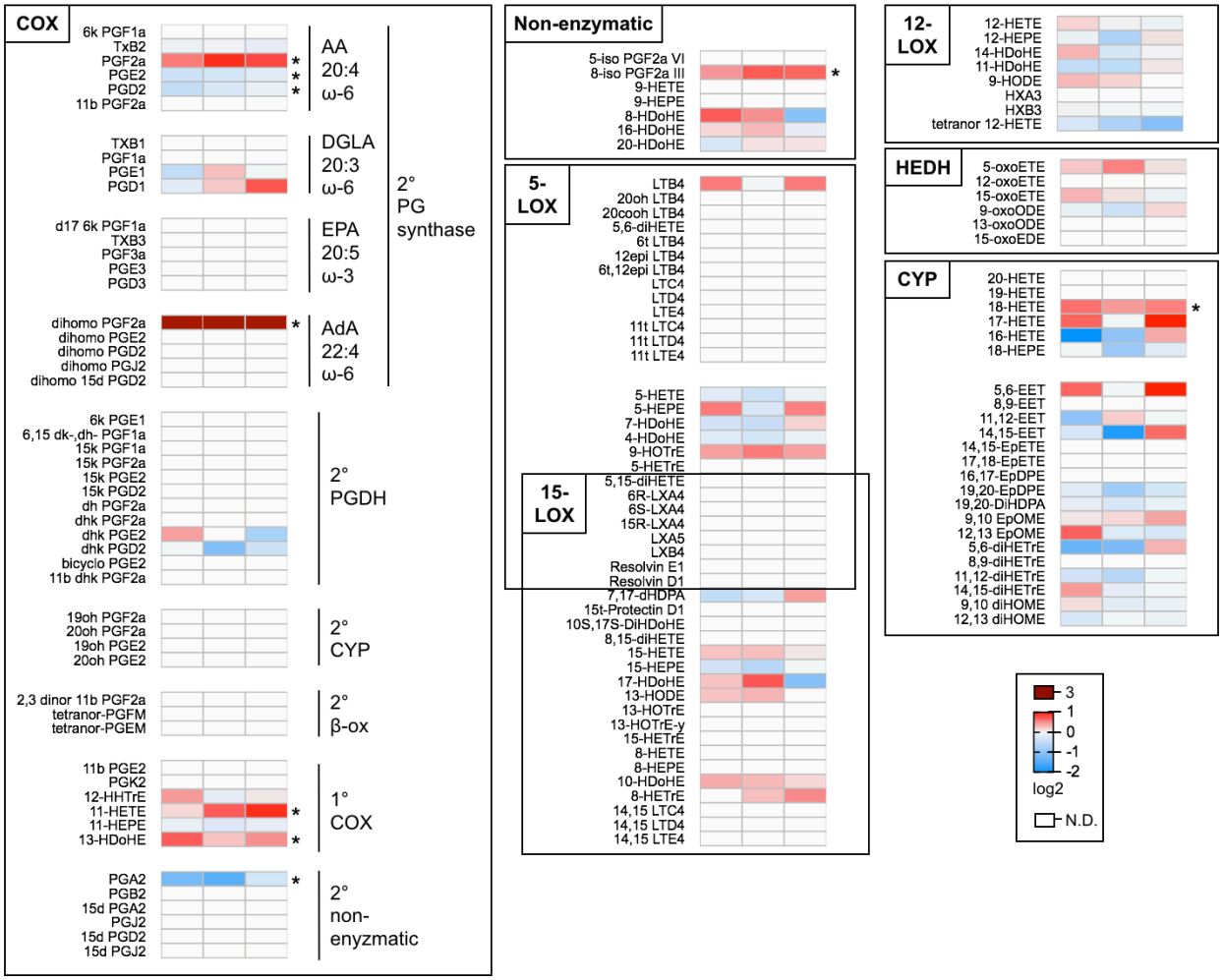

Figure 3.11. Eicosanoid levels are regulated by RECON. Heat map representing fold change values (log2) of eicosanoids (RECON/WT) in cell-free supernatants from *Akr1c13*-deficient or WT TIB73 cells stimulated for 5 minutes with the TLR2 ligand Pam3CSK4 and NOD1 agonist Tri-DAP. In the COX pathway, the products of secondary (2°) synthases and dehydrogenases that act on COX-derived substrates are indicated: arachidonic acid (AA); dihomo γ-linolenic acid (DGLA); eicosapentaenoic acid (EPA); adrenic acid (AdA). Presentation of pathways adapted from Norris and Dennis, 2012. Three biological replicates are shown as separate columns. Increases in metabolite levels are indicated in red, decreases in blue, and detectable but unchanged levels in grey. White boxes indicate eicosanoids that were measured by mass spectrometry but were undetected in the hepatocyte supernatants. Statistical significance was determined by 2way ANOVA with FDR corrected for by the Benjamini-Hochberg procedure and paired Student's t test (*$p<0.05$).

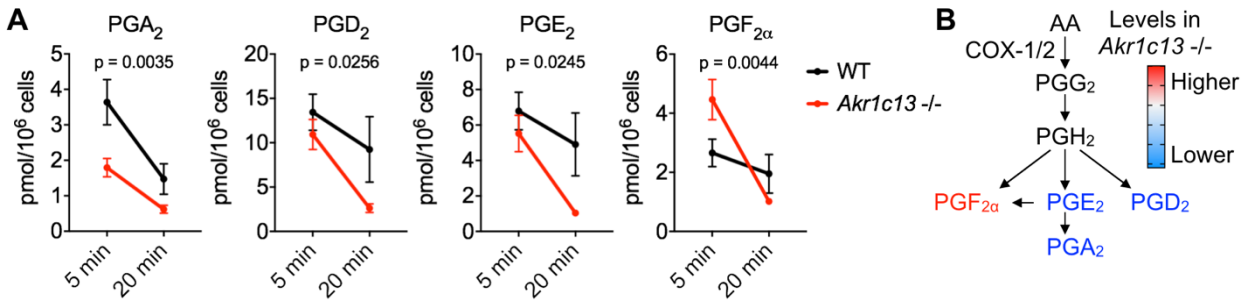

Figure 3.12. Prostaglandin synthesis downstream of PGH_2 is altered in the absence of RECON. (A) Prostaglandin levels (pmol/10^6 cells) measured by mass spectrometry in cell-free supernatants from *Akr1c13*-deficient or WT TIB73 cells stimulated with the TLR2 ligand Pam3CSK4 and NOD1 agonist Tri-DAP. Error bars represent ± SD (N=3). Statistical significance was determined by 2way ANOVA. (B) Schematic depicting COX-mediated arachidonic acid metabolism and PG biosynthesis. Blue indicates prostaglandin species that were less abundant in RECON-deficient cells, red indicates those that were more abundant.

3.6.2 COX-2 promotes *Il6* expression in RECON-deficient hepatocytes

Earlier studies revealed non-enzymatic arachidonic acid peroxidation and production of RLS was involved in promoting *Nos2* but not *Il6* expression in the absence of RECON. We hypothesized that the dysregulation of enzymatic COX-mediated arachidonic acid metabolism and PG biosynthesis may enhance *Il6* expression. To test this, we employed nonsteroidal anti-inflammatory drugs (NSAIDs). The addition of flurbiprofen, a non-selective COX-1/2 inhibitor, resulted in a significant reduction of *Il6* but not *Nos2* expression in RECON-deficient cells (Figure 3.13A). To determine if this effect was mediated by COX-1 or COX-2, we used celecoxib, a well-studied and specific NSAID that targets COX-2 (*113, 114*). Again, we observed that celecoxib significantly reduced the expression of *Il6* but not *Nos2* in RECON-deficient cells (Figure 3.13B). In addition to COX, the two other branches of enzymatic arachidonic acid processing include LOX and CYP450 oxidases. We did not observe an effect of inhibitors targeting these pathways on either *Il6* or *Nos2* expression, consistent with little to no dysregulation in their derived eicosanoids in RECON-deficient cells (Figure 3.13C and 3.13D).

The induction of COX-2 expression in cells during inflammation leads to the temporal production of PG species (*91*). However, the eicosanoid mass spec analysis and results with celecoxib suggested COX-2 may be involved in early PG biosynthesis. Accordingly, we observed high expression of COX-2 at steady-state in hepatocytes in

contrast to its inducibility in macrophages (Figure 3.14). Together, these data suggest that alterations in COX-2-mediated PG production in the absence of RECON enhances *Il6* expression. However, although most of the *Il6* expression is cPLA2-dependent in RECON-deficient cells (Figure 3.5), the COX inhibitors did not completely block *Il6*, suggesting the concerted dysregulation of several arachidonic acid processing pathways are likely involved in mediating expression of this gene.

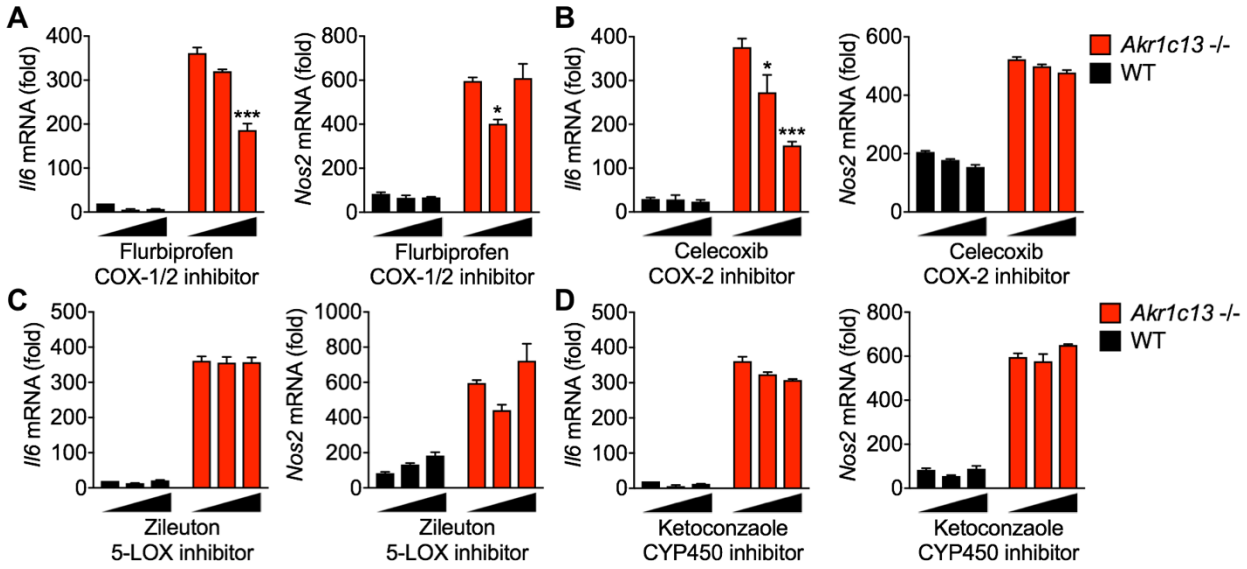

Figure 3.13. COX-2 pathway promotes *Il6* expression in RECON-deficient hepatocytes. Expression of *Il6* and *Nos2* in WT (black bars) or *Akr1c13*-deficient (red bars) TIB73 hepatocytes infected with *L. monocytogenes* for 4 h in the presence of (A) flurbiprofen (COX-1/2 inhibitor; 0.1 and 1.0 μM), (B) celecoxib (COX-2 inhibitor; 0.1 and 1.0 μM), (C) zileuton (5-LOX inhibitor; 2 and 20 μM), or (D) ketoconazole (CYP450 inhibitor; 0.1 and 1 μM). *Hprt* was used as an endogenous control and the data are normalized to uninfected mock-treated WT TIB73 cells. Error bars represent ± SEM of technical duplicate or triplicate. Statistical significance was determined by One-way ANOVA with post-hoc Tukey test (*$p<0.05$; ***$p<0.0001$). The significances indicated in the figure represent the comparison with DMSO mock-treated RECON-deficient cells. Data are representative of at least two independent experiments with similar results.

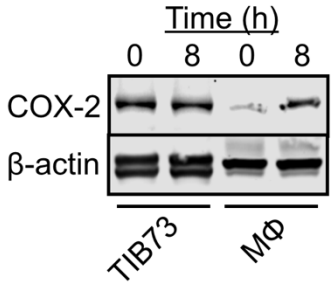

Figure 3.14. TIB73 hepatocytes express COX-2 at steady-state. Western blot of COX-2 protein expression in TIB73 hepatocytes or immortalized bone marrow-derived macrophages infected with *L. monocytogenes* for 8 h or mock treated. β-actin was used as a loading control.

3.6.3 Flux through the arachidonic acid cascade promotes *Il6* expression only in the absence of RECON's enzymatic activity

Comparing the magnitude of *Il6* and *Nos2* augmentation, it is clear that *Il6* follows a different pattern than *Nos2*. *Nos2* is upregulated 3 to 7-fold over WT expression in the absence of RECON. However, *Il6* is upregulated 20 to 50-fold in the absence of RECON. Indeed, *Il6* is only weakly expressed in TLR-stimulated WT cells, suggesting the pathway responsible for its striking expression in RECON-deficient cells is not active in WT cells. Our previous work using an enzymatically dead mutant of RECON (H117A) revealed that loss of RECON's enzymatic activity was responsible for the augmented NF-κB activation (see Chapter 2 and (*78*)). Here, we have found that *Il6* is NF-κB-independent and therefore, we interrogated the impact of RECON enzyme activity on the expression of *Il6*. Complementation of RECON-deficient hepatocytes with WT RECON restored *Il6* expression to WT levels (Figure 3.15A). However, complementation with the H117A mutant did not abrogate the enhanced *Il6* expression. These data demonstrate that, similar to *Nos2*, the catalytic activity of RECON is acting to suppress *Il6* expression.

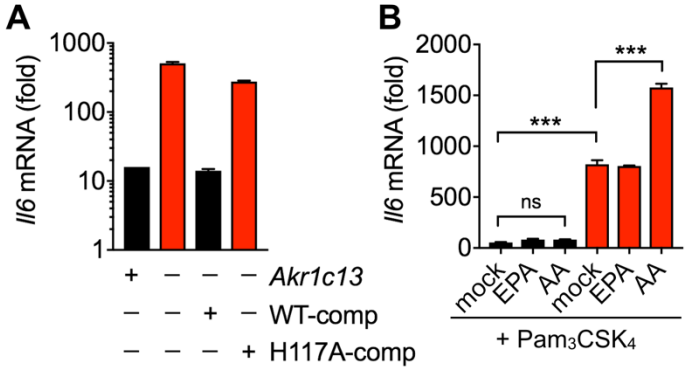

Figure 3.15. Loss of RECON's enzymatic activity drives *Il6* expression downstream of arachidonic acid. (A) Expression of *Il6* in WT, *Akr1c13*-deficient, or *Akr1c13*-deficient complemented with WT (WT-comp) or H117A (H117A-comp) RECON. Cells were stimulated with Pam3CSK4 for 4 h. (B) Expression of *Il6* in WT (black bars) or *Akr1c13*-deficient (red bars) hepatocytes treated with Pam3CSK4 plus arachidonic acid (AA) or eicosapentaenoic acid (EPA) for 4 h. *Hprt* was used as an endogenous control and data are normalized to unstimulated mock-treated WT TIB73. Error bars represent ± SEM of technical duplicate or triplicate. Statistical significance was determined by One-way ANOVA with post-hoc Tukey test (***$p<0.0001$; ns=not significant). Data are representative of at least two independent experiments with similar results.

Collectively, our data indicated that alterations in arachidonic acid metabolism, including oxidation by COX, in the absence of RECON was driving *Il6* expression. We

tested whether we could enhance *Il6* expression by adding exogenous arachidonic acid or eicosapentaenoic acid to hepatocytes during TLR2 stimulation. Addition of either PUFA failed to elicit increased *Il6* expression in WT cells (Figure 3.15B). However, there was a significant increase in *Il6* expression upon arachidonic acid exposure in RECON-deficient cells (Figure 3.15B). These data revealed that the arachidonic acid *Il6*-inducing inflammatory program that is blocked by RECON cannot be overcome by simply increasing flux through the cascade. Therefore, it is likely that *Il6* expression in RECON-deficient cells is not only triggered by the accumulation of a pro-inflammatory arachidonic acid/COX-2-derived eicosanoid, but also by the relief of an inhibitory brake on *Il6* induction itself.

3.7 The absence of RECON relieves a brake on MEK-ERK signaling that induces robust *Il6* expression

Il6 gene expression can be driven by a unique GATE element in its promoter, which is absent in the *Nos2* promoter. The GATE element is bound and activated by a complex containing CCAAT/Enhancer Binding Protein Beta (C/EBPβ), also known as nuclear factor for IL-6 expression (NF-IL6) (*115-117*). C/EBPβ is a liver-specific transcription factor expressed in hepatocytes, and its activation is controlled by MEK1 (mitogen-activated protein kinase kinase/extracellular signal-regulated protein kinase kinase) and ERKs (extracellular signal-regulated protein kinases). Interestingly, as PGs are produced, they can rapidly activate MEK1 via G-protein-coupled receptors (*118-121*). To test whether MEK1 was involved in *Il6* expression, we added the MEK1 inhibitor PD98059 to WT or RECON-deficient hepatocytes and infected the cells with *L. monocytogenes*. Remarkably, the MEK1 inhibitor blocked *Il6* expression in RECON-deficient cells without affecting *Nos2* (Figure 3.16A). To confirm the MEK-ERK pathway was active in the absence of RECON, we determined the phosphorylation status of MEK1/2 and EKR1/2 by Western blot. MEK1/2 and ERK1/2 were rapidly phosphorylated following stimulation of RECON-deficient hepatocytes, while we did not observe their phosphorylation in WT cells (Figure 3.16B). Together, these results indicate that in addition to NF-κB, RECON also controls a cPLA2-MEK-ERK pathway and demonstrates that RECON's enzymatic activity not only modulates inflammation but can also govern whether entire pathways are on or off.

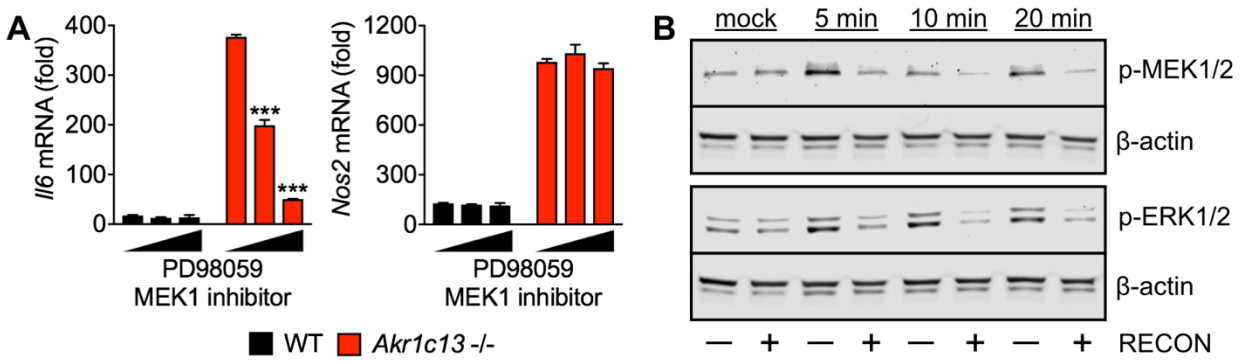

Figure 3.16. RECON puts a brake on MEK-ERK signaling and blocks *Il6* expression. (A) Expression of *Il6* and *Nos2* in cells infected with *L. monocytogenes* for 4 h in the presence of DMSO or PD98059 (MEK1 inhibitor; 25 and 100 μM). The significances indicated in the figure represent the comparison with DMSO mock-treated RECON-deficient cells. (B) Western blot detecting phospho-MEK1/2 and phosho-ERK1/2 in WT (+) or RECON-deficient (-) hepatocytes treated with Pam3CSK4 and Tri-DAP for the indicated times. β-actin was used as a loading control. For qRT-PCR data, *Hprt* was used as an endogenous control and the data are normalized to uninfected mock-treated WT TIB73 cells. Error bars represent ± SEM of technical triplicate. Statistical significance was determined by One-way ANOVA with post-hoc Tukey test (***$p<0.0001$). Data are representative of two independent experiments with similar results.

3.8 Model: RECON suppresses inflammation via targeting inflammatory arachidonic acid oxidation products

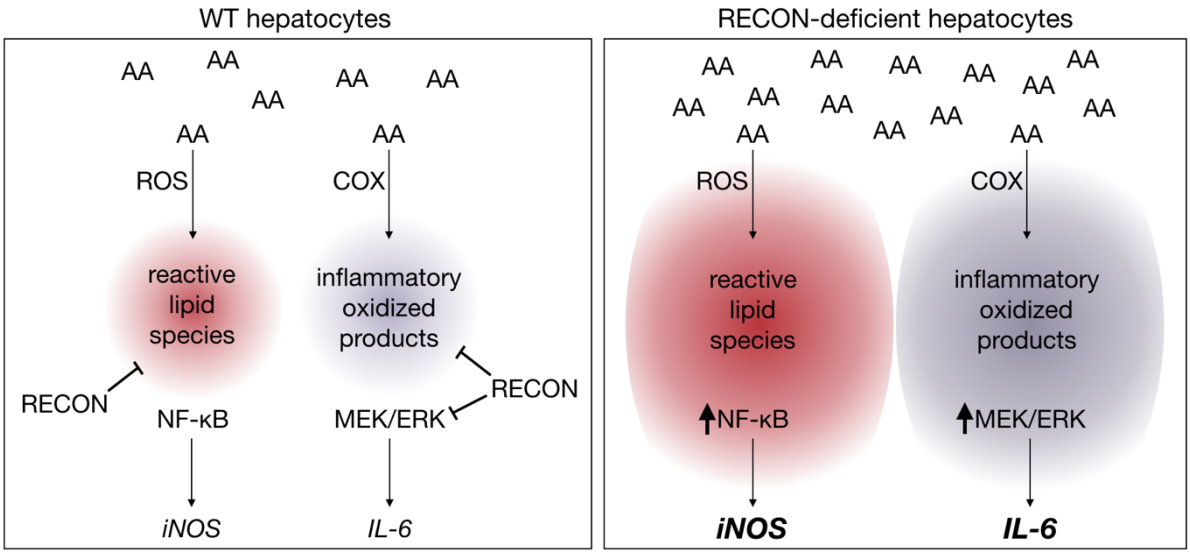

Figure 3.17. RECON suppresses inflammation via targeting inflammatory arachidonic acid oxidation products. In TLR-stimulated hepatocytes, cPLA2 liberates arachidonic acid (AA) which is oxidized via ROS and COX pathways. Reactive lipid species or COX-derived inflammatory oxidized products are suppressed by RECON's enzymatic activity. In the absence of RECON, the free AA pool is increased, and oxidized AA inflammatory products accumulate leading to enhanced expression of iNOS and IL-6.

3.9 Discussion

The work presented in Chapter 2 revealed the requirement of RECON's enzyme activity to modulate inflammatory gene expression during infection, implicating unidentified small molecule metabolites in this process. In this chapter, we provide evidence that RECON's impact on signaling is mediated through modulation of a bifurcated pathway of ROS and COX-2-mediated arachidonic acid signaling. A key finding from these studies is the identification of 4-HNE as a direct substrate of RECON and an RLS involved in RECON-mediated inflammatory responses. 4-HNE is a potent electrophile that is susceptible to nucleophilic conjugation by amino acids (cysteine, lysine, and histidine) and nucleotides. At high concentrations this reactivity promotes cytotoxic aldehyde stress resulting from disruption of protein function and genomic instability, while at low concentrations 4-HNE conjugation to low molecular weight thiols and specific protein receptors has been implicated in signaling that has impacts on a variety of cellular responses (*101*, *103*). While our studies provide evidence that nanomolar levels of 4-HNE can promote inflammatory gene expression, consistent with this later ascribed role, the molecular mechanisms behind these observations are yet to be described.

4-HNE has been reported to be metabolized/detoxified through two primary pathways: enzymatic reduction of the carbonyl by cytosolic reductases (i.e. RECON and AKR1C family members) and Michael addition of glutathione by glutathione transferases (*103*, *104*, *109*, *110*). Glutathione conjugation by the glutathione transferase GSTA4 and subsequent reduction results in the production of glutathione-4-HNE and glutathione-4-dihydroxynonenal (GS-DHN), respectively. GS-DHN has been reported to promote NF-κB activation downstream of LPS sensing in macrophages through an unexplained mechanism (*122*). Another key aspect of 4-HNE cellular signaling is mediated through the activation of the antioxidant stress pathway elicited by the redox sensor Keap1, of which several regulatory cysteines in Keap1 have been reported to be directly alkylated by 4-HNE. Keap1 associates with and regulates the transcription factor Nrf2 and the NF-κB activating kinase IKKβ (*123*, *124*). Interestingly, previous characterization of RECON-mediated control of NF-κB revealed that regulation occurs at the level of IKK, perhaps indicative of a role for Keap1 in this process. The potential role of GS-DHN and Keap1 in mediating NF-κB activation downstream of RECON requires further exploration.

While our findings provide strong evidence for direct turnover of 4-HNE by RECON and regulation of *Nos2* gene expression, the role of this enzyme in PG metabolism is less clear. Following TLR stimulation, loss of RECON enzyme activity has clear impacts on PG metabolites derived from PGH_2. RECON was first cloned from the murine gastrointestinal tract as a PGFS-like synthase due to its cross reactivity with human PGFS antisera. Because PGFS directly metabolizes PGH_2 to $PGF_{2\alpha}$ (*33*), these observations on first pass would imply RECON may have similar enzymatic activity. Interestingly, three of the six eicosanoids that were significantly elevated in the absence of RECON include $PGF_{2\alpha}$, dihomo $PGF_{2\alpha}$, and 8-iso- $PGF_{2\alpha}$. Elevation of these metabolites in the absence of RECON suggests that its enzymatic activity is functionally equivalent to PGFS but may play a role in the oxidation of the 1,3-cyclopentane moiety shared by each of these PGs. However, loss of specific metabolizing enzymes within PG signaling cascades can significantly alter the distribution of other products by increasing flux through alterative pathways, and as such, it is unclear if loss of RECON directly targets the $PGF_{2\alpha}$ moiety or if upstream metabolism shunts PGH_2 metabolism toward these metabolites. Beyond the direct substrate(s) that RECON targets in PG metabolism, the mechanism by which this branch of RECON regulation impacts *Il6* gene expression also remains to be resolved. A thorough record of RECON substrate specificity toward a variety of PGs and characterization of those GPCRs which are differentially activated in the absence of RECON expression will provide significant insight into the molecular mechanisms by which this branch of arachidonic acid metabolism is impacted by this reductase.

The impacts of RECON on inflammatory gene induction are a consequence of RECON's ability to modulate two distinct branches of arachidonic acid metabolism involving enzymatic and ROS-mediated oxidation of this PUFA. A common feature among many murine and human AKRs is the ability to turnover a variety of lipophilic alcohol and aldehyde substrates, including endogenous steroid hormones, isoprenoids, retinoids, as well as oxidized lipids. The ability of RECON to impact NF-κB activation and *Nos2* gene induction through metabolism of ROS-derived 4-HNE and *Il6* expression through turnover of COX-2-derived PGs is likely reflective of a similarly broad substrate repertoire. While addition of exogenous arachidonic acid to RECON-deficient cells resulted in augmented *Il6* expression, this was not observed in WT hepatocytes. These

observations are consistent with an as of yet unidentified brake on *Il6* transcription that is mediated by RECON in an arachidonic acid-independent manner. However, further probing into RECON-controlled regulation of *Il6* expression revealed the importance of the MEK-ERK pathway, which was not active in the presence of RECON. Thus, we have identified a second kinase signaling pathway controlled by RECON in addition to NF-κB. Altogether, it is unlikely that the *in vivo* role of RECON is limited to shaping signaling solely downstream of arachidonic acid, and this enzyme may be involved in a variety of other signaling processes. As such, the impact of RECON on host cell responses is likely versatile and dependent upon substrate availability within distinct cellular and tissue microenvironments.

Surprisingly few studies have interrogated the impact of AKR1C family enzymes during infection conditions, despite a clear role of their substrates in modulating cellular responses to infectious stimuli. Given that loss of RECON enzyme activity and perhaps other AKR1C family enzymes directly enhances inflammation downstream of primary PRRs, it is intriguing to speculate that inhibitors of these enzymes may find utility as host-directed therapies to boost inflammation at sites of infection. One pathological context in which AKR1C family proteins have gained therapeutic notoriety relates to their role in promoting a proliferative environment that drives the progression of malignancies, including prostate cancer, breast cancer, and leukemia. Small molecule inhibitors of human AKRs results in alterations in PG and steroid metabolism, which have shown utility in halting cellular proliferation of malignant cells (*125-127*). The use of cyclic dinucleotides as immunotherapeutics for the treatment of malignant disease has recently garnered significant interest (*128-131*). Within this context, studies have entirely focused on activation of the host cyclic dinucleotide receptor STING. Given our findings that inhibition of RECON enzyme activity alters PG metabolism, which appears key to the antineoplastic activity of AKR1C inhibitors, it is feasible that the therapeutic efficacy of cyclic dinucleotide immunotherapeutics may be beneficially impacted through engagement of this alternative receptor. Given their extensive roles in shaping metabolism of steroid hormones and PGs in a variety of tissues, future studies detailing the impact of AKR1C family enzymes and their inhibitors on both antimicrobial immunity and progression of malignant diseases are more than warranted.

In summary, we have shown that the aldo-keto reductase RECON, which binds to and is enzymatically inhibited by bacterial-derived cyclic dinucleotides, mediates

inflammatory gene expression in hepatocytes following TLR stimulation by altering mobilization of free arachidonic acid pools and impacting levels of arachidonic acid-derived oxidized lipid metabolites. Arachidonic acid signaling during inflammation is of central importance to the development of immune responses and is one of the most pharmacologically targeted branches of inflammation (*90*). As such, these findings are particularly noteworthy in that they provide evidence linking TLR-mediated pattern recognition with cytosolic surveillance of bacterial metabolites through a mechanism involving metabolism of arachidonic acid. The unique integration of cytosolic sensing with metabolism of inflammatory lipid mediators likely provides the host with a means of boosting innate immune responses to cytosolic pathogens. These studies may provide a new paradigm by which AKRs of human and murine origin shape immune responses through sensing of c-di-AMP or other regulatory metabolites from endogenous, infectious, or synthetic sources.

3.10 Materials and Methods

Cell culture and reagents

TIB73 is a spontaneously immortalized hepatocyte cell line from a BALB/c embryo liver (sex unknown, not provided by the original depositor). The cell line was authenticated by and purchased from ATCC. The cells were grown at 37°C in 5% CO2 in phenol red-free DMEM with 10% heat-inactivated FBS and supplemented with 2 mM sodium pyruvate and 1 mM L-glutamine. For passaging, cells were maintained in penicillin-streptomycin (100U/mL) but were plated in antibiotic-free medium for infections and stimulations. J2 immortalized BMDMs (iBMDMs) were grown in the same medium as above except with additional supplementation of 55 μM 2-mercaptoethanol and M-CSF harvested from L929 conditioned medium (final volume 10%).

Stimulations and *L. monocytogenes* infections of cell lines

$1x10^6$/3 mL of TIB73 hepatocytes were seeded per well in 6-well plates the day before stimulation or *L. monocytogenes* (10403S lab strain) infection. *L. monocytogenes* strain 10403S was struck out onto BHI agar, grown overnight at 37°C, and then stored at 4°C for up to one month. For infections, one colony of *L. monocytogenes* was inoculated into 3 mL of BHI and grown overnight, static at 30°C. The morning of infection, 1 mL of culture

(normalized to OD600 1.1) was centrifuged and washed 3x with 1 mL of sterile 1X PBS. The pellet was resuspended in 1 mL of 1X PBS for infections. TIB73 cells were first washed 2x in 1X PBS prior to addition of bacteria. *L. monocytogenes* strains were diluted 1:100 in pre-warmed cell culture medium containing 0.1% FBS. 2 mL of diluted bacteria was overlaid onto the host cells and placed at 37°C for 1 hour. Following infection, the cells were washed 2x with 1X PBS and placed into complete medium containing gentamicin (50 μg/ml) to kill extracellular bacteria. For stimulations with TLR or NOD ligands, the cells were washed 2x in 1X PBS and overlaid with pre-warmed complete medium containing 1 μg/mL LPS, 1 μg/mL Pam_3CSK_4 alone, or 100 ng/mL Pam3CSK4 plus 1 μg/mL Tri-DAP. 4-HNE was exogenously added to cells at 0.1, 1.0, and 10 nM. Arachidonic acid and eicosapentaenoic acid were used at 10 μM final concentrations.

Inhibitor experiments

Inhibitors of signaling pathways were added to cells for 1 hour prior to stimulation/infection. Cells were maintained in the presence of the inhibitors during stimulation/infection and then again after bacteria were washed off, out to 2-4 hpi. All inhibitors were reconstituted in DMSO, which by itself was used as a control treatment (mock). The final concentrations of inhibitors used in experiments are provided in the figure legends and sources are in the Key Resources Table below (Table 3.1).

RNA isolation and real-time qPCR

RNA was extracted with the RNAqueous Total RNA Isolation Kit (Ambion), DNase treated using the TURBO DNA-free Kit (Ambion) and reverse-transcribed with the iScript cDNA synthesis kit (Bio-Rad). TaqMan RT-qPCR assays were used for quantification of mouse *Il6* and *Nos2* and the endogenous control *Hprt*. Primer/probe ID information is provided in the in the supplementary Key Resources Table.

CRISPR/Cas9 mutagenesis

TIB73 hepatocytes deficient in RECON (*Akr1c13*-/-) generated by CRISPR/Cas9-mediated mutagenesis and also complemented with WT or the enzymatically dead H117A mutant have been described previously (1). Cas9 guide sequences specifically targeting *Pla2g4a* were determined using http://crispr.mit.edu/ (sequence information is provided in the in the Key Resources Table below). Annealed *Pla2g4a*-targeting guide sequence oligos were cloned into pSpCas9(BB)-2A-Puro (PX459) V2.0 containing Cas9

and the sgRNA scaffold as previously described (*76*). Cells were transfected with the CRISPR plasmids using TransIT-LT1 transfection reagent (per manufacturer's instructions), placed on puromycin selection (10 μg/mL) at 48 hours, selected for another 48 hours, and the surviving cells were expanded and screened by Western blot.

Immunoblotting

Cells were lysed in Pierce IP lysis buffer in the presence of protease and phosphatase inhibitors (Thermo Fisher). Protein concentrations were determined by BCA assay (Thermo Fisher), 20-60 μg of protein was boiled in Laemmli buffer (Bio-Rad) with 2-mercaptoethanol and Westerns were run using nitrocellulose membranes. Membranes were blocked in 5% non-fat dry milk in 1X TBS for 45 min at room temperature, followed by overnight incubation in primary antibodies diluted 1:1,000 in 5% BSA in 1X TBS-T. Antibody information is provided in the supplementary Key Resources Table.

Comprehensive eicosanoid profiling

WT or *Akr1c13*-/- cells were plated in 6-well dishes and rested overnight. Prior to stimulation, the cells were washed 2x with 1X PBS. The cells were stimulated with 100 ng/mL Pam3CSK4 plus 1 μg/mL Tri-DAP in complete phenol red-free medium and the supernatants were collected at 5 and 20 min post-treatment and snap frozen. Samples were analyzed in biological triplicate. Comprehensive eicosanoid profiling and lipid analysis was performed at the UCSD Lipidomics Core (*132*).

Lipid droplets and microscopy

TIB73 cells were plated on collagen-coated coverslips (Corning BioCoat) deposited in 6-well plates and rested overnight. The cells were co-stimulated with LPS (1 μg/mL) plus arachidonic acid (50 μM) for 1-4 hours and then stained following the Oil Red O staining kit instructions (minus hematoxylin) (Sigma-Aldrich MAK19). Lipid droplets were imaged with a Keyence BZ-X710 microscope and quantified using the BZ-X700 series automated analysis application.

Enzyme activity assays

To measure RECON enzyme activity, 4-HNE was mixed with NADPH (200 μM) in 1X PBS to a final reaction volume of 200 μL and initiated by addition of 5 μM recombinant RECON (purified as described previously (*78*)). Absorbance (340 nm) was measured

using a Synergy HT plate reader. NF-κB luciferase assays were performed as previously described (*78*).

Flow cytometry

$1x10^6$ TIB73 cells treated with 4-HNE or Pam3CSK4 were pelleted, resuspended in 1 mL of cold 1:1 MeOH:Acetone and fixed/permeabilized on ice for 30 min. The cells were washed 2x with 1 mL FACS buffer (1% BSA and 0.1% NaN_3 in PBS). Cells were stained with anti-4-HNE antibody (Abcam ab46545) diluted 1:100 in 50 μL FACS buffer for 1 h on ice. Cells were washed 2x with 1 mL FACS buffer and stained with secondary antibody diluted 1:500 in 50 μL FACS buffer for 1 h on ice in the dark. Cells were washed 2x with 1 mL FACS buffer and resuspended in 300 μL FACS buffer. The cells were analyzed by flow cytometry using a BD LSR II and the data were analyzed with FlowJo software.

Quantification and statistical analysis

All data were plotted and analyzed using Prism 7 software. Specific tests used for determination of statistical significance are detailed in the figure legends.

Table 3.1: Key resources table

Reagent or Resource	Source	Identifier
Antibodies		
Anti-4-hydroxynonenal antibody pAb	Abcam	Cat#ab46545
Anti-mouse/human β-Actin (8H10D10) mouse mAb	Cell Signaling	Cat#3700S
Anti-phospho-MEK1/2 (Ser217/221) (41G9) rabbit mAb	Cell Signaling	Cat#9154
Anti-phospho-ERK1/2 (Thr202/Tyr204) (D13.14.4E) rabbit mAb	Cell Signaling	Cat#4370
Anti-PLA2G4A rabbit pAb	Thermo Fisher Scientific	Cat#PA5-29100; RRID: AB_2546576
Anti-Cox2 (D5H5) rabbit mAB	Cell Signaling	Cat#12282S
IRDye 680RD Goat anti-Mouse IgG	Licor	Cat#926-68070
IRDye 800CW Goat anti-Rabbit IgG	Licor	Cat#926-32211
Anti-rabbit IgG Alexa Fluor 488 secondary	Thermo Fisher Scientific	Cat# A-11034
Bacterial Strains		
Listeria monocytogenes 10403S wild-type	Provided by Dan Portnoy	JW06
Chemicals, Peptides, and Recombinant Proteins		
DMEM, high glucose, no glutamine, no phenol red	Thermo Fisher Scientific	Cat#31053036
Sodium pyruvate	Thermo Fisher Scientific	Cat#11360070
L-Glutamine	Thermo Fisher Scientific	Cat#25030081
Characterized Fetal Bovine Serum	Thermo Fisher Scientific	Cat#SH30071.03
Penicillin-Streptomycin (10,000 U/mL)	Thermo Fisher Scientific	Cat#15140122

Bovine Serum Albumin (BSA)	Fisher BioReagents	Cat#BP9700100
Trypsin-EDTA (0.05%)	Thermo Fisher Scientific	Cat#25300054
Brain Heart Infusion Broth	Research Products International	Cat#B11000
Gentamicin (10 mg/mL)	Thermo Fisher Scientific	Cat#15710072
Puromycin Dihydrochloride	Thermo Fisher Scientific	Cat#A1113803
Dimethyl sulfoxide	Sigma-Aldrich	Cat#D2650
BioCoat Collagen I 22mm round coverslips	Corning	Cat#354089
10% neutral buffered formalin	VWR	Cat#16004-115
Oil Red O	Sigma-Aldrich	Cat#O0625
Celastrol (NF-κB inhibitor; 0.1 and 1.0 μM)	InvivoGen	Cat#ant-cls
PD98059 (MEK1 inhibitor; 25 and 100 μM)	InvivoGen	Cat# tlrl-pd98
Aristolochic acid I (PLA2 inhibitor; 25 and 100 μM)	Sigma-Aldrich	Cat#A5512
Flurbiprofen (COX-1/2 inhibitor; 0.1 and 1.0 μM)	Santa Cruz Biotechnology	Cat# sc-202158
Celecoxib (COX-2 inhibitor; 0.1 and 1.0 μM)	Sigma-Aldrich	Cat#PZ0008
Ketoconazole (CYP450 inhibitor; 0.1 and 1.0 μM)	Santa Cruz Biotechnology	Cat#sc-200496
Zileuton (5-LOX inhibitor; 2.0 and 20 μM)	Santa Cruz Biotechnology	Cat#sc-204417
Diphenyleneiodonium chloride (DPI) (NOX inhibitor; 10 and 100 μM)	Cayman Chemical	Cat#81050
LPS from *E. coli*	Sigma-Aldrich	Cat#L4391
Tri-DAP (NOD1 ligand)	InvivoGen	Cat#tlrl-tdap
Pam_3CSK_4 (TLR2 ligand)	InvivoGen	Cat#tlrl-pms
Arachidonic acid (AA)	Cayman Chemical	Cat#90010
Eicosapentaenoic acid (EPA)	Cayman Chemical	Cat# 90110
Recombinant murine AKR1C13 (RECON)	McFarland et al., 2017	N/A
NADPH	MP Biomedicals	Cat#0215174225
4-hydroxynonenal (4-HNE)	Cayman Chemical	Cat#32100
Halt Protease and Phosphatase Inhibitor Cocktail	Thermo Fisher Scientific	Cat#78442
Pierce IP Lysis Buffer	Thermo Fisher Scientific	Cat#87787
Any kD Mini-PROTEAN TGX Precast Protein Gels	Bio-Rad	Cat#4569034
4x Laemmli Sample Buffer	Bio-Rad	Cat#1610747
Critical Commercial Assays		
TURBO DNA-free Kit	Thermo Fisher Scientific	Cat#AM1907
iScript cDNA synthesis kit	Bio-Rad	Cat#1708891
Maxima SYBR Green/ROX qPCR Master Mix	Thermo Fisher Scientific	Cat#K0221
RNAqueous Total RNA Isolation Kit	Thermo Fisher Scientific	Cat#AM1912
TaqMan pre-designed assay: murine *Nos2*	Thermo Fisher Scientific	Mm00440502_m1
TaqMan pre-designed assay: murine *Il6*	Thermo Fisher Scientific	Mm00446190_m1
TaqMan pre-designed assay: murine *Hprt*	Thermo Fisher Scientific	Mm03024075_m1
TransIT-LT1 Transfection Reagent	Mirus Bio	Cat#MIR2300
Experimental Models: Cell Lines		

TIB73	ATCC	ATCC Cat# BNL CL.2 TIB-73; RRID:CVCL_4383
TIB73 mutant *Akr1c13*	McFarland et al., 2017	N/A
TIB73 mutant *Akr1c13* with MSCV-*Akr1c13*-WT	McFarland et al., 2017	N/A
TIB73 mutant *Akr1c13* with MSCV-*Akr1c13*-H117A	McFarland et al., 2017	N/A
TIB73 mutant *Pla2g4a*	This work	N/A
TIB73 mutant *Akr1c13*, mutant *Pla2g4a*	This work	N/A
Oligonucleotides		
Pla2g4a sgRNA1 forward: CACCGCAGTAAACTTATGGGAGTAC	This work	N/A
Pla2g4a sgRNA1 reverse: AAACGTACTCCCATAAGTTTACTGC	This work	N/A
Pla2g4a sgRNA2 forward: CACCGATAATGATATAAACCCCGTG	This work	N/A
Pla2g4a sgRNA2 reverse: AAACCACGGGGTTTATATCATTATC	This work	N/A
Pla2g4a sgRNA3 forward: CACCGGGTTTCATCCATGACGTAGT	This work	N/A
Pla2g4a sgRNA3 reverse: AAACACTACGTCATGGATGAAACCC	This work	N/A
Pla2g4a sgRNA4 forward: CACCGGATGGATGCCAACTACGTCA	This work	N/A
Pla2g4a sgRNA4 reverse: AAACTGACGTAGTTGGCATCCATCC	This work	N/A
Recombinant DNA		
pSpCas9(BB)-2A-Puro (PX459) V2.0	Ran et al., 2013	Addgene Plasmid #62988
pmaxGFP	Amaxa	N/A
NF-κB promoter luciferase reporter	InvivoGen	Cat#pnifty-luc
Software and Algorithms		
ImageJ	ImageJ Software	https://imagej.nih.gov/ij/
BZ-X700 series microscope analysis application	Keyence	BZ-H3AE
GraphPad Prism 7	GraphPad Software	http://www.graphpad.com/scientificsoftware/prism/
ApE- A plasmid Editor	University of Utah Biology	http://biologylabs.utah.edu/jorgensen/wayned/ape/
Benchling	Benchling Software	https://benchling.com/
CRISPR Design	Zhang Lab, MIT	http://crispr.mit.edu/

Chapter 4

Listeria monocytogenes and RECON: a "Tail" of Nitric Oxide

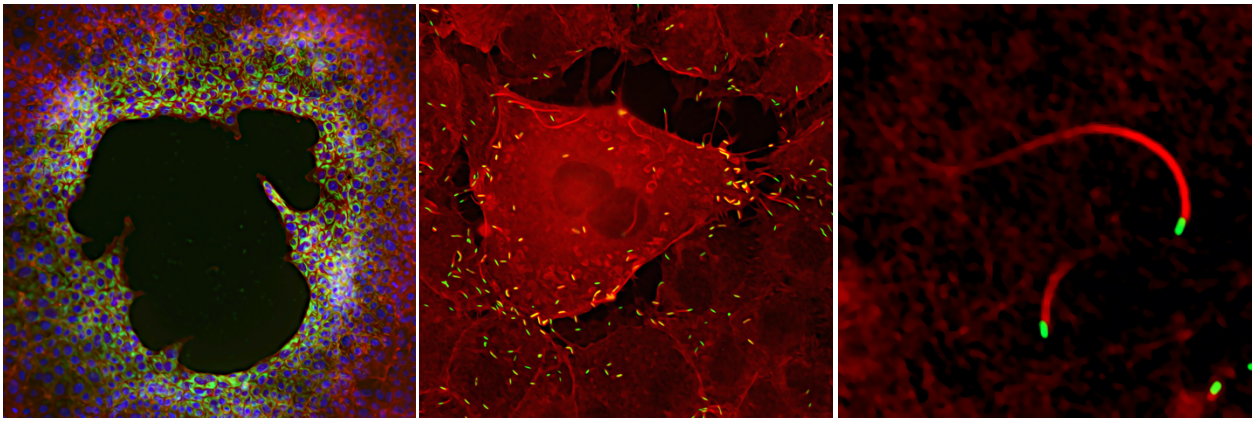

The following work has been published as: McFarland, A.P., Shukun, L., Ahmed-Qadri, F., Zuck, M., Thayer, E.F., Goo, Y.A., Hybiske, K., Tong, L., Woodward, J.J. "Sensing of Bacterial Cyclic Dinucleotides by the Oxidoreductase RECON Promotes NF-κB Activation and Shapes a Proinflammatory Antibacterial State." *Immunity* 9.3 (2018): e00526-18.

4.1 Summary

The oxidoreductase RECON is a high affinity cytosolic sensor of bacterial-derived cyclic dinucleotides (CDNs). CDN binding inhibits RECON's enzymatic activity and subsequently promotes inflammation. In this study, we sought to characterize the effects of RECON on the infection cycle of the intracellular bacterium *Listeria monocytogenes*, which secretes cyclic di-AMP (c-di-AMP) into the cytosol of infected host cells. Here, we report that during infection of RECON-deficient hepatocytes, which exhibit hyper-inflammatory responses, *L. monocytogenes* exhibits significantly enhanced cell-to-cell spread. Enhanced bacterial spread could not be attributed to alterations in PrfA or ActA, two virulence factors critical for intracellular motility and intercellular spread. Detailed microscopic analyses revealed that in the absence of RECON, *L. monocytogenes* actin tail lengths were significantly longer and there was a larger number of faster moving bacteria. Complementation experiments demonstrated that the effect of RECON on *L. monocytogenes* spread and actin tail lengths was linked to its enzymatic activity. RECON enzyme activity suppresses NF-κB activation and is inhibited by c-di-AMP. Consistent

with these previous findings, we found that augmented NF-κB activation in the absence of RECON caused enhanced *L. monocytogenes* cell-to-cell spread and that *L. monocytogenes* spread correlated with c-di-AMP secretion. Finally, we discovered that, remarkably, increased NF-κB-dependent iNOS expression and nitric oxide production was responsible for promoting *L. monocytogenes* cell-to-cell spread. The work presented here supports a model whereby *L. monocytogenes* secretion of c-di-AMP inhibits RECON's enzymatic activity, drives augmented NF-κB activation and nitric oxide production, and ultimately enhances intercellular spread.

4.2 Background

A key feature that distinguishes pathogens from innocuous microorganisms is the purposeful breach of the host cell membrane. The crosstalk between cytosolic surveillance by innate immune receptors and stress sensors has emerged as a key process by which host cells coordinate and amplify their response to eliminate infectious organisms. Cyclic dinucleotides (CDNs) are central mediators of the host cytosolic immune responses to infection. In addition to the well characterized STING-dependent inflammatory response, we recently identified the murine aldo-keto reductase (AKR) RECON, encoded by *Akr1c13*, as a cytosolic sensor of bacterial CDNs and a negative regulator of NF-κB-dependent inflammation (see Chapter 2 and (*78*)).

Bacterial pathogens have evolved to evade immune surveillance, subvert host signaling downstream of sensing, and resist antimicrobial responses by the host. Many human pathogens produce cyclic diadenosine monophosphate (c-di-AMP), the only known essential bacterial CDN. In bacteria, c-di-AMP regulates bacterial growth, cell wall homeostasis and central metabolism (*15-17*). While the role of c-di-AMP-induced inflammation in the host is best characterized with *L. monocytogenes*, its effects on other bacteria, including *M. tuberculosis*, *Chlamydia trachomatis*, *Staphylococcus aureus* and Group B Streptococci (GBS), have recently begun to emerge. GBS evade c-di-AMP-mediated immunity by actively hydrolyzing extracellular nucleotide (*23*). Similarly, *M. tuberculosis* hydrolyzes c-di-AMP during infection, and genetic mutants that produce elevated levels of c-di-AMP are highly attenuated (*19, 27*).

Unlike GBS and *M. tuberculosis*, which appear to evade this branch of immunity, *L. monocytogenes* actively secretes c-di-AMP into the host cytosol via the action of several

multidrug resistant (MDR) transporters with relatively minimal effects on pathogenesis in vivo (*38, 133-135*), suggesting that this pathogen has evolved resistance to the host responses that c-di-AMP elicits. In line with this reasoning, we previously reported that augmented inflammation in RECON-deficient hepatocytes restricted growth of *Chlamydia* spp. whereas the replication of *L. monocytogenes* was unaffected (see Chapter 2 and (*78*)). *L. monocytogenes* has evolved resistance against several key cell intrinsic host defense mechanisms, including the phagolysosomal pathway, autophagy, and reactive oxygen species (*136, 137*). However, the antimicrobial effects elicited by RECON, to which *L. monocytogenes* has seemingly developed resistance, and the consequences on bacterial activity within the host cell are currently unknown.

In this chapter, we investigated the impact of RECON on the intracellular lifecycle of *L. monocytogenes* growing in hepatocytes. Hepatocytes were studied owing to their high expression of RECON as well as their status as a dominant cellular reservoir of *L. monocytogenes* during systemic infection (*62, 138*). Remarkably, we found that *L. monocytogenes* exhibited enhanced cell-to-cell spread in the hyperinflammatory conditions resulting from the absence of RECON. This phenotype was dependent on NF-κB and ensuing nitric oxide production, the latter of which could enhance *L. monocytogenes* spread in a variety of host cells. Furthermore, the intracellular secretion of c-di-AMP correlated with *L. monocytogenes* cell-to-cell spread, a process that was dependent on RECON and NF-κB. Therefore, we propose a model whereby *L. monocytogenes* secretion of c-di-AMP inhibits RECON's enzymatic activity, drives augmented NF-κB activation and nitric oxide production, and ultimately enhances intercellular spread.

To date, bacterial CDNs in eukaryotes are solely appreciated for their capacity to activate cytosolic sensing pathways in innate immunity. However, it remains unclear whether pathogens that actively secrete CDNs benefit from this process. In this chapter, we provide evidence that secretion of CDNs leads to enhancement of *L. monocytogenes* cell-to-cell spread. This is a heretofore unknown role of these molecules and suggests *L. monocytogenes* may benefit from their secretion in certain contexts. Molecular characterization revealed that, surprisingly, nitric oxide was responsible for the enhanced spread. Pathogens act to prevent nitric oxide production or, like *L. monocytogenes*, they have evolved to resist its direct antimicrobial effects. This chapter provides evidence that intracellular bacterial pathogens not only tolerate nitric oxide, which is inevitably

encountered during infection, but can also capitalize on the changes this pleiotropic molecule enacts on the host cell.

4.3 The absence of RECON enhances intercellular spread of *L. monocytogenes*

As part of its intracellular lifecycle, *L. monocytogenes* utilizes cell-to-cell spread to evade extracellular immune defenses while multiplying within the host. We previously reported that the absence of RECON in the murine embryonic hepatocyte cell line TIB73 did not affect the intracellular replication of *L. monocytogenes* (see Chapter 2 and (*78*)). However, when we examined *L. monocytogenes* cell-to-cell spread, which can be

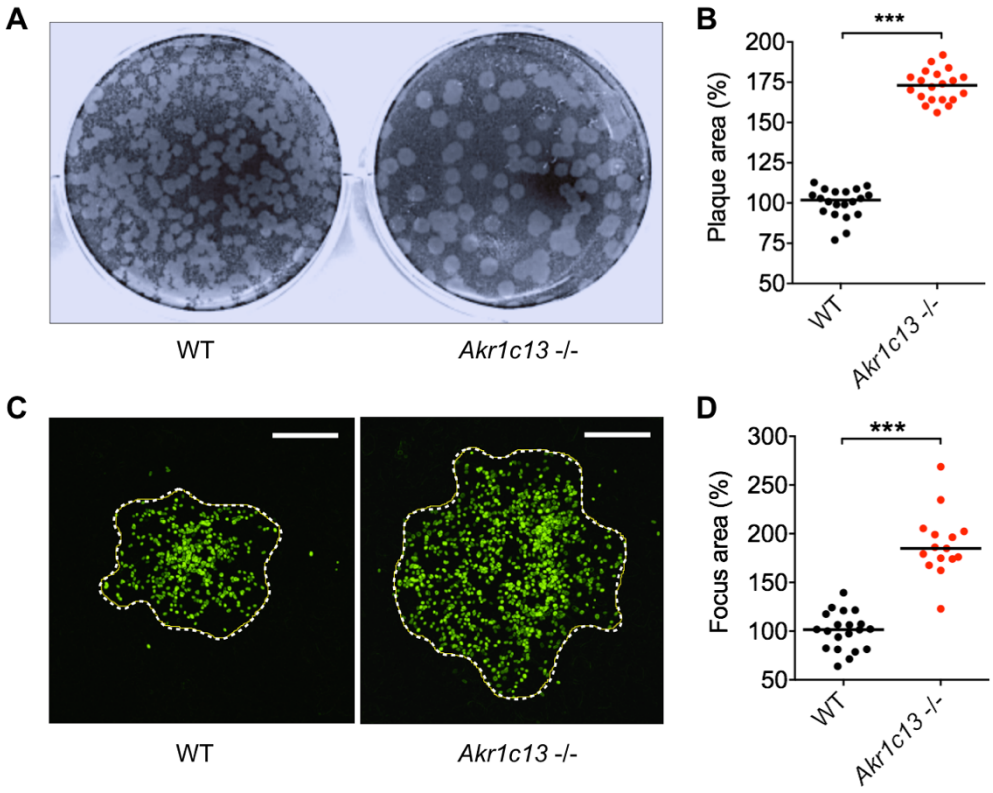

Figure 4.1. *L. monocytogenes* has enhanced cell-to-cell spread in RECON-deficient hepatocytes. (A) Images of *L. monocytogenes* plaques (white) spreading through a monolayer of TIB73 cells (black area) for 72 h in a 6-well plate. (B) Quantification of plaque areas as shown in (A). (C) Images of L. monocytogenes (green) spreading through TIB73 cells (black area) for 8 h. Dotted line indicates the edge of the focus area. Scale=50 μm. (D) Quantification of focus areas as shown in (C). Median values are indicated by a bar. All data points are shown and are plotted as percent of spread in WT TIB73 cells. Data are representative of more than 4 independent experiments. Statistical significance was determined by Mann-Whitney U test (***$p<0.0001$).

visualized and quantified by the presence and size of plaques within a monolayer of cells, we discovered that the loss of RECON resulted in *L. monocytogenes* plaques that were significantly larger than those seen in WT hepatocytes (Figure 4.1A and 4.1B).

The increased spreading was also observed early during infection by microscopy, where the average area of *L. monocytogenes* foci in RECON-deficient cells at 8 hours post-infection (hpi) was increased to a similar magnitude and significance as observed by plaque assay (Figure 4.1C and 4.1D). We chose to focus on the effects of RECON on *L. monocytogenes* cell-to-cell spread in hepatocytes versus macrophages given that hepatocytes are a major cellular reservoir for *L. monocytogenes* during systemic infection and are the predominant cellular constituent of the liver where *L. monocytogenes* focus areas have been visualized in vivo (*138-143*).

4.4 Increased cell-to-cell spread in RECON-deficient cells is likely not due to direct enhancement of *L. monocytogenes* virulence programs

4.4.1 *L. monocytogenes* has increased virulence gene expression in RECON-deficient hepatocytes

L. monocytogenes cell-to-cell spread is governed by the coordinated expression of virulence factors involved in vacuolar escape, actin polymerization, and protrusion formation. We measured the expression of several key virulence genes during infection

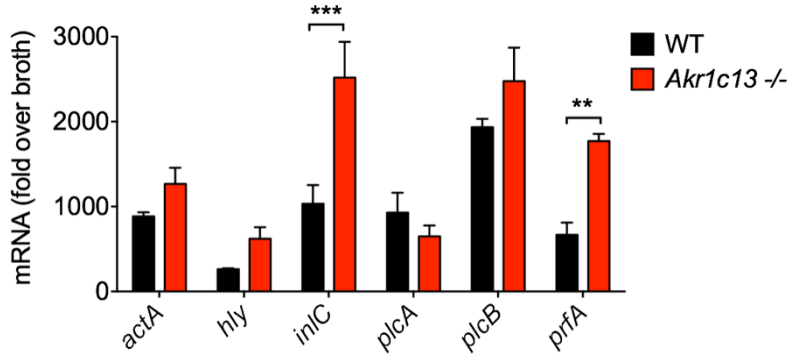

Figure 4.2. Increased expression of *L. monocytogenes inlC* and *prfA* in RECON-deficient hepatocytes. Expression of the indicated *L. monocytogenes* virulence genes during infection of WT or RECON-deficient TIB73 cells at 5 hpi. *16S rRNA* was used an endogenous control. Error bars represent ± SD of biological duplicates. Statistical significance was determined by 2way ANOVA with Bonferroni's multiple comparisons test (**$p \leq 0.001$; ***$p \leq 0.0001$).

of WT or RECON-deficient hepatocytes to determine if increased virulence gene expression could explain the enhanced spread. We observed increased expression of two virulence genes in RECON-deficient cells, *inlC* and *prfA* (Figure 4.2).

4.4.2 Increased InlC, PrfA and ActA levels cannot account for the enhanced spread

InlC encodes for internalin C, an effector protein involved in promoting protrusion formation by disturbing apical cell tight junctions (*144*). To test whether the increased expression of *inlC* might explain the enhanced spread, we infected WT or RECON-deficient hepatocytes with a Δ*inlC* strain. We observed that the Δ*inlC* strain had enhanced spread similar to wild-type *L. monocytogenes* in RECON-deficient cells (Figure 4.3A). Therefore, we concluded that internalin C was not involved in the enhanced spread. PrfA is a master, pleiotropic activator of virulence genes in *L. monocytogenes* (*145*). To test if enhanced PrfA activity could promote increased cell-to-cell spread in TIB73 hepatocytes, we infected cells with a strain of *L. monocytogenes* that expressed a constitutively active form of PrfA (PrfA*), which leads to overexpression of virulence factors (*146*). The PrfA* strain did not form larger foci or plaques in WT TIB73 cells (Figure 4.3B), indicating increased PrfA activity is not sufficient to drive enhanced spread. These data are consistent with previous reports that also found equivalent cell-to-cell spread of wild-type *L. monocytogenes* and the PrfA* strain (*147, 148*). Therefore, we concluded that increased PrfA activity did not underlie the enhanced spread in RECON-deficient cells.

Cell-to-cell spread by *L. monocytogenes* is governed by the polymerization of host cell F-actin into "comet" tails and enables the bacteria to protrude and spread into neighboring cells (*149*). ActA, which is expressed upon entry into the cytosol, is required for the formation of *L. monocytogenes* actin tails. Perpetuation of bacterial motility depends on sufficient actin accumulation on the bacterial cell surface to induce and maintain actin nucleation (*150*). We were not able to directly assess ActA protein levels in TIB73 hepatocytes because even with high concentrations of bacteria the maximum MOI is around 0.02. Therefore, we tested whether increased ActA expression in *L. monocytogenes* could drive enhanced spread in TIB73 hepatocytes by employing a strain that expressed two copies of the *actA* gene. We did not observe increased cell-to-cell spread of this strain in TIB73 cells (Figure 4.3C). This is consistent with two previous reports, where a 10-20% increase in ActA protein level or 400-fold increase in ActA

activity had no effect on *L. monocytogenes* plaque size (*151, 152*). Therefore, we concluded that increased levels of ActA were not sufficient to drive enhanced spread and could not account for enhanced *L. monocytogenes* spread in RECON-deficient cells.

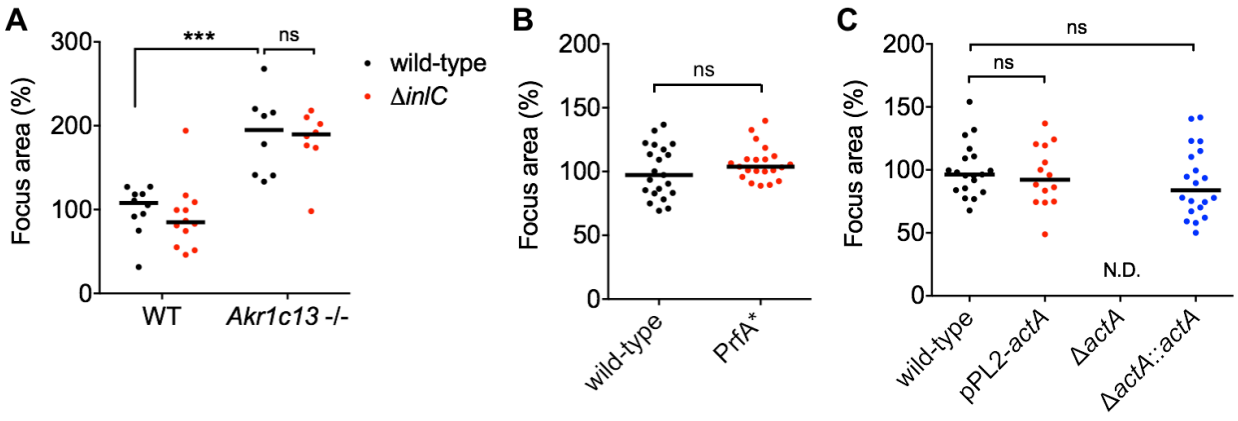

Figure 4.3. Increased cell-to-cell spread in RECON-deficient cells is likely not due to direct enhancement of *L. monocytogenes* virulence programs. (A) Quantification of focus areas in WT or *Akr1c13*-deficient TIB73 cells infected with wild-type or Δ*inlC L. monocytogenes* strains. (B-C) Focus areas of the indicated *L. monocytogenes* strains in WT TIB73 cells. Foci were measured at 8 hpi. Median values are indicated by a bar. All foci measured are shown ($N \geq 8$) and are plotted as percent of wild-type *L. monocytogenes* spread in WT TIB73 cells. Data are representative of at least two independent experiments. Statistical significance was determined by Mann-Whitney U test (***$p \leq 0.0001$; ns = not significant).

4.4.3 RECON controls the intercellular spread of *Burkholderia thailandensis*

Since the increased *L. monocytogenes* cell-to-cell spread was not dependent on InlC or PrfA activation, or elevated ActA levels, we reasoned that perhaps the effect on intercellular spread in the absence of RECON may not be *L. monocytogenes*-specific. We infected monolayers of WT or RECON-deficient hepatocytes with the intracellular pathogen *Burkholderia thailandensis*, which utilizes Arp2/3 complex-mediated cell-to-cell spread analogous to *L. monocytogenes* (*153, 154*). We found *B. thailandensis* plaque size was also significantly increased in the absence of RECON (Figure 4.4). Taken together, these results suggested that the increased spread was likely not due to direct enhancement of *L. monocytogenes*-specific virulence programs but rather may involve alteration of the host cell itself, perhaps though alterations in host factors that affect Arp2/3 complex and F-actin dynamics.

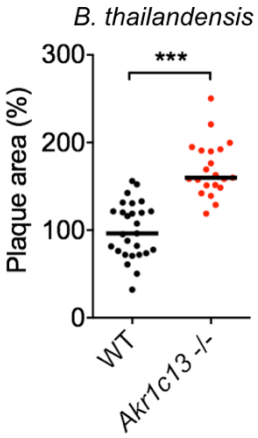

Figure 4.4. *Burkholderia thailandensis* has enhanced cell-to-cell spread in RECON-deficient hepatocytes. Plaque areas in WT or *Akr1c13*-deficient TIB73 cells infected with *B. thailandensis* for 16 h. All plaques measured are shown (N ≥ 20) and are plotted as percent of spread in WT TIB73 cells. Data are representative of two independent experiments. Statistical significance was determined by Mann-Whitney U test (***p ≤ 0.0001).

4.5 *L. monocytogenes* have longer actin tails and increased speed in RECON's absence

4.5.1 *L. monocytogenes* have longer actin tails in RECON-deficient hepatocytes

We next examined the effects of RECON deficiency on *L. monocytogenes* spread through immunofluorescence microscopy. These studies revealed that *L. monocytogenes* actin tails

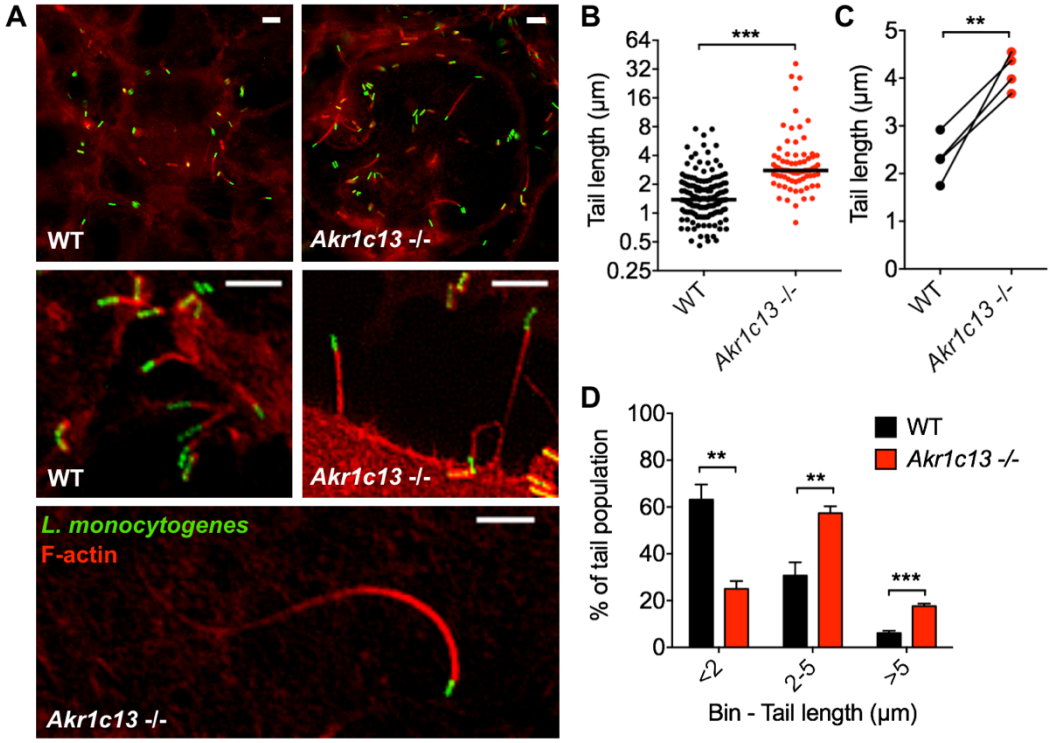

Figure 4.5. *L. monocytogenes* have longer actin tails in RECON-deficient hepatocytes. (A) Images of *L. monocytogenes* (green) associated with F-actin (red) in TIB73 cells at 8 hpi. All scales=5 µm. (B) Quantification of *L. monocytogenes* actin tail lengths in WT or *Akr1c13*-deficient TIB73 hepatocytes. Statistical significance was determined by unpaired, nonparametric, two-tailed Kolmogorov-Smirnov test comparing the cumulative

distributions (***p ≤ 0.0001). (C) Same as in (B) but shown are the mean tail lengths measured from 4 independent experiments each with 75-150 tails quantified. (D) Data from (C) plotted as binned (<2, 2-5, or >5 μm) tail lengths. Actin tail lengths were measured at 6-8 hpi. Median values are indicated by a bar. Data are from four independent experiments. In (C) and (D) statistical significance was determined by Mann-Whitney U test (**p ≤ 0.001; ***p ≤ 0.0001).

were significantly longer in RECON-deficient cells compared to WT (Figure 4.5A and 4.5B), a trend that was consistent across multiple experiments (Figure 4.5C). The profile of tail lengths shifted from predominantly <2 μm in length in WT cells to between 2-5 μm in RECON-deficient cells, with a nearly 3-fold increase in bacteria associated with tails >5 μm (Figure 4.5A and 4.5D).

4.5.2 *L. monocytogenes* exhibits increased rates of movement and longer duration of actin tail association in RECON-deficient cells

Previous work has demonstrated that *L. monocytogenes* tail length directly correlates with the speed of individual bacteria (*155*). However, alterations in the host cell actin disassembly machinery can lead to longer tails without affecting bacterial speed (*156, 157*). Therefore, we sought to determine whether the longer *L. monocytogenes* actin tails in RECON-deficient cells correlated with increased rates of movement or whether the

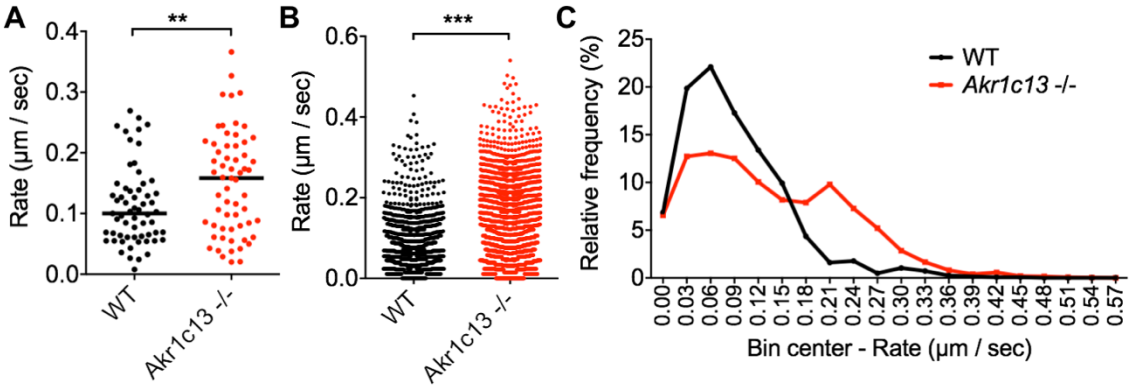

Figure 4.6. *L. monocytogenes* exhibits increased rates of movement in the absence of RECON. (A) Average movement rates of *L. monocytogenes* in TIB73 cells, at 6-8 hpi. Each data point represents an individual bacterium. Images were captured every 10 sec and averaged across at least 6 frames. At least 60 bacteria were measured for each infected cell type. (B-C) Compilation of all *L. monocytogenes* rates from the individual bacteria measured in (A). Data are plotted as unbinned (B) or binned (C). *L. monocytogenes* rates were measured at 6-8 hpi. Median values are indicated by a bar. Statistical significance was determined by unpaired, nonparametric, two-tailed Kolmogorov-Smirnov test comparing the cumulative distributions (**p ≤ 0.001; ***p ≤ 0.0001).

longer tails may be the result of decreased actin depolymerization. We tracked and measured the speed of individual bacteria, and when we compared the average rates of movement for each bacterium across the time course, we observed a significant increase in speed in RECON-deficient cells (Figure 4.6A). *L. monocytogenes* is known to exhibit extreme changes in speed and frequent stops (*150*). Therefore, we also compared the collective rates of movement for each 10 second imaging interval and found that the bacteria in RECON-deficient cells were moving significantly faster between time points than those in WT cells (Figure 4.6B). A binned histogram of these data showed a smooth distribution of rates of *L. monocytogenes* in WT cells, with a peak around 0.05 μm/sec (Figure 4.6C), which is within the range of *L. monocytogenes* speeds reported in other cell types (*158-162*). The histogram in RECON-deficient cells, however, showed a shift toward higher rates, with a second peak emerging at 0.20 μm/sec. Therefore, a significant proportion of the intracellular *L. monocytogenes* population was moving faster than the average rate of movement in the absence of RECON.

4.5.3 *L. monocytogenes* have increased times of motility and association with their actin tails in the absence of RECON

Remarkably, we also found that in the absence of RECON, *L. monocytogenes* had significantly increased times of motility and association with their actin tails (Figure 4.7). These data demonstrate that *L. monocytogenes* exhibits increased rates of movement and longer duration of actin tail association in RECON-deficient cells, suggesting augmented actin-based motility may be promoting the enhanced cell-to-cell spread.

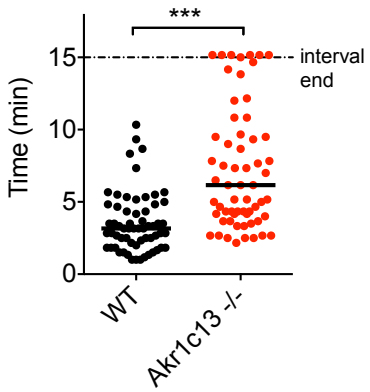

Figure 4.7. *L. monocytogenes* have increased times of motility and association with their actin tails in RECON-deficient hepatocytes. Length of time individual bacteria (N = 60) were associated with their actin tails across 15 min time intervals. *L. monocytogenes* were monitored at 6-8 hpi. Median values are indicated by a bar. Statistical significance was determined by unpaired, nonparametric, two-tailed Kolmogorov-Smirnov test comparing the cumulative distributions (***$p \leq 0.0001$).

4.6 Increased NF-κB-dependent inflammation in the absence of RECON's enzymatic activity drives the enhanced *L. monocytogenes* cell-to-cell spread

4.6.1 Loss of RECON's enzymatic activity drives enhanced cell-to-cell spread of *L. monocytogenes*

Investigation of *L. monocytogenes* virulence gene expression did not yield an explanation for the enhanced spread of these bacteria in RECON-deficient cells (Figure 4.3), implicating alterations in the host cell itself as the underlying cause of the phenotype. RECON is an oxidoreductase belonging to the aldo-keto reductase superfamily of enzymes. We hypothesized that the absence of RECON's enzymatic activity promoted the enhanced *L. monocytogenes* spread and increased actin tail lengths. RECON-deficient TIB73 cells were complemented with stably expressed WT RECON or a catalytically dead mutant of RECON (H117A), as previously reported (see Chapters 2, 3 and (*78*)). Complementation with WT but not the H117A mutant RECON restored focus areas and *L. monocytogenes* actin tails to the sizes and lengths, respectively, observed in WT TIB73 cells (Figure 4.8A and 4.8B), suggesting that loss of RECON's enzymatic activity drives enhanced cell-to-cell spread of *L. monocytogenes*.

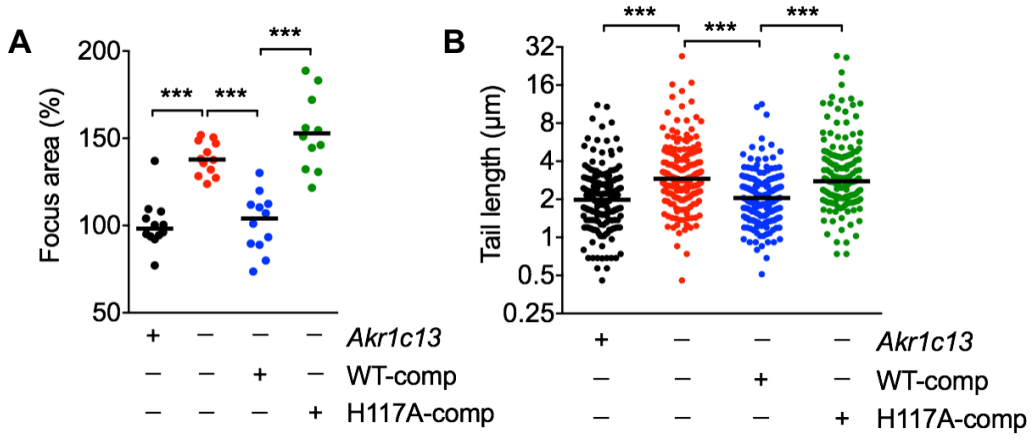

Figure 4.8. Loss of RECON's enzymatic activity drives enhanced cell-to-cell spread of *L. monocytogenes*. *L. monocytogenes* focus areas (A) or tail lengths (B) in WT, *Akr1c13*-deficient, or *Akr1c13*-deficient complemented with WT (WT-comp) or H117A (H117A-comp) RECON. Median values are indicated by a bar and all foci measured are shown. Foci and tail lengths were measured at 8 hpi and foci are plotted as percent of wild-type *L. monocytogenes* in WT TIB73 cells. All data are representative of two independent experiments. Statistical significance was determined by ordinary one-way ANOVA with Bonferroni's multiple comparisons test (***$p \leq 0.0001$).

4.6.2 Augmented NF-κB activation in the absence of RECON promotes *L. monocytogenes* intercellular spread

Our previous characterization of RECON's enzymatic activity revealed its critical role in controlling NF-κB-dependent inflammation, whereby the absence of RECON activity yielded increased inflammation downstream of TLR stimulation and *L. monocytogenes* infection (see Chapter 2 and (*78*)). We characterized the effect of the NF-κB inhibitor celastrol on *L. monocytogenes* cell-to-cell spread and observed a dose-dependent suppression of spread in RECON-deficient hepatocytes (Figure 4.9). Overall these data support the conclusion that the dampening of NF-κB activation by RECON's enzymatic activity in hepatocytes suppresses *L. monocytogenes* cell-to-cell spread.

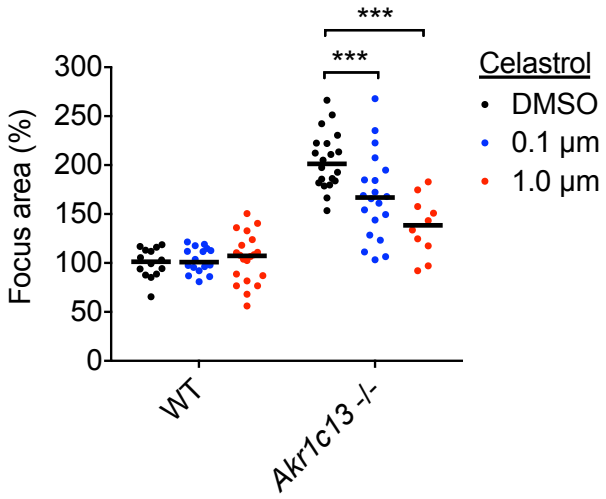

Figure 4.9. Augmented NF-κB activation in the absence of RECON promotes *L. monocytogenes* intercellular spread. Focus areas in WT or *Akr1c13*-deficient TIB73 cells treated with DMSO versus the NF-κB inhibitor celastrol (0.1 or 1.0 μM). Foci were measured at 8 hpi and are plotted as percent of wild-type *L. monocytogenes* in DMSO-treated WT TIB73 cells. Data are representative of two independent experiments. Statistical significance was determined by Mann-Whitney U test (***$p \leq 0.0001$).

4.7 C-di-AMP secreted by *L. monocytogenes* promotes intercellular spread in a RECON and NF-κB-dependent manner

4.7.1 C-di-AMP inhibition of RECON activity promotes *L. monocytogenes* cell-to-cell spread

During infection, c-di-AMP secreted by *L. monocytogenes* binds to and inhibits the enzymatic activity of RECON (*78*). Therefore, we tested the hypothesis that *L.*

monocytogenes strains secreting different levels of c-di-AMP might display altered intercellular spread in TIB73 hepatocytes. Multidrug resistance (MDR) transporters are responsible for secretion of c-di-AMP during infection of host cells (*38*, *133*, *163*). Importantly, mutants with altered c-di-AMP secretion grow normally in broth and exhibit no morphological defects unlike mutants with altered c-di-AMP production. We observed that *L. monocytogenes* lacking the major c-di-AMP transporter MdrM (Δ*mdrM*) had reduced cell-to-cell spread in TIB73 hepatocytes (Figure 4.10A). We also tested *L. monocytogenes* strains that over secrete c-di-AMP due to the loss of negative regulators of MdrM (Δ*marR* and Δ*ladR*), and both strains exhibited increased cell-to-cell spread (Figure 4.10A). To determine whether RECON was involved in mediating the differences in cell-to-cell spread of the *L. monocytogenes* strains secreting different amounts of c-di-AMP, we infected RECON-deficient hepatocytes with these strains. Remarkably, we observed that the focus areas of all the mutant strains, both high and low c-di-AMP secretors, were normalized during infection of the RECON-deficient cells (Figure 4.10B).

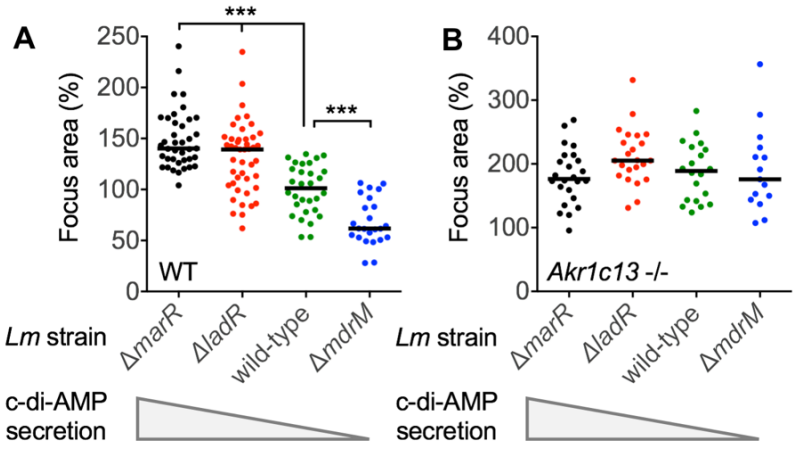

Figure 4.10. C-di-AMP inhibition of RECON activity promotes *L. monocytogenes* cell-to-cell spread. (A-B) Quantification of focus areas in WT (A) or *Akr1c13*-deficient (B) TIB73 cells infected with the indicated *L. monocytogenes* strains. Relative levels of c-di-AMP secretion are indicated. Median values are indicated by a bar and all foci measured are shown. Foci were measured at 8 hpi and are plotted as percent of wild-type *L. monocytogenes* in WT TIB73 cells. Data are representative of two independent experiments. Statistical significance was determined by ordinary one-way ANOVA with Bonferroni's multiple comparisons test (***$p \leq 0.0001$).

4.7.2 C-di-AMP-enhanced spread is dependent on NF-κB activation

The normalization of Δ*mdrM* to that of wild-type *L. monocytogenes* in RECON-deficient hepatocytes suggests that the reduced spread in WT hepatocytes was the result of

diminished interaction of c-di-AMP with RECON. Given that the enhanced spreading of wild-type *L. monocytogenes* in RECON-deficient cells was due to augmented NF-κB activation, we tested whether the increased spread of the c-di-AMP over secreting strains was dependent on NF-κB. Treatment with an NF-κB inhibitor blocked the enhanced spread of both Δ*marR* and Δ*ladR* strains (Figure 4.11). Taken together, these data support the conclusion that c-di-AMP inhibition of RECON activity promotes *L. monocytogenes* cell-to-cell spread via enhanced NF-κB activation.

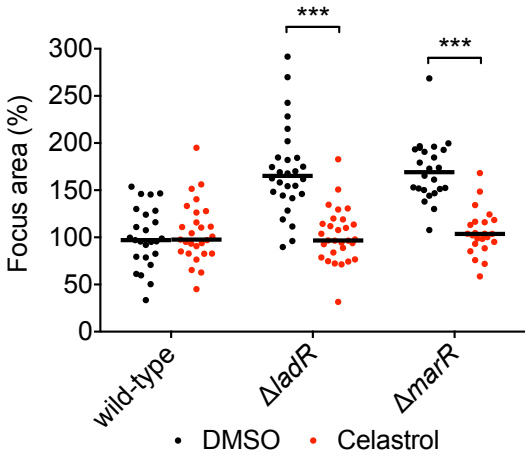

Figure 4.11. C-di-AMP-enhanced spread is dependent on NF-κB. Focus areas of wild-type or c-di-AMP hyper-secreting strains in WT TIB73 cells treated with DMSO (control) or the NF-κB inhibitor celastrol (1.0 μM). Median values are indicated by a bar and all foci measured are shown. Foci were measured at 8 hpi and are plotted as percent of wild-type *L. monocytogenes* in DMSO-treated WT TIB73 cells. Data are representative of two independent experiments. Statistical significance was determined by Mann-Whitney U test (***$p \leq 0.0001$).

4.8 Increased nitric oxide production in the absence of RECON enhances *L. monocytogenes* cell-to-cell spread

4.8.1 Inhibition of iNOS blocks the enhanced cell-to-cell spread in RECON-deficient hepatocytes

To define the aspect of NF-κB-driven inflammation that increased spread in RECON-deficient cells, we considered previous reports of host cell responses involved in controlling *L. monocytogenes* spread. Surprisingly, reports of alterations in host cell genotypes that result in increased intercellular spread are rare. Similarly, we found only one report of *L. monocytogenes* mutants that exhibited significantly enhanced cell-to-cell

spread compared to wild-type *L. monocytogenes* (*152*), which highlights the significance of the finding that c-di-AMP secretion enhances spread. One previous study by Cole and colleagues found that TLR stimulation following *L. monocytogenes* infection of primary macrophages resulted in elevated nitric oxide production that enhanced cell-to-cell spread (*50*). The authors also reported that inhibition of iNOS during *in vivo L. monocytogenes* infection significantly reduced liver burdens in an ActA-dependent manner. This was the second study to find that nitric oxide could enhance *L. monocytogenes* burdens in the liver, a phenomenon first reported in 1993 (*164*). These data

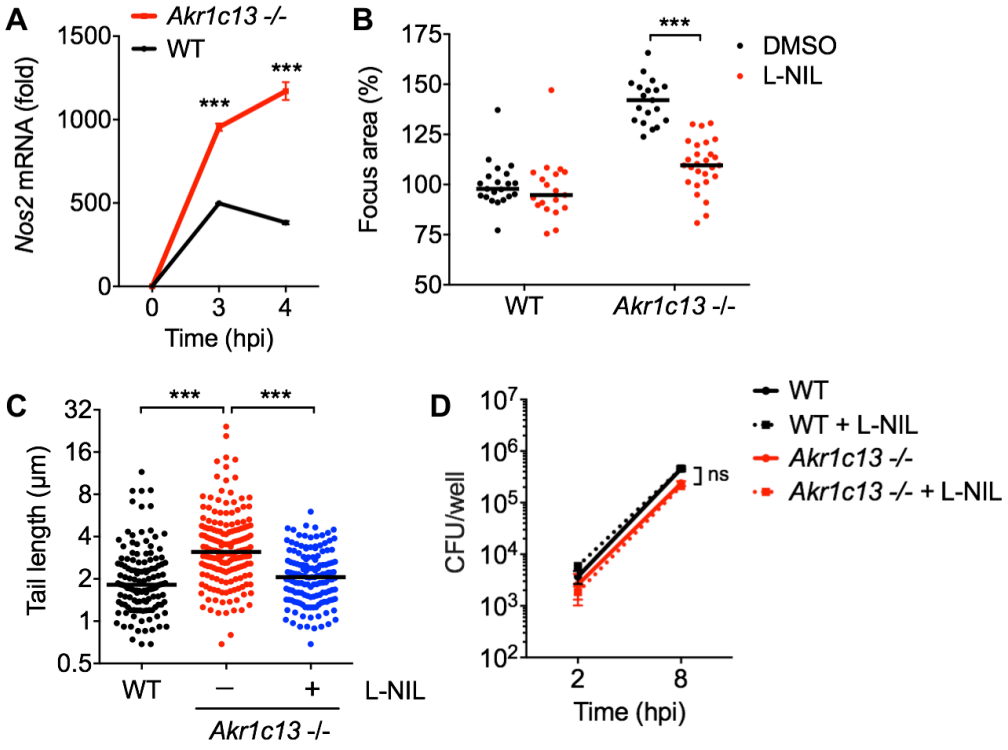

Figure 4.12. Nitric oxide enhances *L. monocytogenes* cell-to-cell spread in RECON-deficient hepatocytes. (A) Expression of *Nos2* in WT or *Akr1c13*-deficient TIB73 hepatocytes 2 h post-infection with *L. monocytogenes*. *Hprt* served as an endogenous control gene. Error bars represent ± SEM of technical triplicates. Statistical significance was determined by 2way ANOVA with Bonferroni's multiple comparisons test (***p ≤ 0.0001). (B-C) *L. monocytogenes* focus areas (B) and tail lengths (C) in WT or *Akr1c13*-deficient TIB73 cells treated with DMSO (control) versus the iNOS inhibitor L-NIL. Statistical significance was determined by Mann-Whitney U test (***p ≤ 0.0001). (D) WT or *Akr1c13*-deficient TIB73 hepatocytes were infected with *L. monocytogenes* in the presence of L-NIL or DMSO (control) and CFU were enumerated at the indicated time points (N=3). Error bars represent ± SD. In (B) and (C) median values are indicated by a bar. All foci and tails measured at 8 hpi are shown. Foci are plotted as percent of wild-type *L. monocytogenes* in untreated WT cells. All data are representative of at least two independent experiments.

led us to test the hypothesis that nitric oxide could enhance *L. monocytogenes* spread in hepatocytes. As we reported on in Chapter 2 (*78*) and Chapter 3, a striking consequence of augmented NF-κB activity in RECON-deficient hepatocytes is the significantly increased expression of the inducible nitric oxide synthase (iNOS, Figure 4.12A). To test whether the overexpression of iNOS was involved in promoting *L. monocytogenes* cell-to-cell spread, we treated cells with a specific inhibitor of iNOS, L-N^{6}-(1-iminoethyl)-L-lysine (L-NIL). Remarkably, L-NIL reduced the enlarged *L. monocytogenes* focus areas and longer actin tails in RECON-deficient hepatocytes back to the size and length of those observed in WT hepatocytes (Figure 4.12B and 4.12C). We did not observe any difference in intracellular bacterial growth in the presence of L-NIL, indicating the inhibitor was affecting cell-to-cell spread and not *L. monocytogenes* growth (Figure 4.12D).

4.8.2 Exogenous nitric oxide can promote *L. monocytogenes* intercellular spread

We also tested whether nitric oxide alone was sufficient to promote *L. monocytogenes* spread in hepatocytes or whether another aspect of RECON deficiency was also required. Treatment of WT TIB73 hepatocytes with the nitric oxide donor NOC-12 significantly increased *L. monocytogenes* spread similar to the level observed in RECON-deficient cells (Figure 4.13A). To test whether the effect of NOC-12 on *L. monocytogenes* spread was specific to a unique aspect of murine TIB73 hepatocytes, we also measured *L. monocytogenes* spread in human Caco-2 (enterocyte line) cells and Huh7 hepatocytes (hepatocellular carcinoma line) (Figure 4.13B and 4.13C). In both cases, the addition of NOC-12 significantly enhanced *L. monocytogenes* cell-to-cell spread, indicating that the effect of nitric oxide on *L. monocytogenes* is not strictly cell type-dependent.

Earlier results on the effects of RECON-deficiency led us to conclude that the virulence protein ActA was not involved in the enhanced *L. monocytogenes* spreading phenotype (Figure 4.3C). Unlike TIB73 hepatocytes, Huh7 cells are highly infectable, and therefore allowed us to directly assess whether nitric oxide affected ActA protein levels. Robust and similar ActA expression was observed in Huh7 cells with or without NOC-12 treatment, indicating that nitric oxide is likely not enhancing spread via increasing ActA protein levels (Figure 4.13D). Taken together, these data indicate that RECON's enzymatic control of nitric oxide production via NF-κB influences *L. monocytogenes* cell-to-cell spread in hepatocytes.

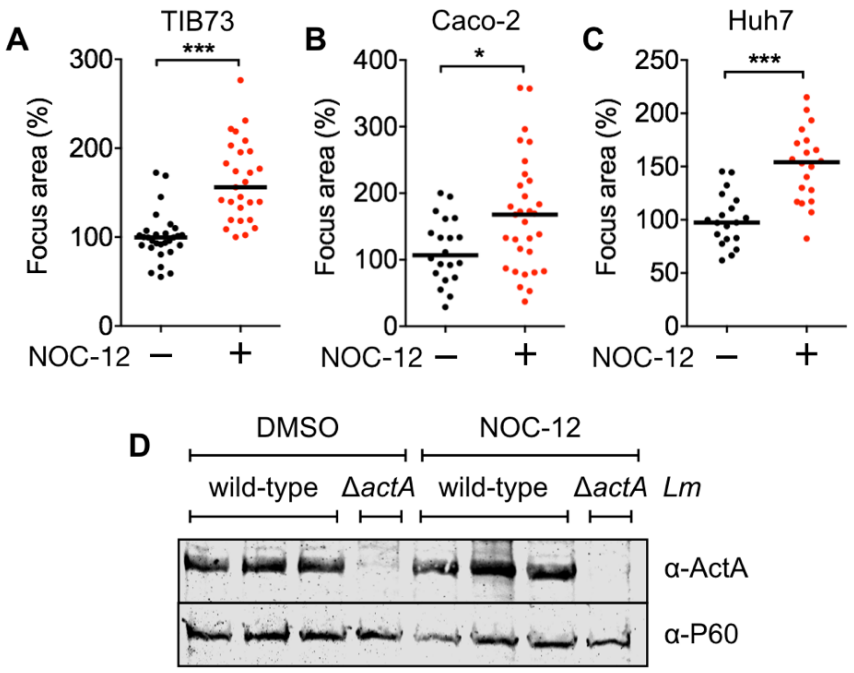

Figure 4.13. *L. monocytogenes* cell-to-cell spread is generally enhanced by nitric oxide in non-phagocytic cells. (A-C) Focus areas of *L. monocytogenes* in WT TIB73 (A), Caco-2 (B) or Huh7 (C) cells treated with the nitric oxide donor NOC-12. (D) Western blot of *L. monocytogenes* ActA and P60 (loading control) proteins expressed at 5 hpi in Huh7 cells plus or minus treatment with NOC-12 performed in biological triplicate. In A-C median values are indicated by a bar. All foci measured at 8 hpi are shown and are plotted as percent of wild-type *L. monocytogenes* in untreated WT cells. All data are representative of two independent experiments, except (D) where three biological replicates are shown together. Statistical significance was determined by Mann-Whitney U test (*$p \leq 0.05$; ***$p \leq 0.0001$).

4.8.3 *L. monocytogenes* is incredibly resistant to nitric oxide

It is little appreciated how incredibly resistant *L. monocytogenes* is to the antimicrobial action of nitric oxide. Many studies have found that *L. monocytogenes* replication is unaltered in iNOS-deficient macrophages or in the presence of nitric oxide *in vitro*, indicating that nitric oxide itself does not directly contribute to restriction of *L. monocytogenes* growth (*50, 51, 164-166*). To demonstrate just how resistant *L. monocytogenes* is to nitric oxide, we compared the growth of several bacterial species in broth cultures containing supraphysiological concentrations of the nitric oxide donors DEA/NO and NOC-12 (Figure 4.14A and 4.14B). *Staphylococcus aureus* colonizes the nasal passage of humans, a site with one of the highest levels of nitric oxide exposure within the host and is considered one of the most nitric oxide-resistant organisms reported. We

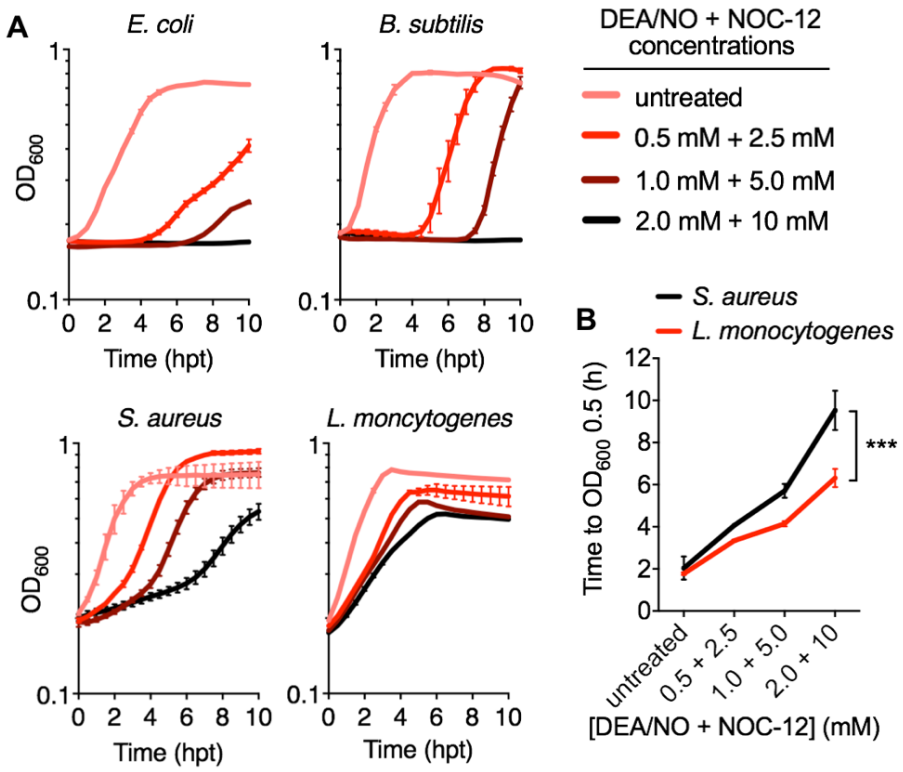

Figure 4.14. *L. monocytogenes* is incredibly resistant to nitric oxide. (A) Growth (OD600 values) of *Escherichia coli*, *Bacillus subtilis*, *Staphylococcus aureus*, or *Listeria monocytogenes* in TSB broth containing the indicated concentrations of the nitric oxide donors DEA/NO and NOC-12 (N=3), error bars represent ± SD. (B) Same as in (A) but plotted are the growth times (h) to OD600 in the presence of increasing concentrations of DEA/NO and NOC-12. Data are representative of two independent experiments. Statistical significance was determined by 2way ANOVA with Bonferroni's multiple comparisons test (***$p \leq 0.0001$).

found that *L. monocytogenes* exhibited higher levels of resistance to nitric oxide growth restriction than even *S. auerus*, while the growth of *Escherichia coli* and *Bacillus subtilis* was severely growth impaired by nitric oxide (Figure 4.14A and 4.14B). Collectively, the data presented in this chapter demonstrate that *L. monocytogenes* not only replicates unhindered in the presence of nitric oxide but that this antimicrobial host metabolite promotes bacterial spread within host cells.

4.9 Model: Inhibition of RECON by c-di-AMP promotes *L. monocytogenes* intercellular spread via increased nitric oxide

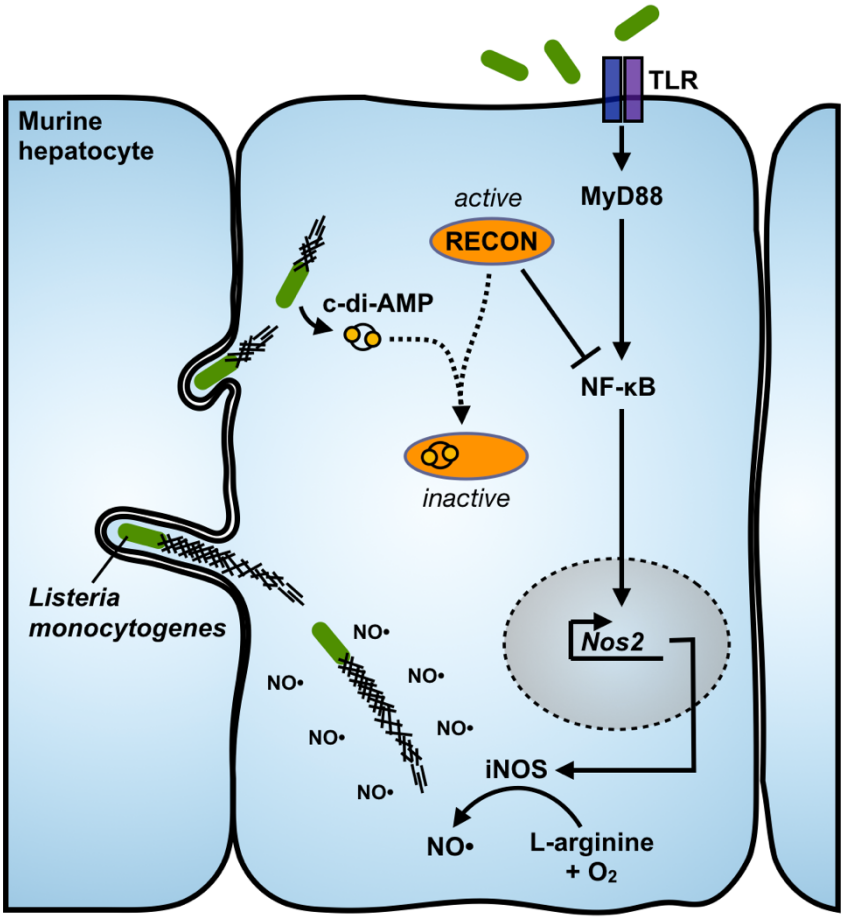

Figure 4.15. During infection, *L. monocytogenes* secretes c-di-AMP into the cytosol which is then bound by RECON. Inhibition of RECON's enzymatic activity by c-di-AMP releases a brake on NF-κB activation downstream of TLR engagement. The augmentation of NF-κB activation leads to increased iNOS levels and nitric oxide production. Elevated nitric oxide promotes elongation of *L. monocytogenes* actin tails, increased bacterial speed in the cytosol, and enhanced cell-to-cell spread.

4.10 Discussion

Successful colonization and replication within host tissues is predicated upon a pathogen's capacity to overcome host immunity. Current evidence suggests that several pathogens utilize evasion strategies to limit c-di-AMP induced inflammation during infection. In contrast, it has been established that *L. monocytogenes* actively secretes c-di-AMP during infection through the action of a variety of multidrug resistance

transporters. These observations suggest that rather than evade host immune sensing of this microbial-associated molecular pattern, *L. monocytogenes* may utilize other mechanisms to counteract c-di-AMP-mediated immunity to promote infection. Here, we provide evidence that c-di-AMP sensing results in elevated inflammatory responses that are unable to limit bacterial replication in hepatocytes. Additionally, elevated production of host nitric oxide can promote spread of this pathogen. These observations support a model in which *L. monocytogenes* utilizes c-di-AMP to promote host cell inflammation and, in combination with its evolved resistance to the direct antimicrobial action of nitric oxide, promote a critical aspect of its infection cycle.

While tissue culture models of infection provide a controlled environment in which to interrogate this aspect of *L. monocytogenes* biology, the complexity of these processes have hampered a clear indication of their *in vivo* impact. Hypersecretion of c-di-AMP associates with ~1.5 log reduction of CFUs specifically in the liver and not the spleen (*38, 135*), while reduced c-di-AMP secretion associates with ~1 log reduction of CFUs in both the liver and spleen (*133, 134*). Although both hypersecretion and reduced secretion of c-di-AMP leads to a reduction in *L. monocytogenes* burdens *in vivo*, it is not clear how altered c-di-AMP secretion impacts the host immune response; increased c-di-AMP secretion may increase spread but may also lead to increased immune responses beneficial for bacterial clearance. Additionally, multiple MDRs are known to transport c-di-AMP (*38, 133*), but their broader roles in *L. monocytogenes* survival within the host are not fully known. MdrT not only transports c-di-AMP but it is important for resistance to bile acid (*134*); therefore, in vivo data with these mutants is confounded by the probable multiple roles of MDRs in mediating *L. monocytogenes* survival within host niches.

The effects of nitric oxide on *in vivo* infection are equally complex. Results from this study and those reported previously, consistently demonstrate that *L. monocytogenes* is resistant to the direct antibacterial action of nitric oxide (*50, 51, 164-166*). Nevertheless, nitric oxide exerts numerous indirect (i.e. non-bacteriostatic/bactericidal) antimicrobial activities including upregulation of autophagy, pathogen iron deprivation, and inhibition of bacterial secretion systems (*167*). Additionally, the immunoprotective function of nitric oxide also transcends the intracellular space, owing to its diverse roles in the differentiation of myeloid cells, tissue regeneration, and regulation of T and B cell responses (*167*). The survival of iNOS-deficient mice with a sub-lethal dose of *L. monocytogenes* is impacted late during infection after day 5, and *L. monocytogenes* burdens

in the liver and spleen are increased by ~2 logs (*51, 168*). These data suggest that the protection imparted by nitric oxide primarily plays out during the adaptive immune response to *L. monocytogenes* infection, as T-cell responses emerge at day 5 and are ultimately responsible for the clearance of *L. monocytogenes* in mice (*169*).

Two studies reported the use of chemical inhibitors of iNOS, rather than fully iNOS-deficient mice (*50, 164*). Interestingly, iNOS inhibition during *L. monocytogenes* infection reduced burdens primarily in the liver and not the spleen, and this reduction did not occur with infections of *L. monocytogenes* Δ*actA* mutants (*50*). Considering that hepatocytes are the dominant cellular reservoir for *L. monocytogenes* in the liver (*62, 138*), these data suggest hepatocytes may be the primary cell type in which nitric oxide promotes spread *in vivo*. Therefore, although nitric oxide production within the context of the entire immune system may act to reduce *L. monocytogenes* survival, it appears that it also promotes cell-to-cell spread and survival of *L. monocytogenes* in the liver.

A single study has reported a connection between nitric oxide and *L. monocytogenes* cell-to-cell spread through delayed phagolysosomal maturation in secondarily infected/recipient macrophages (*50*). In contrast, our investigations in hepatocytes revealed that the absence of RECON did not impact *L. monocytogenes* cytosolic entry but rather increased actin tails and rates of motility in the cytosol, consistent with distinct mechanisms of nitric oxide-induced spread in hepatocytes versus macrophages. It is not immediately clear how nitric oxide promotes elongated *L. monocytogenes* actin tails. Nitric oxide can act as a signaling molecule by modulating the activity of target proteins, through a variety of mechanisms, including changes in cGMP signaling through activation of soluble guanylate cyclase, direct nitrosylation of cysteines in proteins, and protein nitrosation through the action of nitric oxide-derived peroxynitrite. As such, there may exist several mechanisms by which nitric oxide can modify host proteins and influence *L. monocytogenes* spread. Previous studies have found that the rate at which *L. monocytogenes* is moving when it penetrates the plasma membrane to form intercellular protrusions does not positively correlate with speed (*156, 158, 170*). Thus, it is unclear if the increased rate of *L. monocytogenes* movement in RECON-deficient cells is directly responsible for increased spread. However, protrusion formation requires at least a minimum rate of movement, so it is possible that in the absence of RECON, more bacteria meet this threshold requirement to promote protrusion formation and cell-to-cell spread. In line with this, we found that in the absence of RECON, *L. monocytogenes* associate with

their actin tails for an increased length of time, which likely provides those bacteria with increased opportunities for protrusion formation. However, future studies are warranted to determine the exact connection between nitric oxide, actin tail lengths, speed and *L. monocytogenes* spread.

A broader question that arises from this study is if enhanced intercellular spread significantly promotes *L. monocytogenes* virulence. Evidence in support of this proposition is provided by studies of natural isolates of *L. monocytogenes*. Human clinical isolates, including epidemic strains, are more likely to exhibit enhanced spread over the lab reference strain 10403S and compared to strains from ruminants or food sources (*171, 172*). The plaque sizes of these hyperspreading isolates are larger by 1.2 to 1.5-fold, which contextualizes the 1.5- to 2-fold increase in spread areas observed in RECON-deficient cells. Interestingly, amongst natural isolates, cell-to-cell spread phenotypes are not correlated with invasion or replication (e.g. it does not follow that strains that spread more than 10403S also invade better or replicate faster) (*171, 173*). However, for epidemic strains of *L. monocytogenes*, enhanced cell-to-cell spread is the most consistent virulence attribute.

We found that hepatocytes treated with nitric oxide showed enhanced *L. monocytogenes* spread with no impact on *L. monocytogenes* replication. These data suggest that enhancement of intercellular spread does not directly impact replication from either a nutritional or space perspective. How then might enhanced intercellular spread benefit *L. monocytogenes*? One of the most frequently ascribed metrics of infection outcome are the bacterial burdens observed during acute infection. However, several other aspects of the infection process are required for a productive infection cycle, including the initial invasion of deeper tissues and transmission from the host. We found that nitric oxide enhanced spread in enterocytes, which may facilitate initial invasion of the intestinal epithelium. Additionally, when *L. monocytogenes* transits from the bloodstream to the liver, it rapidly infects and resides predominantly within hepatocytes (*138*). From the liver, *L. monocytogenes* has been reported to colonize and replicate within the gallbladder following systemic infection (*174*), which may facilitate transmission through fecal shedding analogous to *Salmonella enterica* serotype Typhi (*175*). Because c-di-AMP and RECON-dependent nitric oxide production affect *L. monocytogenes* spread within hepatocytes, which are intimately entwined with the gallbladder, it is tempting to speculate that enhanced spread within the liver may expedite entry into the gallbladder

to facilitate transmission. Future investigations that interrogate many aspects of the intricate lifecycle of this pathogen beyond systemic bacterial burdens will be necessary to fully understand the in vivo consequences of alterations in intercellular spread.

In summary, this work presented in this chapter establishes that c-di-AMP can promote *L. monocytogenes* cell-to-cell spread in hepatocytes via engagement of RECON and promotion of nitric oxide production downstream of NF-κB activation. These findings provide the basis for novel avenues of inquiry such as the impact that c-di-AMP secretion and nitric oxide have on *in vivo* intercellular spread and host-to-host transmission of *L. monocytogenes*.

4.11 Materials and Methods

Bacterial strains and culture conditions

Listeria monocytogenes 10403S strains were struck out onto BHI agar, grown overnight at 37°C, and then stored at 4°C for up to one month. For infections, one colony of *L. monocytogenes* was inoculated into 3 mL of BHI and grown overnight, static at 30°C. The next morning 1 mL of culture (normalized to OD600 1.1) was centrifuged and washed 3x with 1 mL of sterile 1X PBS. The pellet was resuspended in 1 mL of 1X PBS for infections. *Burkholderia thailandensis* strain E264 Δ*motA2* (*176*) was struck onto BHI agar, grow overnight at 37°C, and stored at room temperature for up to one week. For infections, one colony of *B. thailandensis* was inoculated into 2 mL of BHI and grown overnight shaking at 37°C. The next day, the bacteria were diluted 40x into 2 mL of fresh BHI and grown shaking at 37°C for 4 h until an OD600 of 3-4 was reached. The bacteria were then centrifuged and washed 2x with 1 mL of sterile 1X PBS and the pellet was resuspended in 1mL of 1X PBS for infections.

Cell lines

TIB73 is a spontaneously immortalized hepatocyte cell line from a normal BALB/c embryo liver (sex unknown, not provided by the original depositor). The cell line was authenticated by and purchased from ATCC. TIB73 hepatocytes deficient in RECON (*Akr1c13*-/-) generated by CRISPR/Cas9-mediated mutagenesis have been described previously (*78*). Huh7 and Caco-2 are cancer cell lines derived from human males with hepatocellular carcinoma and colon adenocarcinoma, respectively. Huh7 and Caco-2

cells were obtained from Ram Savan (University of Washington) (*177*, *178*) and tested negative for mycoplasma contamination. They were authenticated by their morphology, infectability, and response to stimuli. Cell lines were grown at 37°C in 5% CO2 in phenol red-free DMEM with 10% heat-inactivated FBS (20% for Caco-2) and supplemented with 2 mM sodium pyruvate and 1 mM L-Glutamine. For passaging, cells were maintained in pen-strep (100U/mL) but were plated in antibiotic-free media for infections.

Bacterial infections of cell lines

$1x10^6$/3 mL (TIB73, Huh7) or $1.75x10^6$/3 mL (Caco-2) cells were seeded per well in 6-well plates the day before infection. For foci analysis, cells were plated on top of collagen-coated coverslips. The morning of infection, the cells were washed 2x in 1X PBS just prior to infection. *L. monocytogenes* strains were diluted 1:100 (growth curves, foci, actin tail lengths, and RNA analyses), 1:500 (TIB73 plaque assays), or 1:15,000 (Huh7, Caco-2 foci analysis) in pre-warmed cell culture media containing 0.1% FBS. 2 mL of diluted bacteria was overlaid onto the host cells and placed at 37°C for 1 hour. Following infection, the cells were washed 2x with 1X PBS and placed into complete medium containing gentamicin (50 μg/ml) to kill extracellular bacteria. For TIB73 growth curves, cells were washed 2x with 1X PBS, lysed in 500 μL cold 1X PBS with 0.1% Triton X-100, and plated as previously described (*179*). TIB73 plaque assays with *L. monocytogenes* were conducted as previously described (*180*).

For live cell imaging of *L. monocytogenes* in WT and RECON-deficient TIB73s, cells were plated at $5x10^5$ per dish onto 20 mM MatTek dishes 24 h prior to infection in FluoroBrite DMEM media containing 10% FBS. Overnight cultures of *L. monocytogenes* expressing GFP under the actA promoter (pPL2-actA-GFP) were washed 2x in 1X PBS and diluted 1:100 into the culture dish. Gentamicin (50 μg/ml) was added at 1 hpi. For *B. thailandensis* infections of TIB73 cells, the washed bacteria were diluted 1:4,000, 1:20,000, or 1:100,000 in 2 mL of cell culture media and each dilution was added to a well of TIB73 cells in 6-well format. Cells were then incubated at 37°C for 30 mins, washed 2x with 1X PBS, and overlaid with media containing 5% FBS, 0.7% agarose, and 1 mg/ml kanamycin. Infected cells were incubated at 37°C and plaques were imaged at 16 hpi.

Microscopy

For microscopic analysis of *L. monocytogenes* foci and actin tails, cells were infected for 8 hours, washed 2x with 1X PBS and fixed in 3.5% formaldehyde for 15 min at room temperature. The coverslips with attached cells were washed in Tris-buffered saline (TBS) with 0.1% Triton X-100 and blocked in TBS with 1% BSA. Cells were stained in TBS with 1% BSA with rabbit *L. monocytogenes* O Antiserum (1:100 dilution), washed, incubated with goat anti-rabbit IgG secondary Alexa Fluor 488 conjugate (1:200 dilution) and Alexa Fluor 568 phalloidin (F-actin probe; 1:1,000 dilution), and washed again. The coverslips were mounted and imaged with a Keyence BZ-X710 microscope. Quantitative analyses of focus areas and tail lengths were performed with ImageJ software. *B. thailandensis* plaques were imaged on a Leica DM IL LED microscope with a 10x objective. Images were analyzed for focus size using ImageJ.

L. monocytogenes rate analysis

WT or *Akr1c13*-/- TIB73 hepatocytes were transduced with rLV-Ubi-LifeAct lentivirus (ibidi) and selected according to the manufacturer's instructions to generate RFP-tagged F-actin for live cell imaging. To measure *L. monocytogenes* movement rates, these cells were infected for 6-8 h prior to imaging. Images were captured using a Nikon Ti Eclipse microscope with a Yokogawa CSU-XI spinning disc confocal, a Clara Interline CCD Camera, 60X (1.4 NA) Plan Apo objective, and MetaMorph software. Two Z-stacks were captured at 10 sec intervals for 15 min per field of view. Individual movements were then tracked using ImageJ software with the Manual Tracking plugin. A minimum of 60 individual bacteria were tracked for each infected cell type. Bacteria that did not migrate ~20 microns from their original location were not tracked, and tracking was stopped when the bacteria stopped migrating.

Isolation of *L. monocytogenes* RNA from host cells

Six 60 x 30 mm dishes of TIB73 cells were infected for 5 hours. At the time of harvest, cells were washed 2x with 1X PBS and then lysed in the dishes on ice for 5 min with 3 mL of 0.1% SDS, 1% acidic phenol, and 19% EtOH to release residing bacteria. Lysates were pooled, and the released bacteria were pelleted at 4,500 rpm for 10 min at 4°C. Pellets containing bacteria were resuspended in 500 μL of 1X PBS, diluted with 500 µL cold methanol and stored at -20°C until RNA extraction. At the time of extraction, bacteria

were pelleted at 4,500 rpm for 10 min at 4°C. Pellets were resuspended in 400 μL of DEPC-treated water with 50 mM NaOAc pH 5.2 and 10 mM EDTA. This bacteria-containing buffer was mixed with 80 μL of 10% SDS and 400 μL 1:1 acidified phenol:chloroform, vortexed for 10 min and then incubated at 65°C for 10 min. The contents were then poured into phase lock tubes and centrifuged for at 17,000 rpm for 5 min. 400 μL of the aqueous layer was transferred to 40 μL 3M NaOAc (pH 5.2) plus 1.0 ml 100% ethanol, vortexed, placed at -20°C for 1 h, and centrifuged at 17,000 rpm for 30 min at 4°C. Samples were aspirated, washed with 500 μL of 70% EtOH and centrifuged at 17,000 rpm for 10 min at room temperature. Samples were aspirated, dried in a speed-vac for 2 min and RNA pellets were resuspended in 50 μL of RNase-free water.

qRT-PCR analysis

RNA was extracted, DNase treated and reverse-transcribed and assayed for gene expression using SYBR (*L. monocytogenes* genes) or TaqMan (host cell genes) chemistries according to the manufacturers' instructions and as previously described (*78*). Primer information is provided in the Key Resources Table below (Table 4.1).

Chemical inhibitors

The NF-κB inhibitor celastrol (used at 0.1 and 1 μM as indicated in the figures) was added to cells for 1 hour prior to infection. Cells were maintained in the presence of celastrol during infection and then again after bacteria were washed off, out to 8 hpi. All inhibitors were reconstituted in DMSO, which by itself was used as a control treatment. For cell culture experiment, L-NIL and the nitric oxide donor NOC-12 were added to a final concentration of 1 mM and 50 μM, respectively, immediately following a 1-hour infection of the cells with *L. monocytogenes*. For *in vitro* bacterial growth curves, bacteria were grown overnight in tryptic soy broth (TSB), subcultured 1:50 in fresh TSB in 96-well plates (200 μL final volume). The nitric oxide donors DEA/NO and NOC-12 were added (concentrations indicated in figures) and bacteria were grown at 37°C with shaking in a BioTek Synergy plate reader.

Immunoblotting

$0.7x10^6$ Huh7 cells were plated in 12-well plates and rested overnight. The cells were infected for 1 h with *L. monocytogenes* at a 1:1,000 dilution of bacteria of overnight culture

as described above (see above "Bacterial infections of cell lines"). NOC-12 (50 μM) was added to the cells 1 hpi and at 5 hpi the cells were lysed in Laemmli Sample Buffer with 5% 2-mercaptoethanol as previously described (*151*). Westerns were run using nitrocellulose membranes blocked in 5% non-fat dry milk in 1X TBS for 45 min at room temperature, followed by overnight incubation in primary antibodies diluted 1:5,000 in 5% BSA in 1X TBS-T. Antibody information is provided in the supplementary Key Resources Table.

Quantification and statistical analysis

Data were analyzed using Prism 7 software. P values correlate with symbols as follows: $^{*}p \leq 0.05$, $^{**}p \leq 0.001$, $^{***}p \leq 0.0001$ and are also denoted in the figure legends. The values for and identify of N (biological replicates) as well as precision measures (e.g., median, SD and SEM) are indicated in the figure legends. Investigators remained unblinded to sample identities throughout. No data was excluded from statistical analysis.

Table 4.1: Key resources table

Reagent or Resource	Source	Identifier
Antibodies		
Difco Listeria O Antiserum Poly Types 1 & 4	Becton Dickinson	Cat#223021
Alexa Fluor 568 Phalloidin	Thermo Fisher Scientific	Cat#A12380
Anti-ActA polyclonal antibody raised against the mature N terminus of the ActA protein	Michelle Reniere	Reniere *et al*. (Nature, 2015); Lauer *et al*. (I&I 2008)
Anti-*Listeria* spp. P60 mAb (P6017)	Adiopgen	Cat#AG-20A-0023
IRDye 680RD Goat anti-Mouse IgG (1:10,000 dilution)	Licor	Cat#926-68070
IRDye 800CW Goat anti-Rabbit IgG (1:10,000 dilution)	Licor	Cat#926-32211
Bacterial and Virus Strains		
rLVUbi-LifeAct-TagRFP: lentiviral vector	Ibidi	Cat#60142
Listeria monocytogenes 10403S wild-type	Provided by Dan Portnoy	JW06
Listeria monocytogenes 10403S Δ*marR*	Provided by Dan Portnoy; Crimmins et al., 2008	JW524
Listeria monocytogenes 10403S Δ*ladR*	Provided by Dan Portnoy; Crimmins et al., 2008	JW523

Listeria monocytogenes 10403S Δ*mdrM*	Provided by Dan Portnoy; Crimmins et al., 2008	JW07
Listeria monocytogenes 10403S Δ*inlC*	Provided by Dan Portnoy	JW551
Listeria monocytogenes 10403S PrfA*	Provided by Dan Portnoy; Wong and Freitag, 2004	JW130
Listeria monocytogenes 10403S Δ*actA*	Provided by Dan Portnoy	JW367
Listeria monocytogenes 10403S pPL2:*actA*	This study	JW618
Listeria monocytogenes 10403S Δ*actA*::*actA*	This study	JW620
Listeria monocytogenes pPL2-actA-GFP	Provided by JD Sauer	JW480
Burkholderia thailandensis strain E264 Δ*motA2*	French et al., 2011	N/A
Escherichia coli XL1 Blue	N/A	N/A
Bacillus subtilis strain 168	Provided by Houra Merrikh	HM01/JW227
Staphylococcus aureus strain Newman	Provided by Dan Portnoy	N/A
Chemicals, Peptides, and Recombinant Proteins		
DMEM, high glucose, no glutamine, no phenol red	Thermo Fisher Scientific	Cat#31053036
Sodium pyruvate	Thermo Fisher Scientific	Cat#11360070
L-Glutamine	Thermo Fisher Scientific	Cat#25030081
Characterized Fetal Bovine Serum	Thermo Fisher Scientific	Cat#SH30071.03
Penicillin-Streptomycin (10,000 U/mL)	Thermo Fisher Scientific	Cat#15140122
Bovine Serum Albumin (BSA)	Fisher BioReagents	Cat#BP9700100
Trypsin-EDTA (0.05%)	Thermo Fisher Scientific	Cat#25300054
Brain Heart Infusion Broth	Research Products International	Cat#B11000
Tryptic soy broth (TSB)	BD Dianostics	Cat#211825
Gentamicin (10 mg/mL)	Thermo Fisher Scientific	Cat#15710072
Dimethyl sulfoxide	Sigma-Aldrich	Cat#D2650
Celastrol	InvivoGen	Cat#ant-cls
L-NIL hydrochloride	Cayman Chemical	Cat#80310
DEA NONOate (DEA/NO)	Cayman Chemical	Cat#82100
NOC-12	Sigma-Aldrich	Cat#487955
Pierce 16% formaldehyde	Thermo Fisher Scientific	Cat#28908
Neutral Red solution	Sigma-Aldrich	Cat#N6264
BioCoat Collagen I 22mm round coverslips	Corning	Cat#354089
Prolong Diamond Antifade Mountant	Thermo Fisher Scientific	Cat#P36961
Critical Commercial Assays		
TURBO DNA-free Kit	Thermo Fisher Scientific	Cat#AM1907
iScript cDNA synthesis kit	Bio-Rad	Cat#1708891
Maxima SYBR Green/ROX qPCR Master Mix	Thermo Fisher Scientific	Cat#K0221
RNAqueous Total RNA Isolation Kit	Thermo Fisher Scientific	Cat#AM1912
TaqMan pre-designed assay: murine *Nos2*	Thermo Fisher Scientific	Mm00440502_m1

TaqMan pre-designed assay: murine *Hprt*	Thermo Fisher Scientific	Mm03024075_m1
Experimental Models: Cell Lines		
TIB73	ATCC	ATCC Cat# BNL CL.2 TIB-73; RRID:CVCL_4383
TIB73 mutant *Akr1c13*	McFarland et al., 2017	N/A
TIB73 mutant *Akr1c13* with MSCV-*Akr1c13*-WT	McFarland et al., 2017	N/A
TIB73 mutant *Akr1c13* with MSCV-*Akr1c13*-H117A	McFarland et al., 2017	N/A
Huh7	Provided by Ram Savan; McFarland et al., 2014; Jarret et al., 2016	RRID:CVCL_0336
Caco-2	Provided by Ram Savan; Lim et al., 2016	RRID:CVCL_0025
Oligonucleotides		
Lm 16S forward primer: CAAGCGTTGTCCGGATTTATTG	This work	N/A
Lm 16S reverse primer: GCACTCCAGTCTTCCAGTTT	This work	N/A
Lm actA forward primer: ACGGGACCAAGATACGAA	This work	N/A
Lm actA reverse primer: GCATGCTAGAATCTAAGTCAC	This work	N/A
Lm hly forward primer: CGCGGATGAATTCGATAG	This work	N/A
Lm hly reverse primer: GTCATACCCGGGAAATCAATG	This work	N/A
Lm inlC forward primer: AATTCCCACAGGACACAACC	This work	N/A
Lm inlC reverse primer: CGGGAATGCAATTTTTCACTA	This work	N/A
Lm plcA forward primer: TTCGGGGAATTCCATGATTAG	This work	N/A
Lm plcA reverse primer: CACTACTCCCGGGACTGAG	This work	N/A
Lm plcB forward primer: CCAGTAGGATCCACTGTATC	This work	N/A
Lm plcB reverse primer: CTTATTTCCCGGGTTTTGCTAATG	This work	N/A
Lm prfA forward primer: CAGCTGAGCTATGTGCGAT	This work	N/A
Lm prfA reverse primer: ACCAATGGGATCCACAAG	This work	N/A
Software and Algorithms		
ImageJ	ImageJ Software	https://imagej.nih.gov/ij/
BZ-X700 series microscope analysis application	Keyence	BZ-H3AE

GraphPad Prism 6	GraphPad Software	http://www.graphpad.com/scientificsoftware/prism/
Metamorph	Molecular Devices	https://www.moleculardevices.com/systems/metamorph-research-imaging
Leica Application Suite, V4	Leica Microsystems	https://www.leica-microsystems.com/products/microscope-software/

Chapter 5

The Roles of RECON in Mice

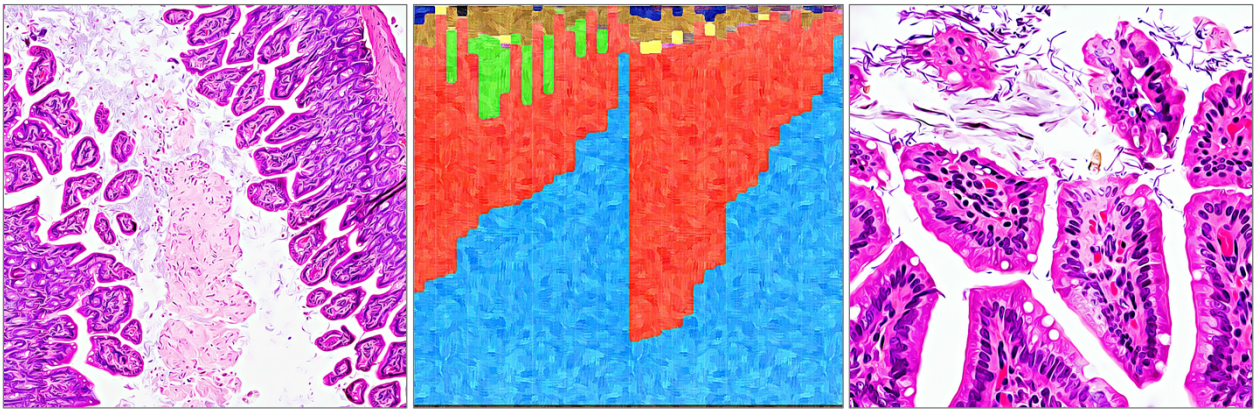

The following work was done in collaboration with: Ahmed-Qadri, F., Carletti, A.A., Snyder, J.M., and Woodward, J.J.

5.1 Summary

The aldo-keto reductase RECON is a high affinity cytosolic sensor of bacterial cyclic dinucleotides produced by commensals and pathogens alike. Binding of cyclic diadenosine monophosphate by RECON results in inhibition of its catalytic activity. How RECON functions *in vivo* is currently an open question. Here, we show that following systemic challenge with the bacterial pathogen *Listeria monocytogenes*, RECON-deficient mice exhibit increased survival and reduced bacterial loads in the liver and spleen. Apart from its role in systemic infection, we also found that RECON deficiency promotes aberrant low-level inflammation in the small intestines characterized by dysregulated IL-17A production. The absence of RECON was associated with alterations in the microbiota particularly in male mice, with aberrant expansion of segmented filamentous bacteria. The findings reported in this chapter indicate that RECON functions in intestinal homeostasis and that the inflammatory programs under its control are protective during systemic bacterial infection.

5.2 Background

Bacterial production of cyclic diadenosine monophosphate (c-di-AMP) within the host inversely correlates with bacterial virulence, whereby elevated c-di-AMP production or

secretion associates with host protection. This effect is observed during infection with prominent human pathogens such as *Mycobacterium tuberculosis*, Group B *Streptococcus*, and *Listeria monocytogenes* (*19, 23, 37, 38*). C-di-AMP functions as an essential second messenger within bacteria (*15-17*) and has been deemed an immunological vita-PAMP (pathogen-associated molecular pattern) as its production signifies to the host the presence of a live bacterium (*24, 25, 181*). The most well-characterized host sensor of c-di-AMP is the ER-localized receptor STING (stimulator of interferon genes). However, STING-deficient mice have no defect in bacterial clearance of c-di-AMP-producing pathogens, including *M. tuberculosis*, *L. monocytogenes*, and *Streptococcus pneumoniae* (*4, 36, 182*). These observations prompted us to investigate the existence of other host c-di-AMP-binding proteins that may be involved in the immune response.

We previously identified that the NADPH-dependent aldo-keto reductase (AKR) RECON (AKR1C13) is a high affinity sensor of c-di-AMP (Chapter 2 and (*78*)). C-di-AMP binds RECON in its nicotinamide binding site, effectively inhibiting its catalytic activity. The absence of RECON within macrophages and hepatocytes results in enhanced NF-κB- and MAPK-dependent inflammatory gene expression downstream of Toll-like receptor (TLR) stimulation (Chapter 2, 3 and (*78*)). Therefore, the interaction between c-di-AMP and RECON serves to amplify the immune response, perhaps because the presence of this vita-PAMP in the cytosol indicates a high threat level. Although the cellular-level effect of RECON has been described, it has remained unclear how RECON would function *in vivo*. Here, we have generated RECON-deficient mice and characterized how the absence of this enzyme at steady-state as well as during bacterial challenge influences homeostasis and immunity. In this chapter, we report that RECON-deficient mice exhibit increased survival and reduced bacterial loads in the liver and spleen after systemic challenge with *L. monocytogenes*. Additionally, RECON deficiency leads to a specific dysregulation in the small intestines, with evidence of dysbiosis and alteration in the IL-17 axis.

5.3 Generation of RECON-deficient mice

5.3.1 CRISPR/Cas9-mediated mutagenesis of C57BL/6J embryos

We previously made CRISPR/Cas9-mediated mutant RECON hepatocytes *in vitro* (Chapter 2 and (*78*)). Complementation studies validated that the observed responses

were specific to the single guide RNA (sgRNA) targeting exon 6 of *Akr1c13* (see Chapters 2 and 3). *In vitro* transcribed sgRNA and Cas9 mRNA were microinjected into C57BL/6J embryos and implanted into pseudo-pregnant female mice. We selected a heterozygous male founder that had a single G insertion in exon 6 of *Akr1c13* (Figure 5.1A-C) and bred the line to homozygosity. The G insertion in the *Akr1c13* coding sequencing caused a frameshift resulting in a premature stop codon after residue 200, which destroyed the catalytic and c-di-AMP binding sites (Figure 5.2A and 5.2B).

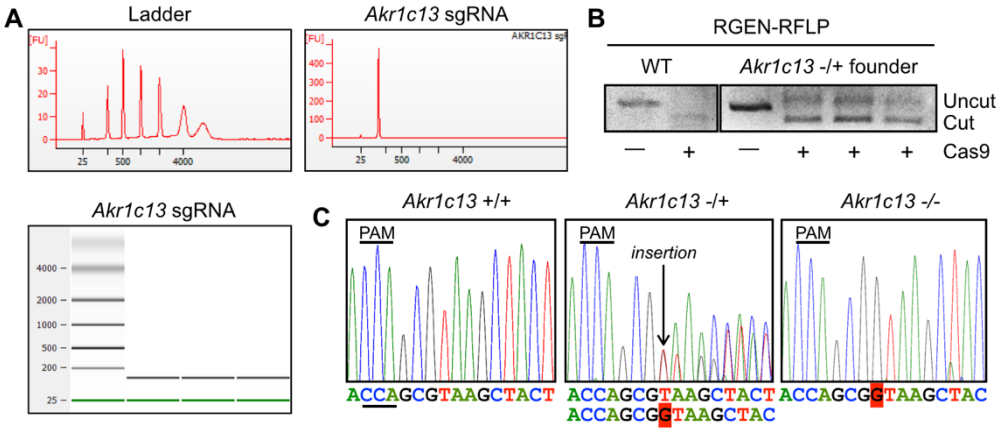

Figure 5.1. CRISPR/Cas9-mutagenesis of *Akr1c13* in C57BL/6J embryos. (A) Agilent Bioanalyzer results with purified sgRNA for injection. (B) RGEN-RFLP analysis of CRISPR-targeted region in the *Akr1c13* gene in the heterozygous founder. (C) Sequence of mutated allele with a single G insertion leading to a frameshift mutation.

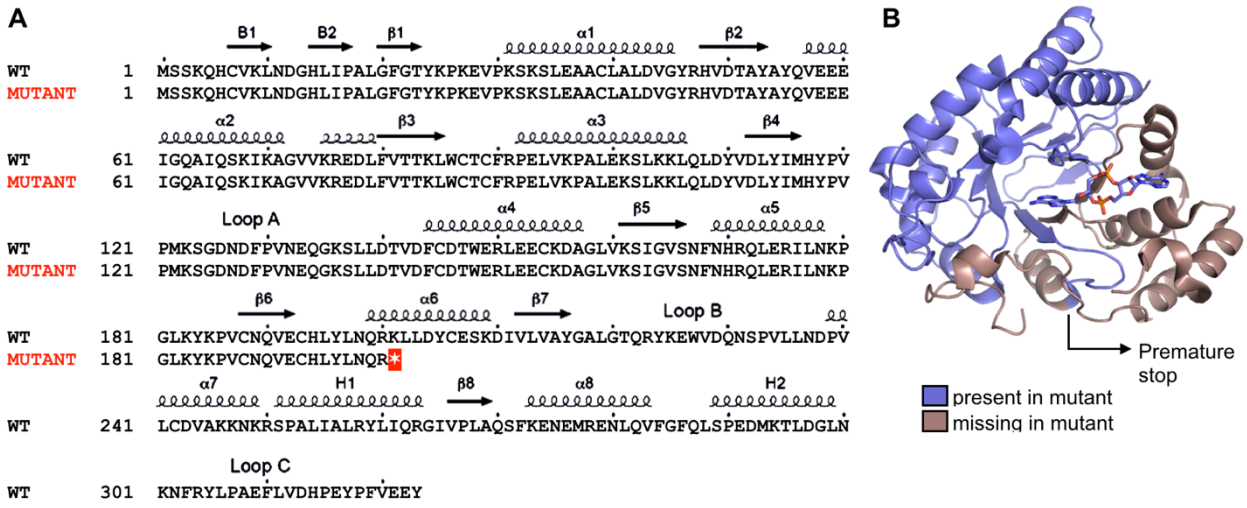

Figure 5.2. Premature stop codon in the mutant *Akr1c13* allele destroys the enzyme structure and the c-di-AMP binding site. (A) Sequence comparison of WT and mutant RECON proteins. The mutant allele encodes for a stop codon after residue 200 (red star). (B) RECON protein structure with the region missing in the truncated mutant colored in brown. Truncation destroys the active and c-di-AMP binding sites.

5.3.2 Mutant *Akr1c13* mRNA is subjected to nonsense-mediated decay

RECON is highly expressed in the liver, stomach and small intestines (*63, 183*). We examined the expression of RECON by qRT-PCR because specific antibodies against RECON, which has close homology with other murine AKRs, are unavailable. We observed that the CRISPR/Cas9-targeted *Akr1c13* mRNA expressed in the liver and small intestine ileum was highly unstable, likely due to nonsense-mediated decay (Figure 5.3A and 5.3B). These results are consistent with the effect of CRISPR/Cas9-targeting of exon 6 in hepatocytes *in vitro*, whereby the mutant *Akr1c13* mRNA becomes unstable (see Chapter 2 and (*78*)). Therefore, these mice are deficient in RECON as a result of destruction of its catalytic activity, c-di-AMP binding pocket and mRNA stability.

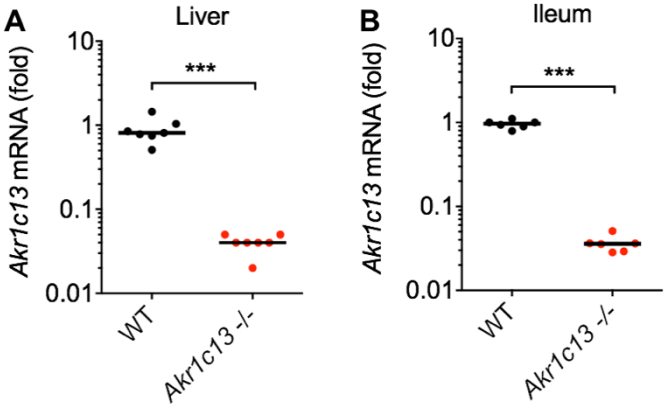

Figure 5.3. Mutant *Akr1c13* mRNA is subjected to nonsense-mediated decay. (A-B) qRT-PCR analysis on mRNA from mouse liver (A) and small intestinal ileum (B) demonstrated the *Akr1c13* mutant mRNA is unstable (N=6 for each genotype). Endogenous control gene was *Hprt* and data are normalized to the mean value of WT mice. Median values are indicated by a bar. Statistical significant was determined by an unpaired Student's t test (***p <0.0001).

5.4 Sex skewing in RECON-deficient mouse litters

RECON-deficient mice appear healthy, with no overt signs of disease. Homozygous knockout females breed normally, with litter sizes on par with those from WT colony breeders (Figure 5.4A). However, we observed significant sex skewing in the knockout litters, with an increased incidence of male versus female pups (Figure 5.4B and 5.4C). It is unclear what aspect of RECON deficiency would cause sex skewing in the litters. However, prior work has shown that diets high in saturated fats can skew sex ratios towards male offspring in mice by altering sex hormone concentrations (*184, 185*). Given

our finding that RECON regulates metabolites of arachidonic acid (see Chapter 3), which is an omega-6 polyunsaturated fatty acid, one interpretation of these data is that RECON deficiency significantly alters PUFA metabolism *in vivo*.

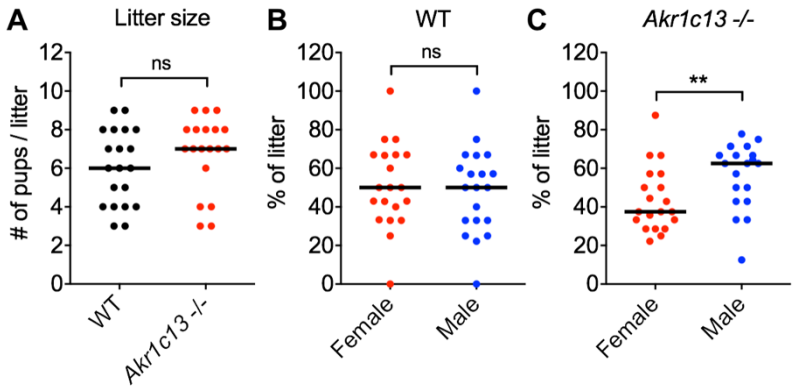

Figure 5.4. Sex skewing in RECON-deficient mouse litters. (A) Number of pups per litter from WT and *Akr1c13*-deficient crosses (N=17). (B-C) Percent female and male pups within WT (B) and *Akr1c13*-deficient (C) litters. Median values are indicated by a bar. Statistical significant was determined by Mann-Whitney U test (**p <0.001; ns=not significant).

5.5 RECON has unique functions in bone marrow-derived versus peritoneal macrophages

5.5.1 RECON-deficient primary BMDMs exhibit augmented inflammatory responses

Previous work with shRNA knockdown of RECON in immortalized bone marrow-derived macrophages (BMDMs) demonstrated that RECON suppresses inflammatory gene expression. Therefore, we investigated whether RECON functioned similarly in primary BMDMs (pBMDMs). WT or RECON-deficient pBMDMs were infected with *L. monocytogenes* or stimulated with Pam3CSK4 and Tri-DAP (PTD) for 4 h. Gene expression analyses revealed that loss of RECON promoted expression of *Il1b*, *Nos2* and *Tnf* (Figure 5.5). These results are consistent with RECON functioning as a suppressor of NF-κB signaling. Examination of STING-dependent genes, however, revealed some unexpected findings. Loss of RECON promoted *Ifnb1* expression during pBMDM infection with *L. monocytogenes*, as we had previously seen in iBMDMs. RECON's control of *Ifnb1* was attributed to it acting as sink for c-di-AMP, whereby loss of RECON resulted in increased bioavailability of c-di-AMP which promoted STING signaling (Chapter 2: Model Figure 2.19). Curiously, this effect was only observed for *Ifnb1* in pBMDMs. *Ccl5* and *Cxcl10*,

which are both STING-dependent genes in pBMDMs (see Chapter 2, Figure 2.7), were unaffected by the absence of RECON during infection with *L. monocytogenes* (Figure 5.5). It is unclear why *Ifnb1* but not *Ccl5* or *Cxcl10* is controlled by RECON in pBMDMs. However, one could speculate that because type I IFN can be detrimental to the host during infection with c-di-AMP-producing bacteria, including *M. tuberculosis*, *L. monocytogenes*, and *S. aureus* (reviewed in (*186*)), RECON functions to suppress *Ifnb1* expression while sparing *Ccl5* and *Cxcl10*, which are important chemoattractants that aid in bacterial clearance (*187*). The mechanism by which RECON exerts differential control of STING-dependent genes in pBMDMs merits further investigation.

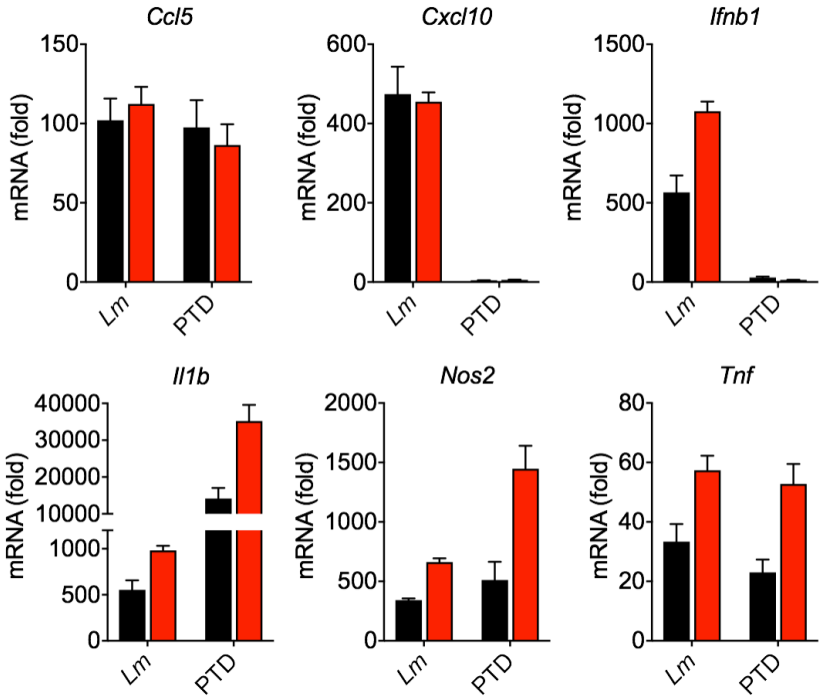

Figure 5.5. RECON controls select inflammatory gene expression in primary BMDMs. WT or *Akr1c13*-deficient primary BMDMs were infected with *L. monocytogenes* (*Lm*) or stimulated with Pam3CSK4 and Tri-DAP (PTD) for 4 h. qRT-PCR data were performed in technical triplicates and were normalized to uninfected WT BMDMs. In all panels, error bars represent ± SEM.

5.5.2 The response of peritoneal macrophages to infection or stimulation is significantly different than that of primary BMDMs

Although primary BMDMs are widely used to study signaling pathways, these cells, which are differentiated *ex vivo* in cell culture, are arguably not the best representation of inflammatory macrophages that are elicited *in vivo* during infection. Therefore, we

investigated inflammatory gene expression in peritoneal macrophages (PEMs) to *L. monocytogenes* infection or stimulation with PTD.

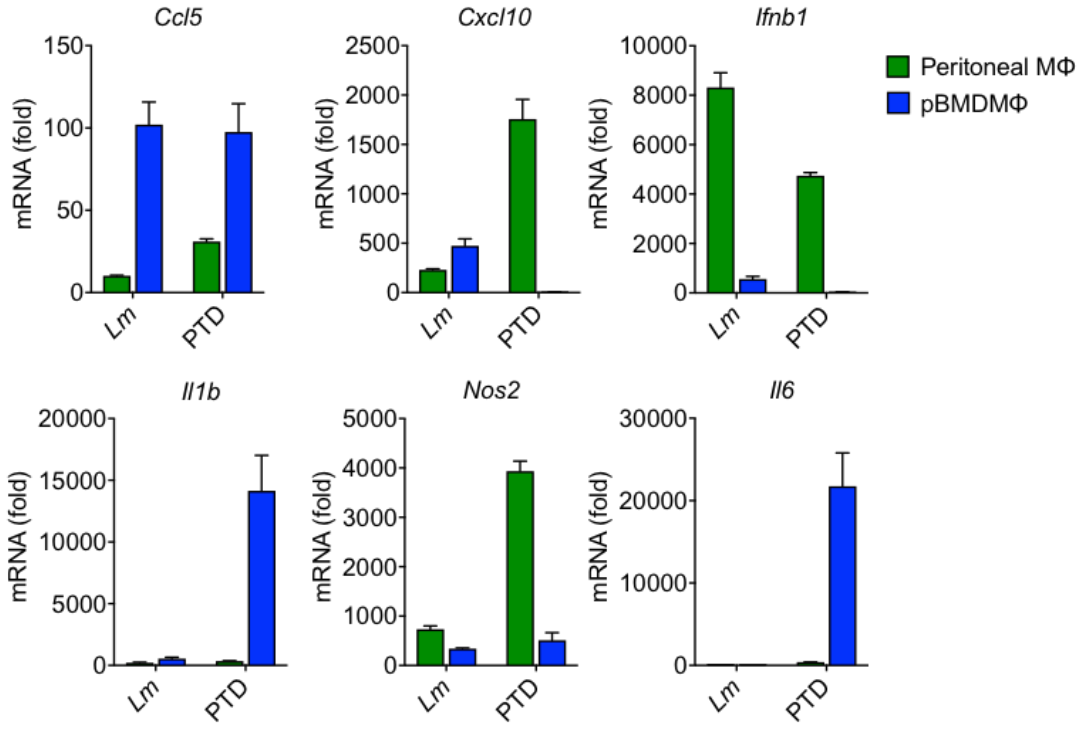

Figure 5.6. Differential response of peritoneal macrophages versus primary BMDMs. Macrophages were infected with *L. monocytogenes* (*Lm*) or stimulated with Pam3CSK4 and Tri-DAP (PTD) for 4 h. qRT-PCR data were performed in technical triplicates and were normalized to uninfected WT cells. In all panels, error bars represent ± SEM.

Infection and stimulation of pBMDMs and PEMs were performed in tandem under the same conditions (including cell plating, concentration of ligands, and time point). Gene expression analyses of these two macrophage types revealed several interesting differences. Compared to PEMs, primary BMDMs exhibited relatively weak expression of *Ifnb1* with *L. monocytogenes* infection (Figure 5.6). Furthermore, PTD was unable to induce *Ifnb1* in pBMDMs but elicited robust *Ifnb1* expression in PEMs. When stimulated with PTD, the pBMDMs, but not PEMs, expressed significant levels of *Il1b* and *Il6*, suggesting these cells are geared towards the production of these pro-inflammatory genes. In contrast, the PEMs had marked expression of *Nos2*. It is intriguing that the expression of inflammatory genes was so dramatically different in pBMDMs versus PEMs and suggests physiological intrinsic differences are at play.

5.5.3 RECON exhibits unique activity in peritoneal macrophages

PEMs reportedly have a unique phospholipid composition that gives rise to specific lipid species distinct from those produced by BMDMs (*188, 189*). Our work in hepatocytes revealed that RECON controls immune gene expression downstream of TLR stimulation by regulating inflammatory arachidonic acid metabolites (see Chapter 3). Given the differential responses of PEMs and pBMDMs and purported differences in lipid metabolism, we investigated how the loss of RECON affected inflammation in PEMs. We elicited macrophage accumulation in the peritoneum using thioglycollate medium. We confirmed by flow cytometry that recruitment of macrophages using this method was comparable between WT and RECON-deficient mice (Figure 5.7).

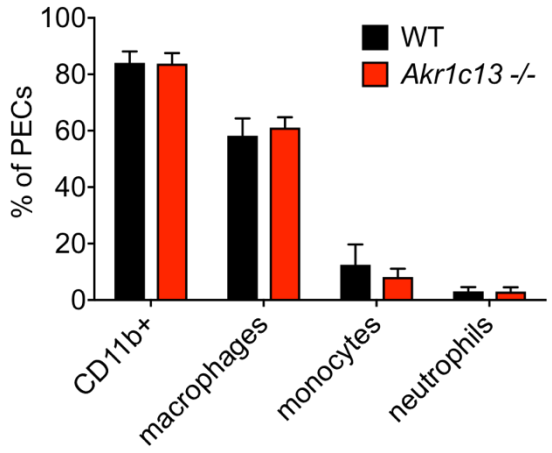

Figure 5.7. Comparable efficacy of thioglycollate medium in eliciting peritoneal macrophage recruitment in WT and RECON-deficient mice. Mice were injected IP with 2 mL of 4% thioglycollate medium and peritoneal exudate cells (PECs) were harvested 4 days later. N=3 mice and error bars represent ± SD.

RECON-deficient PEMs exhibited similar trends in *Ccl5*, *Cxcl10* and *Ifnb1* expression during *L. monocytogenes* infection as pBMDMs, whereby only *Ifnb1* expression was increased in the absence of RECON (Figure 5.7). Unlike iBMDMs, pBMDMs, and TIB73 hepatocytes, PEMs express *Ifnb1* following PTD stimulation (Figure 5.6), and, remarkably, we observed that RECON-deficient PEMs had enhanced expression of *Ifnb1* under these conditions (Figure 5.8). Considering that cyclic dinucleotides are not currently known to be produced during TLR stimulation, these data indicate that RECON can influence *Ifnb1* expression independent of STING activation and that this response is unique to PEMs.

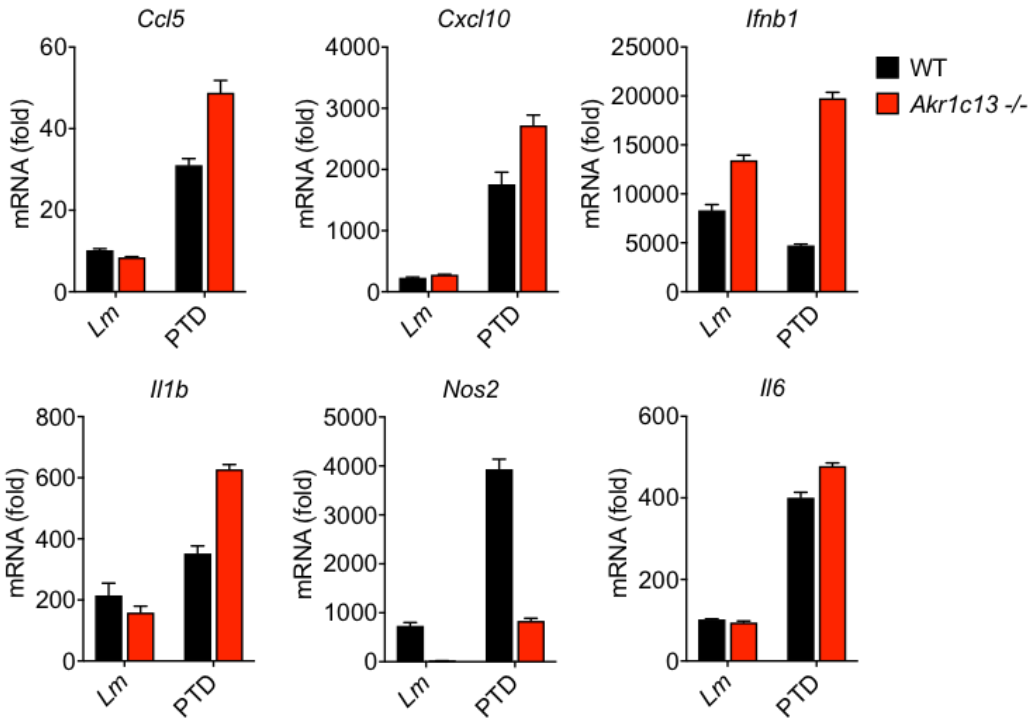

Figure 5.8. RECON controls inflammatory gene expression in peritoneal macrophages. WT or *Akr1c13*-deficient peritoneal macrophages were infected with *L. monocytogenes* (*Lm*) or stimulated with Pam3CSK4 and Tri-DAP (PTD) for 4 h. qRT-PCR data were performed in technical triplicates and were normalized to uninfected WT BMDMs. In all panels, error bars represent ± SEM.

Gene expression analyses also revealed that expression of *Nos2* during PEM infection or stimulation requires RECON, which is opposite to our findings in all other cell types (iBMDMs, pBMDMs, and hepatocytes). Given that RECON exerts its effects on the immune response via its catalytic activity and is engaged in the arachidonic acid cascade, it is intriguing to speculate that the lipid profile of PEMs provides RECON with distinctive substrates that enable its disparate functionality in these cells. The mechanisms by which RECON simultaneously suppresses *Ifnb1* expression while promoting *Nos2* in PEMs warrants further investigation as we continue to expand our understanding of the intersection of RECON biology with immune signaling.

5.6 RECON-deficient mice are more resistant to *L. monocytogenes* systemic infection

5.6.1 RECON-deficient mice are protected against lethal *L. monocytogenes* challenge

We previously found that the inflammatory pathways under RECON's control in macrophages affected the intracellular survival of *L. monocytogenes* (see Chapter 2).

However, *L. monocytogenes* intracellular growth was unhindered by the absence of RECON in hepatocytes, which are a predominant cellular reservoir of these bacteria *in vivo* (*62, 138*). Additionally, we found that enhanced nitric oxide production in RECON-deficient hepatocytes promoted *L. monocytogenes* intercellular spread *in vitro*, suggesting that *L. monocytogenes* may benefit from the augmented cell intrinsic inflammation that occurs in the absence of enzyme (see Chapter 4). Therefore, it has remained an open question as to whether the RECON-controlled inflammatory pathways would promote, impede, or have no effect on *L. monocytogenes* infection *in vivo*. To answer this outstanding question, we infected WT or RECON-deficient littermates IP with a lethal dose of *L. monocytogenes* and observed that RECON deficiency promoted mouse survival (Figure 5.9).

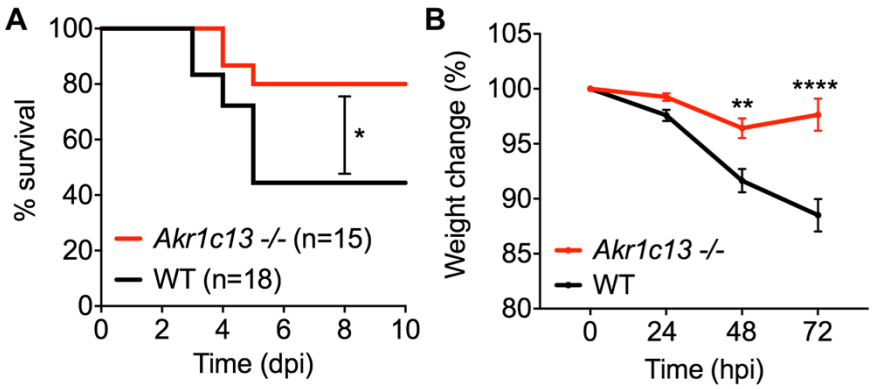

Figure 5.9. RECON-deficient mice are more resistant to lethal *L. monocytogenes* challenge. WT or *Akr1c13*-deficient mice were injected IP with $2x10^6$ CFU. Survival (A) and weight loss (B) were monitored. Statistical significance was assessed by 2-way ANOVA (*p<0.05, **p<0.001, ***p<0.0001).

5.6.2 RECON-deficient mice are more resistant to *L. monocytogenes* infection

In addition to survival analyses, we also enumerated bacterial CFUs from livers and spleens and observed significantly reduced burdens in RECON-deficient mice compared to WT littermates (Figure 5.10). Together these data demonstrate that loss of RECON during infection with *L. monocytogenes* promotes survival of mice and faster clearance of this pathogen during systemic challenge. Therefore, inhibition of RECON during infection is likely to be beneficial to the host. This conclusion supports a harmonious link between the functions of RECON as an innate sensor and anti-inflammatory enzyme.

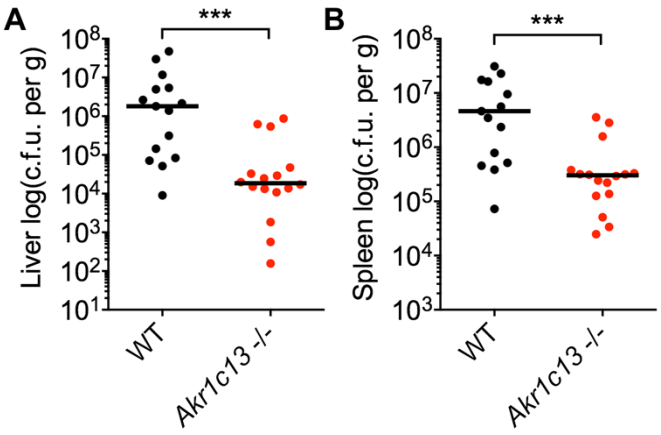

Figure 5.10. RECON-deficient mice have reduced *L. monocytogenes* burdens. WT or *Akr1c13*-deficient mice were injected IP with 1x10^6 CFU. At 72 hours post-infection, CFUs were enumerated from liver (A) and spleen (B). Statistical significance was assessed by Mann-Whitney U test (***p<0.0001).

5.6.3 RECON deficiency enhances myeloid cell recruitment to the peritoneum following *L. monocytogenes* injection

We hypothesized that in the absence of RECON, augmented expression of chemokines might result in enhanced myeloid cell recruitment following IP injection. To test this, we infected mice IP with *L. monocytogenes* and analyzed the inflammatory cell infiltrate at 8 hours. RECON-deficient mice exhibited increased monocyte and neutrophil cell numbers in their peritoneum as compared with WT mice (Figure 5.11). These data suggest that the decreased bacterial burdens in these mice may be the result of increased immune cell recruitment. However, more work is needed to fully understand the mechanisms responsible for the protection.

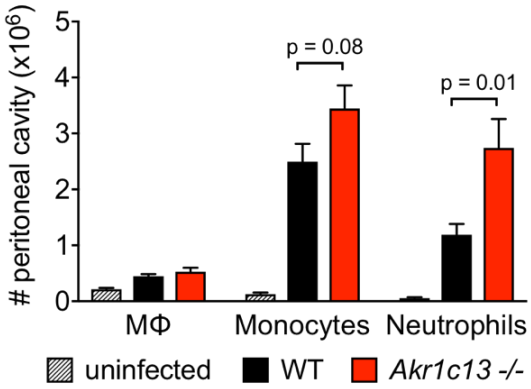

Figure 5.11. RECON deficiency enhances myeloid cell recruitment to the peritoneum. Myeloid cell recruitment into the peritoneum 8 hours post-infection with *L. monocytogenes*. Statistical significance was assessed by unpaired student's t test.

5.7 RECON functions as a regulator of intestinal and microbial homeostasis

5.7.1 RECON deficiency causes low-grade inflammation in the intestinal ileum

The generation of RECON-deficient mice provided us with the opportunity to not only examine the role of RECON during *L. monocytogenes* infection, but to also assess the broader role of this aldo-keto reductase *in vivo*. RECON is expressed at important immunological sites, such as the small intestines, which is in contact with commensal bacteria of the microbiota. To determine whether the absence of RECON influenced

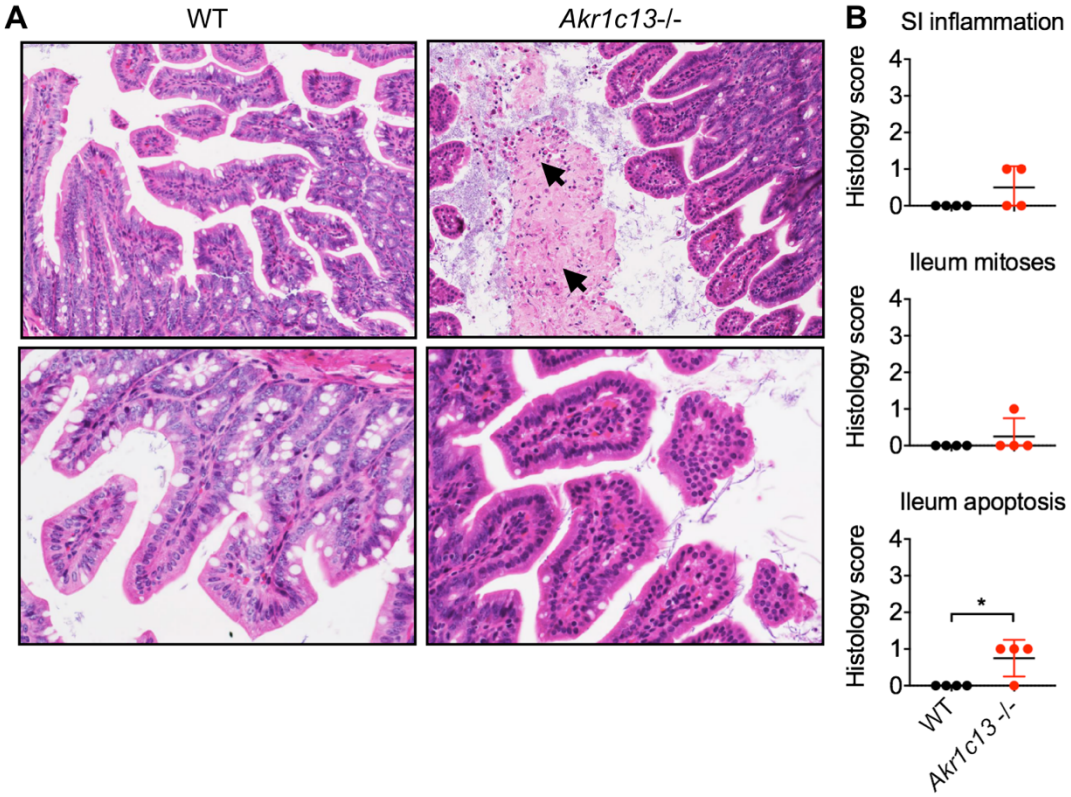

Figure 5.12. Localized low-grade inflammation in RECON-deficient small intestines. (A) Histopathology on distal ileum. Arrows indicate the presence of sloughed apoptotic cells in the lumen of *Akr1c13*-deficient mice. (B) Histology scores indicate dysregulation in ileum. Mean ± SD are indicated (*p=0.024, unpaired Student's t test).

steady-state tissue homeostasis, we performed a thorough histopathological work-up of 8-week-old *Akr1c13*-deficient mice and WT littermate controls. The findings were unremarkable in the heart, kidney, liver, lung, lymph nodes, pancreas, spleen, stomach and thymus. However, there were specific alterations observed in the small intestines, with changes most pronounced in the distal ileum. RECON deficiency was associated

with low-grade inflammation, and sloughed apoptotic enterocytes were observed in the lumen of the ileum as well as mildly reactive Peyer's patches (Figure 5.12A and 5.12B). These findings establish that RECON is required for homeostasis in the small intestines.

5.7.2 RECON deficiency causes a bloom in segmented filamentous bacteria and expression of associated inflammatory genes

As an AKR family member, RECON likely participates in the metabolism of xenobiotics. We hypothesized that the low-grade inflammation observed specially in the ilea of RECON-deficient mice might correlate with perturbations in the microbiota. Histopathology on ilea from these animals revealed the marked abundance of segmented filamentous bacteria (SFB) (Figure 5.13A). SFB, or *Candidatus* Arthromitus, are uncultivable, spore-forming, c-di-AMP-producing bacteria of the phylum Firmicutes. Aberrant expansion of SFB was reported in mice deficient in intestinal IgA production over a decade ago (*190*). More recently, SFB have been recognized for their unique role in promoting maturation of gut immune functions, specifically those involving T helper type 17 (Th17) cells (*191-193*). To quantitatively determine the absolute levels of SFB in the RECON-deficient mice, we performed copy number analyses of SFB *16S rRNA* in DNA isolated from feces and cecal contents using qRT-PCR. Consistent with the histology findings, we detected high copy numbers of SFB *16S rRNA* in the RECON-deficient animals (Figure 5.13B-D).

SFB preferentially colonize the terminal ileum and adhere to the follicle-associated epithelium and M cells present in the Peyer's patches (*194*), two sites in which RECON is highly expressed. The presence of SFB has been shown to specifically promote the expression of *Il17a*, associated with Th17 cells, and serum amyloid A genes, *Saa1*/*2*, in the intestinal epithelium (*191, 192, 195*). Therefore, we investigated whether the expression of these genes was altered in RECON-deficient mice. We confirmed that SFB were adhering to and blooming in the ileum of RECON-deficient mice by examining the expression of SFB *16S rRNA* in RNA isolated from ilea tissue (Figure 5.13E). Additionally, we found that RECON deficiency resulted in elevated levels of *Il17a* and *Saa1*/*2* expression at this site (Figure 5.13F and 5.13G). Together these results demonstrate that the absence of RECON causes a dysbiosis that correlates with low-grade inflammation and perturbation of immune homeostasis.

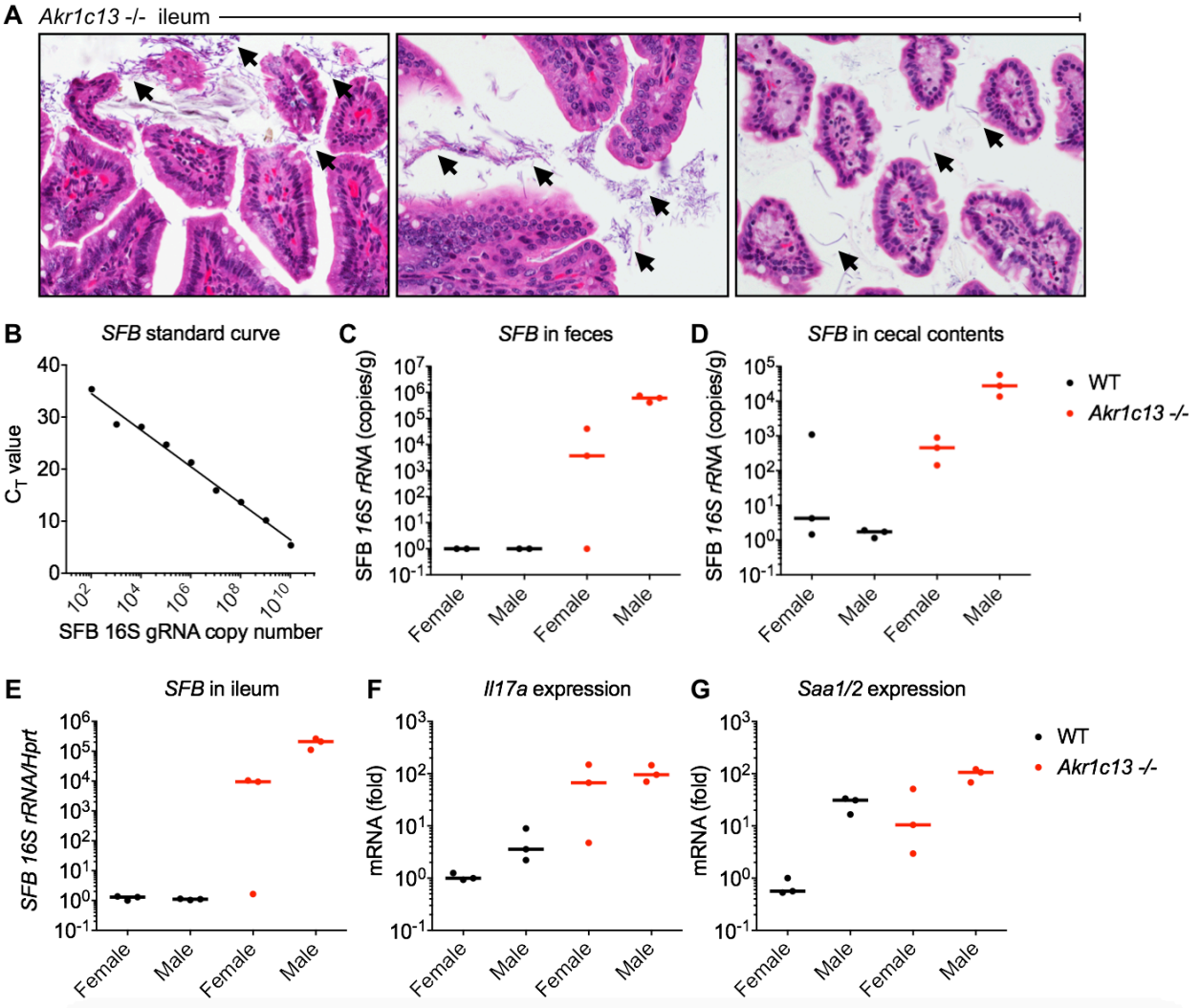

Figure 5.13. RECON deficiency causes an SFB bloom and alteration in immune gene expression in the small intestines. (A) Segmented filamentous bacteria (SFB), indicated by black arrows, were seen in the ileum of *Akr1c13*-deficient mice. (B) Standard curve allowing for copy number calculations generated by TOPO plasmids containing the SFB 16S gRNA gene. (C-D) Copy numbers of SFB *16S gRNA* detected in DNA isolated from feces (C) and cecal contents (D) of mice. Data are plotted as copies per gram of content. (E-G) qRT-PCR expression analysis of SFB *16S rRNA* (E), *Il17a* (F), and *Saa1/2* (G) mRNA in RNA isolated from the ilea of mice. *Hprt* was used as the endogenous control. (C-G) N=6 mice per genotype, with 3 females and 3 males analyzed. Median values are indicated by a bar.

5.7.3 RECON-deficient mice may have increased retinoic acid in their intestines

To gain insight into the alterations occurring in the intestines of RECON-deficient mice, we profiled nuclear hormone receptor (NRs) activation from fecal contents of these animals. NRs are a family of small molecule-activated transcription factors that respond

to hormones, vitamins, and xenobiotics, and most of these receptors are expressed in the intestinal epithelium (*196*). We employed a NR one-hybrid assay in which the DNA binding domain (DBD) of each human nuclear receptor was replaced with a GAL4 DNA binding domain, resulting in a chimeric NR. This fusion protein directly activates a luciferase reporter when the appropriate NR ligand binds to the ligand binding domain (LBD, Figure 5.14A) (*197*). HEK293 cells were transfected with a human NR reporter library and treated with fecal extracts. We observed some interesting differences between the activation profiles of WT versus RECON-deficient fecal extracts (Figure 5.14B).

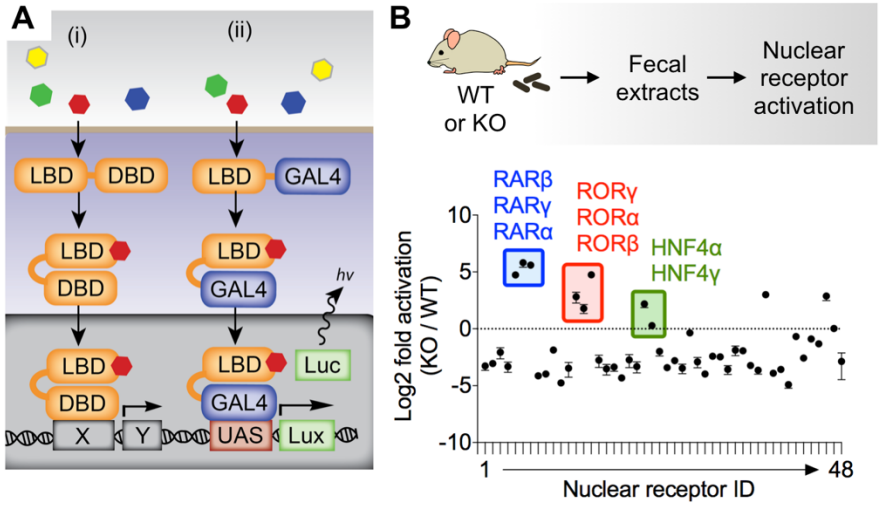

Figure 5.14. Fecal extracts from RECON-deficient mice enhance activation of retinoic acid and retinoid-related nuclear receptors. (A) Nuclear receptor (NR) one-hybrid assay: (i) The DNA binding domain (DBD) of each human NR was replaced with (ii) the GAL4 DNA binding domain, providing luciferase-dependent activity readout. (B) Profiling of NR activation by fresh fecal extracts was carried out using HEK293 cells transfected with the NR library and luciferase reporter. Data is plotted as log2 fold difference in activation (KO/WT).

Fecal extracts from RECON-deficient mice resulted in increased activation of the retinoic acid receptors (RARs; RARβ, RARγ, and RARα), which are activated in response to vitamin A metabolites, such as all-trans-retinoic acid. Retinoic acid is a central molecule that orchestrates immune responses in the intestine. In particular, retinoic acid is a key determinant in maintaining the balance of regulatory T cells (Tregs) versus proinflammatory Th17 cells (*198, 199*). In addition to the RARs, we also observed increased activation of the retinoid-related orphan receptors (RORs; RORγ, RORα, and RORβ). RORγ is an important transcription factor in the intestinal immune system, where it directs lymphoid tissue organogenesis and the development of immune cells, such as

innate lymphoid cells type 3 (ILC3s) and Th17 cells (*199*). Finally, there was also increased activation of hepatocyte nuclear factor 4 alpha (HNF4α) by the RECON-deficient fecal extracts. HNF4α, together with its intestine-specific transcriptional partner CDX2, is critical for the maturation of microvilli and dietary lipid absorption (*200*). Together, these data suggest that the absence of RECON alters intestinal metabolites, and that retinoic acid levels may be increased in the absence of RECON, which may potentiate inflammation in the intestines.

5.8 Discussion

Perhaps the most outstanding question about RECON has been whether its influence over inflammation that we have observed in cell culture would translate to measurable affects at the organismal level. Our studies with RECON-deficient mice have confirmed that RECON does indeed impact infection outcomes *in vivo*, as these animals exhibited increased survival and clearance of *L. monocytogenes*. Although we observed enhanced monocyte and neutrophil recruitment to the site of infection in RECON-deficient animals, much remains to be revealed about how the absence of RECON affords protection against *L. monocytogenes*. In several cell types, RECON deficiency results in augmented expression of chemokines, including *Ccl5* and *Cxcl10*, pro-inflammatory cytokines, including *Il1b*, *Il6* and *Tnf*, as well as *Nos2*. In hepatocytes, RECON controls the expression of these genes via its action on inflammatory metabolites derived from the omega-6 polyunsaturated fatty acid (PUFA) arachidonic acid (see Chapter 3). RECON-deficient hepatocytes have increased reactive lipid species and altered prostaglandin production. The perturbation in the arachidonic acid cascade is what drives enhanced NF-κB activation and relieves a brake on MEK-ERK signaling.

In mice, arachidonic acid-derived metabolites can have profound consequences on *L. monocytogenes* infection outcome. Perturbations in the balance of omega-6 (pro-inflammatory) versus omega-3 (anti-inflammatory) PUFAs can alter host resistance and the immune response to *L. monocytogenes* (*201, 202*). Specific species of COX-derived prostaglandins can suppress or boost immunity to *L. monocytogenes* (*203-205*). Finally, certain PUFAs are directly bactericidal against *L. monocytogenes*, including arachidonic acid (*206, 207*). Therefore, it is possible that in addition to augmented inflammatory gene expression, the perturbation of fatty acids that is caused by the absence of RECON could

directly function as an antimicrobial response. These ideas warrant further investigation and could illuminate our understanding of RECON's function within the host as an aldo-keto reductase and as an innate immune sensor.

An intriguing aspect of RECON biology is its tissue expression profile, whereby it is highly expressed in the stomach, small intestines, large intestines and liver (*63, 183*). This expression profile is in sharp contrast to STING, which is poorly expressed in the liver and intestines (*48, 208, 209*). Within the small intestines, RECON is most highly expressed in enterocytes, the follicle-associated epithelium and M cells located within Peyer's patches (*210, 211*). M cells are specialized cells that facilitate the transcytosis of luminal antigens across the gut epithelium to underlying immune cells (*212*). Given what we have discovered about RECON's role in surveying the cytosol for bacterial pathogens, its high expression at important mucosal immune sites in the small intestines raised the question as to whether RECON acts as part of the intestinal immune system. This question is especially relevant because >95% of intestinal bacteria belong to phyla that are predicted to produce c-di-AMP.

Examination of the small intestines of RECON-deficient mice revealed low-grade inflammation and dysbiosis. These data support the idea that RECON functions within intestinal immunity and homeostasis. The aberrant expansion of SFB, a c-di-AMP-producing organism, is an intriguing observation that may help to elucidate the function of RECON within the gut. Initial work in adult humans found little evidence for SFB colonization. However, recent work has revealed that SFB commonly colonizes the intestines of humans early in life but disappears by three years of age (*213*). SFB preferentially colonizes the terminal ileum and adheres to the follicle-associated epithelium and M cells present in the Peyer's patches (*194*). Although there is currently no direct evidence, SFB may be able to deliver effectors capable of manipulating host cells as they are known to stimulate actin rearrangement (*194, 214*). This raises the possibility that SFB may be able to deliver c-di-AMP directly to the cells they are attached to. This could result in RECON inhibition and perhaps potentiate a more favorable environment for this organism to grow, a hypothesis supported by the fact that we see increased levels of SFB in the RECON-deficient mice.

In addition to the low-grade inflammation and SFB bloom, preliminary studies on mouse feces suggested RECON deficiency may increase retinoic acid levels. There is a

clear link between retinoic acid and the gut microbiome (*215*). Mice fed a vitamin A-deficient diet exhibit a reduced number of Firmicutes, including SFB, in their ilea (*216*). Colonization of mice with SFB also results in the expression of SAA proteins in the intestinal ileum (*191*). SAA proteins were recently shown to be microbe-inducible retinol binding proteins expressed by hepatocytes and the intestinal epithelium (*217*). There are several ways in which we hypothesize RECON could be influencing the microbiota and retinoic acid levels. First, the increased *Saa1/2* expression in the ilea of RECON-deficient mice could promote retinol uptake and subsequent retinoic acid production. Second, RECON, as an aldo-keto reductase, could directly participate in retinoic acid metabolism by reducing retinaldehyde to retinol. Future work characterizing the lipidome and metabolome of the intestines would clarify the specific perturbations caused by RECON deficiency. Additionally, it would be interesting to explore the connection between retinoic acid and SFB colonization. For instance, can we reverse the low-grade inflammation and SFB colonization by feeding the mice a vitamin A-deficient diet? Or perhaps the increased retinoic acid is a symptom of SFB colonization and dysbiosis rather than the cause.

Beyond what we report in this chapter, there is currently nothing known about the contribution of RECON to intestinal homeostasis. The mechanism of c-di-AMP binding and inhibiting RECON's enzymatic function that we have reported on (see Chapters 2-3 and (*78*)) is a new paradigm in pattern recognition. It also intuitively explains why the absence of RECON may promote inflammation in the intestines – because the regulation of its enzymatic activity by the microbiota may be a key mechanism by which it guards the intestinal barrier.

5.9 Materials and methods

Generation of RECON-deficient mice

CRISPR/Cas9-engineered mice were generated as previously described (*76*, *77*) with the University of Washington Transgenic Resources Program. Guide RNAs targeting exon 6 of *Akr1c13* were cloned into pX330-U6-Chimeric_BB-CBh-hSpCas9 (Addgene #42230). A T7-sgRNA PCR product was amplified and *in vitro* transcribed as previously described (*77*) using the MEGAshortscript T7 kit and purified with the MEGAclear kit (Thermo

Fisher Scientific). *Cas9* mRNA used for injections was purchased from Sigma (#CAS9MRNA). Oligo and primer sequences are provided in the Key Resources Table.

RGEN-RFLP assay

Genotyping of founder mice using CRISPR/Cas-derived RNA-guided engineered nucleases (RGEN) restriction fragment length polymorphism (RFLP) analysis was done as previously described (*76, 218*). Guide RNAs were cloned and purified as detailed above (see "Generation of RECON-deficient mice"). A 1.2kB amplicon spanning the *Akr1c13* exon 6 genomic region was used as substrate DNA. Primer sequences are provided in the Key Resources Table (Table 5.1). The RGEN-RFLP assay with Cas9 nuclease from *S. pyrogenes* was carried out according to manufacturer's instructions (NEB #M0386) with 30 nM sgRNA and 3 nM substrate DNA final concentrations.

SNP PCR genotyping of mice

Mouse genotyping was performed using a custom multiplex *Akr1c13* SNP-based genotyping assay (primer information provided in Key Resources Table 5.1). An end-point PCR was first performed to amplify *Akr1c13* exon 6. The product was diluted 1:1,000 in nuclease-free water, and 1.0 μL was used in a 20 μL qRT-PCR reaction, along with TaqMan Master Mix, primers that amplify *Akr1c13* exon 6 (500 nM final concentration) and FAM probes that detect the WT allele mixed with HEX probes that detect the mutant allele (250 nM final probe concentrations).

Isolation of RNA from mouse tissue

Pieces of liver, spleen or ileum were dissected, snap frozen in RNAlater stabilization solution (Thermo Fisher Scientific) and stored at -80c until RNA isolation. At the time of isolation, the tissue was transferred into RLT lysis buffer (Qiagen), and the tissue was homogenized using a bead mill. RNA was isolated from the homogenized lysate using RNeasy Mini Kit (Qiagen).

qRT-PCR gene expression analysis

RNA was extracted from macrophages with the RNAqueous Total RNA Isolation Kit (Thermo Fisher Scientific). RNA from cells or tissues were DNase treated using the TURBO DNA-free Kit and reverse-transcribed with the iScript cDNA synthesis kit (Bio-

Rad). TaqMan qRT-PCR assays were used for quantification of gene expression with *Hprt* as an endogenous control (see Key Resources Table 5.1 for primer information).

Cell culture

HEK293 cells were grown at 37°C in 5% CO2 in phenol red-free DMEM medium (GIBCO) with 10% heat-inactivated FBS (HyClone) and supplemented with 2 mM sodium pyruvate and 1 mM L-Glutamine (Thermo Fisher). Primary bone marrow-derived were grown in the same media as above except with additional supplementation of 55 μM 2-mercaptoethanol and M-CSF harvested from L929 conditioned medium (final volume 10%). Primary BMDMs were generated as previously described (*74*). For peritoneal macrophages (PEMs), mice were injected IP with 2 mL of 4% thioglycollate medium and peritoneal exudate cells (PECs) were recovered 4 days later. $2x10^6$ PECs were plated in 1 mL of RPMI supplemented as above but with 2% FBS. The cells were incubated for 3 h and then washed 3x in warm media to remove non-adherent cells and enrich for PEMs. Cells were rested overnight. PEMs and pBMDMs were simultaneously infected with *L. monocytogenes* or stimulated with 500 ng/mL Pam3CSK4 (InvivoGen) plus 1 μg/mL Tri-DAP (InvivoGen) for 4 h.

Infection of mice

Age-matched (8-12 weeks) and sex-matched WT or RECON-deficient littermates (cross-fostered from 3 days post-birth) were used for experiments. For infections, wild-type 10403S *L. monocytogenes* was grown in Brain Heart Infusion (BHI) media at 30°C overnight without shaking to stationary phase (OD600, 1.1-1.3). The bacteria were back-cultured (1.2 mL into 4.8 mL) and grown for 1 h at 37°C shaking (OD600 ~0.3). For mouse survival studies, bacteria were resuspended in sterile 1X PBS at a concentration of $2x10^6$ CFU/200 μL/mouse and injected IP. For experiments enumerating tissue CFUs, $1x10^6$ CFU/200 μL/mouse was injected IP. 72 hpi the livers and spleen of animals were collected, weighed, homogenized in 0.1% IGEPAL, and plated for CFUs.

Flow cytometry

PECs were recovered from the peritoneal cavities of mice treated with thioglycollate medium or infected IP with *L. monocytogenes* ($1x10^7$/200 μL/mice) for 8 h. PECs were washed 2x in cold FACS buffer (1X PBS, 1% BSA, and 0.1% NaN3). $1x10^6$ PECs were

stained with Fc Block for 15 min and then fixed/permeabilized per the manufacturer's instructions (BD Cytofix/Cytoperm). Cells were stained for myeloid markers (see Key Resources Table 5.1 for antibody information), data was collected on an LSR II and analyzed with FlowJo software. Macrophages identified as CD45+ CD11b+ F4/80+ Ly6C-; monocytes identified as CD45+ CD11b+ F4/80+ Ly6C+; neutrophils identified as CD45+ CD11b+ F4/80- Ly6C+ Ly6G+.

SFB copy number PCR

The SFB *16S rRNA* sequence was cloned into a pCR2.1-TOPO vector (Thermo Fisher Scientific). The plasmid was used to generate a standard curve correlating copy number with C_T values. DNA from feces or cecal contents was isolated using the QIAamp DNA Stool Mini Kit (Qiagen). Equivalent volumes of DNA were used for qRT-PCR and copy number analyses so that data could be back calculated and plotted as copy number per gram of sample. Primer information is provided in the Key Resources Table 5.1.

Nuclear receptor activation assay

The human nuclear receptor library was a generous gift from Patrick Griffin (Department of Molecular Medicine, Scripps Research Institute). Sequences encoding the ligand binding domains of the human nuclear receptors were cloned into the pCM-pBIND plasmid, where they were fused with a GAL4 binding domain. These plasmids were used in tandem with the UAS-LUC plasmid, which has the luciferase gene under the control of GAL4. For experiments, HEK293 cells (25,000/100 μL/well) were seeded in a 96-well plate. 24 hours after plating, the cells were transfected with NR-pCM-pBIND (15ng), UAS-LUC (45 ng), and eGFP (40ng) per well using TransIT-LT1 Transfection Reagent (Mirus Bio). 24 hours post-transfection, the cells were treated with fresh fecal extracts (5 mg feces in 1 mL 1XPBS, vortexed, and filtered) for 24 hours. The cells were lysed in 50 μL TNT lysis buffer (20 mM Tris, 100 mM NaCl, 1% Triton X-100, pH to 8.0) and GFP fluorsence was measured. 40 μL of lysate was mixed with 40 μL luciferase substrate ((20 mM Tricine, 2.67 mM MgS047H20, 0.1 mM EDTA, 33.3 mM DTT, 530 μM ATP, 270 μM acetyl CoA lithium salt, 470 μM luciferin, 5 mM NaOH, 265 μM magnesium carbonate hydroxide) and luminescence was measured immediately using a Synergy HT (BioTek).

Mouse housing and histology

Prior to and during experiments mice were maintained in specific pathogen free conditions and given irradiated chow and water. Daily care was provided, and SPF conditions were ensured through the rodent health monitoring program overseen by the Department of Comparative Medicine at the University of Washington. Necropsy and tissue collection were performed by the University of Washington Histology and Imaging Core. Mice were euthanized via CO_2 asphyxiation, tissue were fixed in 10% NBF, paraffin embedded, cut into 4- to 5-micron sections, and stained with hematoxylin and eosin. Small intestines were scored semi-quantitatively in an unblinded fashion using a 0-4 scale in which 0 indicated no lesions and 1 through 4 generally indicated "minimal", "mild", "moderate", and "severe" changes, respectively.

Ethics Statement

All experiments involving mice were performed in compliance with guidelines set by the American Association for Laboratory Animal Science (AALAS) and were approved by the Institutional Animal Care and Use Committee (IACUC) at the University of Washington.

Table 5.1: Key resources table

Reagent or Resource	Source	Identifier
Antibodies		
PE anti-mouse F4/80	BioLegend	Cat#123109
PerCP/Cy5.5 anti-mouse CD45	BioLegend	Cat#103131
FITC anti-mouse/human CD11b	BioLegend	Cat#101205
APC anti-mouse Ly6C	BioLegend	Cat#128015
PE/Cy7 anti-mouse Ly6G	BioLegend	Cat#127617
Purified Rat Anti-Mouse CD16/CD32 (Mouse BD Fc Block) Clone 2.4G2	Thermo Fisher Scientific	Cat# BDB553142
Bacterial Strains		
Listeria monocytogenes 10403S wild-type	Provided by Dan Portnoy	JW06
Chemicals, Peptides, and Recombinant Proteins		
DMEM, high glucose, no glutamine, no phenol red	Thermo Fisher Scientific	Cat#31053036
Sodium pyruvate	Thermo Fisher Scientific	Cat#11360070
L-Glutamine	Thermo Fisher Scientific	Cat#25030081
Characterized Fetal Bovine Serum	Thermo Fisher Scientific	Cat#SH30071.03
Penicillin-Streptomycin (10,000 U/mL)	Thermo Fisher Scientific	Cat#15140122
Bovine Serum Albumin (BSA)	Fisher BioReagents	Cat#BP9700100
Trypsin-EDTA (0.05%)	Thermo Fisher Scientific	Cat#25300054

Brain Heart Infusion Broth	Research Products International	Cat#B11000
Gentamicin (10 mg/mL)	Thermo Fisher Scientific	Cat#15710072
Thioglycollate	Sigma	Cat#T9032
Tri-DAP (NOD1 ligand)	InvivoGen	Cat#tlrl-tdap
Pam_3CSK_4 (TLR2 ligand)	InvivoGen	Cat#tlrl-pms
Critical Commercial Assays		
QIAamp DNA Stool Mini Kit	Qiagen	Cat#51504
RNeasy Mini Kit	Qiagen	Cat#74104
TURBO DNA-free Kit	Thermo Fisher Scientific	Cat#AM1907
iScript cDNA synthesis kit	Bio-Rad	Cat#1708891
RNAqueous Total RNA Isolation Kit	Thermo Fisher Scientific	Cat#AM1912
TaqMan pre-designed assay: murine *Nos2*	Thermo Fisher Scientific	Mm00440502_m1
TaqMan pre-designed assay: murine *Il6*	Thermo Fisher Scientific	Mm00446190_m1
TaqMan pre-designed assay: murine *Hprt*	Thermo Fisher Scientific	Mm03024075_m1
TaqMan pre-designed assay: murine *Tnf*	Thermo Fisher Scientific	Mm00443258_m1
TaqMan pre-designed assay: murine *Ccl5*	Thermo Fisher Scientific	Mm01302427_m1
TaqMan pre-designed assay: murine *Cxcl10*	Thermo Fisher Scientific	Mm00445235_m1
TaqMan pre-designed assay: murine *Ifnb1*	Thermo Fisher Scientific	Mm00439552_s1
TaqMan pre-designed assay: murine *Il1b*	Thermo Fisher Scientific	Mm00434228_m1
TaqMan pre-designed assay: murine *Il17a*	Thermo Fisher Scientific	Mm00439618_m1
TaqMan pre-designed assay: murine *Saa1/2*	Thermo Fisher Scientific	Mm04208126_mH
TaqMan pre-designed assay: murine *Akr1c13*	Thermo Fisher Scientific	Mm00657347_m1
TransIT-LT1 Transfection Reagent	Mirus Bio	Cat#MIR2300
Experimental Models: Cell Lines		
HEK293	ATCC	ATCC Cat# CRL-1573
Oligonucleotides		
Akr1c13 genotyping end-point forward primer: CAGAAGAATGCTCCCAAGTTA	This work	N/A
Akr1c13 genotyping end-point reverse primer: CTTAGTTTCTTTTCCTGTTGCTCTG	This work	N/A
Akr1c13 genotyping qPCR forward primer: TCTATGGTAGGTTGAATGTCATCTC	This work	N/A
Akr1c13 genotyping qPCR reverse primer: AGCAACGAGAACAATGTCTTTTG	This work	N/A
Akr1c13 WT allele qPCR genotyping FAM probe: 5′ FAM-CAGCGTAAGCTACTGGATTACT 3′	This work	N/A
Akr1c13 mutant allele qPCR genotyping HEX probe: 5′ FAM-CAGCGGTAAGCTACTGGATTACT 3′	This work	N/A
Akr1c13-targeting sgRNA oligo FWD: 5′-AGTAATCCAGTAGCTTACGC-3′	McFarland et al., 2017	N/A
Akr1c13-targeting sgRNA oligo REV: 5′- GCGTAAGCTACTGGATTACT -3′	McFarland et al., 2017	N/A

In vitro transcription of *Akr1c13* sgRNA (T7-sgRNA_F) ttaatacgactcactatagggAGTAATCCAGTAGCTTACG CTGG	Yang et al., 2014	N/A
T7-px330-sgRNA_R: AAAAGCACCGACTCGGTGCC	Yang et al., 2014	N/A
Akr1c13 substrate DNA for RGEN-RFLP FWD: TTGCAGCTGGCGTCTTTACC	This work	N/A
Akr1c13 substrate DNA for RGEN-RFLP REV: CAGACAGCACTTGACTGACAATGC	This work	N/A
SFB 16S rRNA primers for qPCR FWD: GACGCTGAGGCATGAGAGCAT	Barman et al., 2008 (I&I)	N/A
SFB 16S rRNA primers for qPCR REV: GACGGCACGGATTGTTATTCA	Barman et al., 2008 (I&I)	N/A
Recombinant DNA		
pX330-U6-Chimeric_BB-CBh-hSpCas9	A gift from Feng Zhang	Addgene plasmid #42230
Software and Algorithms		
GraphPad Prism 7	GraphPad Software	http://www.graphpad.com/scientificsoftware/prism/
ApE- A plasmid Editor	University of Utah Biology	http://biologylabs.utah.edu/jorgensen/wayned/ape/
Benchling	Benchling Software	https://benchling.com/
CRISPR Design	Zhang Lab, MIT	http://crispr.mit.edu/

Chapter 6

Concluding Remarks

6.1 RECON-TLR cooperation: a new testament to an old doctrine

The magnitude of an immune response is dictated by the nature of the activating ligands and the context in which they are sensed. Each bacterium has a unique molecular footprint comprised of its cell membrane constituents, nucleic acid species, secretion systems, and effectors. It has been appreciated for over a decade that simultaneous sensing of multiple kinds of bacterial products results in a synergistic response greater than the additive sum of each response alone (reviewed in (*219*)). Simultaneous activation of TLRs, for instance TLR2 with TLR4 or TLR3 with TLR9, causes synergistic cytokine production (*220, 221*). Such effects are seen across PRR families as well, exemplified by NOD1 and NOD2 synergy with TLR2, TLR3, TLR4 and TLR9 (*222-224*).

In addition to synergy, cooperation between PRRs can also take place in a step-wise fashion, whereby the activation of the first PRR sets in motion events that enable the functionality of a second PRR. For example, TLR activation leads to the production of inactive pro-IL-1β and pro-IL-18 which are processed into their mature forms downstream of NALP activation (*225, 226*). It is within this modality of PRR cooperation that RECON functions. TLR or NOD activation sets up the cellular conditions in which inhibition of RECON would carry with it any consequence on the immune response. Stimulation of TLRs or NODs causes 1) the activation of cPLA2, 2) assembly of the NADPH oxidase, and 3) phosphorylation of NF-κB (*87-91, 227*). Each of these features of TLR/NOD activation are critical for RECON's function as a PRR as we currently

understand it. Because RECON sensing of cytosolic bacterial CDNs boosts inflammation following initial TLR/NOD activation, the nature of this cooperation suggests engagement of RECON allows host cells to discriminate friend from foe.

6.2 RECON and 4-HNE: partners in stranger-danger amplification

RECON is an aldo-keto reductase with the potential to reduce reactive carbonyls of host and xenobiotic origins. In Chapter 3 we determined that the reactive lipid species 4-HNE, which is a byproduct of arachidonic acid peroxidation, is a bonafide substrate of RECON. Intriguingly, only a handful of studies have reported on the formation of 4-HNE during bacterial infection of the host, where it has been used mainly a biomarker of oxidative stress (*228-232*). Due to its reactivity with cysteine, lysine and histidine residues, 4-HNE has the potential to affect many processes within the cell. In hepatocytes, we found that 4-HNE can specifically enhance *Nos2* expression. However, the mechanism that underlies this activity remains to be elucidated.

The partnering of PRRs that sense "strangers" with molecules that signify "danger" enables host cells to achieve a coordinated, appropriate and effective immune response (Figure 6.1). TLR activation leads to the generation of ROS and RNS via assembly of the NADPH oxidase and expression of the inducible nitric oxide synthase, respectively (*227, 233*). ROS and RNS are antimicrobial molecules that also moonlight as mediators of signaling (*233, 234*). The generation of ROS and RNS is a critical facet of TLR-mediated immunity. The relationship between RECON and 4-HNE may be viewed in a similar regard, although in their case the sensor component and enzyme component are one in the same. While we have evidence that 4-HNE augments TLR-dependent inflammatory gene expression, another interesting avenue to explore is whether 4-HNE itself is directly antimicrobial. It is well appreciated that fatty acids can be antimicrobial, especially against gram-positive bacteria (*207, 235, 236*). In the case of *S. aureus*, the peroxidation of arachidonic acid in the presence of bacterial-derived H_2O_2 is seriously detrimental to bacterial viability (*206*). Preliminary data suggest 4-HNE is particularly toxic to non-host-adapted bacteria such as *B. subtilis* whereas *L. monocytogenes* can tolerate high levels of the aldehyde (Figure 6.2). These observations deserve further attention in order to fully understand the link between RECON, 4-HNE and antibacterial defense. Incidentally, it is of note that our newfound appreciation for 4-HNE came by way of

studying RECON and suggests novel aspects of innate immunity may be revealed by further characterizing its enzymatic targets.

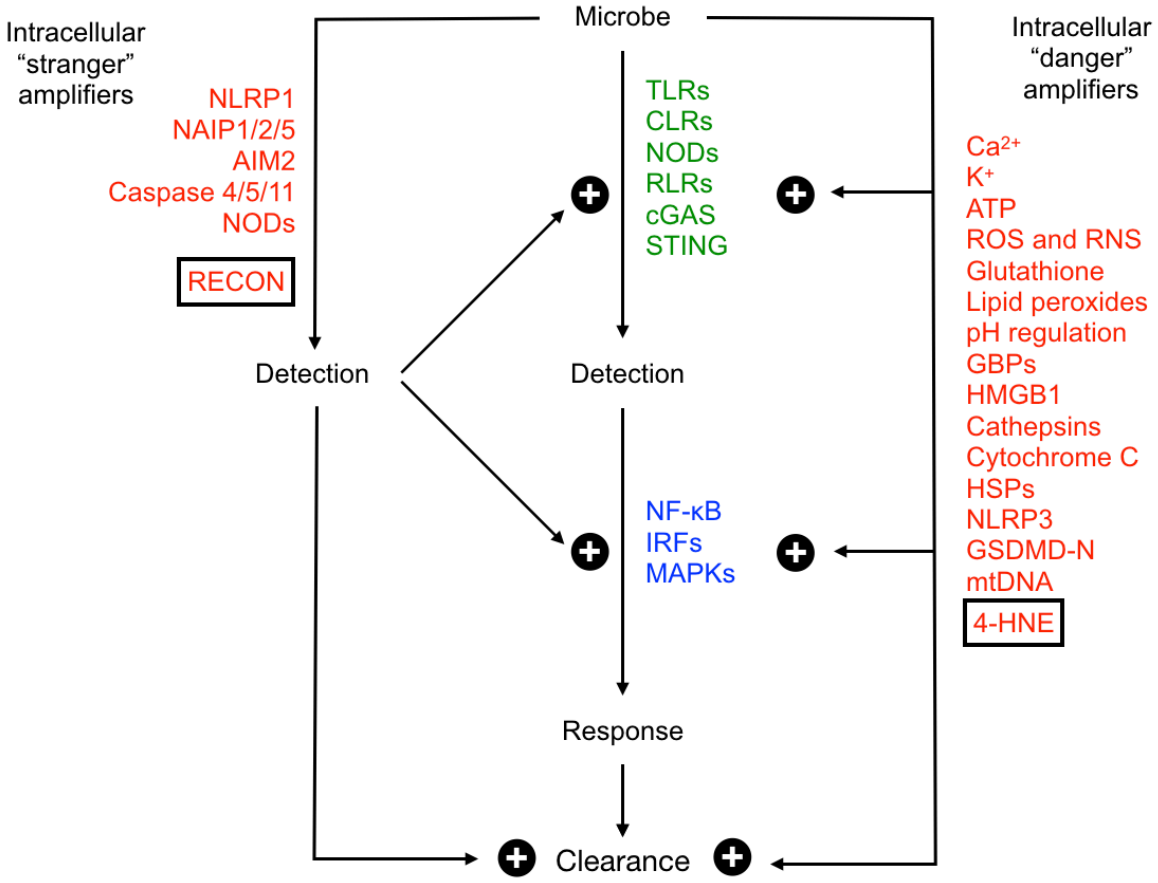

Figure 6.1. Coordination between extracellular/intracellular PRRs that directly sense microbes and danger-associated molecules that are derived, produced or released following the initial sensing enables an appropriate and effective immune response.

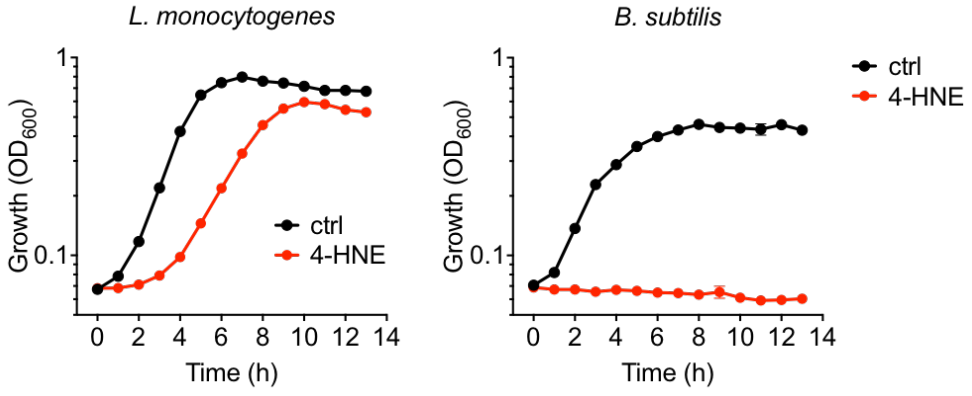

Figure 6.2. 4-HNE exhibits antimicrobial activity. *L. monocytogenes* and *B. subtilis* were grown in LB in the presence of 4-HNE (640 μM) or the equivalent volume of ethanol (control).

6.3 Cell type-specific functionality of RECON and differential effects on bacteria

In our investigation of RECON, we examined its role in modulating immune gene expression in several different cell types, including primary bone marrow-derived macrophages, peritoneal macrophages and hepatocytes. In each cell type, RECON influenced immune gene expression in distinct ways, which was largely influenced by the expression of other immune sensors, such as STING, as well as the steady-state physiology of the cells (for example, high expression of COX-2 in hepatocytes in the absence of stimuli). Therefore, it is clear that RECON affects immune responses in a context-dependent manner and that there is not likely to be a one-size-fits-all model for its function as a sensor or anti-inflammatory enzyme. Although this variable nature complicates the big-picture view of RECON, it may be advantageous in bringing to light potentially novel actors in immunity. For instance, we have found that 4-HNE is generated during TLR stimulation and that this molecule can significantly amplify the magnitude of the response. Therefore, RECON can be used as a tool to probe how inflammatory responses are cell-intrinsically coordinated and controlled.

In Chapter 2, we found that bacteria are differentially affected by RECON. The growth of *Chlamydia pneumoniae* and *Chlamydia muridarum* was restricted in the absence of RECON *in vitro*. Conversely, the intracellular replication of *L. monocytogenes* was largely unaffected by the presence or absence of RECON. In Chapter 4 we report on the surprising finding that *L. monocytogenes* capitalizes on the increased inflammation in RECON-deficient cells by exhibiting enhanced cell-to-cell spread. However, as detailed in Chapter 5, *L. monocytogenes* was attenuated in RECON-deficient mice. Although the study of mice globally deficient in RECON provided some interesting and unexpected findings (i.e. RECON's role in intestinal homeostasis), the response of these mice to *L. monocytogenes* infection are likely to be quite different than what occurs normally. Because RECON acts as a brake on inflammation, it could be expected that in RECON-deficient mice any cell that is exposed to a TLR ligand, infected or not, will have an augmented inflammatory response. The data presented in Chapter 5 are evidence that RECON controls immune responses *in vivo* in such a way that may impart an advantage to the host during infection; however, what those data do not reveal is the true nature of the relationship between RECON and *L. monocytogenes*. Mice in which RECON is

conditionally lost in hepatocytes, macrophages, or other cell types may be of greater use in that venture.

6.4 Tip of the iceberg: perspective on aldo-keto reductases in innate immunity

Our understanding of PRR-mediated responses to microbial products has dramatically advanced in the last decade. Conventional models connecting a surface-bound PRR to a transcription factor inside a cell depict only one aspect of immune activation. Indeed, activation of many distinct transcriptional responses is hard-wired downstream of surface PRRs. However, the importance of non-transcriptional responses that give rise to cytosolic, small-molecule mediators produced *de novo* within seconds of PRR activation is increasingly coming to light. The repertoire of mediators produced for a given response depends on many factors, including the starting substrate pool and the cell type-specific expression of enzymes that metabolize those lipids. The work presented in this dissertation has revealed RECON to be a potent modulator of immune activation owning to its participation in the arachidonic acid cascade. However, the broader function of AKRs, which have distinct substrate repertoires and exhibit idiosyncratic expression in different tissues and cell types, within the immune system is largely unknown.

In addition to RECON, preliminary data indicate that murine AKR1C12, a closely-related enzyme, also binds c-di-AMP. This observation reveals a broader role of AKRs in immunity. RECON and AKR1C12 are similarly expressed in mouse tissues and cell types. Previous *in vitro* work with recombinant AKR1C12 has indicated that it can reduce steroid hormones and prostaglandins (*237*), so the substrate repertoire of this enzyme may be distinct from that of RECON. Although these *in vitro* data are informative, the effects of AKR1C12 on endogenous metabolite pools have not been explored. Furthermore, the consequence of c-di-AMP binding to AKR1C12 is currently unknown, as is whether this enzyme affects immune responses. Given all that we have learned about immune modulation by studying RECON, future work exploring the role of AKR1C12 in immunity are warranted.

An important line of investigation that we have been pursuing is whether there is a RECON-like AKR in humans because there is no direct human ortholog of RECON or AKR1C12. Pulldown studies from HepG2 cells revealed human AKR1C1 was highly enriched in c-di-AMP-beads versus control (see Chapter 2 and (*78*)). We also detected

some enrichment for AKR1C2 and AKR1C3, although they did not reach significance. In mice, there are eight AKR1C family members, including RECON and AKR1C12, encoded by genes clustered on chromosome 13 (*63*). This region of the chromosome has shared synteny with a region on human chromosome 10 that encodes the four human AKR1C members: AKR1C1, AKR1C2, AKR1C3 and AKR1C4 (Figure 6.3) (*79*).

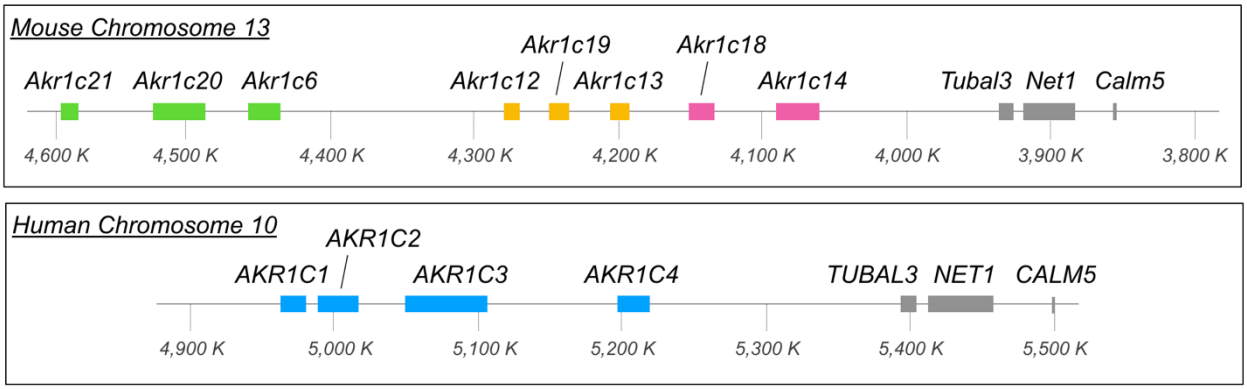

Figure 6.3. Mouse and human AKR1C subfamily chromosomal configuration. The regions of shared synteny in mouse and human are shown. The color-coding corresponds to close homology of the enzymes within the species.

Considering this synteny, the preliminary pulldown data indicating that AKR1C1, C2 and C3 may interact with c-di-AMP is especially encouraging. However, there are multiple isoforms of these enzymes as well as potential for post-translational modifications that are specific to proteins produced in mammalian cells. This complexity may contribute to binding ability as we have yet to confirm binding of c-di-AMP to any human AKR using their reference sequences expressed in and purified from *E. coli*. To definitively determine whether any human AKRs bind to c-di-AMP or other bacterial CDNs, it will likely be necessary to express and purify all isoforms of these enzymes in a mammalian expression system, perhaps in the presence of TLR ligands or other stress-inducing conditions.

Apart from their c-di-AMP-binding ability, much remains to be revealed about the function of the human AKR1C proteins in immunity. While all human AKR1C family members are expressed in the liver, AKR1C1, C2 and C3 are also expressed in the intestinal and lung epithelium (mined from deposited mRNA-seq data using Genevestigator software (*238*)). AKR1C1, C2 and C3 are expressed at low levels in monocytes and macrophages at steady-state but are highly induced following TLR

stimulation or infection with *L. monocytogenes* (Genevestigator (*238*)). Interestingly, AKR1C3 is highly expressed in NK cells, making it the only AKR1C member expressed in a lymphocyte. AKR1C3 is also the only member that efficiently reduces prostaglandin D2 (*79*), whereas AKR1C1, AKR1C2 and AKR1C4 are all capable of reducing 5α-dihydrotestosterone (*63*), a molecule previously associated with blocking NF-κB responses (*239*). The role of these enzymes following immune stimulation or infection have never been examined. Our identification and characterization of RECON as an important factor in immune sensing, modulator of cellular inflammation, and regulator of intestinal microbial homeostasis has opened the door to many lines of inquiry. Future work may ultimately prove AKRs to be more than a class of enzymes – they may be a class of immunity proteins unto themselves.

References

1. A. Iwasaki, R. Medzhitov, Regulation of adaptive immunity by the innate immune system. *Science* **327**, 291-295 (2010).
2. T. Kawai, S. Akira, Toll-like receptor and RIG-I-like receptor signaling. *Ann N Y Acad Sci* **1143**, 1-20 (2008).
3. D. L. Burdette *et al.*, STING is a direct innate immune sensor of cyclic di-GMP. *Nature* **478**, 515-518 (2011).
4. J. D. Sauer *et al.*, The N-ethyl-N-nitrosourea-induced Goldenticket mouse mutant reveals an essential function of Sting in the in vivo interferon response to Listeria monocytogenes and cyclic dinucleotides. *Infect Immun* **79**, 688-694 (2011).
5. C. Shu, G. Yi, T. Watts, C. C. Kao, P. Li, Structure of STING bound to cyclic di-GMP reveals the mechanism of cyclic dinucleotide recognition by the immune system. *Nat Struct Mol Biol* **19**, 722-724 (2012).
6. Y. H. Huang, X. Y. Liu, X. X. Du, Z. F. Jiang, X. D. Su, The structural basis for the sensing and binding of cyclic di-GMP by STING. *Nat Struct Mol Biol* **19**, 728-730 (2012).
7. X. Cai, Y. H. Chiu, Z. J. Chen, The cGAS-cGAMP-STING pathway of cytosolic DNA sensing and signaling. *Mol Cell* **54**, 289-296 (2014).
8. E. J. Diner *et al.*, The innate immune DNA sensor cGAS produces a noncanonical cyclic dinucleotide that activates human STING. *Cell Rep* **3**, 1355-1361 (2013).
9. L. Sun, J. Wu, F. Du, X. Chen, Z. J. Chen, Cyclic GMP-AMP synthase is a cytosolic DNA sensor that activates the type I interferon pathway. *Science* **339**, 786-791 (2013).
10. A. Ablasser *et al.*, cGAS produces a 2'-5'-linked cyclic dinucleotide second messenger that activates STING. *Nature* **498**, 380-384 (2013).
11. D. Kalia *et al.*, Nucleotide, c-di-GMP, c-di-AMP, cGMP, cAMP, (p)ppGpp signaling in bacteria and implications in pathogenesis. *Chem Soc Rev* **42**, 305-341 (2013).
12. B. W. Davies, R. W. Bogard, T. S. Young, J. J. Mekalanos, Coordinated regulation of accessory genetic elements produces cyclic di-nucleotides for V. cholerae virulence. *Cell* **149**, 358-370 (2012).
13. C. A. Kellenberger *et al.*, GEMM-I riboswitches from Geobacter sense the bacterial second messenger cyclic AMP-GMP. *Proc Natl Acad Sci U S A* **112**, 5383-5388 (2015).
14. E. Mills, I. S. Pultz, H. D. Kulasekara, S. I. Miller, The bacterial second messenger c-di-GMP: mechanisms of signalling. *Cell Microbiol* **13**, 1122-1129 (2011).
15. C. E. Witte *et al.*, Cyclic di-AMP is critical for Listeria monocytogenes growth, cell wall homeostasis, and establishment of infection. *MBio* **4**, e00282-00213 (2013).
16. K. Sureka *et al.*, The cyclic dinucleotide c-di-AMP is an allosteric regulator of metabolic enzyme function. *Cell* **158**, 1389-1401 (2014).
17. R. M. Corrigan, A. Grundling, Cyclic di-AMP: another second messenger enters the fray. *Nat Rev Microbiol* **11**, 513-524 (2013).
18. J. R. Barker *et al.*, STING-dependent recognition of cyclic di-AMP mediates type I interferon responses during Chlamydia trachomatis infection. *MBio* **4**, e00018-00013 (2013).
19. B. Dey *et al.*, A bacterial cyclic dinucleotide activates the cytosolic surveillance pathway and mediates innate resistance to tuberculosis. *Nat Med* **21**, 401-406 (2015).

20. J. J. Woodward, A. T. Iavarone, D. A. Portnoy, c-di-AMP secreted by intracellular Listeria monocytogenes activates a host type I interferon response. *Science* **328**, 1703-1705 (2010).
21. J. Yang *et al.*, Deletion of the cyclic di-AMP phosphodiesterase gene (cnpB) in Mycobacterium tuberculosis leads to reduced virulence in a mouse model of infection. *Mol Microbiol* **93**, 65-79 (2014).
22. U. Romling, Great times for small molecules: c-di-AMP, a second messenger candidate in Bacteria and Archaea. *Sci Signal* **1**, pe39 (2008).
23. W. A. Andrade *et al.*, Group B Streptococcus Degrades Cyclic-di-AMP to Modulate STING-Dependent Type I Interferon Production. *Cell Host Microbe* **20**, 49-59 (2016).
24. J. M. Blander, L. E. Sander, Beyond pattern recognition: five immune checkpoints for scaling the microbial threat. *Nat Rev Immunol* **12**, 215-225 (2012).
25. R. E. Vance, R. R. Isberg, D. A. Portnoy, Patterns of pathogenesis: discrimination of pathogenic and nonpathogenic microbes by the innate immune system. *Cell Host Microbe* **6**, 10-21 (2009).
26. C. M. Gries *et al.*, Cyclic di-AMP Released from Staphylococcus aureus Biofilm Induces a Macrophage Type I Interferon Response. *Infect Immun* **84**, 3564-3574 (2016).
27. R. J. Dey *et al.*, Inhibition of innate immune cytosolic surveillance by an M. tuberculosis phosphodiesterase. *Nature chemical biology* **13**, 210-217 (2017).
28. A. J. Wolf *et al.*, Hexokinase Is an Innate Immune Receptor for the Detection of Bacterial Peptidoglycan. *Cell* **166**, 624-636 (2016).
29. M. B. Fessler, The Intracellular Cholesterol Landscape: Dynamic Integrator of the Immune Response. *Trends Immunol* **37**, 819-830 (2016).
30. S. B. Joseph, A. Castrillo, B. A. Laffitte, D. J. Mangelsdorf, P. Tontonoz, Reciprocal regulation of inflammation and lipid metabolism by liver X receptors. *Nat Med* **9**, 213-219 (2003).
31. E. S. Gold *et al.*, 25-Hydroxycholesterol acts as an amplifier of inflammatory signaling. *Proc Natl Acad Sci U S A* **111**, 10666-10671 (2014).
32. E. V. Dang, J. G. McDonald, D. W. Russell, J. G. Cyster, Oxysterol Restraint of Cholesterol Synthesis Prevents AIM2 Inflammasome Activation. *Cell* **171**, 1057-1071 e1011 (2017).
33. S. Ikeda *et al.*, Cloning and characterization of two novel aldo-keto reductases (AKR1C12 and AKR1C13) from mouse stomach. *FEBS Lett* **459**, 433-437 (1999).
34. C. J. Desmet, K. J. Ishii, Nucleic acid sensing at the interface between innate and adaptive immunity in vaccination. *Nat Rev Immunol* **12**, 479-491 (2012).
35. E. E. Gray *et al.*, The AIM2-like Receptors Are Dispensable for the Interferon Response to Intracellular DNA. *Immunity* **45**, 255-266 (2016).
36. A. C. Collins *et al.*, Cyclic GMP-AMP Synthase Is an Innate Immune DNA Sensor for Mycobacterium tuberculosis. *Cell Host Microbe* **17**, 820-828 (2015).
37. T. Yamamoto *et al.*, Listeria monocytogenes strain-specific impairment of the TetR regulator underlies the drastic increase in cyclic di-AMP secretion and beta interferon-inducing ability. *Infect Immun* **80**, 2323-2332 (2012).
38. G. T. Crimmins *et al.*, Listeria monocytogenes multidrug resistance transporters activate a cytosolic surveillance pathway of innate immunity. *Proc Natl Acad Sci U S A* **105**, 10191-10196 (2008).
39. S. Endo *et al.*, Characterization of rat and mouse NAD+-dependent 3alpha/17beta/20alpha-hydroxysteroid dehydrogenases and identification of

substrate specificity determinants by site-directed mutagenesis. *Arch Biochem Biophys* **467**, 76-86 (2007).
40. J. M. Jez, M. J. Bennett, B. P. Schlegel, M. Lewis, T. M. Penning, Comparative anatomy of the aldo-keto reductase superfamily. *Biochem. J.* **326**, 625-636 (1997).
41. J. F. Couture *et al.*, Human 20alpha-hydroxysteroid dehydrogenase: crystallographic and site-directed mutagenesis studies lead to the identification of an alternative binding site for C21-steroids. *J Mol Biol* **331**, 593-604 (2003).
42. A. T. Jacobs, L. J. Ignarro, Cell density-enhanced expression of inducible nitric oxide synthase in murine macrophages mediated by interferon-beta. *Nitric Oxide* **8**, 222-230 (2003).
43. P. M. Murphy *et al.*, International union of pharmacology. XXII. Nomenclature for chemokine receptors. *Pharmacol Rev* **52**, 145-176 (2000).
44. F. C. Fang, Perspectives series: host/pathogen interactions. Mechanisms of nitric oxide-related antimicrobial activity. *J Clin Invest* **99**, 2818-2825 (1997).
45. B. T. Edelson, E. R. Unanue, MyD88-dependent but Toll-like receptor 2-independent innate immunity to Listeria: no role for either in macrophage listericidal activity. *J Immunol* **169**, 3869-3875 (2002).
46. A. Mosa *et al.*, Nonhematopoietic cells control the outcome of infection with Listeria monocytogenes in a nucleotide oligomerization domain 1-dependent manner. *Infect Immun* **77**, 2908-2918 (2009).
47. I. Lavon *et al.*, High susceptibility to bacterial infection, but no liver dysfunction, in mice compromised for hepatocyte NF-kappaB activation. *Nat Med* **6**, 573-577 (2000).
48. M. K. Thomsen *et al.*, Lack of immunological DNA sensing in hepatocytes facilitates hepatitis B virus infection. *Hepatology*, (2016).
49. L. Di Costanzo, T. M. Penning, D. W. Christianson, Aldo-keto reductases in which the conserved catalytic histidine is substituted. *Chem Biol Interact* **178**, 127-133 (2009).
50. C. Cole, S. Thomas, H. Filak, P. M. Henson, L. L. Lenz, Nitric oxide increases susceptibility of Toll-like receptor-activated macrophages to spreading Listeria monocytogenes. *Immunity* **36**, 807-820 (2012).
51. M. U. Shiloh *et al.*, Phenotype of mice and macrophages deficient in both phagocyte oxidase and inducible nitric oxide synthase. *Immunity* **10**, 29-38 (1999).
52. T. M. Penning, M. C. Byrns, Steroid hormone transforming aldo-keto reductases and cancer. *Ann N Y Acad Sci* **1155**, 33-42 (2009).
53. H. Yun, J. Xie, A. F. Olumi, R. Ghosh, A. P. Kumar, Activation of AKR1C1/ERbeta induces apoptosis by downregulation of c-FLIP in prostate cancer cells: A prospective therapeutic opportunity. *Oncotarget* **6**, 11600-11613 (2015).
54. H. J. Martin *et al.*, Purification and characterization of akr1b10 from human liver: role in carbonyl reduction of xenobiotics. *Drug Metab Dispos* **34**, 464-470 (2006).
55. T. Shimizu, Y. Tatano, H. Tomioka, Aldose reductase participates in the downregulation of T cell functions due to suppressor macrophages. *Sci Rep* **6**, 21093 (2016).
56. X. Zhang *et al.*, Cyclic GMP-AMP containing mixed phosphodiester linkages is an endogenous high-affinity ligand for STING. *Mol Cell* **51**, 226-235 (2013).
57. G. Yi *et al.*, Single nucleotide polymorphisms of human STING can affect innate immune response to cyclic dinucleotides. *PLoS One* **8**, e77846 (2013).
58. K. M. Monroe, S. M. McWhirter, R. E. Vance, Induction of type I interferons by bacteria. *Cell Microbiol* **12**, 881-890 (2010).

59. R. O. Watson *et al.*, The Cytosolic Sensor cGAS Detects Mycobacterium tuberculosis DNA to Induce Type I Interferons and Activate Autophagy. *Cell Host Microbe* **17**, 811-819 (2015).
60. K. W. Bruhn, N. Craft, J. F. Miller, Listeria as a vaccine vector. *Microbes Infect* **9**, 1226-1235 (2007).
61. I. Skrnjug *et al.*, The mucosal adjuvant cyclic di-AMP exerts immune stimulatory effects on dendritic cells and macrophages. *PLoS One* **9**, e95728 (2014).
62. L. P. Cousens, E. J. Wing, Innate defenses in the liver during Listeria infection. *Immunol Rev* **174**, 150-159 (2000).
63. L. Vergnes, J. Phan, A. Stolz, K. Reue, A cluster of eight hydroxysteroid dehydrogenase genes belonging to the aldo-keto reductase supergene family on mouse chromosome 13. *J Lipid Res* **44**, 503-511 (2003).
64. I. Moreno-Indias, F. Cardona, F. J. Tinahones, M. I. Queipo-Ortuno, Impact of the gut microbiota on the development of obesity and type 2 diabetes mellitus. *Front Microbiol* **5**, 190 (2014).
65. X. Yang, L. Xie, Y. Li, C. Wei, More than 9,000,000 unique genes in human gut bacterial community: estimating gene numbers inside a human body. *PLoS One* **4**, e6074 (2009).
66. R. M. Corrigan, J. C. Abbott, H. Burhenne, V. Kaever, A. Grundling, c-di-AMP is a new second messenger in Staphylococcus aureus with a role in controlling cell size and envelope stress. *PLoS Pathog* **7**, e1002217 (2011).
67. U. Hellman, C. Wernstedt, J. Gonez, C. H. Heldin, Improvement of an "In-Gel" digestion procedure for the micropreparation of internal protein fragments for amino acid sequencing. *Anal Biochem* **224**, 451-455 (1995).
68. J. Rosenfeld, J. Capdevielle, J. C. Guillemot, P. Ferrara, In-gel digestion of proteins for internal sequence analysis after one- or two-dimensional gel electrophoresis. *Anal Biochem* **203**, 173-179 (1992).
69. Z. S. Derewenda, P. G. Vekilov, Entropy and surface engineering in protein crystallization. *Acta Crystallogr D Biol Crystallogr* **62**, 116-124 (2006).
70. Z. Otwinowski, W. Minor, C. C. W Jr, Processing of X-ray diffraction data collected in oscillation mode. *Methods in Enzymology* **276**, 307-326 (1997).
71. P. D. Adams *et al.*, PHENIX: building new software for automated crystallographic structure determination. *Acta Crystallogr D Biol Crystallogr* **58**, 1948-1954 (2002).
72. P. Emsley, K. Cowtan, Coot: model-building tools for molecular graphics. *Acta Crystallogr D Biol Crystallogr* **60**, 2126-2132 (2004).
73. K. G. Roelofs, J. Wang, H. O. Sintim, V. T. Lee, Differential radial capillary action of ligand assay for high-throughput detection of protein-metabolite interactions. *Proc Natl Acad Sci U S A* **108**, 15528-15533 (2011).
74. S. Jones, D. A. Portnoy, Characterization of Listeria monocytogenes pathogenesis in a strain expressing perfringolysin O in place of listeriolysin O. *Infect Immun* **62**, 5608-5613 (1994).
75. J. D. Sauer *et al.*, Listeria monocytogenes triggers AIM2-mediated pyroptosis upon infrequent bacteriolysis in the macrophage cytosol. *Cell Host Microbe* **7**, 412-419 (2010).
76. F. A. Ran *et al.*, Genome engineering using the CRISPR-Cas9 system. *Nat Protoc* **8**, 2281-2308 (2013).
77. H. Yang, H. Wang, R. Jaenisch, Generating genetically modified mice using CRISPR/Cas-mediated genome engineering. *Nat Protoc* **9**, 1956-1968 (2014).

78. A. P. McFarland *et al.*, Sensing of Bacterial Cyclic Dinucleotides by the Oxidoreductase RECON Promotes NF-kappaB Activation and Shapes a Proinflammatory Antibacterial State. *Immunity* **46**, 433-445 (2017).
79. P. Velica *et al.*, Lack of functional and expression homology between human and mouse aldo-keto reductase 1C enzymes: implications for modelling human cancers. *Mol Cancer* **8**, 121 (2009).
80. T. M. Penning, The aldo-keto reductases (AKRs): Overview. *Chem Biol Interact* **234**, 236-246 (2015).
81. O. A. Barski, S. M. Tipparaju, A. Bhatnagar, The aldo-keto reductase superfamily and its role in drug metabolism and detoxification. *Drug Metab Rev* **40**, 553-624 (2008).
82. C. M. Zeng *et al.*, Aldo-Keto Reductase AKR1C1-AKR1C4: Functions, Regulation, and Intervention for Anti-cancer Therapy. *Front Pharmacol* **8**, 119 (2017).
83. W. D. Chen, Y. Zhang, Regulation of aldo-keto reductases in human diseases. *Front Pharmacol* **3**, 35 (2012).
84. D. Hyndman, D. R. Bauman, V. V. Heredia, T. M. Penning, The aldo-keto reductase superfamily homepage. *Chem Biol Interact* **143-144**, 621-631 (2003).
85. Y. Jin, T. M. Penning, Aldo-keto reductases and bioactivation/detoxication. *Annu Rev Pharmacol Toxicol* **47**, 263-292 (2007).
86. F. X. Ruiz *et al.*, Retinaldehyde is a substrate for human aldo-keto reductases of the 1C subfamily. *Biochem J* **440**, 335-344 (2011).
87. J. Balsinde, M. V. Winstead, E. A. Dennis, Phospholipase A(2) regulation of arachidonic acid mobilization. *FEBS Lett* **531**, 2-6 (2002).
88. H. Y. Qi, J. H. Shelhamer, Toll-like receptor 4 signaling regulates cytosolic phospholipase A2 activation and lipid generation in lipopolysaccharide-stimulated macrophages. *J Biol Chem* **280**, 38969-38975 (2005).
89. Y. Alvarez *et al.*, Eicosanoids in the innate immune response: TLR and non-TLR routes. *Mediators Inflamm* **2010**, (2010).
90. E. A. Dennis, P. C. Norris, Eicosanoid storm in infection and inflammation. *Nat Rev Immunol* **15**, 511-523 (2015).
91. P. C. Norris, E. A. Dennis, Omega-3 fatty acids cause dramatic changes in TLR4 and purinergic eicosanoid signaling. *Proc Natl Acad Sci U S A* **109**, 8517-8522 (2012).
92. W. L. Smith, L. J. Marnett, D. L. DeWitt, Prostaglandin and thromboxane biosynthesis. *Pharmacol Ther* **49**, 153-179 (1991).
93. Z. Zhou, M. J. Xu, B. Gao, Hepatocytes: a key cell type for innate immunity. *Cell Mol Immunol* **13**, 301-315 (2016).
94. P. C. Calder, Omega-3 polyunsaturated fatty acids and inflammatory processes: nutrition or pharmacology? *Br J Clin Pharmacol* **75**, 645-662 (2013).
95. H. A. Saka, R. Valdivia, Emerging roles for lipid droplets in immunity and host-pathogen interactions. *Annu Rev Cell Dev Biol* **28**, 411-437 (2012).
96. L. S. Moreira *et al.*, Cytosolic phospholipase A2-driven PGE2 synthesis within unsaturated fatty acids-induced lipid bodies of epithelial cells. *Biochim Biophys Acta* **1791**, 156-165 (2009).
97. E. Kikawada, J. V. Bonventre, J. P. Arm, Group V secretory PLA2 regulates TLR2-dependent eicosanoid generation in mouse mast cells through amplification of ERK and cPLA2alpha activation. *Blood* **110**, 561-567 (2007).
98. S. Jayaraja *et al.*, Cytosolic phospholipase A2 contributes to innate immune defense against Candida albicans lung infection. *BMC Immunol* **17**, 27 (2016).

99. R. Bhowmick, S. Clark, J. V. Bonventre, J. M. Leong, B. A. McCormick, Cytosolic Phospholipase A2alpha Promotes Pulmonary Inflammation and Systemic Disease during Streptococcus pneumoniae Infection. *Infect Immun* **85**, (2017).
100. D. Wang, R. N. Dubois, Eicosanoids and cancer. *Nat Rev Cancer* **10**, 181-193 (2010).
101. A. Higdon, A. R. Diers, J. Y. Oh, A. Landar, V. M. Darley-Usmar, Cell signalling by reactive lipid species: new concepts and molecular mechanisms. *Biochem J* **442**, 453-464 (2012).
102. S. S. Fam, J. D. Morrow, The isoprostanes: unique products of arachidonic acid oxidation-a review. *Curr Med Chem* **10**, 1723-1740 (2003).
103. A. Ayala, M. F. Munoz, S. Arguelles, Lipid peroxidation: production, metabolism, and signaling mechanisms of malondialdehyde and 4-hydroxy-2-nonenal. *Oxid Med Cell Longev* **2014**, 360438 (2014).
104. H. Zhong, H. Yin, Role of lipid peroxidation derived 4-hydroxynonenal (4-HNE) in cancer: focusing on mitochondria. *Redox Biol* **4**, 193-199 (2015).
105. J. R. Requena *et al.*, Lipoxidation products as biomarkers of oxidative damage to proteins during lipid peroxidation reactions. *Nephrol Dial Transplant* **11 Suppl 5**, 48-53 (1996).
106. S. Toyokuni, Reactive oxygen species-induced molecular damage and its application in pathology. *Pathol Int* **49**, 91-102 (1999).
107. A. M. Gioacchini *et al.*, Determination of 4-hydroxy-2-nonenal at cellular levels by means of electrospray mass spectrometry. *Rapid Commun Mass Spectrom* **13**, 1573-1579 (1999).
108. J. Hintzpeter, H. J. Martin, E. Maser, Reduction of lipid peroxidation products and advanced glycation end-product precursors by cyanobacterial aldo-keto reductase AKR3G1-a founding member of the AKR3G subfamily. *FASEB J* **29**, 263-273 (2015).
109. K. V. Ramana *et al.*, Selective recognition of glutathiolated aldehydes by aldose reductase. *Biochemistry* **39**, 12172-12180 (2000).
110. M. E. Burczynski, G. R. Sridhar, N. T. Palackal, T. M. Penning, The reactive oxygen species--and Michael acceptor-inducible human aldo-keto reductase AKR1C1 reduces the alpha,beta-unsaturated aldehyde 4-hydroxy-2-nonenal to 1,4-dihydroxy-2-nonene. *J Biol Chem* **276**, 2890-2897 (2001).
111. U. C. Yadav, K. V. Ramana, Regulation of NF-kappaB-induced inflammatory signaling by lipid peroxidation-derived aldehydes. *Oxid Med Cell Longev* **2013**, 690545 (2013).
112. P. Needleman, J. Turk, B. A. Jakschik, A. R. Morrison, J. B. Lefkowith, Arachidonic acid metabolism. *Annu Rev Biochem* **55**, 69-102 (1986).
113. C. J. Hawkey, COX-2 inhibitors. *Lancet* **353**, 307-314 (1999).
114. A. Zarghi, S. Arfaei, Selective COX-2 Inhibitors: A Review of Their Structure-Activity Relationships. *Iran J Pharm Res* **10**, 655-683 (2011).
115. S. Akira *et al.*, A nuclear factor for IL-6 expression (NF-IL6) is a member of a C/EBP family. *EMBO J* **9**, 1897-1906 (1990).
116. S. K. Roy *et al.*, MEKK1 plays a critical role in activating the transcription factor C/EBP-beta-dependent gene expression in response to IFN-gamma. *Proc Natl Acad Sci U S A* **99**, 7945-7950 (2002).
117. J. Hu *et al.*, ERK1 and ERK2 activate CCAAAT/enhancer-binding protein-beta-dependent gene transcription in response to interferon-gamma. *J Biol Chem* **276**, 287-297 (2001).

118. A. N. Hata, R. M. Breyer, Pharmacology and signaling of prostaglandin receptors: multiple roles in inflammation and immune modulation. *Pharmacol Ther* **103**, 147-166 (2004).
119. E. Goupil *et al.*, Biasing the prostaglandin F2alpha receptor responses toward EGFR-dependent transactivation of MAPK. *Mol Endocrinol* **26**, 1189-1202 (2012).
120. W. C. Chung, S. H. Ryu, H. Sun, D. C. Zeldin, J. S. Koo, CREB mediates prostaglandin F2alpha-induced MUC5AC overexpression. *J Immunol* **182**, 2349-2356 (2009).
121. I. H. Tveteraas *et al.*, Mechanisms involved in PGE2-induced transactivation of the epidermal growth factor receptor in MH1C1 hepatocarcinoma cells. *J Exp Clin Cancer Res* **31**, 72 (2012).
122. K. V. Ramana *et al.*, Aldose reductase mediates the lipopolysaccharide-induced release of inflammatory mediators in RAW264.7 murine macrophages. *J Biol Chem* **281**, 33019-33029 (2006).
123. K. Taguchi, H. Motohashi, M. Yamamoto, Molecular mechanisms of the Keap1-Nrf2 pathway in stress response and cancer evolution. *Genes Cells* **16**, 123-140 (2011).
124. J. E. Kim *et al.*, Suppression of NF-kappaB signaling by KEAP1 regulation of IKKbeta activity through autophagic degradation and inhibition of phosphorylation. *Cell Signal* **22**, 1645-1654 (2010).
125. D. R. Bauman *et al.*, Development of nonsteroidal anti-inflammatory drug analogs and steroid carboxylates selective for human aldo-keto reductase isoforms: potential antineoplastic agents that work independently of cyclooxygenase isozymes. *Mol Pharmacol* **67**, 60-68 (2005).
126. T. L. Rizner, Enzymes of the AKR1B and AKR1C Subfamilies and Uterine Diseases. *Front Pharmacol* **3**, 34 (2012).
127. J. C. Desmond *et al.*, The aldo-keto reductase AKR1C3 is a novel suppressor of cell differentiation that provides a plausible target for the non-cyclooxygenase-dependent antineoplastic actions of nonsteroidal anti-inflammatory drugs. *Cancer Res* **63**, 505-512 (2003).
128. J. Fu *et al.*, STING agonist formulated cancer vaccines can cure established tumors resistant to PD-1 blockade. *Sci Transl Med* **7**, 283ra252 (2015).
129. T. Nakamura *et al.*, Liposomes loaded with a STING pathway ligand, cyclic di-GMP, enhance cancer immunotherapy against metastatic melanoma. *J Control Release* **216**, 149-157 (2015).
130. L. Corrales, T. F. Gajewski, Molecular Pathways: Targeting the Stimulator of Interferon Genes (STING) in the Immunotherapy of Cancer. *Clin Cancer Res* **21**, 4774-4779 (2015).
131. D. Chandra *et al.*, STING ligand c-di-GMP improves cancer vaccination against metastatic breast cancer. *Cancer Immunol Res* **2**, 901-910 (2014).
132. O. Quehenberger *et al.*, Lipidomics reveals a remarkable diversity of lipids in human plasma. *J Lipid Res* **51**, 3299-3305 (2010).
133. M. Kaplan Zeevi *et al.*, Listeria monocytogenes multidrug resistance transporters and cyclic di-AMP, which contribute to type I interferon induction, play a role in cell wall stress. *J Bacteriol* **195**, 5250-5261 (2013).
134. S. J. Quillin, K. T. Schwartz, J. H. Leber, The novel Listeria monocytogenes bile sensor BrtA controls expression of the cholic acid efflux pump MdrT. *Mol Microbiol* **81**, 129-142 (2011).

135. K. T. Schwartz *et al.*, Hyperinduction of host beta interferon by a Listeria monocytogenes strain naturally overexpressing the multidrug efflux pump MdrT. *Infect Immun* **80**, 1537-1545 (2012).
136. A. Camejo *et al.*, The arsenal of virulence factors deployed by Listeria monocytogenes to promote its cell infection cycle. *Virulence* **2**, 379-394 (2011).
137. M. Cemma, J. H. Brumell, Interactions of pathogenic bacteria with autophagy systems. *Curr Biol* **22**, R540-545 (2012).
138. S. H. Gregory, A. J. Sagnimeni, E. J. Wing, Bacteria in the bloodstream are trapped in the liver and killed by immigrating neutrophils. *J Immunol* **157**, 2514-2520 (1996).
139. J. W. Conlan, R. J. North, Early pathogenesis of infection in the liver with the facultative intracellular bacteria Listeria monocytogenes, Francisella tularensis, and Salmonella typhimurium involves lysis of infected hepatocytes by leukocytes. *Infect Immun* **60**, 5164-5171 (1992).
140. J. L. Gaillard, F. Jaubert, P. Berche, The inlAB locus mediates the entry of Listeria monocytogenes into hepatocytes in vivo. *J Exp Med* **183**, 359-369 (1996).
141. S. H. Gregory, L. K. Barczynski, E. J. Wing, Effector function of hepatocytes and Kupffer cells in the resolution of systemic bacterial infections. *J Leukoc Biol* **51**, 421-424 (1992).
142. N. Leung, A. Gianfelice, S. D. Gray-Owen, K. Ireton, Impact of the Listeria monocytogenes protein InlC on infection in mice. *Infect Immun* **81**, 1334-1340 (2013).
143. H. W. Rogers, M. P. Callery, B. Deck, E. R. Unanue, Listeria monocytogenes induces apoptosis of infected hepatocytes. *J Immunol* **156**, 679-684 (1996).
144. T. Rajabian *et al.*, The bacterial virulence factor InlC perturbs apical cell junctions and promotes cell-to-cell spread of Listeria. *Nat Cell Biol* **11**, 1212-1218 (2009).
145. A. de las Heras, R. J. Cain, M. K. Bielecka, J. A. Vazquez-Boland, Regulation of Listeria virulence: PrfA master and commander. *Curr Opin Microbiol* **14**, 118-127 (2011).
146. K. K. Wong, N. E. Freitag, A novel mutation within the central Listeria monocytogenes regulator PrfA that results in constitutive expression of virulence gene products. *J Bacteriol* **186**, 6265-6276 (2004).
147. C. Becavin *et al.*, Comparison of widely used Listeria monocytogenes strains EGD, 10403S, and EGD-e highlights genomic variations underlying differences in pathogenicity. *MBio* **5**, e00969-00914 (2014).
148. M. L. Reniere, A. T. Whiteley, D. A. Portnoy, An In Vivo Selection Identifies Listeria monocytogenes Genes Required to Sense the Intracellular Environment and Activate Virulence Factor Expression. *PLoS Pathog* **12**, e1005741 (2016).
149. L. G. Tilney, D. A. Portnoy, Actin filaments and the growth, movement, and spread of the intracellular bacterial parasite, Listeria monocytogenes. *J Cell Biol* **109**, 1597-1608 (1989).
150. S. M. Rafelski, J. A. Theriot, Bacterial shape and ActA distribution affect initiation of Listeria monocytogenes actin-based motility. *Biophys J* **89**, 2146-2158 (2005).
151. M. L. Reniere *et al.*, Glutathione activates virulence gene expression of an intracellular pathogen. *Nature* **517**, 170-173 (2015).
152. L. M. Shetron-Rama *et al.*, Isolation of Listeria monocytogenes mutants with high-level in vitro expression of host cytosol-induced gene products. *Mol Microbiol* **48**, 1537-1551 (2003).
153. E. L. Benanti, C. M. Nguyen, M. D. Welch, Virulent Burkholderia species mimic host actin polymerases to drive actin-based motility. *Cell* **161**, 348-360 (2015).

154. M. D. Welch, M. Way, Arp2/3-mediated actin-based motility: a tail of pathogen abuse. *Cell Host Microbe* **14**, 242-255 (2013).
155. J. A. Theriot, T. J. Mitchison, L. G. Tilney, D. A. Portnoy, The rate of actin-based motility of intracellular Listeria monocytogenes equals the rate of actin polymerization. *Nature* **357**, 257-260 (1992).
156. A. M. Talman, R. Chong, J. Chia, T. Svitkina, H. Agaisse, Actin network disassembly powers dissemination of Listeria monocytogenes. *J Cell Sci* **127**, 240-249 (2014).
157. J. Rosenblatt, B. J. Agnew, H. Abe, J. R. Bamburg, T. J. Mitchison, Xenopus actin depolymerizing factor/cofilin (XAC) is responsible for the turnover of actin filaments in Listeria monocytogenes tails. *J Cell Biol* **136**, 1323-1332 (1997).
158. J. R. Robbins *et al.*, Listeria monocytogenes exploits normal host cell processes to spread from cell to cell. *J Cell Biol* **146**, 1333-1350 (1999).
159. M. Diakonova *et al.*, Adapter protein SH2-Bbeta stimulates actin-based motility of Listeria monocytogenes in a vasodilator-stimulated phosphoprotein (VASP)-dependent fashion. *Infect Immun* **75**, 3581-3593 (2007).
160. G. A. Dabiri, J. M. Sanger, D. A. Portnoy, F. S. Southwick, Listeria monocytogenes moves rapidly through the host-cell cytoplasm by inducing directional actin assembly. *Proc Natl Acad Sci U S A* **87**, 6068-6072 (1990).
161. J. A. Theriot, J. Rosenblatt, D. A. Portnoy, P. J. Goldschmidt-Clermont, T. J. Mitchison, Involvement of profilin in the actin-based motility of L. monocytogenes in cells and in cell-free extracts. *Cell* **76**, 505-517 (1994).
162. G. A. Smith, J. A. Theriot, D. A. Portnoy, The tandem repeat domain in the Listeria monocytogenes ActA protein controls the rate of actin-based motility, the percentage of moving bacteria, and the localization of vasodilator-stimulated phosphoprotein and profilin. *J Cell Biol* **135**, 647-660 (1996).
163. K. Tadmor *et al.*, Listeria monocytogenes MDR transporters are involved in LTA synthesis and triggering of innate immunity during infection. *Front Cell Infect Microbiol* **4**, 16 (2014).
164. S. H. Gregory, E. J. Wing, R. A. Hoffman, R. L. Simmons, Reactive nitrogen intermediates suppress the primary immunologic response to Listeria. *J Immunol* **150**, 2901-2909 (1993).
165. L. E. Bermudez, Differential mechanisms of intracellular killing of Mycobacterium avium and Listeria monocytogenes by activated human and murine macrophages. The role of nitric oxide. *Clin Exp Immunol* **91**, 277-281 (1993).
166. J. N. Higginbotham, T. L. Lin, S. B. Pruett, Effect of macrophage activation on killing of Listeria monocytogenes. Roles of reactive oxygen or nitrogen intermediates, rate of phagocytosis, and retention of bacteria in endosomes. *Clin Exp Immunol* **88**, 492-498 (1992).
167. C. Bogdan, Nitric oxide synthase in innate and adaptive immunity: an update. *Trends Immunol* **36**, 161-178 (2015).
168. J. D. MacMicking *et al.*, Altered responses to bacterial infection and endotoxic shock in mice lacking inducible nitric oxide synthase. *Cell* **81**, 641-650 (1995).
169. E. G. Pamer, Immune responses to Listeria monocytogenes. *Nat Rev Immunol* **4**, 812-823 (2004).
170. D. M. Monack, J. A. Theriot, Actin-based motility is sufficient for bacterial membrane protrusion formation and host cell uptake. *Cell Microbiol* **3**, 633-647 (2001).

171. M. J. Gray *et al.*, Listeria monocytogenes isolates from foods and humans form distinct but overlapping populations. *Appl Environ Microbiol* **70**, 5833-5841 (2004).
172. C. Guldimann *et al.*, Increased spread and replication efficiency of Listeria monocytogenes in organotypic brain-slices is related to multilocus variable number of tandem repeat analysis (MLVA) complex. *BMC Microbiol* **15**, 134 (2015).
173. M. Wiedmann *et al.*, Ribotypes and virulence gene polymorphisms suggest three distinct Listeria monocytogenes lineages with differences in pathogenic potential. *Infect Immun* **65**, 2707-2716 (1997).
174. T. Zhang *et al.*, Deciphering the landscape of host barriers to Listeria monocytogenes infection. *Proc Natl Acad Sci U S A* **114**, 6334-6339 (2017).
175. J. Hardy *et al.*, Extracellular replication of Listeria monocytogenes in the murine gall bladder. *Science* **303**, 851-853 (2004).
176. C. T. French *et al.*, Dissection of the Burkholderia intracellular life cycle using a photothermal nanoblade. *Proc Natl Acad Sci U S A* **108**, 12095-12100 (2011).
177. C. Lim, M. Hong, R. Savan, Human IL-22 binding protein isoforms act as a rheostat for IL-22 signaling. *Sci Signal* **9**, ra95 (2016).
178. A. P. McFarland *et al.*, The favorable IFNL3 genotype escapes mRNA decay mediated by AU-rich elements and hepatitis C virus-induced microRNAs. *Nat Immunol* **15**, 72-79 (2014).
179. A. Kuhbacher, P. Cossart, J. Pizarro-Cerda, Internalization assays for Listeria monocytogenes. *Methods Mol Biol* **1157**, 167-178 (2014).
180. A. N. Sun, A. Camilli, D. A. Portnoy, Isolation of Listeria monocytogenes small-plaque mutants defective for intracellular growth and cell-to-cell spread. *Infect Immun* **58**, 3770-3778 (1990).
181. J. Moretti *et al.*, STING Senses Microbial Viability to Orchestrate Stress-Mediated Autophagy of the Endoplasmic Reticulum. *Cell* **171**, 809-823 e813 (2017).
182. J. S. Ruiz-Moreno *et al.*, The cGAS/STING Pathway Detects Streptococcus pneumoniae but Appears Dispensable for Antipneumococcal Defense in Mice and Humans. *Infect Immun* **86**, (2018).
183. IMMGEN. pp. Akr1c13.
184. C. S. Rosenfeld *et al.*, Striking variation in the sex ratio of pups born to mice according to whether maternal diet is high in fat or carbohydrate. *Proc Natl Acad Sci U S A* **100**, 4628-4632 (2003).
185. J. J. Whyte *et al.*, Maternal diet composition alters serum steroid and free fatty acid concentrations and vaginal pH in mice. *J Endocrinol* **192**, 75-81 (2007).
186. P. Kovarik, V. Castiglia, M. Ivin, F. Ebner, Type I Interferons in Bacterial Infections: A Balancing Act. *Front Immunol* **7**, 652 (2016).
187. M. Durr, A. Peschel, Chemokines meet defensins: the merging concepts of chemoattractants and antimicrobial peptides in host defense. *Infect Immun* **70**, 6515-6517 (2002).
188. C. C. Akoh, R. S. Chapkin, Composition of mouse peritoneal macrophage phospholipid molecular species. *Lipids* **25**, 613-617 (1990).
189. L. S. Bisgaard *et al.*, Bone marrow-derived and peritoneal macrophages have different inflammatory response to oxLDL and M1/M2 marker expression - implications for atherosclerosis research. *Sci Rep* **6**, 35234 (2016).
190. K. Suzuki *et al.*, Aberrant expansion of segmented filamentous bacteria in IgA-deficient gut. *Proc Natl Acad Sci U S A* **101**, 1981-1986 (2004).
191. Ivanov, II *et al.*, Induction of intestinal Th17 cells by segmented filamentous bacteria. *Cell* **139**, 485-498 (2009).

192. V. Gaboriau-Routhiau *et al.*, The key role of segmented filamentous bacteria in the coordinated maturation of gut helper T cell responses. *Immunity* **31**, 677-689 (2009).
193. H. J. Wu *et al.*, Gut-residing segmented filamentous bacteria drive autoimmune arthritis via T helper 17 cells. *Immunity* **32**, 815-827 (2010).
194. M. Caselli, J. Holton, P. Boldrini, D. Vaira, G. Calo, Morphology of segmented filamentous bacteria and their patterns of contact with the follicle-associated epithelium of the mouse terminal ileum: implications for the relationship with the immune system. *Gut Microbes* **1**, 367-372 (2010).
195. N. Kamada, G. Nunez, Regulation of the immune system by the resident intestinal bacteria. *Gastroenterology* **146**, 1477-1488 (2014).
196. A. Lundin *et al.*, Gut flora, Toll-like receptors and nuclear receptors: a tripartite communication that tunes innate immunity in large intestine. *Cell Microbiol* **10**, 1093-1103 (2008).
197. N. Kumar *et al.*, The benzenesulfoamide T0901317 [N-(2,2,2-trifluoroethyl)-N-[4-[2,2,2-trifluoro-1-hydroxy-1-(trifluoromethyl)ethy l]phenyl]-benzenesulfonamide] is a novel retinoic acid receptor-related orphan receptor-alpha/gamma inverse agonist. *Molecular pharmacology* **77**, 228-236 (2010).
198. M. N. Erkelens, R. E. Mebius, Retinoic Acid and Immune Homeostasis: A Balancing Act. *Trends Immunol*, (2017).
199. C. Ohnmacht, Tolerance to the Intestinal Microbiota Mediated by ROR(gammat)(+) Cells. *Trends Immunol* **37**, 477-486 (2016).
200. A. K. San Roman, B. E. Aronson, S. D. Krasinski, R. A. Shivdasani, M. P. Verzi, Transcription factors GATA4 and HNF4A control distinct aspects of intestinal homeostasis in conjunction with transcription factor CDX2. *J Biol Chem* **290**, 1850-1860 (2015).
201. K. L. Fritsche, L. M. Shahbazian, C. Feng, J. N. Berg, Dietary fish oil reduces survival and impairs bacterial clearance in C3H/Hen mice challenged with Listeria monocytogenes. *Clin Sci (Lond)* **92**, 95-101 (1997).
202. M. A. Puertollano, M. A. de Pablo, G. Alvarez de Cienfuegos, Relevance of dietary lipids as modulators of immune functions in cells infected with Listeria monocytogenes. *Clin Diagn Lab Immunol* **9**, 352-357 (2002).
203. J. C. Petit, G. Richard, B. Burghoffer, G. L. Daguet, Suppression of cellular immunity to Listeria monocytogenes by activated macrophages: mediation by prostaglandins. *Infect Immun* **49**, 383-388 (1985).
204. E. Theisen *et al.*, Cyclooxygenase-1 and -2 Play Contrasting Roles in Listeria-Stimulated Immunity. *J Immunol*, (2018).
205. S. Noor *et al.*, Activation of cytosolic phospholipase A2alpha in resident peritoneal macrophages by Listeria monocytogenes involves listeriolysin O and TLR2. *J Biol Chem* **283**, 4744-4755 (2008).
206. H. R. Knapp, M. A. Melly, Bactericidal effects of polyunsaturated fatty acids. *J Infect Dis* **154**, 84-94 (1986).
207. L. L. Wang, E. A. Johnson, Inhibition of Listeria monocytogenes by fatty acids and monoglycerides. *Appl Environ Microbiol* **58**, 624-629 (1992).
208. T. H. P. Atlas, Protein Expression; http://www.proteinatlas.org/ENSG00000184584-TMEM173/tissue; TMEM173/STING.
209. D. L. Burdette, R. E. Vance, STING and the innate immune response to nucleic acids in the cytosol. *Nat Immunol* **14**, 19-26 (2013).

210. M. Lizio *et al.*, Gateways to the FANTOM5 promoter level mammalian expression atlas. *Genome Biol* **16**, 22 (2015).
211. FANTOM5, http://fantom.gsc.riken.jp/5/sstar/EntrezGene:27384; Akr1c13; EntrezGene 27384.
212. N. A. Mabbott, D. S. Donaldson, H. Ohno, I. R. Williams, A. Mahajan, Microfold (M) cells: important immunosurveillance posts in the intestinal epithelium. *Mucosal Immunol* **6**, 666-677 (2013).
213. Y. Yin *et al.*, Comparative analysis of the distribution of segmented filamentous bacteria in humans, mice and chickens. *ISME J* **7**, 615-621 (2013).
214. M. A. Jepson, M. A. Clark, N. L. Simmons, B. H. Hirst, Actin accumulation at sites of attachment of indigenous apathogenic segmented filamentous bacteria to mouse ileal epithelial cells. *Infect Immun* **61**, 4001-4004 (1993).
215. A. L. Kau, P. P. Ahern, N. W. Griffin, A. L. Goodman, J. I. Gordon, Human nutrition, the gut microbiome and the immune system. *Nature* **474**, 327-336 (2011).
216. H. R. Cha *et al.*, Downregulation of Th17 cells in the small intestine by disruption of gut flora in the absence of retinoic acid. *J Immunol* **184**, 6799-6806 (2010).
217. M. G. Derebe *et al.*, Serum amyloid A is a retinol binding protein that transports retinol during bacterial infection. *Elife* **3**, e03206 (2014).
218. J. M. Kim, D. Kim, S. Kim, J. S. Kim, Genotyping with CRISPR-Cas-derived RNA-guided endonucleases. *Nat Commun* **5**, 3157 (2014).
219. G. Trinchieri, A. Sher, Cooperation of Toll-like receptor signals in innate immune defence. *Nat Rev Immunol* **7**, 179-190 (2007).
220. E. Beutler, T. Gelbart, C. West, Synergy between TLR2 and TLR4: a safety mechanism. *Blood Cells Mol Dis* **27**, 728-730 (2001).
221. M. M. Whitmore *et al.*, Synergistic activation of innate immunity by double-stranded RNA and CpG DNA promotes enhanced antitumor activity. *Cancer Res* **64**, 5850-5860 (2004).
222. H. Tada, S. Aiba, K. Shibata, T. Ohteki, H. Takada, Synergistic effect of Nod1 and Nod2 agonists with toll-like receptor agonists on human dendritic cells to generate interleukin-12 and T helper type 1 cells. *Infect Immun* **73**, 7967-7976 (2005).
223. J. H. Fritz *et al.*, Synergistic stimulation of human monocytes and dendritic cells by Toll-like receptor 4 and NOD1- and NOD2-activating agonists. *Eur J Immunol* **35**, 2459-2470 (2005).
224. D. A. van Heel *et al.*, Synergistic enhancement of Toll-like receptor responses by NOD1 activation. *Eur J Immunol* **35**, 2471-2476 (2005).
225. J. Tschopp, F. Martinon, K. Burns, NALPs: a novel protein family involved in inflammation. *Nat Rev Mol Cell Biol* **4**, 95-104 (2003).
226. L. Agostini *et al.*, NALP3 forms an IL-1beta-processing inflammasome with increased activity in Muckle-Wells autoinflammatory disorder. *Immunity* **20**, 319-325 (2004).
227. F. S. Laroux, X. Romero, L. Wetzler, P. Engel, C. Terhorst, Cutting edge: MyD88 controls phagocyte NADPH oxidase function and killing of gram-negative bacteria. *J Immunol* **175**, 5596-5600 (2005).
228. X. Wang *et al.*, 4-hydroxy-2-nonenal mediates genotoxicity and bystander effects caused by Enterococcus faecalis-infected macrophages. *Gastroenterology* **142**, 543-551 e547 (2012).
229. N. Deighton, I. I. Muckenschnabel, B. A. Goodman, B. Williamson, Lipid peroxidation and the oxidative burst associated with infection of capsicum

annuum by botrytis cinerea. *The Plant journal : for cell and molecular biology* **20**, 485-492 (1999).
230. R. Tanaka, K. Shigeta, Y. Sugiura, H. Hatate, T. Matsushita, Accumulation of hydroxyl lipids and 4-hydroxy-2-hexenal in live fish infected with fish diseases. *Lipids* **49**, 385-396 (2014).
231. L. Kolodziejczyk, E. Siemieniuk, E. Skrzydlewska, Antioxidant potential of rat liver in experimental infection with Fasciola hepatica. *Parasitology research* **96**, 367-372 (2005).
232. J. H. Kavouras *et al.*, Herpes simplex virus type 1 infection induces oxidative stress and the release of bioactive lipid peroxidation by-products in mouse P19N neural cell cultures. *Journal of neurovirology* **13**, 416-425 (2007).
233. F. C. Fang, Antimicrobial reactive oxygen and nitrogen species: concepts and controversies. *Nat Rev Microbiol* **2**, 820-832 (2004).
234. V. J. Thannickal, B. L. Fanburg, Reactive oxygen species in cell signaling. *Am J Physiol Lung Cell Mol Physiol* **279**, L1005-1028 (2000).
235. A. P. Desbois, V. J. Smith, Antibacterial free fatty acids: activities, mechanisms of action and biotechnological potential. *Appl Microbiol Biotechnol* **85**, 1629-1642 (2010).
236. J. J. Kabara, D. M. Swieczkowski, A. J. Conley, J. P. Truant, Fatty acids and derivatives as antimicrobial agents. *Antimicrob Agents Chemother* **2**, 23-28 (1972).
237. S. Endo *et al.*, Substrate specificity of a mouse aldo-keto reductase (AKR1C12). *Biol Pharm Bull* **29**, 2488-2492 (2006).
238. T. Hruz *et al.*, Genevestigator v3: a reference expression database for the meta-analysis of transcriptomes. *Adv Bioinformatics* **2008**, 420747 (2008).
239. E. T. Keller, C. Chang, W. B. Ershler, Inhibition of NFkappaB activity through maintenance of IkappaBalpha levels contributes to dihydrotestosterone-mediated repression of the interleukin-6 promoter. *J Biol Chem* **271**, 26267-26275 (1996).